CHANGE NO. 3

FOR

THE TRAPPED RADIATION HANDBOOK
(DNA 2524H)

2 December 1974

Instructions

The recipient is requested to remove the pages listed below from his or her copy of DNA 2524H, add the attached pages per DNA letter of approval dated 12 August 1975, and record this and all previous actions on page iii.

REMOVE	ADD
Title Page (1 November 1973)	Title Page (2 December 1974)
ii (1 November 1973)	ii (2 December 1974)
iii thru iv (1 November 1973)	iii thru iv (2 December 1974)
ix thru xxxvi (1 November 1973)	ix thru xxxvi (2 December 1974)
3-19 thru 3-24 (Original)	3-19 thru 3-24 (2 December 1974)
3-37 thru 3-46 (Original)	3-37 thru 3-46 (2 December 1974)
3-69 thru 3-98 (Original)	3-69 thru 3-100 (2 December 1974)
5-1 thru 5-2 (Original)	5-1 thru 5-2 (2 December 1974)
5-9 thru 5-12 (2 January 1973)	5-9 thru 5-126 (2 December 1974)
5-13 thru 5-44 (Original)	.
5-45 thru 5-46 (2 January 1973)	.
5-47 thru 5-100 (Original)	.
8-9 thru 8-10 (Original)	8-9 thru 8-10 (2 December 1974)
15-1 thru 15-16 (Original)	15-1 thru 15-18 (2 December 1974)
D1 thru D8 (1 November 1973)	D1 thru D8 (2 December 1974)

NOTE: If the recipient did not receive a copy of DNA 2524H (The Trapped Radiation Handbook), Change 1, or Change 2, they can be obtained by addressing a request to the below named individual. A limited supply will be available for this purpose.

M. J. Dudash
General Electric Company– TEMPO
DASIAC
816 State Street
Santa Barbara, CA 93102

DNA 2524H-
Change-3

THE TRAPPED RADIATION HANDBOOK

Compilers and Editors-in-Chief:

John B. Cladis
Gerald T. Davidson
Lester L. Newkirk

~~Revised~~
2 December 1974

Project Officer: Dr. Charles A. Blank

Prepared for:
Defense Nuclear Agency
Washington, D.C. 20305
by Lockheed Palo Alto Research Laboratory
~~Under Contract~~ DNA 001-73-C-0065
NWER ~~Subtask~~-HC047-08

Published by:
DASIAC
General Electric Company—TEMPO
Santa Barbara, California 93102
Under Contract DNA 001-75-C-0023
NWED Subtask DC008-01

LIST OF EFFECTIVE PAGES

PAGE	LAST CHANGE
Title Page	2 December 1974
ii	2 December 1974
iii thru iv	2 December 1974
v thru viii	1 November 1973
ix thru xxxvi	2 December 1974
xxxvii thru xxxviii	1 November 1973
1-1 thru 1-22	Original
2-1 thru 2-6	Original
2-7 thru 2-8	2 January 1973
2-9 thru 2-10	Original
2-11 thru 2-12	2 January 1973
2-13 thru 2-32	Original
2-33 thru 2-34	2 January 1973
2-35 thru 2-66	Original
3-1 thru 3-6	Original
3-7 thru 3-8	2 January 1973
3-9 thru 3-18	Original
3-19 thru 3-24	2 December 1974
3-25 thru 3-36	Original
3-37 thru 3-46	2 December 1974
3-47 thru 3-68	Original
3-69 thru 3-100	2 December 1974
4-1 thru 4-88	Original
5-1 thru 5-2	2 December 1974
5-3 thru 5-8	Original
5-9 thru 5-126	2 December 1974
6-1 thru 6-60	Original
7-1 thru 7-30	Original
8-1 thru 8-2	1 November 1973
8-3 thru 8-4	Original
8-5 thru 8-6	1 November 1973
8-7 thru 8-8	Original
8-9 thru 8-10	2 December 1974
8-11 thru 8-12	Original
8-13 thru 8-35	1 November 1973
8-35A thru 8-35D	1 November 1973
8-36	1 November 1973
8-37 thru 8-80	Original
8-81 thru 8-82	2 January 1973
8-83 thru 8-84	Original
8-85 thru 8-86	1 November 1973
8-87 thru 8-88	Original
8-89 thru 8-90	1 November 1973
9-1 thru 9-36	Original
10-1 thru 10-9	Original
11-1 thru 11-34	Original
11-35 thru 11-36	2 January 1973
11-37 thru 11-60	Original
12-1 thru 12-6	Original
13-1 thru 13-20	Original
14-1 thru 14-2	Original
14-3 thru 14-4	2 January 1973
15-1 thru 15-18	2 December 1974
D1 thru D8	2 December 1974

2 December 1974

RECORD OF REVISIONS

Revision No.	Date of Issue	Date of Receipt	Entered By

2 December 1974

ACKNOWLEDGMENTS

The Defense Nuclear Agency sincerely appreciates the contributions of these people to the publication and contents of this Handbook:

Mr. A.D. Anderson	Lockheed Palo Alto Research Laboratory
Dr. C.A. Blank	HQ, Defense Nuclear Agency
Dr. J.B. Cladis	Lockheed Palo Alto Research Laboratory
Mr. D.L. Crowther	Lockheed Palo Alto Research Laboratory
Dr. G.T. Davidson	Lockheed Palo Alto Research Laboratory
Dr. J.F. Fennell	St. Louis University
Mr. W.E. Francis	Lockheed Palo Alto Research Laboratory
Dr. J.A. George	St. Louis University
Mr. W.H. Harless, Jr.	Lockheed Palo Alto Research Laboratory
Dr. R.W. Hendrick, Jr.	General Electric Company—TEMPO
Dr. J.L. Hickerson	St. Louis University
Dr. R.T. Hoverter	St. Louis University
Dr. C.H. Humphrey	Lockheed Palo Alto Research Laboratory
Maj. S. Kennedy	HQ, Defense Nuclear Agency
Dr. G.V. Maldonado	St. Louis University
Dr. D.J. Manson	St. Louis University
Dr. B.M. McCormac	Lockheed Palo Alto Research Laboratory
Dr. G.H. Nakano	Lockheed Palo Alto Research Laboratory
Dr. L.L. Newkirk	Lockheed Palo Alto Research Laboratory
Dr. S.L. Ossakow	Lockheed Palo Alto Research Laboratory
Dr. A.M. Peterson	Stanford Research Institute
Mr. F.H. Sage, III	General Electric Company—TEMPO
Mr. J.W. Schallau	Lockheed Palo Alto Research Laboratory
Dr. J.F. Vesecky	Stanford Research Institute
Dr. J.I. Vette	NASA—Goddard Space Flight Center
Dr. M. Walt	Lockheed Palo Alto Research Laboratory
Dr. A.H. Weber	St. Louis University

CONTENTS

Next Page Over

ILLUSTRATIONS

5

TABLES

The particle does not return to the point from which it started but experiences a drift in the direction perpendicular to the gradient of the field, $\nabla_\perp B$. The motion is quite similar to the $\bar{F} \times \bar{B}$ drift except that the trajectory in this case is not truly cycloidal—the guiding center "wobbles" about a straight line perpendicular to $\nabla_\perp B$ (Reference 4). The calculated drift velocities are only approximate. Their accuracy becomes poorer as the scale of the field variation approaches the gyro-radius. The gradient-B drift velocity to first order in $\nabla_\perp B$ (References 4 and 22) is

$$\bar{V}_g = -\frac{p_\perp^2}{2\gamma m^2} \frac{\nabla_\perp B \times \bar{B}}{\omega_c B^2} \quad . \tag{3-36}$$

The gradient-B drift and curvature drift velocities may be combined in one expression:

$$\bar{V}_g = -\left(\frac{p_\perp^2}{2} + p_{\parallel}^2\right) \frac{\nabla_\perp B \times \bar{B}}{\gamma m^2 \omega_c B^2}$$

$$= -\left(\frac{v_\perp^2}{2} + v_{\parallel}^2\right) \gamma \frac{\nabla_\perp B \times \bar{B}}{\omega_c B^2} \quad . \tag{3-37}$$

The total drift velocity of Equation 3-37 often is called the gradient-B drift velocity. For simplicity, it will be thus designated throughout the remainder of this volume.

In the geomagnetic field that decreases with $1/r^3$, the drift velocity is proportional approximately to L^2 . The drift velocity in the azimuthal direction at any latitude, λ , is

$$\bar{V}_g = -\left(\frac{p_\perp^2}{2} + p_{\parallel}^2\right) \frac{3cL^2}{\gamma mqR_E B_E} \frac{(1 + \sin^2\lambda)\cos^5\lambda}{(1 + 3\sin^2\lambda)^2} \quad . \tag{3-38a}$$

At the equator where $\sin\lambda = 0$, the latitude-dependent part of Equation 3-38 equals 1, and the drift velocity (eastward) for electrons becomes

$$V_g(\text{km/sec}) = 14.76\left(p_\perp^2 + 2p_\parallel^2\right)\frac{L^2}{\gamma} = 3.86\left(\frac{v_\perp^2}{c^2} + 2\frac{v_\parallel^2}{c^2}\right)\gamma L^2 \quad . \tag{3-38b}$$

The corresponding drift velocity (westward) for protons is

$$V_g(\text{km/sec}) = -8.04 \times 10^{-3}\left(p_\perp^2 + 2p_\parallel^2\right)\frac{L^2}{\gamma} \quad -7080\left(\frac{v_\perp^2}{c^2} + 2\frac{v_\parallel^2}{c^2}\right)\gamma L^2 \tag{3-39a}$$

which in the nonrelativistic limit is

$$V_g(\text{km/sec}) \sim -15.1(T_\perp + 2T_\parallel)\frac{L^2}{\gamma} \quad . \tag{3-39b}$$

Momentum here is in MeV/c units and energy in MeV. For relativistic electrons, the magnitudes of the energy "components" may be used in place of the momentum. In Equations 3-39a and 3-39b, a positive velocity results when the drift motion is toward the east. Electrons generally drift toward the east and positively charged particles drift toward the west.

The gradient-B drift current induces a magnetic field that, inside a region enclosed by the path of the guiding center, opposes the main field of the earth. The drift current may be thought of as a diamagnetic current (Section 3.3.2; References 1 and 20).

The gradient-B drift is much faster than the gravitational drift for electrons and fast protons. The mean of $(v_\perp^2/2 + v_\parallel^2)$ for isotropically distributed thermal particles is 3 kT/m . k is Boltzmann's constant 1.38×10^{-16} cgs, and T is the temperature (Reference 2). The mean drift velocity of thermal particles at the equator due to the nonhomogeneity of the field is

$$V_g(\text{km/sec}) \cong 4 \times 10^{-9}\, TL^2 \quad . \tag{3-40}$$

A mean temperature of about 2,000°K appears to be a fair assumption for both electrons and ions in the trapped radiation belts (References 23 through 27). The drift velocity of thermal particles then is

$$V_g(\text{km/sec}) \cong 8 \times 10^{-6}\, L^2 \quad , \tag{3-41}$$

which is comparable with the gravitational drift velocity of protons (Equation 3-32).

3.3.2 Magnetic Reflection

Generally, a nonhomogeneous magnetic field has regions where the field lines converge. In those regions, the magnetic force $(q/c)\vec{v} \times \vec{B}$ has a small component directed along the field lines. This component tends to deflect a charged particle away from a region of increasing field strength.

The magnetic force components are depicted in Figure 3-9. The relative magnitudes of the force components are variable. Usually the centripetal force is the major part of the magnetic force. When the retarding force along the field lines is relatively weak, the equation of motion yields an acceleration (or deceleration) in the field direction $\vec{B}$ (References 4 and 21):

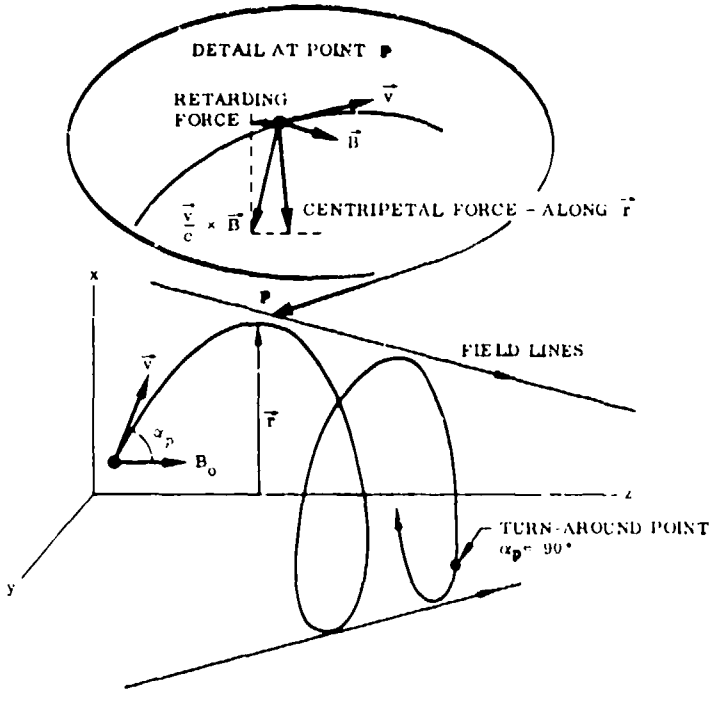

Figure 3-9. Components of the force acting on a positively charged particle in a converging magnetic field.

$$\frac{dv_{\parallel}}{dt} \cong - \frac{1}{2} \frac{v_{\perp}^2}{\gamma B} \frac{d\bar{B}}{dS} \qquad (3\text{-}42a)$$

to first order in the variation of B with distance S along the field line. The similarity to the drift velocity Equation 3-37 especially should be noted. Here, too, gravitational effects are comparable with the field inhomogeneity effects for thermal velocity protons.

The radial component of the equation of motion reduces to:

$$\frac{dv_{\perp}}{dt} \cong \frac{1}{2} \frac{v_{\parallel} v_{\perp}}{\gamma B} \frac{dB}{dS} \quad . \qquad (3\text{-}42b)$$

But $v_{\parallel}\, dB/dS$ is just the time rate of change of magnetic field intensity as experienced by a spiraling particle. Equation 3-42b, therefore, yields the simple relation:

$$v_{\perp}^2 \propto B \quad . \qquad (3\text{-}43)$$

Charged particles in a converging magnetic field travel toward the "ends" of the field only as far as the turnaround or mirror points (Reference 1) where $p_{\perp}^2$ is equal to p^2, the total momentum squared. This definition of the turnaround points is not in exact accord with Section 3.2.3. For all practical purposes, the turnaround point is regarded simply as the location where there is no component of momentum along the general direction of the field. To avoid confusion, the term mirror point will be used here except when the specific meaning of Section 3.2.3 is intended.

If the magnetic field is closed at two ends, charged particles will continue to "bounce" back and forth until they either lose energy or are deflected by some external process. Figure 1-3 shows how charged particles move in the earth's field (ignoring drift motion).

It is convenient to define the pitch angle α_p as the angle between the particle's momentum and the magnetic field (some of the early literature on magnetic trapping refers to the pitch angle as the compliment of the angle defined here). The pitch angle is indicated in Figures 1-3 and 3-9. Equation 3-43 is equivalent to a simple relation which gives, at any point, the pitch angle variation in a magnetic field:

$$\sin \alpha_p = \sqrt{B/B_m} \qquad 3\text{-}44$$

Equation 3-44 is presented numerically in Figure 3B-1. B_m is the field strength at the mirror point. The pitch angle attains its minimum, α_o, at the equator. A smallest allowed α_o, the cutoff pitch angle, exists for any field line. Particles with smaller pitch angles would be lost rapidly because they penetrate deeply into the atmosphere (References 28, 29, and 30). The cutoff pitch angle:

$$\alpha_c = \arcsin\left(\sqrt{B_o/B\left[\text{atmosphere}\right]}\right) \tag{3-45}$$

is plotted in Figures 3B-3 and 3B-4.

THE MAGNETIC MOMENT OF A CHARGED PARTICLE. The proportionality of $p_\perp^2$ and B ensures that the magnetic flux $\pi\rho_c^2 B$ within an orbit remains constant. This result can be shown to be true generally, even in a magnetic field that varies with time (Reference 21). Charged particles behave as a diamagnetic medium—their motion induces a magnetic field in opposition to the externally applied field (References 1, 20, 31, and 32). The product of the area enclosed by the orbit multiplied by the current around the perimeter is the magnetic moment of a single gyrating particle. The magnetic moment of a charged particle in a magnetic field:

$$M = \frac{p_\perp^2}{2mB} = \frac{p^2}{2m\,B_m} \tag{3-46}$$

is a constant if Equation 3-43 is valid. The energy-dependent factor in the latter equation is plotted in Figure 3B-7.

THE BOUNCE AND DRIFT PERIODS. The total time elapsed between successive reflections of a trapped particle is the bounce period:

$$t_b = \frac{4}{v}\int_o^{S_m} \frac{dS}{\cos\alpha_p} \equiv \frac{R_o}{v}\,\mathcal{J}(\alpha_o) \quad . \tag{3-47}$$

A quite satisfactory empirical approximation (with errors of less than 1 percent) for particles trapped in the geomagnetic field (Reference 33) is

$$t_b(\text{sec}) \approx 0.177\,\frac{L}{v/c}\left[1 - 0.4635\,(\sin\alpha_o)^{0.73}\right] \quad . \tag{3-48}$$

It is often more convenient to replace the exponent of the $\sin\alpha_o$ term by 0.75; in that case the accuracy at large pitch angles is improved with a slight sacrifice of accuracy at moderate pitch angles. Bounce periods are generally several orders of magnitude greater than the

gyro periods ($\approx 10^{-1}$ second versus $\approx 10^{-6}$ to 10^{-5} second, respectively, for the trapped electrons). Computed bounce periods are shown in Figures 3B-10 through 3B-12.

Because it varies along a geomagnetic field line, the azimuthal drift velocity (Equations 3-38 and 3-39) must be averaged over a complete bounce period. The average drift velocity has been computed and tabulated by several workers, particularly Lew (Reference 34). At the equator the average is given quite well by the empirical formula (which agrees with computed values within 0.5 percent) (References 33, 34, 35, and 36).

$$V_g \approx \frac{c}{eB_E R_E} L^2 E\left(\frac{v}{c}\right)^2 / [1 - 0.3333 (\sin \alpha_o)^{0.62}] \quad . \tag{3-49}$$

The drift period is the time taken for drifting particles to make a complete circuit of the earth; Equation 3-49 gives

$$t_d \approx \frac{2\pi eB_E R_E^2}{mc^3} \frac{1}{L\gamma(v/c)^2} [1 - 0.3333(\sin \alpha_o)^{0.62}] \tag{3-50a}$$

for electrons:

$$\frac{2\pi eB_E R_E^2}{mc^3} \approx 1.557 \times 10^4 \text{ second} \tag{3-50b}$$

and for protons:

$$\approx 8.481 \text{ second.} \tag{3-50c}$$

Drift periods are generally several orders of magnitude greater than bounce periods. The computed values are shown in Figures 3B-10, 3B-11, and 3B-13.

3.3.3 The Motion of Field Lines

If charged particles gyrating in a magnetic field are to maintain a constant magnetic moment during changes in the field strength, their kinetic energies also must change. Energy normally is not exchanged between a static magnetic field and charged particles. However, a variable magnetic field induces an electric field that can accelerate charged particles. The induced electric field $\bar{E}_i$ is given by Faraday's law, which states that the integral $\oint E_i \cdot d\bar{s}$ taken

(often written with a subscript, i.e., J_o or $J_{[omni]}$). The omnidirectional flux is just 4π times the intensity averaged over all angles. The omnidirectional flux should not be confused with the net flux:

$$F = \int_{[\text{all angles}]} j \cos\zeta \, d\Omega \tag{3-86}$$

which is the rate per unit area at which particles cross a plane surface; ζ is the angle between the velocity vector and the normal to the surface, $d\Omega$ is the increment of solid angle. The flux, F, can be negative or positive, depending on whether more particles cross the surface from one side or the other. With regard to the trapped particles, F has a meaning only when referred to a solid detector surface, otherwise:

$$F = 2\pi \cos\zeta' \int_{-1}^{1} j(\mu)\, \mu d\mu \sim 0 \tag{3-87}$$

where ζ' is the angle between the field line and the normal to the surface.

Since J is a function of B, it also may be regarded as a function of $\mu_o' = \sqrt{1 - B_o/B}$. With the aid of Liouville's equation (Equation 3-82), the omnidirectional flux can be written as an integral involving the equatorial intensity $j(\mu_o, \mu_o') = j(\mu_o, B_o)$:

$$J(B) = J(\mu_o') = 4\pi \int_{\mu_o'}^{1} j(\mu_o, B_o) \frac{B\mu_o \, d\mu_o}{B_o \sqrt{1 - B(1-\mu_o^2)/B_o}} \tag{3-88a}$$

$$= 4\pi \int_{\mu_o'}^{1} j(\mu_o, \mu_o') \frac{\mu_o \, d\mu_o}{(1-\mu_o'^2)\sqrt{1 - (1-\mu_o^2)/(1-\mu_o'^2)}} \tag{3-88b}$$

The inverse relation that yields j as a function of J cannot be written in a closed form except for certain special cases. For a pitch-angle distribution of the form

$$j = C(\mu_c - \mu_o^2)^{n/2} \Big\} \; \mu_o < \mu_c \tag{3-89a}$$

the omnidirectional flux is

$$J = 2\pi C \frac{\Gamma(1+\frac{n}{2})}{\Gamma(\frac{3}{2}+\frac{n}{2})} \frac{(\mu_c^2 - \mu_o'^2)^{n/2 + 1/2}}{(1 - \mu_o'^2)^{1/2}} \quad . \tag{3-89b}$$

The distribution Equation 3-89b is particularly useful because it approximates the steady-state solutions of a pitch-angle diffusion equation (see Chapter 5).

Detailed solutions of the relation of j to J are available (References 61 and 62 ; a computer code which performs the integration is listed in Appendix 3C).

3.6 HYDROMAGNETIC MODEL OF A PLASMA

3.6.1 Collisions Between Charged Particles— Collective Behavior

In any ensemble of particles, collisions occur between particles. These result in transfer of momentum. The electrostatic forces between charged particles decrease slowly as the mutual separation increases. Therefore, where a plasma is relatively tenuous, the most important interactions are between charged particles. The interaction forces between charged particles become negligible only beyond the Debye length or Debye shielding radius:

$$\lambda_D = \sqrt{\frac{kT_e}{4\pi n_e e^2}} \tag{3-89c}$$

$$\lambda_D(\text{cm}) = 6.9 \sqrt{\frac{T_e(k)}{n_e(\text{cm}^{-3})}} \tag{3-89d}$$

where T_e and n_e are, respectively, the effective temperature and number density of "thermal" electrons. The shielding of electrostatic forces is due to thermal fluctuations in the free electron gas (References 1 and 2). The effective temperature of the free electrons, the electron temperature T_e, therefore should be expected to appear in the Debye length formula. The electron temperature above the atmosphere is about 1,500 to 2,000 K (References 23 through 27),

which results in a Debye length of

$$\lambda_D(\text{cm}) \approx \frac{300}{\sqrt{n_e(\text{cm}^{-3})}} \quad . \tag{3-90}$$

The Debye length in the lower trapped radiation belts is about 2 to 10 centimeters.

The number of particles within a sphere of radius λ_D, the Debye sphere, is a measure of the importance of collective behavior. When few particles occur within a Debye sphere, each particle interacts only with its nearest neighbors. But when each particle interacts simultaneously with thousands of other particles, any perturbation in the particle distribution will result in transient electric and magnetic fields that are felt by many particles. These fields tend to restore the original particle distribution. Oscillations can occur as in any mechanical system where restoring forces restrain the excursions from equilibrium. The trapped particle belts are subject to a wide variety of oscillation phenomena. Oscillations and waves in the magnetosphere are discussed briefly in Section 4. A systematic treatment of oscillations in ionized gases demands more space than is available here. For further reading, see especially References 63 and 64.

3.6.2 Boltzmann's Equation

It is advantageous to treat the behavior of a plasma statistically through the evolution of a distribution function f. Liouville's equation must be modified to take account of interparticle collisions and nonconservation of f. The generalization of Liouville's equation is Boltzmann's equation (References 20, 65, 66, and 75):

$$\frac{\partial f}{\partial t} + \frac{1}{\gamma m}\,\vec{p}\cdot\nabla f + \vec{F}\cdot\nabla_p f = \left(\frac{\delta f}{\delta t}\right)_{[\text{collisions}]} \quad . \tag{3-91}$$

The notation ∇_p has been used to denote the gradient $(\partial/\partial p_1, \partial/\partial p_2, \partial/\partial p_3)$ in momentum space. Considering the strictly relativistic Boltzmann equation usually is not necessary. Most of the particles in the radiation belts have velocities not significantly greater than the thermal speed. Throughout the remainder of this section, the momentum is replaced by $m\vec{v}$.

Boltzmann's equation in the absence of collisions is entirely equivalent to the orbit equations of Sections 3.2 and 3.3 (References 20, 40, and 41).

MOMENTS OF BOLTZMANN'S EQUATION. Boltzmann's equation can be approximately solved if fluid-like equations are constructed by means of an averaging procedure (References 1, 20, and 40). Two important quantities are the number density:

$$n_k = \iiint f_k(\bar{x}, \bar{v}, t)\, d^3v \tag{3-92}$$

and the streaming velocity:

$$\bar{u}_k = \frac{1}{n_k} \iiint f_k(\bar{x}, \bar{v}, t)\, \bar{v}\, d^3v \qquad \langle \bar{v} \rangle \tag{3-93}$$

of particles of species k. These may be regarded as moments of the distribution function weighted by powers of v. Another useful moment is the stress tensor or pressure tensor:

$$\bar{\bar{P}}_k = m_k \iiint f_k(\bar{x}, \bar{v}, t)\, \bar{v}\bar{v}\, d^3\bar{v} - n_k m_k \bar{u}_k \bar{u}_k \quad . \tag{3-94}$$

Dyadic notation has been employed for the tensor $\bar{\bar{P}}$ (Reference 67). Another way of writing $\bar{\bar{P}}$ is in terms of the components:

$$P_{ij} = nm \langle v_i v_j \rangle - nm \langle v_i \rangle \langle v_j \rangle \quad . \tag{3-95}$$

The first moment of Boltzmann's equation (averaged over $\iiint d^3v$) is the equation of continuity:

$$\frac{\partial n_k}{\partial t} + \nabla \cdot n_k \bar{u}_k = 0 \quad , \tag{3-96}$$

which guarantees that particles are conserved.

The second moment of Boltzmann's equation (averaged over $\iiint \bar{v} d^3v$) is the momentum conservation equation:

$$n_k m_k \left(\frac{\partial \bar{u}_k}{\partial t} + \bar{u}_k \cdot \nabla \bar{u}_k \right) - n_k q_k \left(\bar{E} + \frac{1}{c}\, \bar{u}_k \times \bar{B} \right) + \nabla \cdot \bar{\bar{P}}_k = \bar{F}_c \quad . \tag{3-97}$$

The effects of collisions between different types of particles are combined in the term $\bar{F}_c$.

The third moment is of less immediate interest. It describes the transfer of energy and is somewhat analogous to a heat-transfer equation (Reference 20).

3.6.3 Hydromagnetic Equations

The similarity of Equations 3-96 and 3-97 to the equations of hydrodynamics is obvious. A plasma often can be considered as a continuous fluid in which the total mass velocity (or average streaming velocity) is

$$\bar{V} = \frac{\sum_k n_k m_k \bar{u}_k}{\sum_k n_k m_k} = \frac{1}{\rho} \sum_k n_k m_k \bar{u}_k \qquad (3\text{-}98)$$

The density ρ is the sum of all $n_k m_k$'s. The electrical current density (in emu) is

$$\bar{J} = \frac{1}{c} \sum_k n_k q_k \bar{u}_k = \frac{e}{c} \left[\sum_{\text{ions}} (n_i Z_i) \bar{u}_i - \sum_{\text{electrons}} n_e \bar{u}_e \right] . \qquad (3\text{-}99)$$

$+Z_i e$ is the total charge on an ion. When the Boltzmann equations for electrons and ions are combined, the result is the hydromagnetic equations (References 1, 20, 38, 40, 41, and 42) or magnetohydrodynamic equations. The mechanical force equation is

$$\rho \frac{\partial \bar{v}}{\partial t} = \bar{J} \times \bar{B} - \nabla \cdot \ddot{P} , \qquad (3\text{-}100)$$

and Ohm's law is

$$\frac{m_e c}{n_e c^2} \frac{\partial \bar{J}}{\partial t} = \bar{E} + \frac{1}{c} \bar{V} \times \bar{B} - \frac{1}{n_e e} \nabla \cdot \ddot{P}_e - \frac{1}{n_e e} \bar{J} \times \bar{B} - \frac{\bar{J}}{\sigma} . \qquad (3\text{-}101)$$

Spatial derivatives and terms of order m_e/m_i have been ignored.

Equation 3-100 is still recognizable as the basic equation of motion of a fluid. Equation 3-101 has been called Ohm's law because of its similarity to the conventional Ohm's law for a conductor. The last term on the right in Equation 3-101 contains all the effects of collisions between positive and negative particles. The proportionality of this term to $\bar{J}$ does not follow directly from Boltzmann's equation, but

rather from the assumption that the momentum exchange between unlike particles should be proportional to their relative velocities (Reference 1). The constant of proportionality $1/\sigma$ is called the electrical resistivity because, in a uniform, steady state plasma with no magnetic fields, Equation 2-121 reduces to the familiar form of Ohm's law. The inverse of electrical resistivity is the electrical conductivity. The conductivity is approximately

$$\sigma \approx \frac{n_e e^2}{m_e c^2 \nu_c} \tag{3-102}$$

where ν_c represents the frequency of collisions between electrons and ions (References 1, 68, and 69).

FIELD EQUATIONS. A continuity equation for electrical charge follows immediately from Boltzmann's equation. It is (Reference 1) the charge conservation equation:

$$\frac{\partial Q}{\partial t} + c \nabla \cdot \bar{J} = 0 \quad . \tag{3-103}$$

The localized excess charge density is

$$Q = \sum_k n_k q_k \quad . \tag{3-104}$$

The diamagnetism of a plasma, mentioned in Section 3.3.3, is a general result which makes possible including the gyro-motion part of the current in the total magnetic field. Maxwell's equations, which describe the electric and magnetic fields of a plasma, are ther (References 1 and 70)

$$\nabla \cdot \bar{E} = 4\pi Q \tag{3-105}$$

$$\nabla \cdot \bar{B} = 0 \tag{3-106}$$

$$\nabla \times \bar{E} = -\frac{1}{c} \frac{\partial \bar{B}}{\partial t} \tag{3-107}$$

$$\nabla \times \bar{B} = \frac{1}{c} \frac{\partial \bar{E}}{\partial t} + 4\pi \bar{J} \quad . \tag{3-108}$$

The units of these equations are discussed in Appendix 3A. $\bar{J}$ is only that part of the current due to the relative motion of different components of the plasma. The appropriate measure of the magnetic field is $\bar{B}$, which here is called the magnetic field intensity. ($\bar{B}$ conventionally is referred to as the flux density or magnetic induction. The designation magnetic intensity or field strength conventionally is reserved for $H = B/(\text{permitivity})$.) The magnetic moments of individual particles are included in B, which is the field that would be measured at any point.

SOLUTIONS OF THE HYDROMAGNETIC EQUATIONS. A complete description of a plasma requires one more equation—an equation of state relating n_e and P. Employing a simplified equation of state usually is sufficient and desirable; in the trapped radiation belt, n_e can be assumed nearly independent of P.

The dynamics of a plasma, including flow and wave motions, can be treated by methods similar to those developed for the solution of problems in classical hydrodynamics (References 38 and 71). A special complication of hydromagnetics is that the pressure is a tensor (References 40, 41, and 42). This means that motion along the magnetic field direction is not simply related to the transverse motion, nor does the motion along the field correspond very well with the motion of a massive fluid. Only for waves and flow transverse to the magnetic field is the hydrodynamic analogy entirely valid.

TRANSVERSE DRIFT CURRENTS. A rather confusing aspect of Equation 3-101 is that it does not predict a steady current due to a gradient in the magnetic field strength (as in Equation 3-37). This drift current actually is contained implicitly in the pressure gradient term. If $\nabla P = 0$, the density of guiding centers of particles drifting in some arbitrary direction is balanced exactly by the density of guiding centers of particles drifting in the opposite direction. However, if the plasma is of finite extent or has a region in which ∇P is finite, it is possible for a current to flow (Reference 1).

3.6.4 Electrical Conductivity Tensor

When pressure gradients can be ignored, the Ohm's law equation (Equation 3-101) resembles the conventional Ohm's law in that J and E appear only linearly, although they may be in different directions. If the fields and current have parts that vary sinusoidally proportional to real part $(e^{i\omega t})$, the time derivatives can be replaced by

$$\frac{\partial}{\partial t}\left(e^{i\omega t}\right) \rightarrow i\omega\left(e^{i\omega t}\right) \quad .$$

Equation 3-101 reduces to (Reference 2)

$$\frac{m n_e c}{n_e e^2} i\omega \bar{J} = \bar{E} + \frac{1}{n_e e} \bar{J} \times \bar{B} - \frac{\bar{J}}{\sigma} \quad . \tag{3-109}$$

The current and electric field may be decomposed into vectors parallel and perpendicular to $\bar{B} = \bar{B}_o + \bar{B}\,(e^{i\omega t})$:

$$\bar{E} = \bar{E}_{\parallel} + \bar{E}_{\perp} \tag{3-110}$$

$$\bar{J} = c\sigma_o \bar{E}_{\parallel} + c\sigma_1 \bar{E}_{\perp} + c\sigma_2 \frac{\bar{B}}{B_o} \times \bar{E}_{\perp} \quad . \tag{3-111}$$

The tensor equations:

$$\bar{J} = c\bar{\bar{\sigma}} \cdot \bar{E} \tag{3-112}$$

$$\bar{\bar{\sigma}} = \begin{bmatrix} \sigma_1 & -\sigma_2 & 0 \\ \sigma_2 & \sigma_1 & 0 \\ 0 & 0 & \sigma_o \end{bmatrix} \tag{3-113}$$

are identical with the preceding equations and usually are preferred. Note that no universal agreement exists on the choice of signs in the off-diagonal (σ_2) components of $\bar{\bar{\sigma}}$. The notation here is perhaps the more frequently used.

CONDUCTIVITY TENSOR IN AN IONIZED GAS. Equations 3-109, 3-110, and 3-111 can be solved readily for the specific electrical conductivity σ_o, the Pederson conductivity σ_1, and the Hall conductivity σ_2. The total current is the sum of contributions from all types of particles. The total conductivity is the sum of ion and electron contributions:

$$\bar{\bar{\sigma}} = \bar{\bar{\sigma}}_i + \bar{\bar{\sigma}}_e \quad . \tag{3-114}$$

The components of the conductivity tensor (in emu) (References 72, 73, and 74) are

$$\sigma_o = -i \frac{n_e e^2}{c^2} \left[\frac{1}{m_i(\omega - i\nu_i)} + \frac{1}{m_e(\omega - i\nu_e)} \right] \tag{3-115}$$

$$\sigma_1 = -i \frac{n_e e^2}{c^2} \left\{ \frac{(\omega - i\nu_i)}{m_i[(\omega - i\nu_i)\omega_i^2]} + \frac{(\omega - i\nu_e)}{m_e[(\omega - i\nu_e)^2 - \omega_e^2]} \right\} \tag{3-116}$$

$$\sigma_2 = \frac{n_e e^2}{c^2} \left\{ \frac{\omega_i}{m_i[(\omega - i\nu_i)^2 - \omega_i^2]} - \frac{\omega_e}{m_e[(\omega - i\nu_e)^2 - \omega_e^2]} \right\} . \tag{3-117}$$

The frequencies ν_i and ν_e are, respectively, the rate of collisions of ions with neutral particles and the rate of collisions of electrons with all heavy particles.

The conductivities in the zero-frequency limit are

$$\sigma_o \sim \frac{n_e e^2}{c^2} \left(\frac{1}{m_i \nu_i} + \frac{1}{m_e \nu_e} \right) \sim \sigma \tag{3-118}$$

$$\sigma_1 \sim \frac{n_e e^2}{c^2} \left[\frac{\nu_i}{m_i(\nu_i^2 + \omega_i^2)} + \frac{\nu_e}{m_e(\nu_e^2 + \omega_e^2)} \right] \tag{3-119}$$

$$\sigma_2 \sim \frac{n_e e^2}{c^2} \left[\frac{\omega_i}{m_i(\nu_i^2 + \omega_i^2)} + \frac{\omega_e}{m_e(\nu_e^2 + \omega_e^2)} \right] \tag{3-120}$$

As the collision frequency become negligible, σ_o becomes very large whereas σ_1 and σ_2 approach zero. The contribution of each component,

$$\left(\frac{\pm n_e e^2}{m_e c^2 \omega_c} \right) ,$$

to the Hall conductivity is exactly the same as would be given by the $\bar{E} \times \bar{B}$ drift. The total Hall current is zero. The current transverse to the magnetic field must be equivalent to the $\bar{E} \times \bar{B}$ drift current. However, in a steady state ($\omega \sim 0$), electrons and ions drift together so that no transverse current is expected.

The actual direction of Hall current flow depends on the relative importance of two terms. With the sign selected here, σ_2 is generally positive in the ionosphere between 70 and several hundred kilometers altitude (References 27, 73, and 74). The Hall conductivity in the ionosphere is quite large; it is responsible for the polar electrojets — strong currents which flow across the geomagnetic field lines (Reference 73).

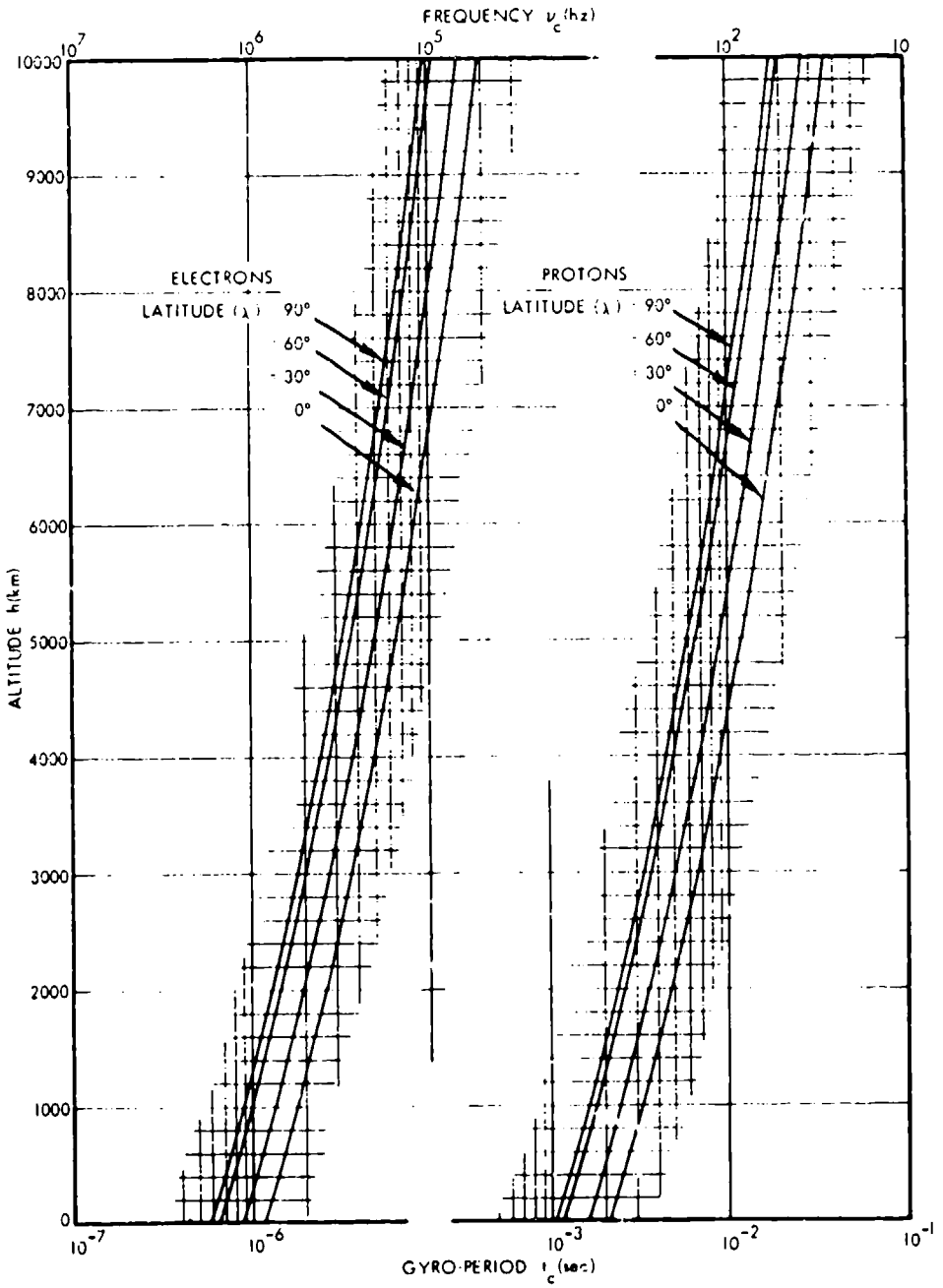

Figure 3B-9. The gyro-period of a charged particle in the geomagnetic field.

Figures 3B-10 and 3B-11 give the bounce and drift periods of trapped electrons and protons, respectively. The abscissas are the kinetic energies. Separate curves are plotted for selected values of $L \approx R_o/R_E$. These figures were constructed for particles with 90-degree equatorial pitch angles; the detailed pitch-angle variation can be found in Figures 3B-12 and 3B-13. (The guiding center approximation and trapping conditions break down at very high energies where the bounce and drift periods become comparable.)

Figure 3B-12 shows the bounce period and the second adiabatic invariant as functions of equatorial pitch angle. The bounce period t_b and the second adiabatic invariant J contain, respectively, the integrals

$$\mathcal{S} = \frac{4}{R_o}\int_0^{S_m} dS/\mu$$

and

$$\mathcal{J} \equiv \frac{4}{R_o}\int_0^{S_m} \mu\, dS \quad ,$$

integrated along the field line from the equator to the mirror point. The factor of 4 accounts for a complete bounce period (Equations 3-47 and 3-75). These integrals are shown in this figure (also in Table 3B-1). The length, S, of a field line would yield a curve $4S/R_o$ falling between and passing through zero-ordinate at a 90-degree pitch angle.

The complete J integral is

$$J = R_o \mathcal{J} p = LR_E \mathcal{J} p$$

and the bounce period is

$$t_b = R_o \mathcal{S}/v = LR_E \mathcal{S}/v \quad .$$

The momentum p and velocity v can be found from Figures 3B-6 and 3B-7. Any of several units may be employed for J. The most common are cgs units or mixed units—(MeV/c) cm, or (MeV/c) (earth radii). A third alternative, MeV sec, is less useful. The appropriate numerical conversion is J(MeV second) = 0.02125 Lp(MeV/c).

For example: A 1-MeV electron has a velocity 2.8×10^{10} centimeters per second (Figure 3B-6). If the equatorial pitch angle is 30 degrees and L = 2, the ordinate $\mathcal{S}$ is 4.0 and the bounce period is $t_b = 6.37 \times 10^8 \times 2.0 \times 4.0/2.8 \times 10^{10} = 0.18$ second. The momentum is

Figures 3B-10 and 3B-11 give the bounce and drift periods of trapped electrons and protons, respectively. The abscissas are the kinetic energies. Separate curves are plotted for selected values of $L \approx R_o/R_E$. These figures were constructed for particles with 90-degree equatorial pitch angles; the detailed pitch-angle variation can be found in Figures 3B-12 and 3B-13. (The guiding center approximation and trapping conditions break down at very high energies where the bounce and drift periods become comparable.)

Figure 3B-12 shows the bounce period and the second adiabatic invariant as functions of equatorial pitch angle. The bounce period t_b and the second adiabatic invariant J contain, respectively, the integrals

$$\mathcal{S} = \frac{4}{R_o}\int_0^{S_m} dS/\mu$$

and

$$\mathcal{J} \equiv \frac{4}{R_o}\int_0^{S_m} \mu\, dS \quad ,$$

integrated along the field line from the equator to the mirror point. The factor of 4 accounts for a complete bounce period (Equations 3-47 and 3-75). These integrals are shown in this figure (also in Table 3B-1). The length, S, of a field line would yield a curve $4S/R_o$ falling between and passing through zero-ordinate at a 90-degree pitch angle.

The complete J integral is

$$J = R_o \mathcal{J} p = L R_E \mathcal{J} p$$

and the bounce period is

$$t_b = R_o \mathcal{S}/v = L R_E \mathcal{S}/v \quad .$$

The momentum p and velocity v can be found from Figures 3B-6 and 3B-7. Any of several units may be employed for J. The most common are cgs units or mixed units—(MeV/c) cm, or (MeV/c) (earth radii). A third alternative, MeV sec, is less useful. The appropriate numerical conversion is J(MeV second) = 0.02125 Lp(MeV/c).

For example: A 1-MeV electron has a velocity 2.8×10^{10} centimeters per second (Figure 3B-6). If the equatorial pitch angle is 30 degrees and $L = 2$, the ordinate $\mathcal{S}$ is 4.0 and the bounce period is $t_b = 6.37 \times 10^8 \times 2.0 \times 4.0/2.8 \times 10^{10} = 0.18$ second. The momentum is

1.4 MeV/c. The second adiabatic invariant is therefore $J = 2 \times 1.8 \times 1.4 = 5.0$ (MeV/c) R_E. The degenerate adiabatic invariant is $\mathcal{J} = J/p = 3.6\ R_E$.

The velocity of a 1-MeV proton is only 1.4×10^9 centimeters per second (Figure 3B-7). If the pitch angle and L are the same as for the electron in the first example, the proton's bounce period is $t_b = 6.37 \times 10^8 \times 2 \times 4.0/1.4 \times 10^9 = 3.6$ seconds. The corresponding gyro-periods of electrons and protons at L = 2 on the equator are 9×10^{-6} seconds and 1.7×10^{-2} seconds, respectively (Figure 3B-9).

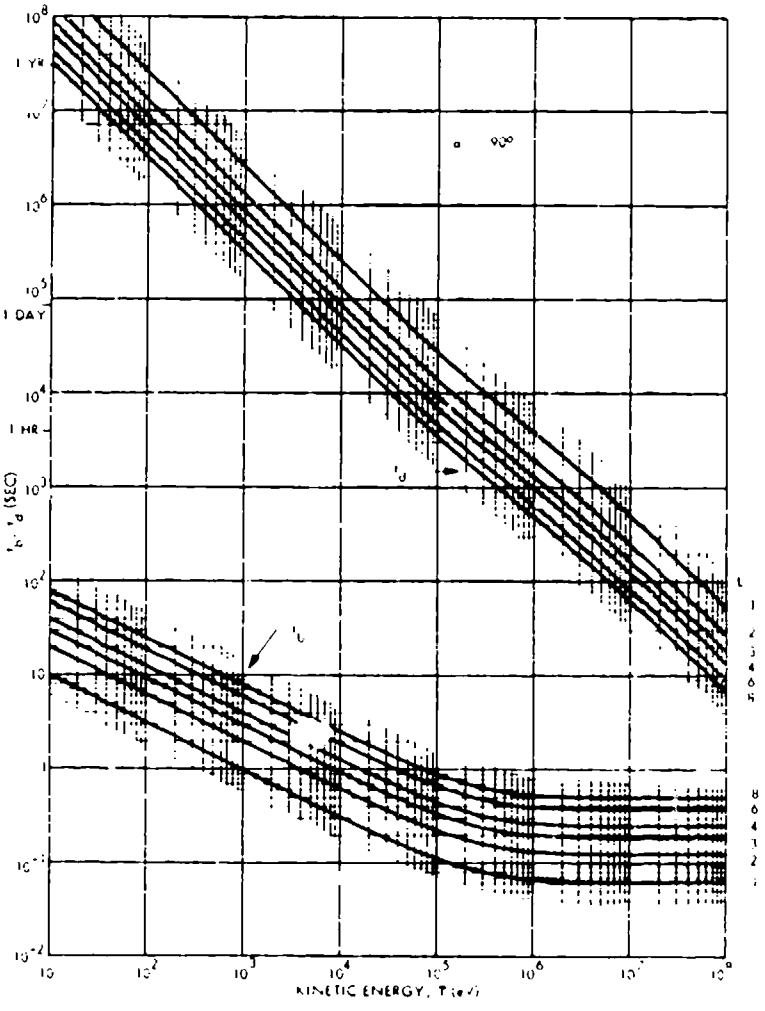

Figure 3B-10. The bounce and drift periods of trapped electrons as a function of kinetic energy.

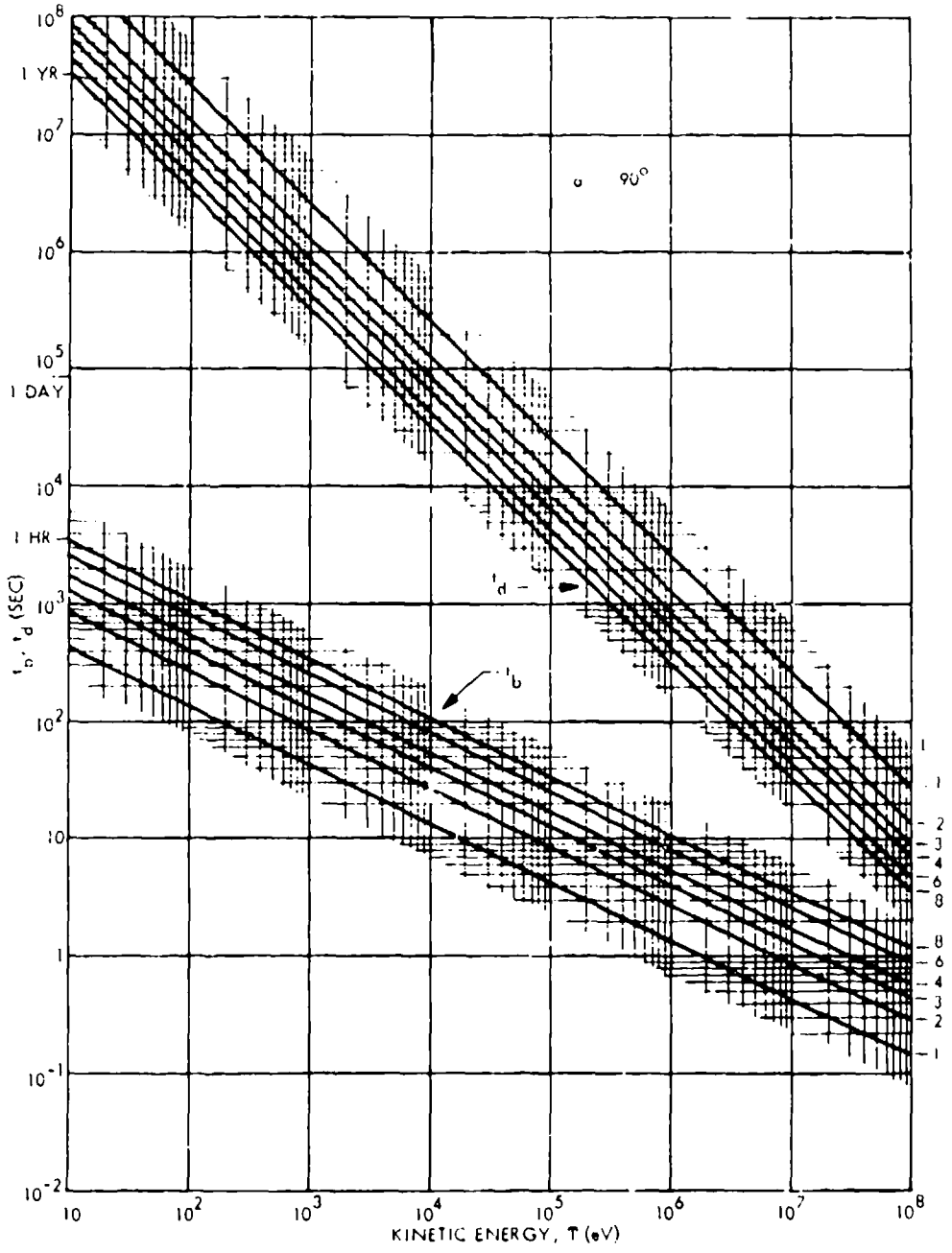

Figure 3B-11. The bounce and drift periods of trapped protons as a function of kinetic energy.

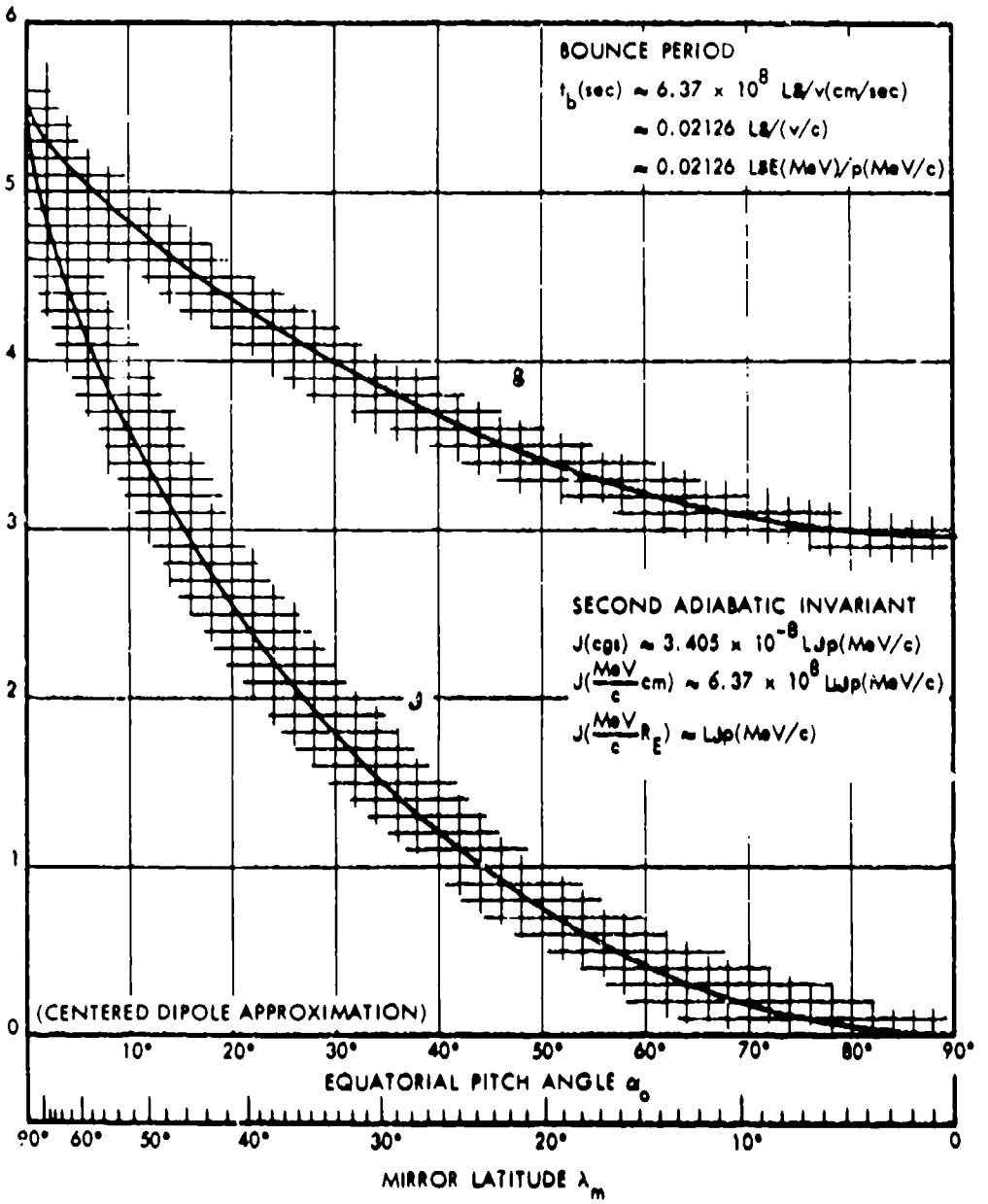

Figure 3B-12. The bounce period and second adiabatic invariant as functions of equatorial pitch angle.

Figure 3B-13 presents the azimuthal drift period as a function of the equatorial pitch angle in the earth's field. This figure, together with Figure 3B-14, which provides the energy-dependent factor, can be used to determine the azimuthal drift periods of particles trapped in the earth's magnetic field (Equation 3-50). The average angular drift velocity is simply

$$\omega_d = \frac{2\pi}{t_d} = \frac{2\pi L E(v^2/c^2)}{\mathcal{E}}$$

The drift velocity at the equator is the angular drift velocity multiplied by the equatorial radius $R_o = LR_E$ or

$$V = \frac{2\pi L^2 R_E E(v^2/c^2)}{\mathcal{E}} .$$

For example: The energy-dependent factor for a 1-MeV electron is $E(v^2/c^2) = p^2/\gamma m = 1.3$ MeV (Figure 3B-14). If the electron has an equatorial pitch angle of 30 degrees, the ordinate of this graph is 6,250, which, at L = 2, results in a drift period $t_d = 6,250/2 \times 1.3 = 2,400$ seconds = 0.67 hour. The average angular drift rate is $2\pi/2,400 = 0.0026$ radian per second = 0.15 degree per second or 0.83 degree per bounce (Figure 3B-10). The average drift velocity is $V = 4.0 \times 10^4 \times (2)^2 \times 1.3/6,250 = 33$ kilometers per second.

For a 1-MeV proton, the ordinate of Figure 3B-14 is so small that the approximation $E(v^2/c^2) \approx 2$ may be used. If the pitch angle and L-value are the same as for the electron in the first example, the drift period is $t_d = 6,250/2 \times 2 = 1,560$ seconds = 0.43 hour.

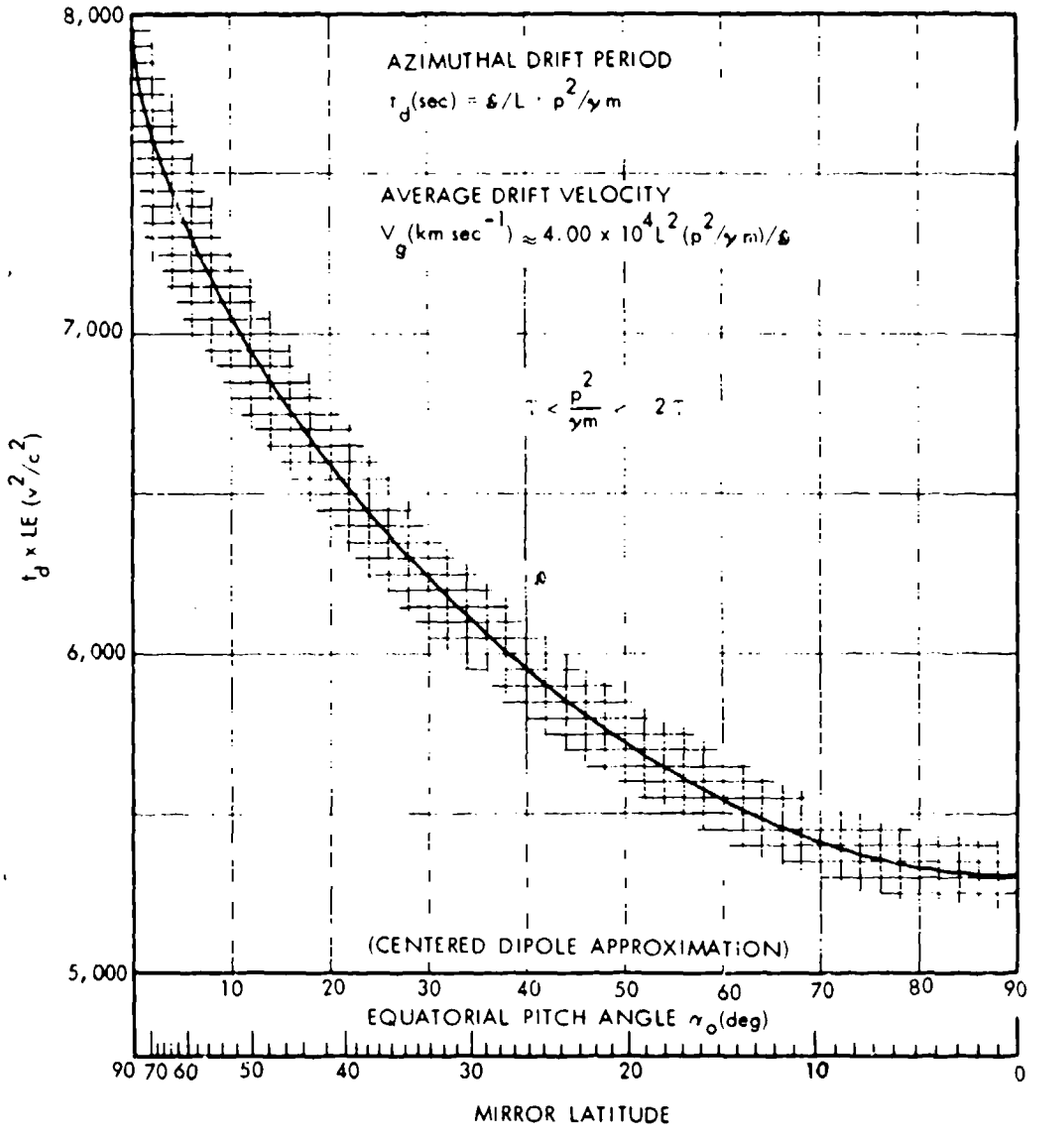

Figure 3B-13. Azimuthal drift period as a function of the equatorial pitch angle in the earth's field.

Figure 3B-14 contains the energy-dependent factor employed in azimuthal drift computations. The square of particle momentum divided by γ (or total energy multiplied by velocity squared) occurs frequently, particularly in computations relating to particle drift motions. For nonrelativistic particles, this factor is nearly equal to 2. Accurate values at higher energies can be found from the formula:

$$p^2/\gamma m = \frac{T(T + 2mc^2)}{T + mc^2}$$

or from Figure 3B-14. The ordinate and abscissa are in the same units.

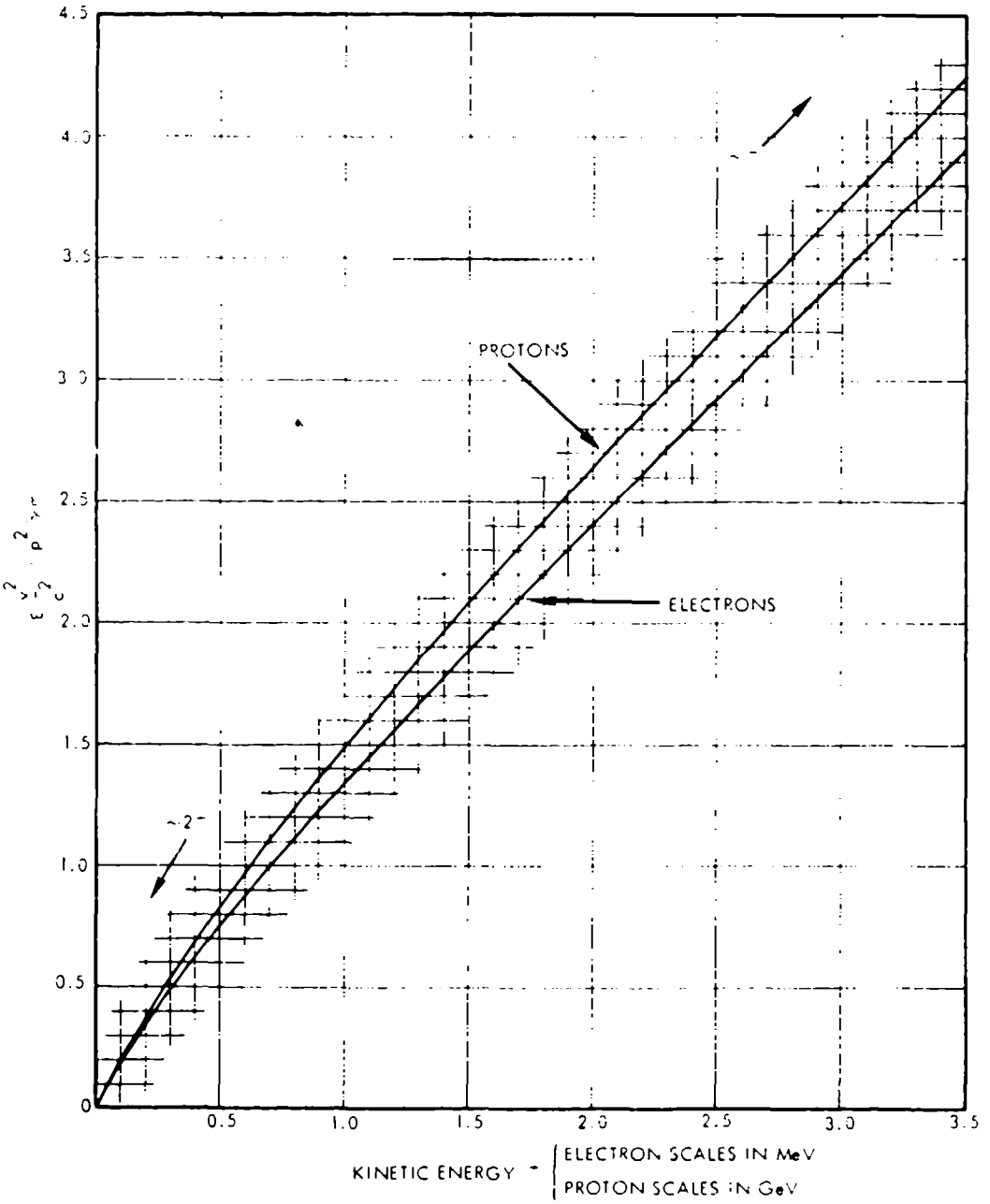

Figure 3B-14. Energy-dependent factor employed in azimuthal drift computations.

Figure 3B-15 shows constant-$\mathcal{J}$ curves in a dipole field. The upper half of this figure shows some selected contours of constant degenerate adiabatic invariant, $\mathcal{J} = J/p$ (in units of earth radii, R_E) in a dipole field. These curves contain the mirror points of all particles having a particular value of $\mathcal{J}$. The constant-$\mathcal{J}$ surfaces, constructed by rotating these curves about the polar axis are open and funnel shaped. The curves are labeled with the value of $\mathcal{J}$ in R_E. Several dipole field lines also are shown.

The constant-$\mathcal{J}$ curves are not the mirror point traces of particles that preserve adiabatic invariants while drifting across L-shells. The constant adiabatic invariant curves, labeled with the values of $J^2/Mm \propto \mathcal{J}^2 B_m$ in gauss square centimeters or gauss R_E^2, are shown in the lower part of the figure.

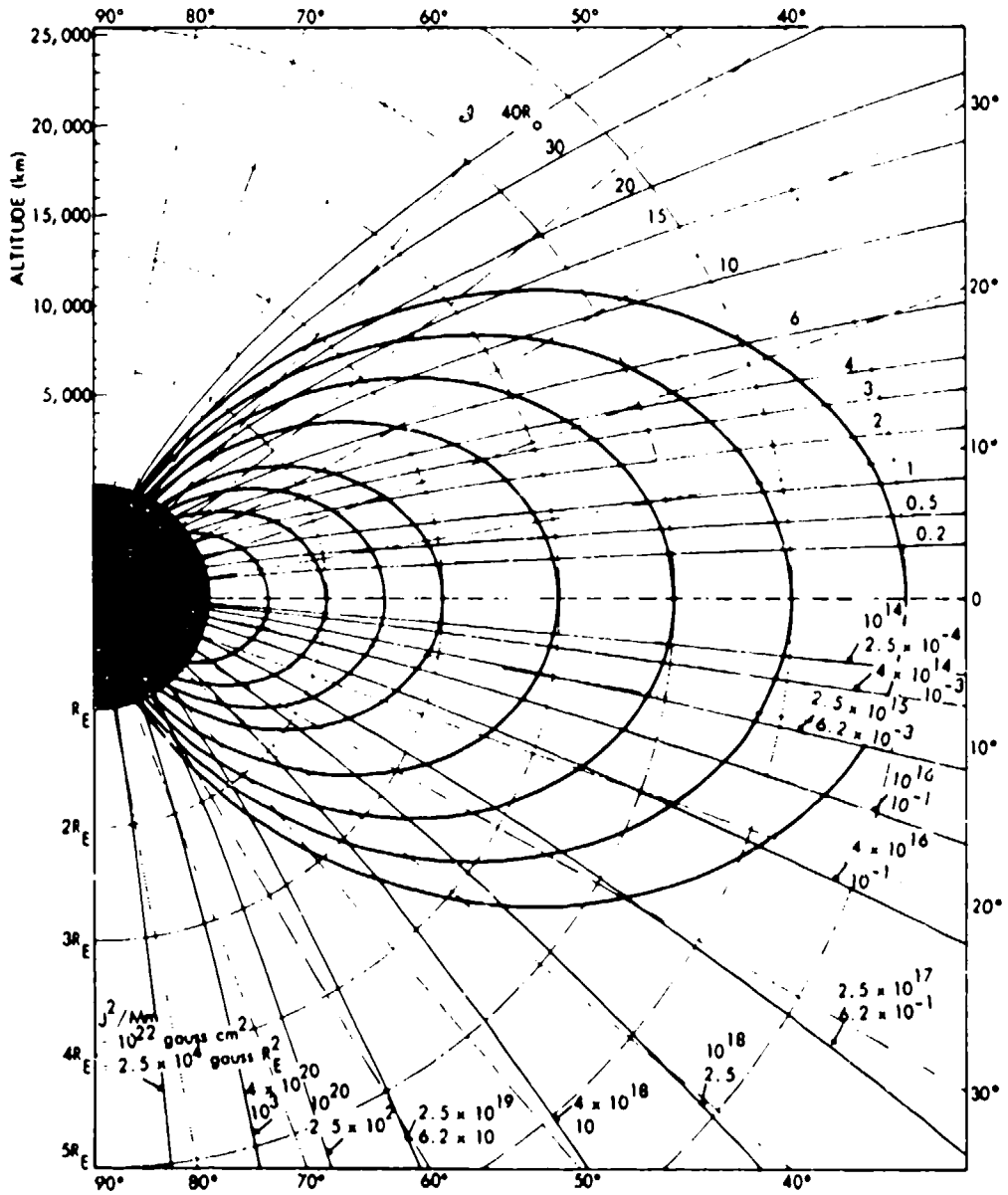

Figure 3B-15. Constant adiabatic invariant curves in a dipole field.

Figure 3B-16 contains constant adiabatic invariant curves in B, L coordinates. Constant J^2/Mm contours, such as in the lower part of Figure 3B-15, are shown in Figure 3B-16 in B, L coordinates. The mirror point of a particle drifting across L-shells while preserving the first two adiabatic invariants will follow a trajectory such as these.

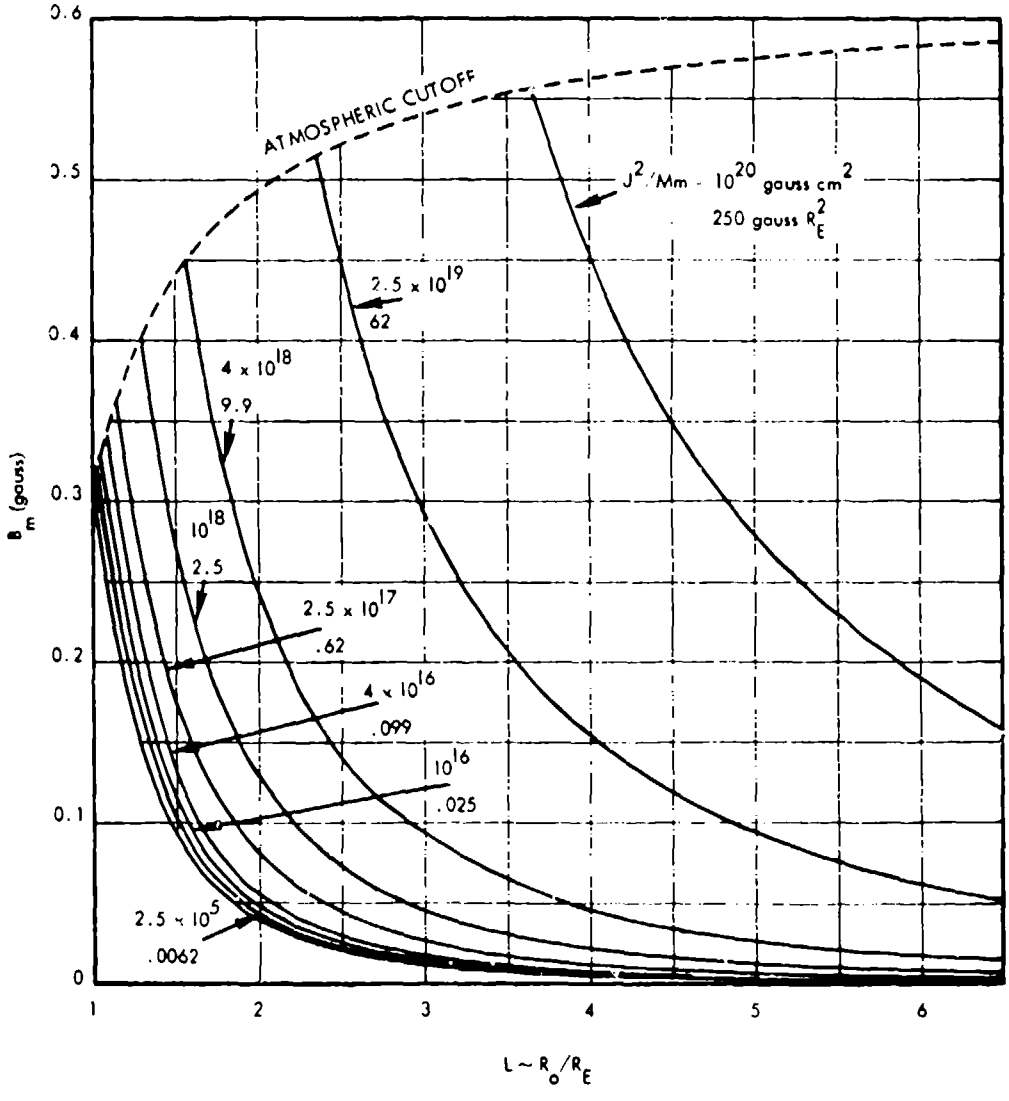

Figure 30-16. Constant adiabatic invariant curves in B, L coordinates.

Figure 3B-17 presents adiabatic invariants of particles entering the atmosphere. The quantity J^2/Mm is shown as a function of L for particles entering the atmosphere mirroring at 100-kilometers altitude. J, M, and m may be in cgs units, or J may be in MeV/c cm, M in MeV/gauss, and M in MeV.

For example: A 1-MeV electron mirrors at 100-kilometers altitude on L = 2. From this figure, the ratio of its adiabatic invariants is $J^2/Mm = 30$ gauss R_E^2. If the electron started at L = 6 and drifted across L-shells while preserving its adiabatic invariants, the ratio of initial and final mirror fields, Bm, can be found from Figure 3B-19. The ratio is $B_m(LJ^2/Mm = 180), B_m(LJ^2/Mm = 60) = 1.3 \times 10^{-6}/1.8 \times 10^{-5} = 0.07$. The constancy of the magnetic moment ensures that the ratio of initial and final momentum squared is the same as the ratio of the B_m's. When observed on L = 2, $p^2/2m$ was 2 MeV (Figure 3B-8). Initially, $p^2/2m$ must have been $2 \times 0.07 = 0.14$ MeV. The initial energy was approximately the same (0.14 MeV).

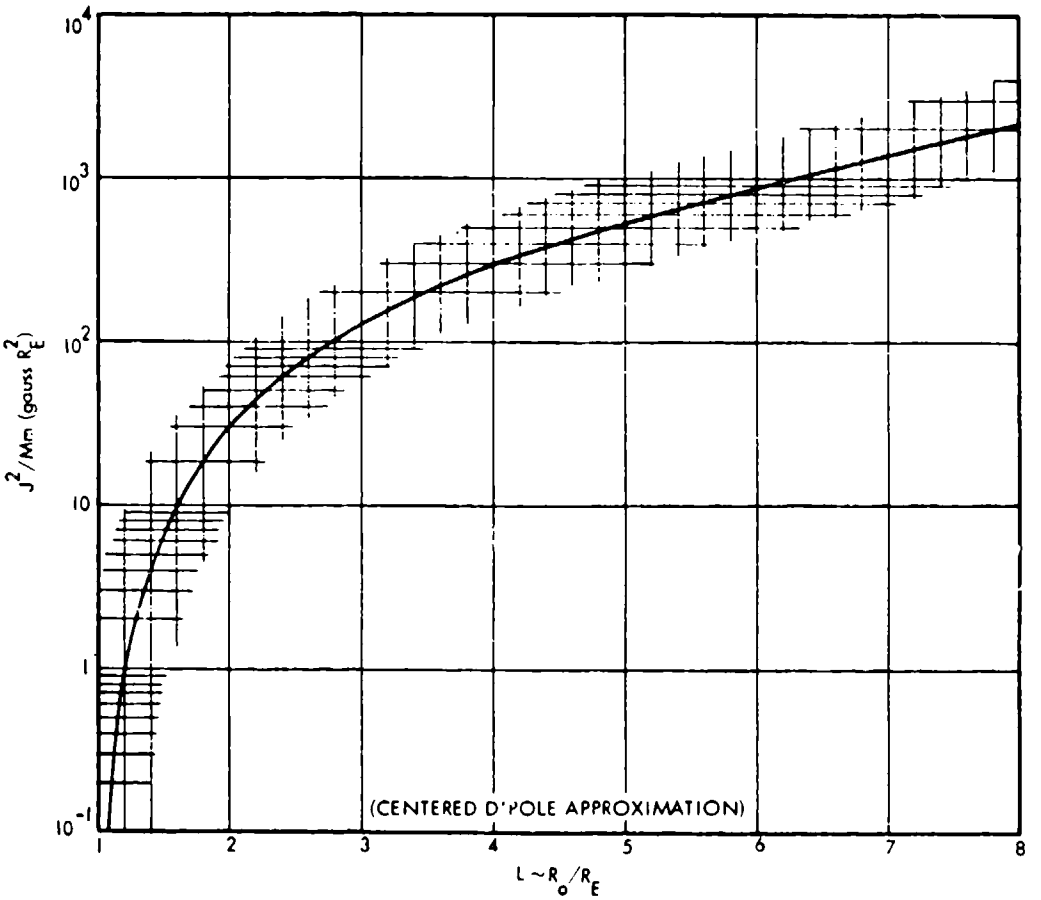

Figure 38-17. Adiabatic invariants of particles entering the atmosphere.

Figure 3B-18 contains an equatorial pitch angle as a function of L for constant adiabatic invariants. The equatorial pitch angle α_o varies so slowly with L that this figure has been folded over many times. The value of L can be found by multiplying the coordinate on the lower scale by the factor above the appropriate segment of the curve and dividing by J^2/Mm. The dimensions of J, M, and m are the same as in the preceding figures. If J^2/Mm is an integral power of 10, for example 10^n, L and α_o may be read directly from the curve labeled $\times 10^n$.

Small changes in α_o can be computed accurately by using the average slopes given on the right side together with the formula:

$$\alpha_o = [\text{constant}] + [\text{slope}] \times \log_{10} L \quad .$$

For example: A trapped particle is initially at L = 6 with an equatorial pitch angle of 50 degrees. The abscissa of this figure is at $LJ^2/Mm = 6 \times 10^{-1}$ gauss R_E^2. Therefore, J^2/Mm is 10^{-1} gauss R_E^2. The L-values may be read directly from the scale at the bottom. If the particle drifts to L = 2 while preserving its adiabatic invariants, the new equatorial pitch angle is 57.8 degrees. When the preceding simplified formula is used, the new pitch angle is computed to be

$$\alpha_o = 50 \text{ degrees} + (-16.1) \log_{10} \frac{L=2}{L=6} = 57.7 \text{ degrees} \quad .$$

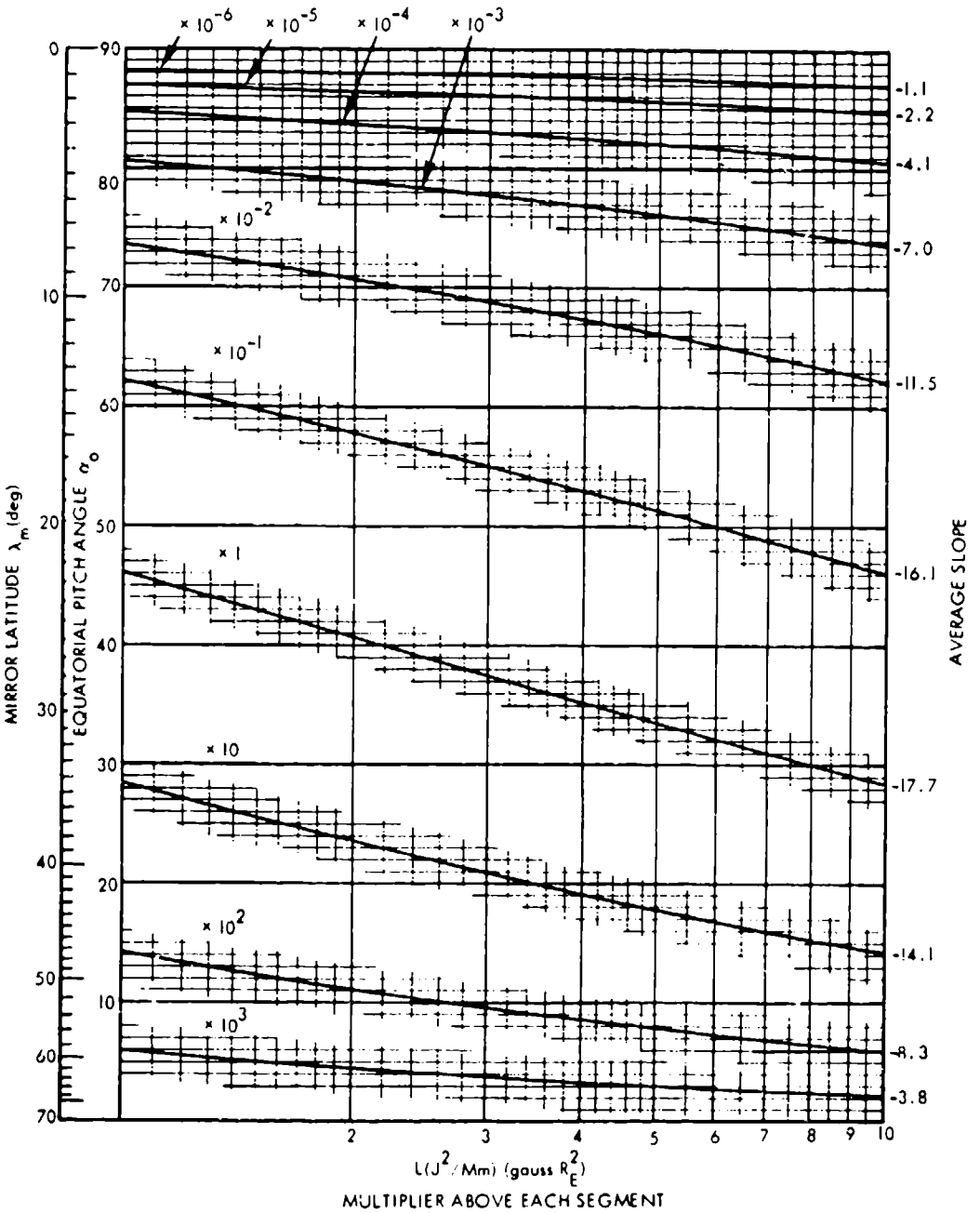

Figure 3B-18. Equatorial pitch angle as a function of L for constant adiabatic invariants.

Figures 3B-19a and 3B-19b show a mirror point field as a function of L for constant adiabatic invariants. These figures contain essentially the same information as the last several figures, except that P_m has been multiplied by $(Mm_o)^3/J^6$ to obtain a unique function of L (J^2/Mm). The parameter J^2/Mm common to the ordinate and abscissa may be computed or, alternatively, determined from the preceding figure. If J^2/Mm is an integral power of 10, for example 10^n, L may be read directly from the curve labeled $x10^n$.

Constancy of the magnetic moment requires that $p^2/2m$ varies directly with B_m. The kinetic energy can be found, therefore, from Figure 3B-8.

Small changes in B_m can be computed with the aid of the average slopes at the right side and the formula:

$$\log_{10} B_m \cong [\text{constant}] + [\text{slope}] \times \log_{10} L \quad .$$

The figure has not been continued beyond $L = 10^3$ because, for smaller L values ($\alpha_o > 80$ degrees), B_m is given quite accurately by the simple formula:

$$B_m \propto L^{-3} \quad .$$

For example: The equatorial pitch angle and L of a trapped particle are 50 degrees and 6, respectively. From the preceding figure, J^2/Mm is 10^{-1} gauss R_E^2. The mirror field may be read directly from the curve labeled 10^{-1} (after multiplication of the ordinate by 10^{-3}). If the particle drifts to L = 4 while preserving adiabatic invariants, the mirror field changes from $B_m = 0.0024$ gauss to $B_m = 0.0076$ gauss. If the particle is an electron with initial energy of 1 MeV, $p^2/2m$ is about 2 MeV (Figure 3B-8). The momentum squared is proportional to the mirror field if the magnetic moment is preserved. Finally, $p^2/2m$ is $2.0 \times (0.0076/0.0024) = 6.3$ MeV. The final kinetic energy is about 2.2 MeV. The energy of a trapped proton is more nearly proportional to B_m. If the drifting particle were a proton, its energy change would be from 1.0 MeV to $1.0 \times (0.076/0.024) = 3.2$ MeV.

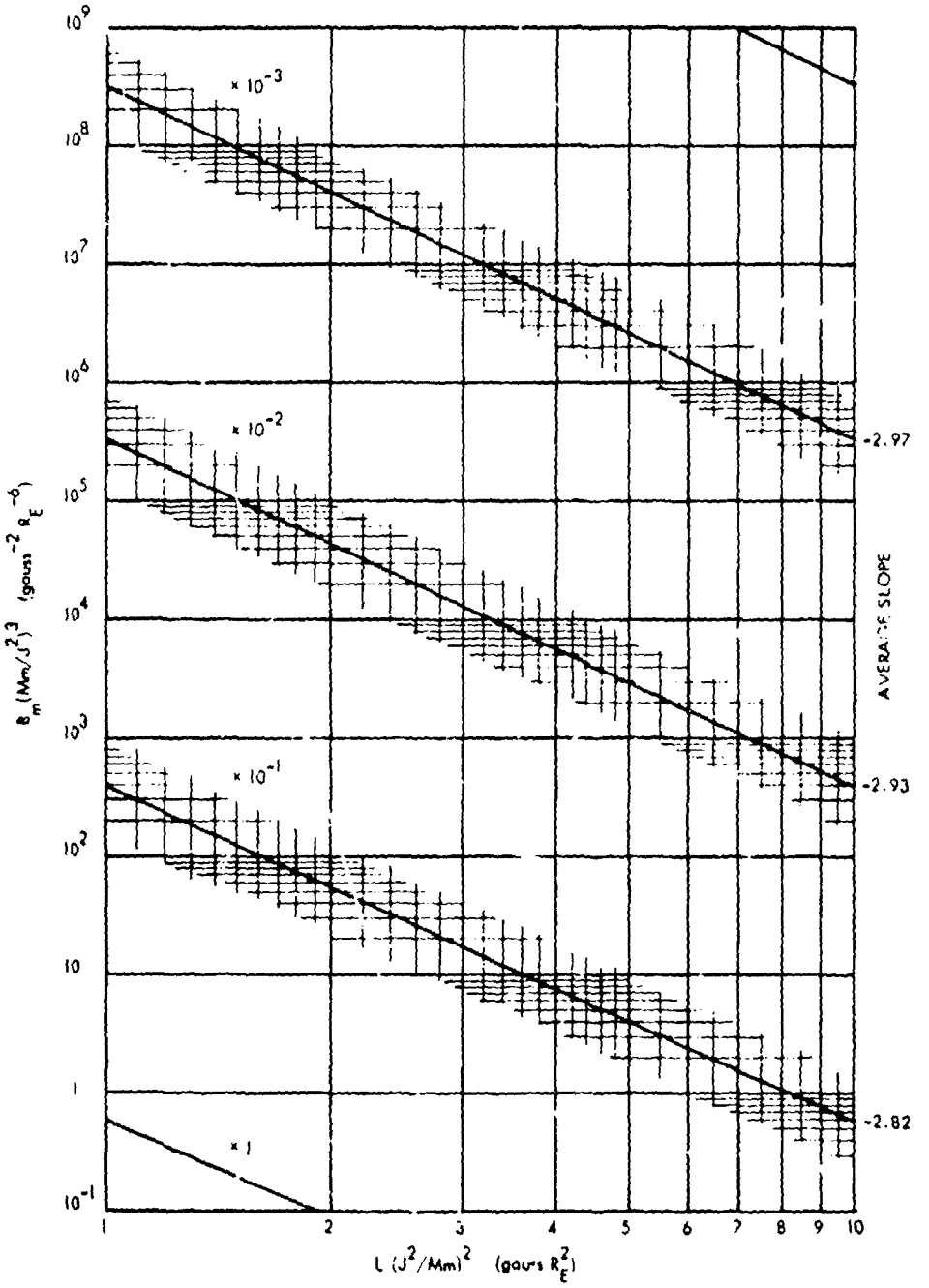

Figure 3B-19a. Mirror point field as a function of L for constant adiabatic invariants.

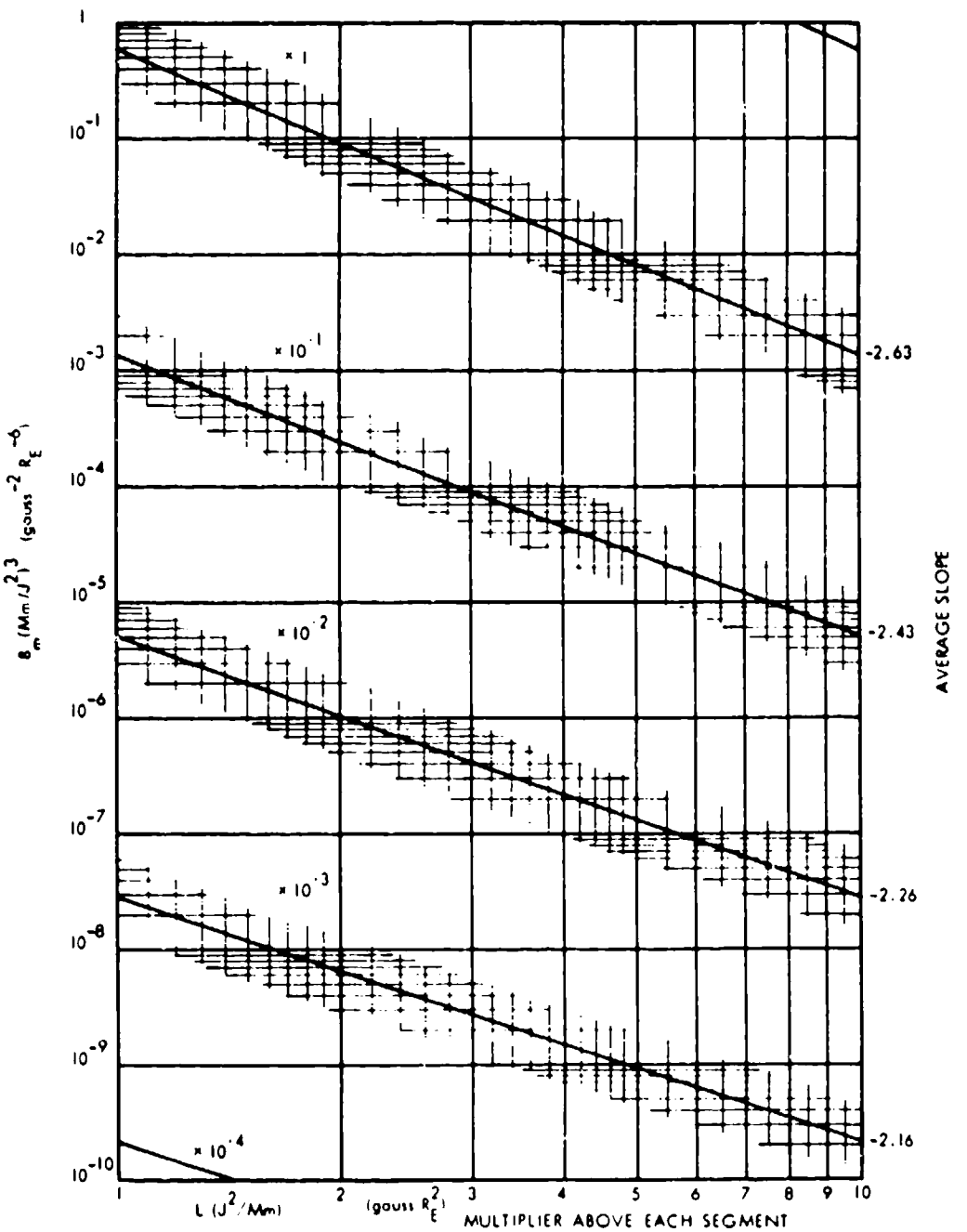

Figure 3B-19b. Mirror point field as a function of L for constant adiabatic invariants.

APPENDIX 3C

CONVERSION OF OMNIDIRECTIONAL FLUX TO DIRECTIONAL FLUX

This Fortran subroutine integrates a tabulated set of values of omnidirectional flux to obtain directional fluxes and the beta parameter (see Chapter 5). There is also an option which allows the program to perform the integration from j to J. The dimensions of the arrays are set at 1; with some computer systems, it may be necessary to enter the desired dimensions in the dimension statement.

```
      SUBROUTINE OMNINV(FDIR,OMNI,BETA,CPA,SSQ,NC,ARRAY,IBETA,IFORJ,
     1 IBOUND,IFLAG)
C          CONVERTS OMNIDIRECTIONAL FLUX TO DIRECTIONAL FLUX
C          RUNNING TIME  APROX 1 SEC FOR 100 INTERVALS
C
C          FDIR = DIRECTIONAL FLUX AT EQUATOR AS A FUNCTION OF
C                    COSINE(PITCH ANGLE)--IN UNITS OF /CM**2 SEC STER
C          OMNI = OMNIDIRECTIONAL FLUX AT  CX = SQRT(1- B(EQ)/B)
C                    --IN UNITS OF /CM**2 SEC
C          BETA = TRANSVERSE PRESSURE / MAXWELL STRESS
C                    --MUST BE MULTIPLIED BY 2.2E-15 *(RELATIVISTIC
C                    GAMMA)*(L**4) TO GET PROPER VALUE AT EQUATOR
C                    (PARTICLE ENERGY / FIELD ENERGY)
C          CPA = TABLE OF COSINE(PITCH ANGLE) OR CX
C                    FDIR, OMNI, AND BETA ARE SPECIFIED AT THE SAME
C                    POINTS RELATIVE TO THE ARRAY CPA
C          NC = SIZE OF TABLE = INDEX OF CUTOFF
C          ARRAY = TABLE OF MATRIX ELEMENTS. ALLOW  2*NC  DIMENSIONS
C                    (NC IF BETA IS NOT DESIRED)
C          IBETA = 1  IF BETA IS DESIRED IN OUTPUT, 0  OTHERWISE
C          IFORJ = 1  IF FDIR IS INPUT, 2  IF OMNI IS INPUT
C          IBOUND = 0  IF FDIR = 0 AT CUTOFF, 1  IF DERIVATIVE IS ZERO
C                     FDIR = 0 CORRESPONDS TO LOSS CONE SOLUTION
C                    (NO FLUX BEYOND CUTOFF), DERIVATIVE OF FDIR IS
C                    ZERO FOR STRONG DIFFUSION CASE (ISOTROPIC FLUX
C                    IN LOSS CONE--BEYOND CUTOFF). IN THIS CASE
C                    SPECIFY INPUT VALUES AT NC
C          IFLAG MAY BE SPECIFIED IN CALL OR ARGUMENTS OR COMMON.
C                    IFLAG = 0 CAUSES PRINTOUT OF COEFFICIENTS
C
      DIMENSION FDIR(1),OMNI(1),BETA(1),CPA(1),SSQ(1),ARRAY(1)
      DATA TWOPI/6.283185/
C---- ------------------------------------------------------------------
C
C          COMPUTE ELEMENTS OF FDIR-TO-OMNI MATRIX
      NM1=NC-1
      NNN=NM1
      IF(IBOUND.GT.0)NNN=NC
      NNNP1=NNN+1
      DO 80 I=1,NNN
      J=NNNP1-I
```

```
42            JP1=J+1
43      C           SET CONSTANTS
44            CSQJ=CPA(J)**2
45            SSQ(J)=1.-CSQJ
46            SPA=SQRT(SSQ(J))
47            A=SPA/TWOPI
48            B=1./(SPA*TWOPI)
49            IF(J.GE.NC)GO TO 26
50            DELKM1=0.
51            DELKP1=CPA(JP1)-CPA(J)
52            UK=0.
53            UKP1=SQRT(DELKP1*(CPA(JP1)+CPA(J)))
54            IF(J.EQ.1)GO TO 10
55            VK=ALOG(CPA(J))
56            GO TO 11
57         10 VK=0
58         11 VKP1=ALOG(CPA(JP1)+UKP1)
59            ARRAY(J)=(CPA(JP1)*UKP1+CSQJ*(VK-VKP1))/DELKP1
60            IF(IBETA.NE.0)ARRAY(NNN+J)=SSQ(J)*ARRAY(J)
61            IF(JP1.GE.NC)GO TO 24
62            DO 22 K=JP1,NM1
63            KM1=K-1
64            KP1=K+1
65            DELKM1=DELKP1
66            DELKP1=CPA(KP1)-CPA(K)
67            UKM1=UK
68            UK=UKP1
69            UKP1=SQRT((CPA(KP1)**2)-CSQJ)
70            VKM1=VK
71            VK=VKP1
72            VKP1=ALOG(CPA(KP1)+UKP1)
73            CPAU=CPA(K)*UK
74            ARRAY(K)=(CPA(KM1)*UKM1-CPAU+CSQJ*(VK-VKM1))/DELKM1
75           1 +(CPA(KP1)*UKP1-CPAU+CSQJ*(VK-VKP1))/DELKP1
76         22 IF(IBETA.NE.0)ARRAY(NNN+K)=SSQ(K)*ARRAY(K)
77         24 IF(IBOUND.EQ.0)GO TO 30
78            ARRAY(NC)=(CPA(NM1)*UK-CPA(NC)*UKP1+CSQJ*(VKP1-VK))/DELKP1
79            IF(IBETA.NE.0)ARRAY(NNN+NC)=SSQ(NC)*ARRAY(NC)+(SPA*SSQ(J)
80           1 -UKP1**3)/.75
81            ARRAY(NC)=ARRAY(NC)+2.*SPA
82            GO TO 30
83         26 ARRAY(NC)=2.*SPA
```

```
      IF(IBETA.NE.0)ARRAY(NNN+NC)=ARRAY(NC)*SSQ(NC)/1.5
   30 IF(IBETA.GT.1)GO TO 70
      IF(IFLAG.EQ.0.)WRITE(6,660) (ARRAY(K),K=J,NNN)
  660 FORMAT(10X,6E20.8)
      GO TO (40,50),IFORJ
C-----------------------------------------------------------------------
C
C           COMPUTE OMNIDIRECTIONAL FLUX FROM EQUATORIAL PITCH ANGLE
C                     DISTRIBUTION
   40 TOTAL=0.
      DO 42 K=J,NNN
   42 TOTAL=TOTAL+FDIR(K)*ARRAY(K)
   44 OMNI(J)=TOTAL/A
      GO TO 60
C-----------------------------------------------------------------------
C
C           COMPUTE EQUATORIAL PITCH ANGLE DISTRIBUTION FROM
C                     OMNIDIRECTIONAL FLUX DISTRIBUTION BY INVERTING
C                     MATRIX
   50 TOTAL=OMNI(J)*A
      IF(J.EQ.NNN)GO TO 54
      DO 52 K=JP1,NNN
   52 TOTAL=TOTAL-FDIR(K)*ARRAY(K)
   54 FDIR(J)=TOTAL/ARRAY(J)
      IF(IBOUND.EQ.0)FDIR(NC)=0.
C-----------------------------------------------------------------------
C
C           COMPUTE BETA FROM EQUATORIAL PITCH ANGLE DISTRIBUTION
   60 IF(IBETA.NE.1)GO TO 80
      TOTAL=0.
      DO 62 K=J,NNN
   62 TOTAL=TOTAL+FDIR(K)*ARRAY(NNN+K)
   64 BETA(J)=TOTAL/B
      GO TO 80
C-----------------------------------------------------------------------
C
C           COMPUTE EQUATORIAL DISTRIBUTION FROM BETA
C                     (CAUTION--THIS WILL NOT ALWAYS WORK IF BETA DOES
C                     NOT FALL OFF RAPIDLY ENOUGH NEAR THE ATMOSPHERIC
C                     CUTOFF)
   70 TOTAL=BETA(J)*B
      IF(J.EQ.NNN)GO TO 74
      DO 72 K=JP1,NNN
   72 TOTAL=TOTAL-FDIR(K)*ARRAY(   N+K)
   74 FDIR(J)=TOTAL/ARRAY(NNN+J)
      IF(IBOUND.EQ.0)FDIR(NC)=0.
      GO TO 40
   80 CONTINUE
C-----------------------------------------------------------------------
C
      IF(IFLAG.GT.0)RETURN
      IFLAG=99
      WRITE(6,661)
  661 FORMAT(10X/////)
      END
```

REFERENCES

1. L. Spitzer. Physics of Fully Ionized Gases, 102, Interscience, New York, 1956.

2. J. L. Delcroix. Introduction a la théorie des gas ionisés, Dunod, Paris, 1959, trans.: Introduction to the Theory of Ionized Gases, 146, trans. by Ben Daniel Clark, Interscience, New York, 1960.

3. H. Goldstein. Classical Mechanics, 383, Addison Wesley, Cambridge, 1950.

4. H. Alfvén and C.-G. Fälthammar. Cosmical Electrodynamics Fundamental Principles, Oxford U. Press, London, 1963.

5. H. Alfvén. Cosmical Electrodynamics, 232, Clarendon Press, Oxford, 1950.

6. L. Davis and D. B. Chang. "On the Effect of Geomagnetic Fluctuations on Trapped Particles," J. Geophys. Res., 67, 2169-2179, 1962.

7. C.-G. Fälthammar. "Effects of Time-Dependent Electric Fields on Geomagnetically Trapped Radiation," J. Geophys. Res., 70, 2503-2516, 1965.

8. H. Alfvén. "On the Electrical Field Theory of Magnetic Storms and Aurorae," Tellus, 7, 50-64, 1955.

9. H. Alfvén. "On the Theory of Magnetic Storms and Aurora," Tellus, 10, 104-116, 1958.

10. L. Block. "The Present State of the Electric Field Theory of Magnetic Storms and Aurorae," IAU Symposium 6, 58, 1956.

11. C. Störmer. The Polar Aurora, 392, Clarendon Press, Oxford, 1955.

12. P. Lanzano. "Analytic Contributions to the Störmer Problem," Astphys. Sp. Sci., 2, 319-333, 1968.

13. S.F. Singer. Bull. Am. Phys. Soc., Ser. II 1, 229, abs., 1956.

14. J.W. Chamberlain. "Motion of Charged Particles in the Earth's Magnetic Field," Geophysics the Earth's Environment, 141-174, ed. by C. DeWitt, J. Hieblot, and A. Lebeau, Gordon and Breach, New York, 1963.

15. G. Hellwig. "Über die Bewegung geladener Teilchen in schwach veränderlichen Magnetfeldern," Zeit. Naturforsch, 10a, 508-516, 1955.

16. E.C. Ray. "On the Motion of Charged Particles in the Geomagnetic Field," Ann. Phys., 24, 1-18, 1963.

17. K.S. Viswanathan and P. Venkatarangan. "The Geomagnetic Cavity and the Van Allen Radiation Belts, Pl. Sp. Sci., 14, 641-647, 1966.

18. V.P. Shalimov and I.N. Svachunov. "The Use of Störmer's Method for the Investigation of the Motion of Charged Particles in the Field of a Magnetic Dipole Situated in an External Magnetic Field II," Kosm Issled, 4, 394-403, 1966, trans: Cos Res 4, 350-357, 1966.

19. D. Stern. "Störmer Theory and Euler Potentials," Pl. Sp. Sci., 15, 1525-1530, 1967.

20. S. Chandrasekhar. Plasma Physics, 214, U. of Chicago, 1960.

21. T.G. Northrop. The Adiabatic Motion of Charged Particles, 105, Interscience, New York, 1963.

22. P.O. Vandervoort. "The Relativistic Motion of a Charged Particle in an Inhomogeneous Electromagnetic Field," Ann. Phys., 10, 401-453, 1960.

23. D.R. Bates. "The Temperature of the Upper Atmosphere," P.R.S. Lon, B64, 805-821, 1951.

24. F.S. Johnson. "Temperature in the High Atmosphere," Ann. Geophys., 14, 94-108, 1958.

25. L.H. Brace, N.W. Spencer, and A. Dalgarno. "Electrostatic Probe Data and Interpretation," Trans. Am. Geophys. U., 45, 82, 1964.

26. F.S. Johnson. "Structure of the Upper Atmosphere," Satellite Environment Handbook, 1-20, second ed, ed. by F.S. Johnson, Stanford Press, Stanford, Calif. 1965.

27. W.B. Hanson. "Structure of the Ionosphere," Satellite Environment Handbook, 21-49, ed. by F.S. Johnson, Stanford Press, Stanford, Calif. 1965.

28. S.F. Singer. "Radiation Belt and Trapped Cosmic-Ray Albedo," Phys. Rev. Letters, 1, 171, 1958, trapped albedo theory of the radiation belt, Phys. Rev. Letters, 1, 181, 1958.

29. R.C. Wentworth, W.M. MacDonald, and S.F. Singer. "Lifetimes of Trapped Radiation Belt Particles Determined by Coulomb Scattering," Phys. Fluids, 2, 499-509, 1959.

30. M. Walt and W.M. MacDonald. "The Influence of the Earth's Atmosphere on Geomagnetically Trapped Particles," Rev. Geophys., 2, 543-577, 1964.

31. J.G. Linhart. Plasma Physics, 274, North Holland, Amsterdam, 1960.

32. W.B. Thompson. An Introduction to Plasma Physics, 247, Pergamon Press, Oxford, London, 1962.

33. D.A. Hamlin, R. Karplus, R.C. Vik, and K.M. Watson. "Mirror and Azimuthal Drift Frequencies for Geomagnetically Trapped Particles," J. Geophys. Res., 66, 1-4, 1961.

34. J.S. Lew. 'Drift Rate in a Dipole Field," J. Geophys. Res., 66, 2681-2686, 1961.

35. A.M. Lenchek, S.F. Singer, and R.C. Wentworth. "Geomagnetically Trapped Electrons From Cosmic Albedo Neutrons," J. Geophys. Res., 66, 4027-4046, 1961.

36. L.L. Newkirk and M. Walt. "Longitudinal Drift Velocity of Geomagnetically Trapped Particles," J. Geophys. Res., 69, 1759-1763, 1964.

37. E.N. Parker. "Disturbance of the Geomagnetic Field by the Solar Wind," Physics of Geomagnetic Phenomena, II, 1153-1202, ed. by S. Matsushita and W.H. Campbell, Academic Press, New York, 1967.

38. T.G. Cowling. Magnetohydrodynamics, 112, Interscience, New York, 1957.

39. W.A. Newcomb. "The Motion of Magnetic Lines of Force," Princeton U. Observ., Tech. Rept. No. 1, 1955.

40. K.M. Watson. "Use of the Boltzmann Equation for the Study of Ionized Gases of Low Density I," Phys. Rev., 102, 12-19, 1956.

41. K.A. Brueckner and K.M. Watson. "Use of the Boltzmann Equation for the Study of Ionized Gases of Low Density II," Phys. Rev., 102, 19-27, 1956.

42. G.F. Chew, M.L. Goldberger, and F.E. Low. "The Boltzmann Equation and the One-Fluid Hydromagnetic Equations in the Absence of Particle Collisions," Proc. Roy. Soc., A236, 112-118, 1956.

43. H. Grad and H. Rubin. Proceedings of the Second United Nations Conference on the Peaceful Use of Atomic Energy, 31, 190, U.N., Geneva, 1958.

44. T.G. Northrop and E. Teller. "Stability of the Adiabatic Motion of Charged Particles in the Earth's Field," Phys. Rev., 117, 215-225, 1960.

45. D.P. Stern. "The Motion of Magnetic Field Lines," Sp. Sci. Rev., 6, 147-173, 1966.

46. D. P. Stern. "Geomagnetic Euler Potentials," J. Geophys. Res., 72, 3995-4010, 1967.

47. D. P. Stern. Euler Potentials and Geomagnetic Drift Shells, GSFC Document X-641-67-329, 1967.

48. D. P. Stern. "Euler Potentials and Geomagnetic Drift Shells," J. Geophys. Res., 73, 4373-4378, 1968.

49. J. B. Taylor. "Equilibrium and Stability of Plasma in Arbitrary Mirror Fields," Phys. Fluids, 7, 767-773, 1964.

50. C. S. Gardner. "Adiabatic Invariants of Periodic Classical Systems," Phys. Rev., 115, 791-794, 1959.

51. D. Ter Haar. "Adiabatic Invariance and Adiabatic Invariants," Contemp. Physics, 7, 447-458, 1966.

52. G. F. Chew, M. L. Goldberger, and F. E. Low. The Individual Particle Equations of Motion in the Adiabatic Approximation, Los Alamos Rept. LA-2055, T-759, 1955.

53. M. Kruskal. The Spiraling of a Charged Particle, Princeton U. Project, Materhorn Rept. PM-S-33, NYO-7903, March 1958.

54. M. Kruskal. "Assymptotic Theory of System of Ordinary Differential Equations With All Solutions Nearly Periodic," The Theory of Neutral and Ionized Gases, 277-284, ed. by C. DeWitt and J. F. Detoeuf, Wiley, New York, 1960.

55. S. Chandrasekhar, A. N. Kaufman, and K. M. Watson. "Properties of an Ionized Gas of Low Density in a Magnetic Field, IV," Ann. Phys. 5, 1-25, 1958.

56. G. F. Chew, M. L. Goldberger, and F. E. Low. An Adiabatic Invariant for Motion Along the Magnetic Lines of Force, Los Alamos Rept. LA-2055, T-767, September 1955.

57. R. L. Kauffmann. "Conservation of First and Second Adiabatic Invariants," J. Geophys. Res., 70, 2181-2186, 1965.

58. J.D. Roederer. "On the Adiabatic Motion of Energetic Particles in a Model Magnetosphere," J. Geophys. Res., 72, 981-992, 1967.

59. C.E. McIllwain. "Coordinates for Mapping the Distribution of Magnetically Trapped Particles, J. Geophys. Res., 66, 3681-3691, 1961.

60. E.C. Stone. "The Physical Significance and Application of L, B_o, and R_o to Geomagnetically Trapped Particles," J. Geophys. Res., 68, 4157-4166, 1963.

61. A.M. Lenchek, S.F. Singer, and R.C. Wentworth. "Geomagnetically Trapped Electrons from Cosmic Ray Albedo Neutrons," J. Geophys. Res., 66, 4027-4046, 1961.

62. W.N. Hess. The Radiation Belt and Magnetosphere, 63-66, Blaisdell, Waltham, Mass. 1968.

63. J.F. Denisse and J.L. Delcroix. Theorie des Ondes dans les Plasmas, Dunod, Paris, 1961, trans: Plasma Waves, 140, Interscience, New York, 1963.

64. T.H. Stix. The Theory of Plasma Waves, 268, McGraw-Hill, New York, 1962.

65. S. Chapman and T.G. Cowling. The Mathematical Theory of Non-Uniform Gases, 319-379, University Press, Cambridge, 1952.

66. D.C. Montgomery and D.A. Tidman. Plasma Kinetic Theory, 286, McGraw-Hill, New York, 1964.

67. H.B. Phillips. Vector Analysis, 215-231, Wiley, New York, 1933.

68. R.S. Cohen, L. Spitzer, and P. Routly. "The Electrical Conductivity of an Ionized Gas," Phys. Rev., 80, 230-238, 1950.

69. L. Spitzer and R. Härm. "Transport Phenomena in a Completely Ionized Gas," Phys. Rev., 89, 977-981, 1953.

70. M. Abraham and R. Becker. The Classical Theory of Electricity and Magnetism, 283, Hafner, New York, trans.

71. H. Lamb. Hydrodynamics, 730, Dover, N. Y., 1945; and Cambridge, 1879.

72. S. Chapman and J. Bartels. Geomagnetism, II, 609-669, Oxford U. Press, London, 1940.

73. S. Chapman. "The Electrical Conductivity of the Ionosphere, A Review," Nuovo Cimento, 4, 1385-1412, 1956.

74. J.A. Fejer. "Atmospheric Tides and Associated Magnetic Effects," Rev. Geophys., 2, 275-309, 1964.

SECTION 5
SOURCES AND LOSSES OF TRAPPED PARTICLES

G.T. Davidson, Lockheed Palo Alto Research Laboratory

5.1 INTRODUCTION

Most of the unsolved problems relating to the trapped radiation belts have to do with two broad question: (1) Where do such large numbers of energetic particles come from and (2) Why, after they have been trapped, do they disappear again? Only partial answers are available. The source of high-energy trapped protons has been ascribed with a fair degree of success to decay of cosmic-ray-produced albedo neutrons. The same mechanism is quite inadequate to explain trapped electrons and low-energy protons.

Observations of the decay of artificial radiation belts have shown that the principal loss mechanism on low L-shells ($L < 1.25$) must be collisions in the atmosphere. Some additional loss mechanism must certainly exist that affects particles on higher L-shells. A large amount of effort has been expended in analyzing the effects of diffusion of particles across L-shells, and limited success has been achieved for some special instances. Otherwise, the L-shell diffusion theory is far from complete.

Many interesting particular effects have been explained, but their relevance to the overall picture of trapping and losses is not well understood. A recent subject of much attention has been the interaction of plasma waves with trapped particles. This topic is still rather controversial.

The Sections 5.2 and 5.3 treat the pure loss or source mechanisms, such as loss through repeated collisions with atmospheric particles and the neutron decay injection theory. Succeeding subsections discuss more complicated processes that may be responsible not only for injection and removal of particles but also for redistribution within the trapping regions.

Unfortunately, space limitations prohibit citing all the important reference materials. The references in this section are intended

primarily as a guide to further reading. For more detailed treatments of the subjects in this section, see References 1 and 210.

5.2 LOSSES IN THE ATMOSPHERE

5.2.1 Particle Collisions

Section 3 considered the motion of isolated particles. The results of Section 3 hold if particle collisions do not substantially alter the motions. Not obvious, however, is that collision effects can be ignored when dealing with large numbers of particles. In the lowest parts of the atmosphere, the air behaves as a collision-dominated fluid with only rare manifestations of plasma-like behavior. One should expect that intermediate regions exist in the high atmosphere in which the effects of collisions and electromagnetic fields are comparable.

A fast, charged particle in an un-ionized medium loses energy efficiently through collisions with atomic electrons and nuclei. Orbital electrons involved in a collision may be excited to higher energy states or may be removed completely from the parent atoms. The resulting energy lost per unit trajectory distance by a fast particle of charge $\pm e$ and velocity v encountering stationary particles of charge $\pm e$ is the stopping power (References 2, 3, and 4):

$$-\frac{dE}{ds} = -\frac{dT}{ds} = \frac{2\pi e^4}{m_r v^2} n \ln \frac{(\text{maximum energy exchange})}{(\text{minimum energy exchange})} . \qquad (5\text{-}1)$$

The energy loss is proportional to the number density of stationary charged particles, n. The mass that frequently appears in formulas related to collisions between two particles is the reduced mass (Reference 5):

$$m_r = \frac{m_1 m_2}{m_1 + m_2} . \qquad (5\text{-}2)$$

When both particles are electrons, the reduced mass is $m_e/2$. When both are protons, the reduced mass is $m_p/2$. Otherwise, if one particle is an electron and the other is much heavier, the reduced mass is nearly equal to the electron mass, m_e. Because the reduced mass in collisions with electrons is small, the slowing of heavy, charged particles is due almost entirely to collisions with bound and free electrons (Reference 1).

Table 5-1. Excitation ionization potentials (Reference 23).

Material	I^* (eV)	$\log_{10} I^*$	Predominates in Altitude Range (km)
Air (nitrogen)	87	1.94	< 300
Oxygen	97	1.99	300 < h < 800
Helium	44	1.64	800 < h < 5000
Hydrogen	18	1.26	5000 < h

Equation 5-7, the first two terms in the square brackets become $6.60 + \log_{10}(m_e/m_p)\bar{T}$(MeV). The difference between Equations 5-7 and 5-9b is only about 10 percent when particles of comparable velocities are considered.

The energy loss lifetime is of order

$$\tau_E \approx \frac{\bar{T}}{(-d\bar{T}/dt)} \quad . \tag{5-11}$$

In the upper part of the trapped radiation belts where the total average electron density may be of order 10^3 per cubic centimeter (References 20, 21, and 22), the predicted lifetimes of trapped electrons and protons would be of order 20 and 60 years, respectively. A particle of sufficient energy could very well remain trapped for a long time if the only effect of collisions were a degradation of kinetic energy.

5.2.2 Cumulative Deflections—the Fokker-Planck Equation

An energy loss formula is not quite adequate to describe the relaxation of charged particles in a plasma. The total accumulated deflections of a particle can become so great that eventually there is no longer a well-defined "forward" velocity. Additionally, the described stopping power formulas are not very accurate when the speed of the particle under scrutiny is not much greater than the thermal speed. A complete treatment of collision effects must include explicitly the random nature of individual collisions; the

expected deflection after many collisions should be related to the probable deflections in individual collision events. The Fokker-Planck equation satisfies these criteria quite neatly in predicting the evolution of a single-particle distribution function $f(\bar{x}, \bar{v}, t)$ (References 24 through 27). Because of considerable confusion about its proper use, a brief derivation of the Fokker-Planck equation (Reference 28) is given here. Suppose that $S(\bar{v}, \delta\bar{v}, t)\, d^3v\, \delta t$ is the probability that a test particle within the element of velocity space defined by $\bar{v}$ and d^3v (momentum space could as well be employed) experiences a small deflection $\delta\bar{v}$ sometime between t and $t + \delta t$. One may assume that S does not contain time as an explicit variable; this assumption defines a Markov process in which the expected behavior of a dynamical system does not depend on its past history (Reference 24). (Many interactions between particles are not Markovian, particularly if the test particles have internal energy states that may be excited during or between collisions.) During a time interval, δt, long enough to include a considerable number of collisions, the distribution function evolves according to the formula:

$$f(u_i, t + \delta t) = \left[\int\int\int_{[\text{all } \delta u_i]} f(u_i - \delta u_i, t)\, S(u_i - \delta u_i, \delta u_i)\, J\, d^3(\delta u_i)\right] \delta t \quad . \tag{5-12}$$

The velocity coordinates have been generalized so that the components of v are linear functions of some set of u_i. The infinitesimal volume element $d^3(\delta\bar{v})$ is equivalent to $d(\delta u_1)\, d(\delta u_2)\, d(\delta u_3)$. The $\delta\bar{v}_i$ are related to cartesian coordinates by the Jacobian (Reference 29):

$$J \equiv \frac{\partial(\delta v_x, \delta v_y, \delta v_z)}{\partial(\delta u_1, \delta u_2, \delta u_3)} = \text{Determinant} \begin{vmatrix} \frac{\partial(\delta v_x)}{\partial(\delta u_1)} & \frac{\partial(\delta v_y)}{\partial(\delta u_1)} & \frac{\partial(\delta v_z)}{\partial(\delta u_1)} \\ \frac{\partial(\delta v_x)}{\partial(\delta u_2)} & \frac{\partial(\delta v_y)}{\partial(\delta u_2)} & \frac{\partial(\delta v_z)}{\partial(\delta u_2)} \\ \frac{\partial(\delta v_x)}{\partial(\delta u_3)} & \frac{\partial(\delta v_y)}{\partial(\delta u_3)} & \frac{\partial(\delta v_z)}{\partial(\delta u_3)} \end{vmatrix} \tag{5-13}$$

Of course J can be written as an explicit function of one set of variables, say u_i. A Taylor series expansion about $\delta u_i = 0$ gives to first order.

$$f(u_i, t) = \frac{\partial f(u_i, t)}{\partial t} \delta t$$

$$= \int\int\int \left[f(u_i, t)\, S(u_i, \delta u_i) - \sum_{j=1}^{3} \frac{\partial}{\partial u_j} \left(J(u_i) f(u_i, t) S(u_i, \delta u_i) \right) \delta u_i + \frac{1}{2} \sum_{j=1}^{3} \sum_{k=1}^{3} \frac{\partial}{\partial u_k} \frac{\partial}{\partial u_j} \left(J(u_i) f(u_i, t) S(u_i, \delta u_i) \right) \delta u_j \delta u_k \right] J(\delta u_i) d^3(\delta u_i) \Big\} \delta t / J(u_i)$$

(5-14)

The probability S is normalized so that the total probability of a collision $\int\int\int S\, d^3(\delta \bar{v})$ is equal to 1 (including collisions that result in no deflection). The generalized Fokker-Planck equation may be written immediately from Equation 5-14:

$$\frac{\partial f}{\partial t} = -\frac{1}{J} \sum_{j=1}^{3} \frac{\partial}{\partial u_j} \left(J f \langle \Delta u_j \rangle \right) + \frac{1}{2J} \sum_{j=1}^{3} \sum_{k=1}^{3} \frac{\partial}{\partial u_j} \frac{\partial}{\partial u_k} \left(J f \langle \Delta u_i, \Delta u_k \rangle \right). \qquad (5\text{-}15)$$

The Fokker-Planck coefficients represent averages of the probabilities of deflections, and are defined as:

$$\langle \Delta u_j \rangle = \left[\int\int\int \delta u_j\, J(u_i) S(u_i, \delta u_i) d^3(\delta u_i) \right] \delta t \qquad (5\text{-}16a)$$

$$\langle \Delta u_j, \Delta u_k \rangle = \left[\int\int\int \delta u_j\, \delta u_k\, J(u_i)\, S(u_i, \delta u_i) d^3(\delta u_i) \right] \delta t \qquad (5\text{-}16b)$$

$$j, k = 1, 2, 3$$

The Fokker-Planck equation can be further generalized to apply to any quantity that changes in random, discrete steps; the derivation above also applies to a space of any arbitrary number of dimensions.

In cartesian coordinates, the Fokker-Planck equation has a simple tensor form (Reference 26):

$$\frac{\partial f}{\partial t} = -\nabla_v \cdot f \langle \Delta \bar{v} \rangle + \frac{1}{2} \nabla_v \nabla_v : f \langle \Delta \bar{v}\, \Delta \bar{v} \rangle \qquad (5\text{-}17)$$

The notation $\langle\ \rangle : \langle\ \rangle$ refers to dyadic multiplication (Reference 29). ∇_v is just the velocity space gradient.

Using a coordinate system with a symmetry exis that coincides with some special symmetry axis of the physical system often is convenient. No Fokker-Planck coefficients exist involving the azimuthal angle about the symmetry axis. In cylindrical coordinates, $\bar{v}$ is decomposed into parallel, $\bar{v}_{\parallel}$, and transverse, $\bar{v}_{\perp}$, components. The Jacobian is $2\pi v_{\perp}$. The Fokker-Planck equation that results is

$$\frac{\partial f}{\partial t} = \frac{\partial}{\partial v_{\parallel}} f\langle \Delta v_{\parallel} \rangle - \left(\frac{1}{v_{\perp}} + \frac{\partial}{\partial v_{\perp}}\right) f\langle \Delta v_{\perp} \rangle$$
$$+ \frac{1}{2} \frac{\partial}{\partial_{\parallel}^{2}} \langle f\,(\Delta v_{\parallel})^2 \rangle + \left(\frac{1}{v_{\perp}} \frac{\partial}{\partial v_{\parallel}} + \frac{\partial^2}{\partial v_{\parallel}\, \partial v_{\perp}}\right) f\langle \Delta v_{\parallel}\, \Delta v_{\perp} \rangle$$
$$+ \left(\frac{1}{v_{\perp}} \frac{\partial}{\partial v_{\perp}} + \frac{1}{2} \frac{\partial^2}{\partial v_{\perp}^{2}}\right) f\langle (\Delta v_{\perp})^2 \rangle . \qquad (5\text{-}18)$$

In velocity v and pitch angle α_p coordinates (spherical coordinates), the Jacobian is $2\pi v^2 \sin\alpha_p$. The corresponding Fokker-Planck equation is

$$\frac{\partial f}{\partial t} = -\left(\cot\alpha_p + \frac{\partial}{\partial \alpha_p}\right) f\langle \Delta \alpha_p \rangle - \left(\frac{2}{v} + \frac{\partial}{\partial v}\right) f\langle \Delta v \rangle$$
$$+ \frac{1}{2}\left(-1 + 2\cot\alpha_p \frac{\partial}{\partial \alpha_p} + \frac{\partial^2}{\partial \alpha_p^{2}}\right) f\langle (\Delta \alpha_p)^2 \rangle$$
$$+ \left(\frac{2}{v}\cot\alpha_p + \cot\alpha_p \frac{\partial}{\partial v} + \frac{2}{v}\frac{\partial}{\partial \alpha_p} + \frac{\partial^2}{\partial v\, \partial \alpha_p}\right) f\langle \Delta \alpha_p\, \Delta v \rangle$$
$$+ \left(\frac{1}{v^2} + \frac{2}{v}\frac{\partial}{\partial v} + \frac{1}{2}\frac{\partial^2}{\partial v^2}\right) f\langle (\Delta v)^2 \rangle . \qquad (5\text{-}19)$$

The cosine of the pitch angle, μ, is usually a convenient variable, in which case the Jacobian is $2\pi v^2$ and the Fokker-Planck equation in velocity-pitch angle cosine coordinates becomes

$$\frac{\partial f}{\partial t} = -\frac{\partial}{\partial \mu} f\langle \Delta\mu \rangle - \left(\frac{2}{v} + \frac{\partial}{\partial v}\right) f\langle \Delta v \rangle + \frac{1}{2}\frac{\partial^2}{\partial \mu^2} f\langle (\Delta\mu)^2 \rangle + \left(\frac{2}{v}\frac{\partial}{\partial \mu} + \frac{\partial^2}{\partial \mu\, \partial v}\right) f\langle \Delta\mu \Delta v \rangle + \left(\frac{1}{v^2} + \frac{2}{v}\frac{\partial}{\partial v} + \frac{1}{2}\frac{\partial^2}{\partial v^2}\right) f\langle (\Delta v)^2 \rangle \quad . \tag{5-20}$$

In the last equation, the velocity could have been replaced by the kinetic energy with a resulting Jacobian of just 2π (the number of particles in $dT d\mu$ is $2\pi f(T,\mu)\, dT d\mu$). The Fokker-Planck equation in energy-cosine pitch angle coordinates is

$$\frac{\partial f}{\partial t} = -\frac{\partial}{\partial \mu} f\langle \Delta\mu \rangle - \frac{\partial}{\partial T} f\langle \Delta T \rangle + \frac{1}{2}\frac{\partial^2}{\partial \mu^2} \cdot f\langle (\Delta\mu)^2 \rangle + \frac{\partial^2}{\partial \mu \partial T} f\langle \Delta\mu \Delta T \rangle + \frac{1}{2}\frac{\partial^2}{\partial T^2} f\langle (\Delta T)^2 \rangle \quad . \tag{5-21}$$

The Fokker-Planck equation represents a diffusion in velocity space (References 24 and 26). Particles starting in a group at one point in velocity space eventually will become difficult to identify as members of the original group. However, after a finite time interval, the particles that were originally traveling together have not only different velocities but also different spatial positions. It is necessary to define the distribution function so that it is spatially invariant when collisions are ignored. This requirement is not always trivial. Usually, the distribution of velocities at a fixed point (or surface) is adequate to determine the behavior of the entire ensemble (Section 3.6).

THE DIFFUSION EQUATION AVERAGED ALONG A FIELD LINE. The Fokker-Planck equation can often be reduced to an equation in two variables, say x and t. If it happens that a particular solution, f_s, is known for which $\partial f/\partial t$ is zero, then there is a simple relation between the coefficients $\langle \Delta x \rangle$ and $\langle (\Delta x)^2 \rangle$:

$$f_s \langle \Delta x \rangle = \frac{1}{2}\frac{\partial}{\partial x} f_s \langle (\Delta x)^2 \rangle \tag{5-21a}$$

(For examples of cases where this applies, see Sections 5.4.3 and 5.5.) If the second coefficient is replaced by

$$D_{xx} = 2\left\langle (\Delta x)^2 \right\rangle ,$$

the Fokker-Planck equation reduces to

$$\frac{\partial f}{\partial t} = \frac{\partial}{\partial x}\left[D_{xx}\left(\frac{\partial f}{\partial x} - \frac{f}{f_s}\frac{\partial f_s}{\partial x} \right) \right] . \qquad (5\text{-}21b)$$

This equation (Reference 160), or its more usual form

$$\frac{\partial f}{\partial t} = \frac{\partial}{\partial x}\left[D_{xx}\frac{\partial f}{\partial x} \right] \qquad (5\text{-}21c)$$

is immediately recognizable as the diffusion equation.

When the variable x is changed to a new variable, say y, the diffusion coefficient, D, must be altered to preserve the form of the diffusion Equation 5-21c. From the remarks above, it follows that the new diffusion coefficient is related to D_{xx} by the formula

$$D_{yy} = \left(\frac{\partial y}{\partial x} \right)^2 D_{xx} . \qquad (5\text{-}21d)$$

It is often feasible to establish a coordinate system in which the diagonal Fokker-Planck coefficients (e.g. $\langle \Delta_\mu \Delta T \rangle$) are zero, and pitch angle or some closely related variable is the primary variable. The contributions to $\partial f/\partial t$ due to energy diffusion and pitch-angle diffusion are additive, so it is meaningful to speak of the pitch-angle diffusion equation:

$$\left(\frac{\partial f}{\partial t} \right)_{T = \text{const}} = \frac{\partial}{\partial \mu}\left[D_{\mu\mu}\frac{\partial f}{\partial \mu} \right] . \qquad (5\text{-}21e)$$

Pitch-angle diffusion in the geomagnetic field is complicated by the fact that the phase space element ($d\mu dT$) changes with B along a field line. Equation 5-21e can be averaged over the length of a field line by using Liouville's equation (Equation 3-82) to relate the changes in the pitch-angle distribution at the equator to changes induced by diffusive processes at any arbitrary point.

If the variable μ is transformed to its value at the equator, μ_o, and the pitch-angle diffusion equation averaged over a trapped particle trajectory, the result is

$$\bar{D}_{\mu_o\mu_o} = \oint D_{\mu_o\mu_o} \frac{dS}{\mu} \Big/ \oint \frac{dS}{\mu}$$

$$= \oint D_{\mu\mu} \left(\frac{B_o}{B} \frac{\mu}{\mu_c}\right)^2 \frac{dS}{\mu} \Big/ \mathcal{A} \qquad (5\text{-}21f)$$

$$\frac{\partial f_o}{\partial t} = \frac{1}{t_b \mu_o} \frac{\partial}{\partial \mu_o} \left[\bar{D}_{\mu_o\mu_o} t_b \mu_o \frac{\partial f_o}{\partial \mu_o} \right] \qquad (5\text{-}21g)$$

where the subscripts o imply that a variable is evaluated at the equator. If the pitch angle, α_o, is selected as a variable, the averaged diffusion equation is

$$\frac{\partial f_o}{\partial t} = \frac{1}{t_b \sin 2\alpha_o} \frac{\partial}{\partial \alpha_o} \left[\bar{D}_{\alpha_o\alpha_o} t_b \sin 2\alpha_o \frac{\partial f_o}{\partial \alpha_o} \right] . \qquad (5\text{-}21h)$$

(Note that $\bar{D}_{\mu_o\mu_o} = \bar{D}_{\alpha_o\alpha_o} (\sin \alpha_o)^2$.)

A useful way to treat the loss cone is to assume that particles within the loss cone ($\mu_o > \mu_c$ or $\alpha_o < \mu_c$) are lost, on the average, in half the bounce period. The diffusion equation within the loss cone becomes

$$\frac{\partial f_o}{\partial t} = \frac{1}{t_b \mu_o} \frac{\partial}{\partial \mu_o} \left[\bar{D}_{\mu_o\mu_o} t_b \mu_o \frac{\partial f_o}{\partial \mu_o} \right] - \frac{f_o}{2t_b} \Big\} \mu_o > \mu_c \quad . \qquad (5\text{-}21i)$$

A special caution is necessary in the application of Equation 5-21i; it is strictly valid only in the case of strong diffusion, when the last term on the right is no larger than the other terms. Otherwise, it yields distributions which fall off precipitously at the edge of the loss cone and which give nearly correct loss rates, but the observable distribution in the loss cone does not necessarily resemble the solution of Equation 5-21i.

A diffusion equation like Equation 5-21c can be solved by finite-difference techniques. However, care must be exercised in constructing the finite-difference matrices to ensure stability and conservation of particles. The iterated solutions at the points $t_i + \delta t$ must be used to correct the approximations to the x derivatives used in stepping forward from t_i to $t_i + \delta t$

or the solution will be unstable no matter how small the time step δt (References 207 and 208). Some general methods are described in References 208 and 209. The treatment of the boundary of the loss cone is another troublesome problem in any solution of the pitch-angle diffusion equation.

An eigen-function solution is often more practical and more illuminating than a finite-difference solution to the pitch-angle diffusion equation (References 10, 35, and 36). Each eigen-mode decays exponentially with the time parameter τ_k. The complete solution (subject to appropriate boundary conditions) is

$$f(\mu_o, t) = \sum_k g_k(\mu_o)\, e^{-t/\tau_k} \qquad (5\text{-}21j)$$

The eigen-value equation for the g_k's is

$$\frac{t_b}{\tau_k} g_k + \frac{1}{\mu_o} \frac{\partial}{\partial \mu_o} \left[\bar{D}_{\mu_o \mu_o} \; t_b \mu_o \; \frac{\partial g_k}{\partial \mu_o} \right] = 0 . \qquad (5\text{-}21k)$$

If solutions to Equation 5-21k exist, the eigen-mode approach is feasible; frequently the diffusion coefficient and bounce period must be rather crudely approximated in order to derive manageable solutions.

CUMULATIVE DEFLECTIONS IN AN IONIZED GAS. Parallel and transverse deflections may be decomposed either with respect to the direction of the initial velocity or to the direction of the magnetic field. A particle traversing an ionized medium will experience small random deflections every time it comes near enough to an electron to be influenced by the field around that electron. Figure 5-3 shows the trajectory of a charged particle in a fully ionized plasma. The dots represent electrons; the dashed circles represent the Debye spheres with a radius equal to the Debye length. (Actually, many electrons might be found within any individual Debye sphere.) A fast charged particle is affected by the nearly stationary electrons only when it penetrates their respective Debye spheres.

The first Fokker-Planck coefficient $\langle \Delta v_{\parallel} \rangle$ is equivalent to a gradual loss of kinetic energy. It usually is called the dynamical friction coefficient (References 30 and 31). The averages of $\langle \Delta v_{\perp} \rangle$ and $\langle \Delta v_{\parallel} \Delta v_{\perp} \rangle$ in a uniform medium are expected to be zero because a transverse velocity increment is equally probable in any direction about the symmetry axis. The effects of random deflections are contained in the remaining coefficients $\langle (\Delta v_{\parallel})^2 \rangle$ and $\langle (\Delta v_{\perp})^2 \rangle$.

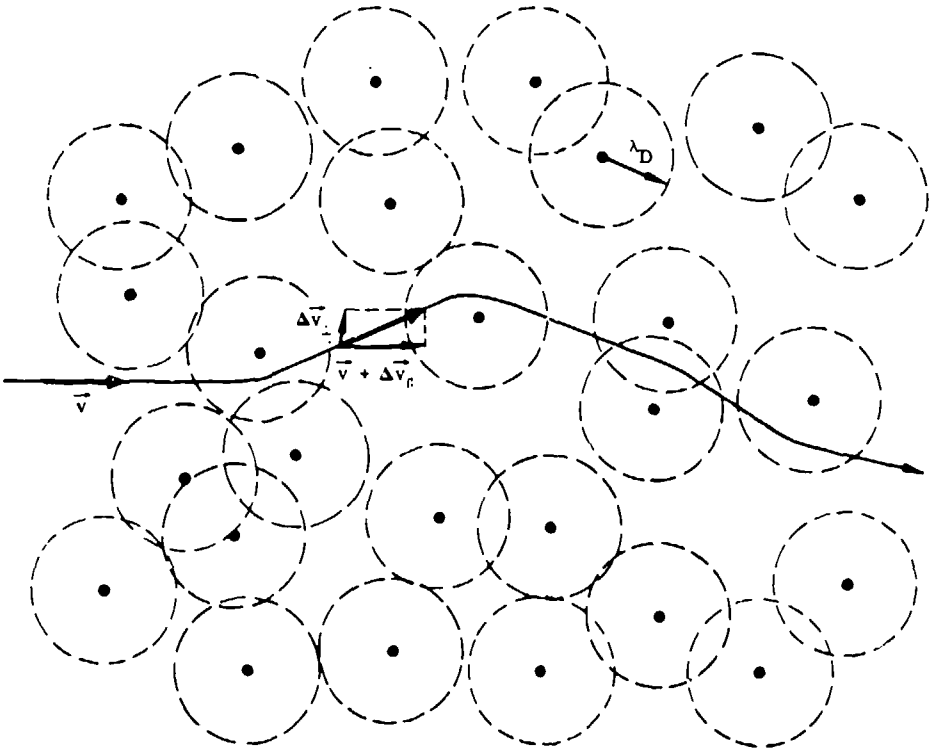

Figure 5-3. The path of a light-charged particle (an electron) in a fully ionized gas.

Chandrasekhar has computed Fokker-Planck coefficients for inverse square-type forces (Reference 31). The significant (nonrelativistic) coefficients for the slowing of a particle of mass m_1 and velocity v by free electrons (Equation 5-3b defines C, also see Reference 32) are

$$\langle \Delta v_{\parallel} \rangle = -2C\, n_e \frac{m_e^2}{m_1 m_r 2kT_e} G\left(\sqrt{\frac{m_e v^2}{2kT_e}}\right) \ln \Lambda \qquad (5\text{-}22)$$

$$\langle (\Delta v_{\parallel})^2 \rangle = 2C\, n_e \frac{m_e}{m_1^2 v} G\left(\sqrt{\frac{m_e v^2}{2kT_e}}\right) \ln \Lambda \qquad (5\text{-}23)$$

$$\langle (\Delta v_{\perp})^2 \rangle = C\, n_e \frac{m_e}{m_1^2 v} \left[\operatorname{erf}\left(\sqrt{\frac{m_e v^2}{2kT_e}}\right) - G\left(\sqrt{\frac{m_e v^2}{2kT_e}}\right) \right] \ln \Lambda \qquad (5\text{-}24)$$

The function G is related to the error function:

$$\text{erf}(x) = \frac{2}{\sqrt{\pi}} \int_0^x \exp(-y^2)\, dy \qquad (5\text{-}25)$$

through the definition:

$$G(x) = \frac{\text{erf}(x) - x\frac{d}{dx}\text{erf}(x)}{2x^2} \quad . \qquad (5\text{-}26)$$

Figure 5-4 gives numerical values of G and erf . The parameter Λ is related to the number of elecrons in a Debye sphere. Generally, $\ln \Lambda$ may be set equal to:

$$\ln \Lambda = \ln\left(\lambda_D \frac{3kT}{e^2}\right) \approx 15 - 20 \quad . \qquad (5\text{-}27)$$

If more accuracy is desired, the tabulations of $\ln \Lambda$ by Spitzer (Reference 32) may be found useful.

The Fokker-Planck coefficients for moderately high velocities are approximately

$$\langle \Delta v_{\parallel} \rangle \cong - C n_e \frac{m_e}{m_1 m_r} \frac{c^2}{v^2} \ln \Lambda \qquad (5\text{-}28)$$

$$\langle (\Delta v_{\parallel})^2 \rangle \cong C n_e \frac{kT}{m_1^2 c} \frac{c^3}{v^3} \ln \Lambda \qquad (5\text{-}29)$$

$$\langle (\Delta v_{\perp})^2 \rangle \cong C n_e \frac{m_e c}{m_1^2} \frac{c}{v} \ln \Lambda. \qquad (5\text{-}30)$$

The similarity between Equations 5-28 and 5-5 is readily apparent; the numerical magnitudes of the logarithmic terms are actually quite close. At incident particle velocities greater than about 4 times the thermal electron speed, the two formulas give nearly identical results. Only for very slow particles is Equation 5-28 preferred over Equation 5-5 (which is also correct at relativistic velocities).

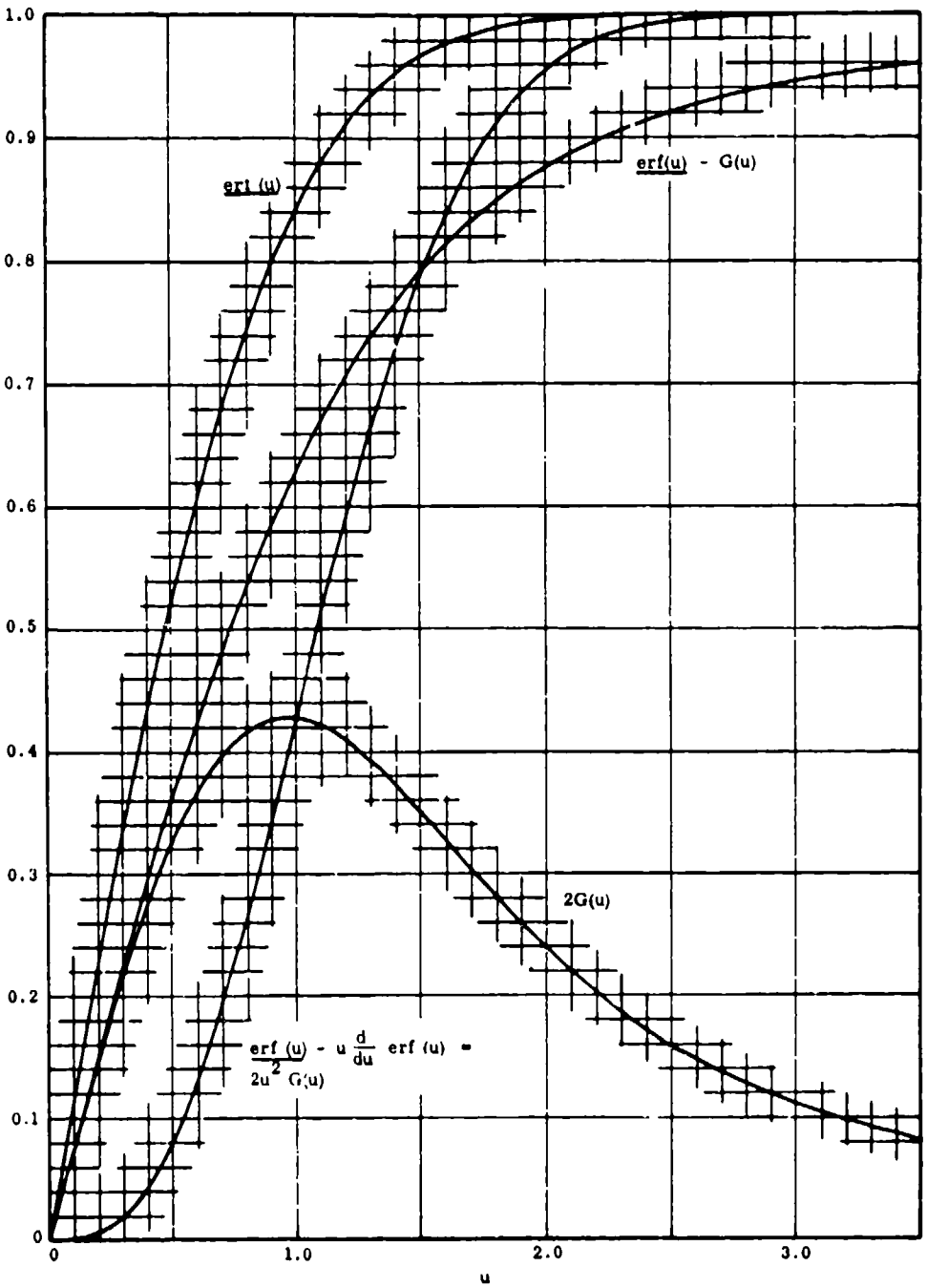

Figure 5-4. Functions used in computing Fokker-Plan k coefficients for the slowing and deflection of a charged particle in an ionized gas.

The ratio of the "diffusion" coefficient $\langle (\Delta v_\perp)^2 \rangle$ to the dynamical friction $\langle \Delta v_\parallel \rangle$ is proportional to m_r/m_1. For protons passing through free electrons, the ratio m_r/m_1 is only 1/1,836; but for electrons passing through a gas of free electrons, the ratio is 1/2. Generally, deflections are much more important for electrons than for fast, heavy particles (Section 5.2.1).

A useful measure of the lifetime of a particle in a plasma is the average time required to deflect the initial velocity through 90 degrees. A deflection relaxation time (Reference 32) might be defined as:

$$\tau_D = \frac{v^2}{\langle (\Delta v_\perp)^2 \rangle} = \frac{mv}{8\pi} n_e e^2 (\text{erf} - G) \ln \Lambda \qquad (5\text{-}31a)$$

$$\approx 0.002 \frac{m^2 v^3}{n_e e^4} \quad . \qquad (5\text{-}31b)$$

The deflection relaxation time is usually less than the energy relaxation time, τ_E, for electrons. The deflection relaxation lifetime of electrons in the outer trapping regions is on the order of 10 to 100 years.

5.2.3 Collisions in the Earth's Atmosphere

A trapped particle is effectively removed if it loses enough energy in successive collisions that it is no longer distinguishable from low-energy ambient particles ($T \approx 1,000$ to $2,000$ K). A trapped particle also is lost if its trajectory is altered by collisions so that it enters a low-altitude region of the atmosphere where it may be stopped within a small fraction of its bounce period. Although a single violent collision would suffice to substantially alter the pitch angle, a large number of successive small deflections can have the same effect.

The earth's atmospheric density, ρ, decreases with altitude, h, roughly according to the hydrostatic equation:

$$\frac{d\rho}{dh} \cong -\frac{\rho}{H} \exp(-h/H) \quad . \qquad (5\text{-}32)$$

The parameter H is called the scale height. The scale height in the lower atmosphere is of the order 7 kilometers, so the number of molecules and atoms per cubic centimeter falls from about 10^{20} at the surface to less than 10^{11} above 120 kilometers. The scale height increases in the upper atmosphere, but the number density still is generally less than 10^6 atoms per cubic centimeter at 1,000-kilometer

altitude. Generally, trapped particles can be found with mirror altitudes down to 120 to 150 kilometers. Below 120 kilometers the atmospheric density increases so fast that stably trapped particles never are found there. Further details regarding atmospheric parameters are in Section 12.

If it is trapped so that it never comes below several thousand kilometers altitude, a charged particle will spend its life in what is essentially a tenuous vacuum. Its lifetime is much greater than its gyro-period, bounce period, drift period, and other time parameters.

5.2.4 Loss of Trapped Protons in the Earth's Atmosphere

The loss of trapped heavy particles is analytically and conceptually simpler than the loss of electrons because the effects of deflections can be ignored. A further simplification can be achieved in neglecting the effects of free electrons below several thousand kilometers altitude. Many more bound electrons exist than free electrons in this region (Figure 5-6). At most altitudes, one constituent of the atmosphere predominates over all the others. In the important altitude range of 200 to 800 kilometers, most of the slowing of fast particles is due to oxygen atoms. For rough computational purposes, the average excitation potential of oxygen, $I^* \approx 97.5$ eV, may be used in Equation 5-3 or Equation 5-7. The total number of bound electrons is about eight times the total number of oxygen atoms. Where an appreciable fraction of the atmosphere is molecular and atomic hydrogen, the appropriate excitation potential is 13.9 eV. Below 200 kilometers, an acceptable average excitation potential is $I^* \approx 87$ eV (the average for air).

Protons with large kinetic energies can be involved in nuclear interactions (References 1, 12, and 15). This is the dominant loss process at very high kinetic energies, above 300 to 500 MeV. The range of protons in air is compared in Figure 5-1 with the mean free paths for nuclear interactions. The relative energy dependence of the competing slowing processes is such that, at energies only slightly below 300 MeV, nuclear interactions are virtually insignificant.

At kinetic energies below 1 MeV, a proton is susceptible to charge-exchange reactions with hydrogen and oxygen atoms. After picking up an orbital electron, the neutralized proton—now a hydrogen atom—likely will escape the trapping region before being reionized. Because of the accidental equality of their ionization potentials, oxygen and hydrogen have a resonance in the charge exchange reaction with protons (References 18 and 19). The charge-exchange cross sections for protons in hydrogen or oxygen is of order 10^{-15} to 10^{-14} square centimeter up to 10 KeV (References 16 and 17). At higher energies, charge-exchange rates fall rapidly. The mean path for charge ex-

change is shown in Figure 5-1. Clearly, charge exchange must be the dominant loss process for protons with energies less than 100 KeV. Above 1 MeV, charge exchange is negligible. (Alternating neutralization and ionization of protons mirroring at low altitudes might result in a diffusion across field lines (References 33 and 34). This process is not likely to be significant except for protons that penetrate so deeply in the atmosphere that they are already near the ends of their trapped lifetimes.)

The total rate of removal of protons from a volume in phase space (References 11 and 12) is

$$\frac{\partial f(T)}{\partial t} = \frac{\partial}{\partial T}\left[f(T)\frac{dT}{dt}\right] - f(T)\, v \sum_k n_k \sigma_k^{[loss]} \quad (5\text{-}33)$$

The first term on the right of the equal sign in Equation 5-33 is due to the gradual energy loss. The last term on the right takes account of violent interactions (nuclear reactions or charge exchange). $\sigma_k^{[loss]}$ is the cross section for the reaction and n_k is the number density of the reacting atoms (or nuclei) of species k. Lifetimes for trapped protons predicted according to Equation 5-33 are shown in Table 5-2.

Table 5-2. Energy loss lifetimes of trapped particles with pitch angles near 90 degrees (References 11 and 12).

Trapped Particles	L = 1.2 (days)	L = 1.6 (years)	L = 3 (years)
300 KeV Electron	10	6	20
2 MeV Electron	100	60	200
10 MeV Proton	50	30	100
100 MeV Proton	1825	1000	(not trapped)

In equilibrium, the trapped proton loss rate must be balanced by the production rate. The production rate will include an exterral source of strength q (per eV per cubic centimeter per second) plus the production rate of secondary protons originating in nuclear reactions. The secondary production rate can be written in terms of a cross section for secondary production $\sigma_k^{[sec]}$ and the fractional probability $W(T', \mu_o' \rightarrow T, \mu_o)$ that a reaction induced by a proton with

energy T' and equatorial pitch angle cosine μ_o' will yield a proton with energy T and equatorial pitch angle cosine μ_o. The loss and production rates should be averaged over the particle trajectories and equated. The result is the steady state equation (References 11, 12, and 35):

$$\frac{\partial}{\partial T}\left[j_o(T, \mu_o)\,\overline{\frac{dT}{ds}}\right] - \overline{j_o(T, \mu_o)\sum_k n_k \sigma_k^{[loss]}} + \overline{q(T, \mu_o)}$$

$$+ \int_T^\infty dT' \int_{-1}^{1} d\mu_o'\; \overline{j_o(T', \mu_o')\sum_k n_k \sigma_k^{[sec]}\, W_k(T', \mu_o' \rightarrow T, \mu_o)} = 0 . \quad (5\text{-}34)$$

$f_o(T, \mu_o)v$ has been replaced by the equatorial intensity $j_o(T, \mu_o)$.

The horizontal bars denote trajectory averages, i.e.,:

$$\bar{x} = \frac{\oint x\, ds}{\oint ds} = \frac{\int_{S_m}^{S_m} x \frac{dS}{\mu}}{\int_{-S_m}^{S_m} \frac{dS}{\mu}} . \quad (5\text{-}35)$$

A solution of Equation 5-33 for the case of negligible secondary production (Reference 35) is

$$j_o(T, \mu_o) = \left(\overline{\frac{dT}{ds}}\right)^{-1} \int_T^\infty dT'\; \overline{q(T', \mu_o)}$$

$$\cdot \exp\left[-\int_T^{T'} dT'' \left(\frac{dT}{ds}\right)^{-1} \overline{\sum_k n_k \sigma_k^{[loss]}}\right] . \quad (5\text{-}36)$$

The exponential function accounts for nuclear collisions. This factor can be significant only for particles with high kinetic energies and pitch angles sufficiently small that they will dip low into the atmosphere and encounter many nuclei with large cross sections, $\sigma^{[loss]}$. If the source q is fairly uniform, the form of j_o is determined primarily by the variation of $\overline{dT/ds}$ due to the atmospheric density distribution. In fact, j_o should be roughly inversely proportional to the total number of electrons encountered along the orbit. Therefore, on low L-shells, j_o and f_o should be strongly dependent on pitch angle.

That j_o depends very strongly on mirror latitude means that the omnidirectional flux J_o on the equator should increase rapidly with L

on low L-shells. The actually observed altitude dependence of J_o is consistent with atmospheric collisions being the predominant loss mechanism for protons below L = 1.4 (References 11 and 35).

Actually, on low L-shells, nearly all the trapped-particle depletion occurs within the South American anomaly region (Section 2.4.2; References 35 and 36). Therefore, the trajectory averages (Equation 5-35) should be average also over longitude.

EAST-WEST ASYMMETRY. The spatial-gradient of proton fluxes at low altitudes results in an excess of protons moving eastward. This is simply because protons moving toward the east have guiding centers above the point observation. Protons moving toward the west have guiding centers below that point. The particles with the lower guiding centers are trapped on lower field lines and, consequently, are lost more rapidly to the atmosphere. The ratio of eastward-to-westward intensities (References 37 and 38) is

$$\frac{j(\text{east})}{j(\text{west})} = \exp\left(2\rho_c \cos I/H\right) \qquad (5\text{-}37)$$

where ρ_c is the gyro-radius and I is the field-line inclination. The east-west asymmetry has been utilized to derive scale heights H within the upper atmosphere (Reference 39).

(The current that results from the inequality of fluxes in opposite directions is analogous to the current in Equation 3-101, which depends on the gradient of particle pressure.)

5.2.5 Loss of Trapped Electrons in the Atmosphere

The deflections of trapped electrons entering the atmosphere are fully as important as their loss of energy. For that reason, the Fokker-Planck equation is especially well-suited to the problem of the depletion of trapped electron belts. The Fokker-Planck coefficients must, however, be averaged over the trajectories of the trapped electrons (see Equation 5-21g); the averaged coefficients in T, μ_o coordinates are (References 10 and 35; see also Equation 5-4)

$$\langle \Delta T \rangle \cong -C \frac{c^2}{v} \sum_k n_k Z_k \ln \frac{T\sqrt{T + m_e c^2}}{2I^* \sqrt{m_e c^2}} \qquad (5\text{-}38a)$$

$$\equiv \overline{\frac{dT}{dt}} \qquad (5\text{-}38b)$$

$$\langle \Delta\mu_o \rangle = -\frac{1}{2} C \frac{c^2}{v} \frac{m_e c^2}{T(T+2m_e c^2)} \frac{1}{\mu_o^3} \frac{(1-\mu_o^2)}{(1-\mu^2)} (\mu^2 - \mu_o^2 + \mu^2 \ldots \sum_k n_k Z_k^2 \ell n \Theta_{[min]}^{-1} \quad (5-39)$$

$$\langle (\Delta\mu_o)^2 \rangle = C \frac{c^2}{v} \frac{m_e c^2}{T(T+2m_e c^2)} \frac{1}{\mu_o^2} \frac{(1-\mu_o^2)}{(1-\mu^2)} (\mu^2 - \mu^2 \mu_o^2) \sum_k n_k Z_k^2 \ell n \Theta_{[min]}^{-1} \quad (5-40a)$$

$$\equiv 2 \frac{c}{v} \frac{m_e c^2}{T(T+2m_e c^2)} D(\mu_o) \quad (5-40b)$$

$$\langle \Delta T \Delta\mu_o \rangle = 0 \quad (5-41)$$

$$\langle (\Delta T)^2 \rangle \approx 0 \quad . \quad (5-42)$$

The number of orbital electrons in an atom of species k has been denoted by Z_k. Only the dynamical friction (Equation 5-38) is proportional to the total number of bound electrons – the other coefficients contain an extra Z factor. The minimum scattering angle in the center-of-mass frame is $\Theta_{[min]}$. The Fokker-Planck coefficients have been evaluated and can be found in References 10, 35, and 36.

The Fokker-Planck equation for the atmospheric loss of trapped electrons reduces to a diffusion-type equation for the distribution function at the equator $f_o(T, \mu_o)$ (in particles per unit energy, per steradian, per unit volume) (Reference 10):

$$\frac{\partial f_o(T,\mu_o)}{\partial t} = \frac{1}{2\pi v t_b} - \frac{\partial}{\partial T}\left[f_o(T,\mu_o) v t_b \overline{\frac{dT}{dt}} \right] + \frac{1}{\mu_o t_b} \frac{\partial}{\partial \mu_o}\left[D(\mu_o)\ \mu_o t_b\ \frac{\partial f_o(T,\mu_o)}{\partial \mu_o} \right] \quad (5-43)$$

where t_b is the bounce period.

The energy loss part of Equation 5-43 could have been written in terms of the total number of particles in a magnetic flux tube per unit μ_o, per unit cross sectional area at the equator:

$$N_o(T,\mu_o) = 2\pi f_o(T,\mu_o)\, v \mu_o\, t_b \quad . \quad (5-44)$$

The pitch-angle deflection part of Equation 5-43 describes a diffusion process in pitch-angle space (for a further discussion of pitch-angle diffusion see Section 5.5.5).

The coefficients $\overline{dT/dt}$ and D are both extremely sensitive to μ_o near the atmospheric cutoff. It is primarily this fact that has prohibited analytic solution of Equation 5-43; the solution has been generally through numerical computations (References 10, 35, 36, 40, and 41). The results of a sample calculation, assuming injection strongly concentrated at one energy and pitch angle, are shown in Figure 5-5. In the figure, injection into the trapped-radiation belts was concentrated at an equatorial pitch angle α_o = arc cos μ_o = arc cos 0.25 and a kinetic energy of T = 1.5 MeV. The successive views represent "snapshots" at the times 90, 190, 365, and 900 days after the initial injection event. The flux intensity $j(cm^{-2}sec^{-1}MeV^{-1}ster^{-1})$ is given as a function of μ and kinetic energy T. The effect of collisions is to broaden the distributions and degrade the energy. Eventually, of those injected at an intermediate pitch angle, the only trapped particles remaining have mirror points near the equatorial plane.

Below $L \approx 1.25$, agreement of theory and observation leaves little doubt that, during periods of weak geomagnetic activity, electrons are lost primarily through atmospheric collisions. The electron fluxes resulting from the Starfish-high-altitude nuclear explosion decayed by as much as an order of magnitude within the first few days. During this time, several competing loss mechanisms may have been effective. After several weeks, the major irregularities in the pitch angle distributions disappeared and the decay leveled off to a nearly exponential behavior. By that time, the exponential decay rates were about the same everywhere on any L-shell. Observed and predicted decay rates are shown later in this section (Figure 5-13).

Above $L \approx 1.25$, the decay after several weeks was exponential but the observed fluxes lay somewhat above the theoretical predictions. This seems to imply either an additional steady source of electrons or displacement of electrons toward lower L-shells (Reference 42). Diffusion of particles across L-shells seems to be the likeliest explanation. This topic is discussed in Section 5.4.

In the outer part of the trapped radiation belts, intensity variations occur over short time intervals that cannot be reconciled with slow diffusion and atmospheric loss. Lifetimes of some outer-belt particles may be as short as several days. Although the depletion of trapped-particle belts through atmospheric collisions is always effective, additional loss processes of comparable importance must be considered.

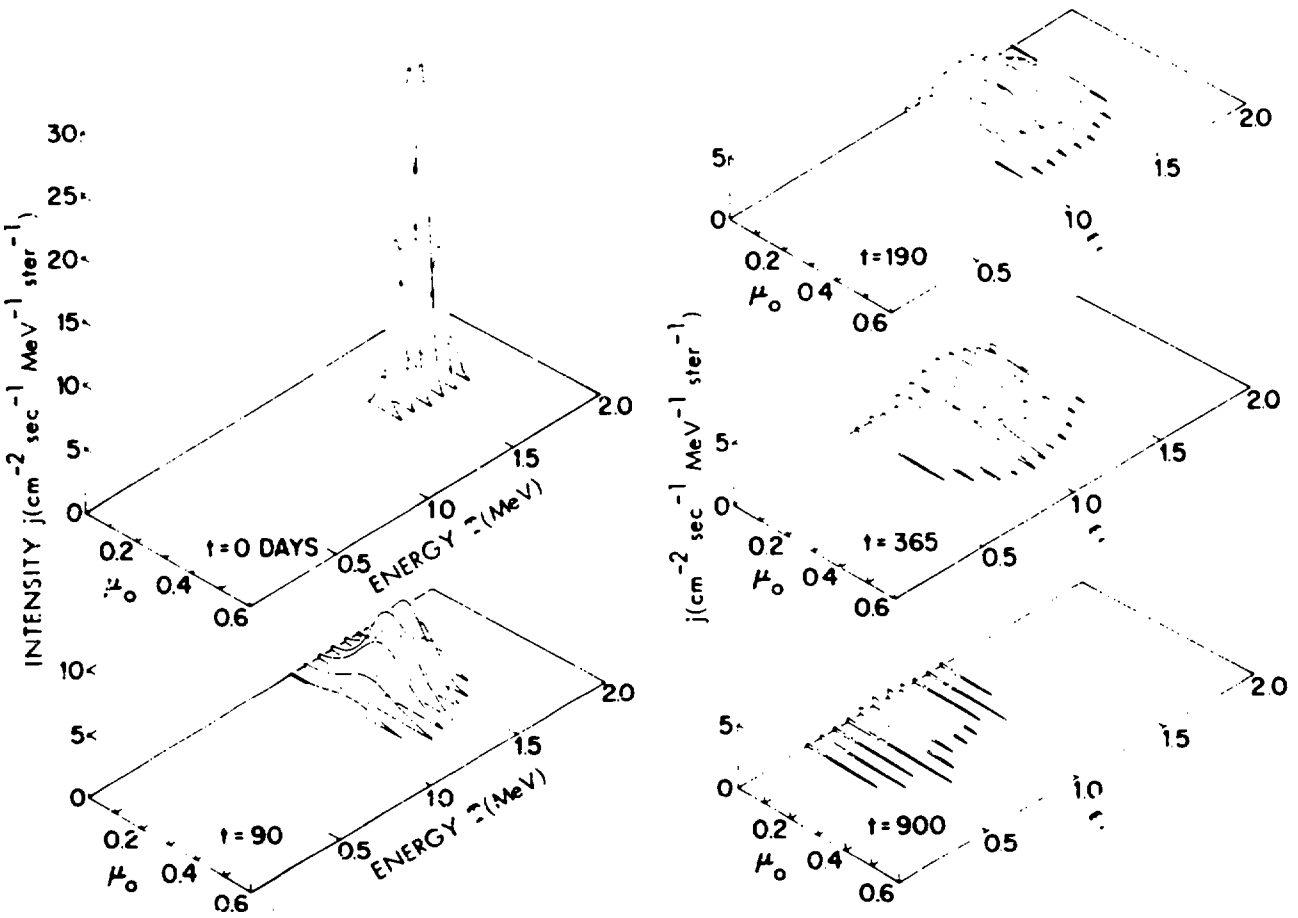

Figure 5-5. Diffusion of a group of electrons in energy, pitch angle space (Reference 40). Injection into the trapped radiation belts was concentrated at an equatorial pitch angle $\alpha_o = \arccos \mu_o = \arccos 0.25$ and a kinetic energy of $T = 1.5$ MeV. The successive views represent "snapshots" at the times 90, 190, 365, and 900 days after the initial injection event. The flux intensity j(cm^{-2} sec^{-1} MeV^{-1} ster^{-1}) is given as a function of μ and kinetic energy T.

5.3 INJECTION OF TRAPPED PARTICLES THROUGH NUCLEAR DECAYS

5.3.1 Injection of Trapped Particles

The source term, $q(T, \mu_o)$, in Equation 5-34 represents the instantaneous appearance of trapped particles with a given energy and pitch angle. Charged particles may be introduced in many ways--as products of fission fragment decays (the decay of fission fragments is discussed in Section 12), as products of neutron decays, as products of ionization, or as products of charge-transfer reactions (between atoms and ions). The decay of a neutron leaves behind a fast proton and a fast electron. This mechanism, which will be discussed in Section 5.3.2, therefore would appear a likely source of either kind of trapped particle.

The rate of injection $q(T, \mu, S, \psi)$ generally depends not only on energy, T, and pitch angle, μ, but also on location on the field line, S, and on azimuthal angle, ψ, referred to the field line. The rate of increase in $f(T, \mu, S)$ (averaged over ψ) due to injection in a segment δS of the field line is

$$\frac{df(T, \mu, S)}{dt} = \frac{\left[\int_o^{2\pi} q(T, \mu, S, \psi)\, d\psi\right] \delta S}{\pi \mu v t_b} \quad . \tag{5-45}$$

Note the factor μ in the denominator—isotropic injection does not result in isotropic trapping. With the aid of Liouville's equation (Equation 3-82) the rate of increase in $f_o(T, \mu_o)$ at the equator due to injection everywhere on the field line can be found. The result is

$$\frac{df(T, \mu_o)}{dt} = \frac{\oint \frac{dS}{\mu} \int_o^{2\pi} d\psi\, q(T, \mu, S, \psi)}{2\pi \oint \frac{dS}{\mu}} \quad . \tag{5-46}$$

The integration must follow a particle trajectory. If the injection rate is independent of ψ, the rate of increase is just $\overline{q(T, \mu_o)}$, as discussed in Section 5.2.4.

5.3.2 The Cosmic Ray Albedo Neutron Theory of Trapped Radiation Belt Formation

The albedo neutron theory of the trapped particle belts may be briefly outlined thus (References 11, 12, 43, and 44): Cosmic rays colliding with atmospheric nuclei produce neutrons; some of these neutrons, the albedo neutrons, leave the atmosphere, whereupon they decay leaving in their place charged particles that can be trapped. The expected numbers of trapped particles depend on the rates at

which neutrons leave at the top of the atmosphere. The outgoing neutron flux is very uncertain though it appears that a substantial portion of the high-energy trapped protons below $L \approx 1.5$ may be accounted for by decay of albedo neutrons (References 11 and 12).

Neutrons are produced by cosmic rays in (p,n) and similar reactions (References 45 and 46). The neutrons may decay in flight, with a half life of about 11 minutes or, more probably, may be lost in atmospheric collisions (Reference 47). Very few neutrons reach low enough altitudes that they can be easily detected. Direct observations of fast neutron fluxes is hindered by experimental difficulties so the neutron flux at high altitudes is poorly known. Most estimates of albedo neutron fluxes have been derived from the basic processes affecting neutrons rather than from extrapolations of observations (References 46 and 48 through 52). The number escaping, which is not a large fraction of the number produced, is therefore very uncertain.

High-energy neutrons, say at kinetic energies greater than 50 MeV, are deflected only slightly in the atmosphere. Therefore, the fast-neutron component of the albedo flux escapes nearly tangential to the horizon—being produced by cosmic rays with paths that do not intersect the earth's surface. The angular spread of the emergent beam of neutrons is determined primarily by the angular distribution of particles produced in cosmic ray "stars" (Reference 45). Fast secondary particles in turn may interact with other atomic nuclei; about three fourths of all neutron-generating interactions are due to secondary particles. Most of the albedo neutrons with kinetic energies greater than 1 GeV are in a beam less than 10 degrees wide. Only below 60 MeV is the width of the beam more than 60 degrees.

There is a latitude variation in the energies of cosmic rays which can penetrate the atmosphere; this is a consequence of the fact that cosmic rays cannot enter the forbidden regions discussed in Section 3.2.3. At latitudes beyond 60 to 70 degrees, solar cosmic rays can penetrate the atmosphere and contribute to the neutron albedo. The kinetic energies involved are moderate, 10 to 100 MeV, and the neutron production rates are expected to vary throughout the 11-year solar cycle. Neutrons are produced nearly isotropically in the center of mass reference frame. The angular distribution of albedo neutrons is therefore fairly broad (References 11 and 12).

Each neutron decay releases a proton with a kinetic energy nearly equal to that of the neutron. High-energy protons can be injected only when the projection of the initial velocity vector is tangent to the top of the atmosphere. The rate of injection can be approximated by:

$$\frac{df(T, \mu_o)}{dt} \cong \bar{q}^{\gamma}(T) \quad \frac{\oint \eta(\mu, S) \frac{dS}{\mu}}{\oint \frac{dS}{\mu}} \tag{5-47}$$

where η is the fraction of the trajectory over which injection is possible and $\overline{q'}$ is an equivalent isotropic injection rate. Figure 5-6 shows how the pitch angle cone of halfwidth α_p at any point on a field line intersects the earth's atmosphere. Only within the shaded strip of the figure can neutrons be emitted (from the top of the atmosphere) that can decay at point P, thus releasing protons with the pitch angle α_p. Some pitch angle cones intersect the earth at all azimuthal angles; others do not intersect the earth anywhere (e.g. small pitch angles near the equator. It is evident that only a very small

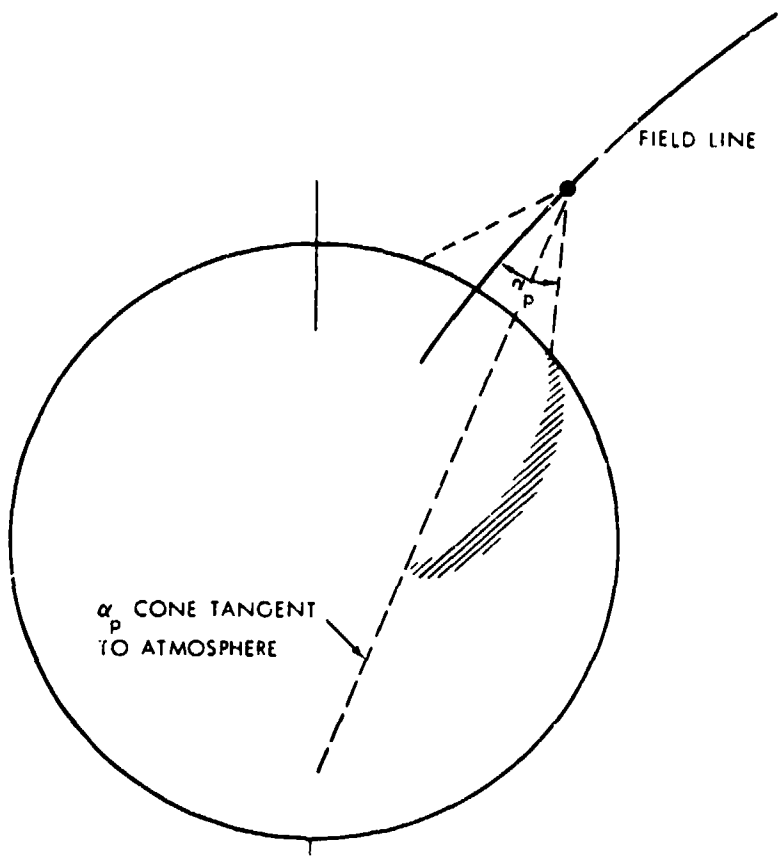

Figure 5-6. The intersection of a pitch angle cone with the earth's surface.

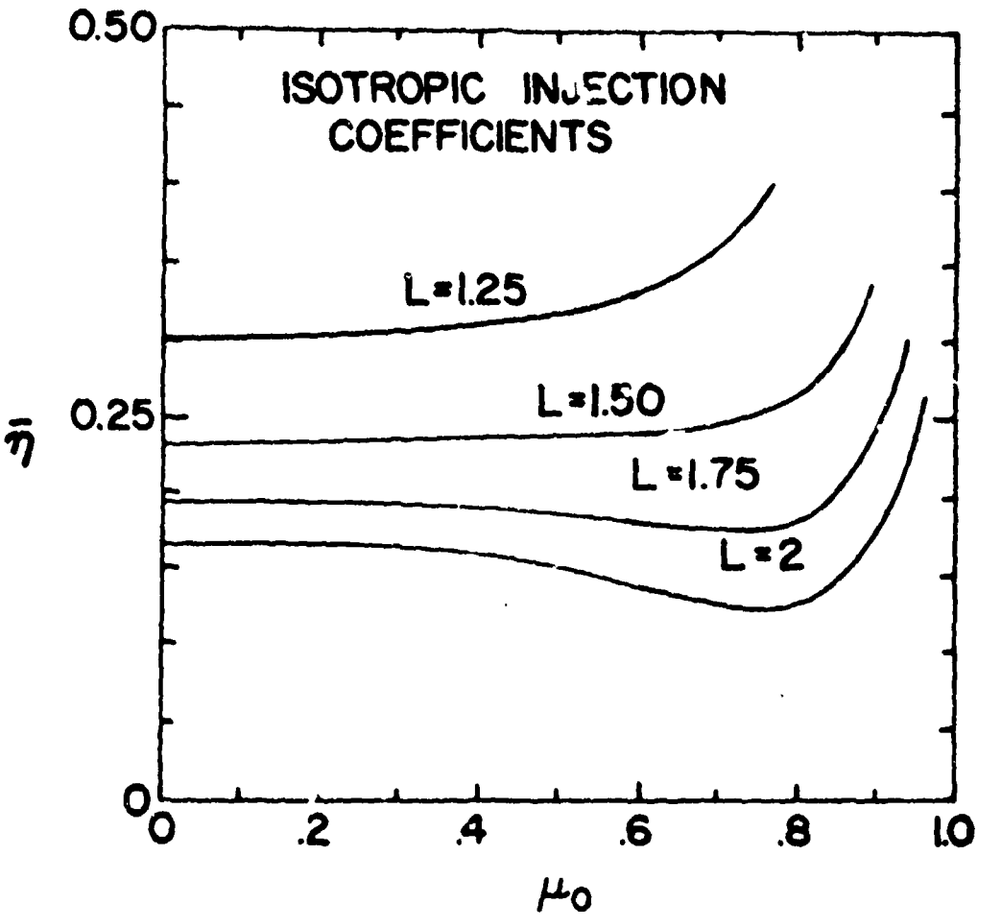

Figure 5-7. Equatorial pitch angle dependence of the average injection coefficient $\bar{\eta}$ for an isotropic neutron flux emerging from the atmosphere (References 11 and 12).

part of the pitch angle cone is within several degrees of being tangential to the atmosphere. Low-energy protons ($T \leq 50$ MeV) are injected nearly isotropically; η is then just the fraction of the pitch angle cone that intersects the earth. Some computed values of η are shown in Figures 5-7 and 5-8. In Figure 5-8, above $T \approx 50$ MeV, the effect of the finite width of the albedo neutron beam is included. The pitch angle dependence is nearly the same as in Figure 5-7.

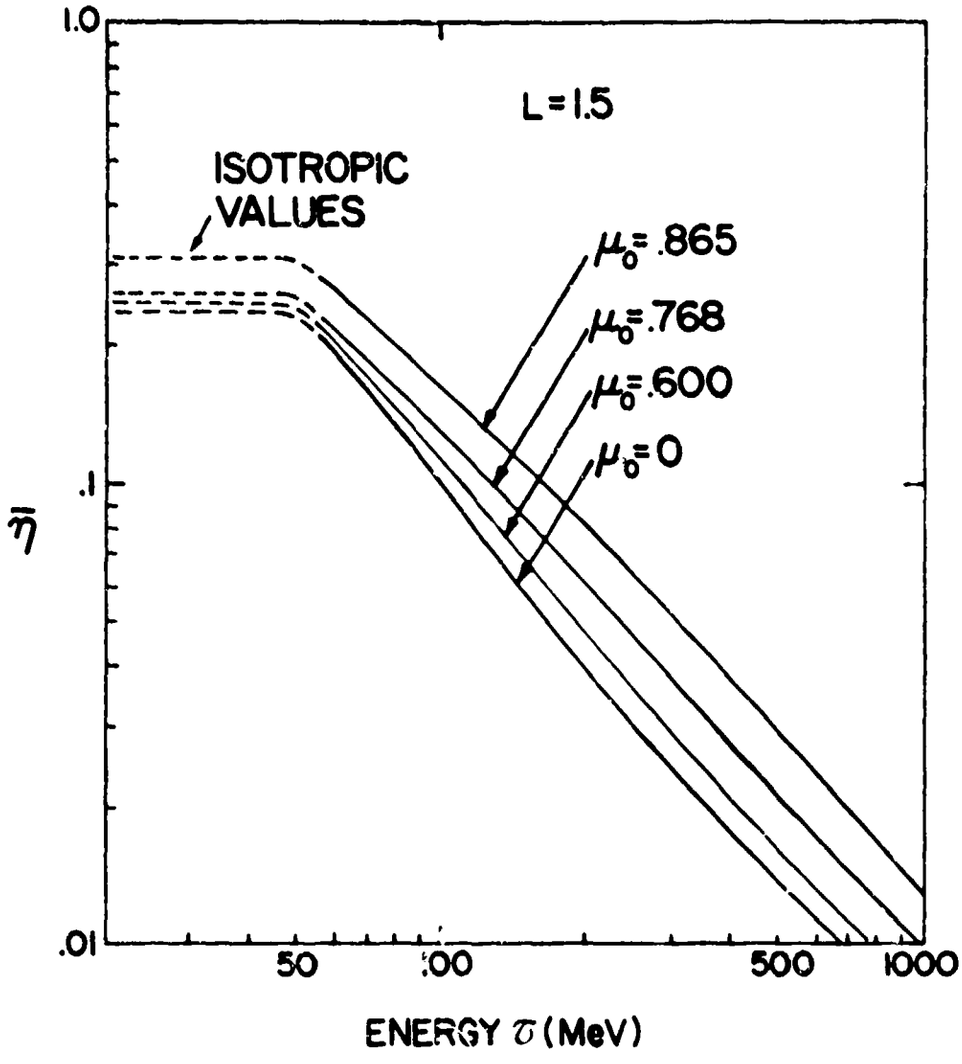

Figure 5-8. Energy dependence of average albedo neutron injection coefficient (References 11 and 12). Above $T \approx 50$ MeV, the effect of the finite width of the albedo neutron beam is included. The pitch angle dependence is nearly the same as in Figure 5-7.

The high-energy protons of the lower trapped radiation belt are fairly well accounted for by the albedo neutron-decay theory (Reference 12). The slope of the observed energy spectrum above 50 MeV is matched well by the predicted spectrum (Section 4.2). Some recent studies combining neutron decay and radial diffusion are discussed in Section 5.4.4. At lower kinetic energies, the numbers of trapped protons are much too great to be attributed solely to decay of fast neutrons. The low-energy albedo neutrons produced by solar cosmic rays might yield appreciable numbers of low-energy protons. However, these solar cosmic ray albedo neutrons cannot reach the equator at low altitudes; they cannot be responsible for an enhancement of trapping of protons with large pitch angles.

LOW ENERGY ALBEDO NEUTRONS. High-energy trapped protons can be attributed to decays of fast neutrons. The same source is relatively ineffective in producing trapped electrons; the low-energy trapped electron number density is nearly everywhere much larger than the trapped proton density. It has been suggested that the electrons could be injected by low-energy albedo neutrons (References 43 and 44). However, neutrons with kinetic energies below 1 MeV are deflected appreciably within the atmosphere. For that reason, considering a diffusion-type problem is necessary to obtain the albdeo flux.

For any quantity that is transported through a material medium, in this case j (the number of neutrons per square centimeter per ster per second), a Boltzmann-type equation can be formulated. The Boltzmann equation (Equation 3-91) gives the rate of change of a number density in a volume element that follows the flow. The general transport equation for j in a plane-layered medium (References 53, 54, and 55) is

$$\zeta \frac{\partial j(T, \zeta, h)}{\partial h} + j(T, \zeta, h)\, n\sigma(T, \zeta) = q(T, \zeta, h) + \int_{T}^{\infty} dT' \int_{-1}^{1} d\zeta'\, j(T', \zeta', h)\, n\sigma(T', h)\, W(T', \zeta' \rightarrow T, \zeta) \qquad (5\text{-}48)$$

where h is the depth measured perpendicular to the layers. The first term on the left denotes the rate of depletion (or augmentation) of a stream of particles moving at an angle arc cos ζ from the normal to the plane (note the similarity to Equation 3-34 when ζ is replaced by μ_0). The second term is the rate of loss by collisions, σ is the

total cross section, and n is the number density of scatterers. Particles are added to the stream by a source of strength q, or by scattering, with a fractional probability W, from all other energies, T', and angles, arc cosine ζ'. Slow neutrons scatter almost isotropically, in which case the scattering probability σW is equal to the product of a constant σ_s (which, of course, must be less than or equal to σ) and $W(T' \rightarrow T)$.

When Equation 5-48 is integrated over ζ, a simplified equation is obtained in terms of the omnidirectional neutron flux J and the flux across a constant-h surface F (Section 3.5.2; Reference 53):

$$4\pi \frac{\partial F(T)}{\partial h} + J(T)\, n\sigma = Q(T, h) + \int_{T}^{\infty} dT'\, J(T')\, n\sigma_s\, W(T' \rightarrow T) \qquad (5\text{-}49)$$

where Q now represents an average source strength:

$$Q(T, h) = \frac{1}{2} \int_{-1}^{1} d\zeta\, q(T, \zeta, h) \; . \qquad (5\text{-}50)$$

Equation 5-49 can be solved by standard numerical methods (References 48, 53, 54, 55, and 56).

Equation 5-49 has a form that resembles a conventional diffusion equation. In the lower atmosphere, where the mean path lengths are so short that j is nearly independent of ζ, the first term in Equation 5-49 may be replaced by

$$\frac{\partial}{\partial h}\left(D \frac{\partial J}{\partial h}\right) \; .$$

D is a diffusion coefficient (References 46, 51, 52, and 54). Unfortunately, the free paths of neutrons near the top of the atmosphere are large compared with other dimensional parameters. Consequently, the anisotropies are great enough that the diffusion equation solution does not give entirely reliable results for the flux at the top of the atmosphere.

An additional complication is that neutrons of energies much less than 1 eV cannot leave the earth's gravitational field. This has the effect of increasing the rate of neutron decays near the earth, though the albedo is diminished only slightly (Reference 46).

Various solutions to the neutron-transport problem have appeared. They are all normalized to measured fluxes of neutrons of cosmic rays observed at low altitudes. Figure 5-9 shows computed rates of neutron decays near the earth. These should be the same as the rates of electron injection (References 44, 45, and 46). The electrons released from slow neutron decays above the atmosphere are injected into the trapping regions nearly isotropically.

Albedo neutron decay is definitely inadequate as the sole source of trapped electrons (References 35, 43, and 44). Additionally, it is significant that the energy spectrum of trapped electrons is much different from that of the neutron decay component (Reference 57).

5.4 NONCONSERVATION OF THE THIRD ADIABATIC INVARIANT

15

5.4.1 Hydromagnetic Stability of Trapped Radiation

Simple two-particle interactions are inadequate to explain all the observations relevant to trapped particle sources and losses. The remainder of this chapter is concerned with the effects of plasma oscillations and collective behavior of large numbers of particles. A first consideration is whether the trapped radiation belts are always stable against gross instabilities, primarily involving violation of the third adiabatic invariant Φ.

The $\bar{J} \times \bar{B}$ term in the mechanical force equation (Equation 3-100) can be simplified readily with the aid of Maxwell's Equations (Equation 3-108). The result is

$$\bar{J} \times \bar{B} = - \nabla \frac{B^2}{8\pi} + \nabla \cdot \frac{\bar{B}\bar{B}}{4\pi} \qquad (5\text{-}51)$$

The expression on the right of Equation 5-51 may be identified with the divergence of the Maxwell stress tensor (Reference 58):

$$\bar{\bar{T}} = \frac{1}{4\pi} \begin{bmatrix} \frac{1}{2}B_x^2 + \frac{1}{2}B_y^2 + \frac{1}{2}B_z^2 & - B_x B_y & - B_x B_z \\ - B_y B_x & \frac{1}{2}B_x^2 - \frac{1}{2}B_y^2 + \frac{1}{2}B_z^2 & - B_y B_z \\ - B_z B_x & - B_z B_y & \frac{1}{2}B_x^2 + \frac{1}{2}B_y^2 - \frac{1}{2}B_z^2 \end{bmatrix} \qquad (5\text{-}52)$$

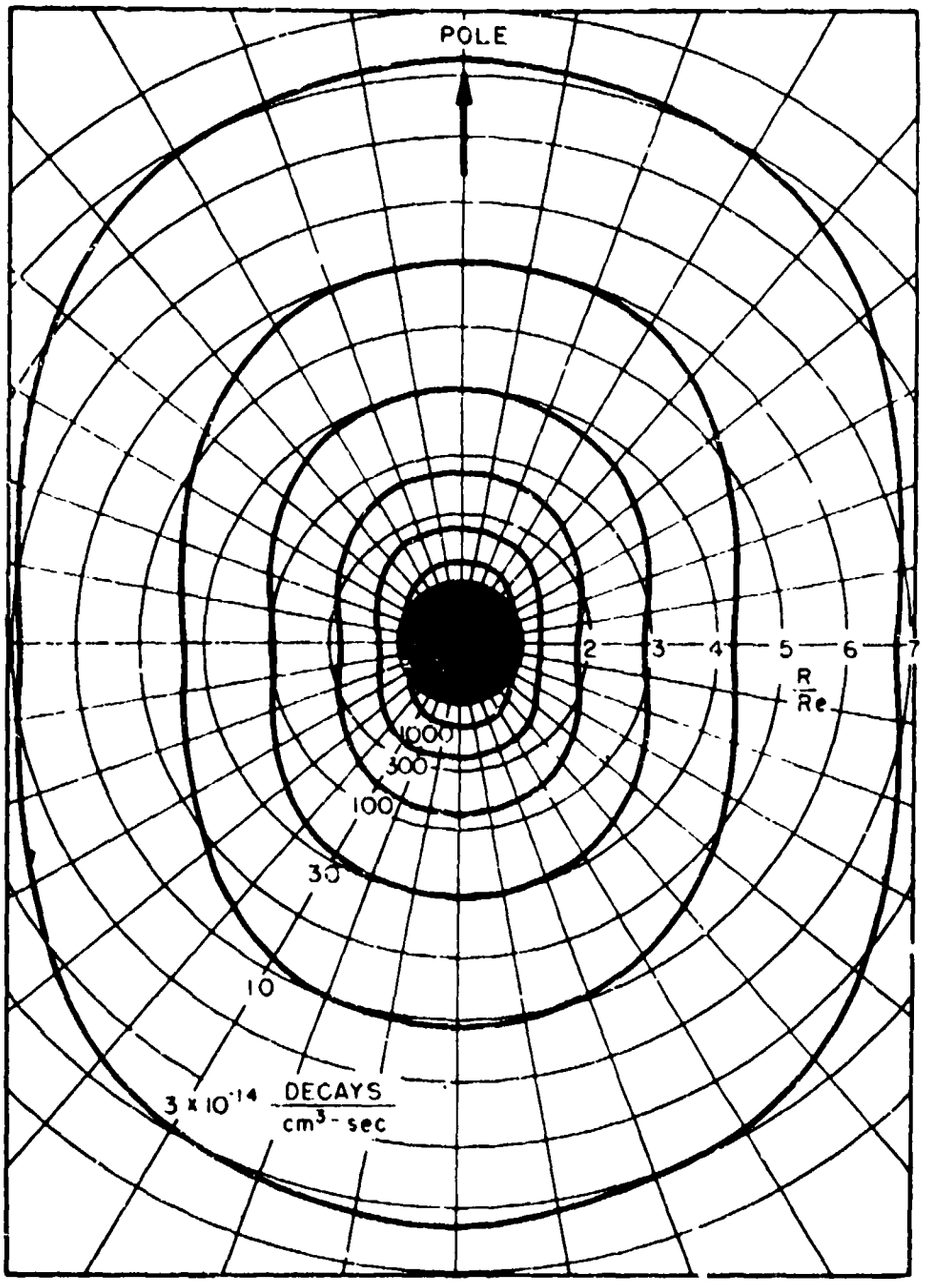

Figure 5-9. Neutron decay rate contours near the earth (Reference 46).

The mechanical force equation then can be written in the concise form:

$$\rho \frac{\partial \bar{v}}{\partial t} = - \nabla \cdot (\bar{\bar{T}} + \bar{\bar{P}}) \quad . \tag{5-53}$$

The magneto-mechanical stresses are equivalent to a pressure $B^2/8\pi$ transverse to the field lines and a tension $B^2/8\pi$ along the field lines (References 32, 58, and 59).

The ratio of the transverse particle pressure to the magnetic pressure is a useful criterion of the relative importance of particles versus field (Reference 60). If the ratio

$$\beta_p = \frac{\sum_{[\text{all particles}]} \gamma m v_\perp^2}{B^2/8\pi} \tag{5-54}$$

is much greater than unity, the medium behaves as a classical fluid and the magnetic field has little effect on the gross motion. Conversely, if β_p is extremely small, so little energy is contained in the particles that the effects of collective behavior are likely to be insignificant. When β_p is computed for observed naturally trapped particles, the result is generally much less than 1. If β_p (in any part of the radiation belts) should ever exceed about 0.1, the radiation belts would very likely exhibit all the types of plasma instabilities observed in mirror machines in the laboratory (References 60, 61, and 62).

The parameter β_p is nearly the ratio of particle kinetic energy to magnetic field energy. The magnetic field energy contained within a narrow range, δL, of L shells between the two conjugate intersections with the atmosphere is

$$\delta W = \frac{1}{2} R_E^3 B_E^2 \frac{\sqrt{L-1}}{L^{5/2}} \delta L \quad . \tag{5-55}$$

The total integrated magnetic energy between the earth's surface and a shell of field lines is shown in Figure 5-10. (The unit of energy in the figure is equivalent megatons of TNT explosive energy; 1 MT = 4.2×10^{22} erg.) The total kinetic energy of the particles trapped within an L shell is not expected to appreciably exceed the magnetic field energy.

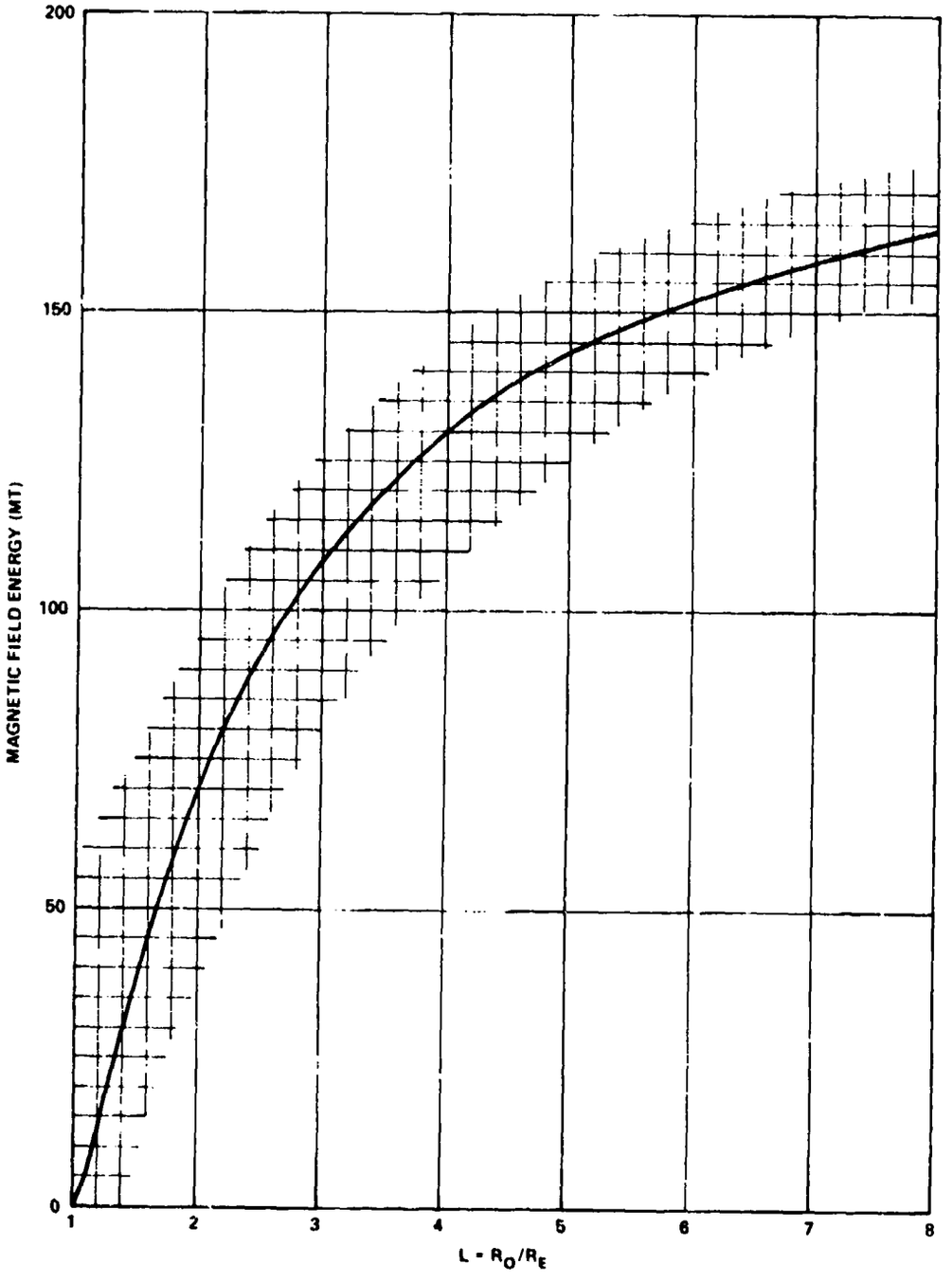

Figure 5-10. Total magnetic field energy in the volume contained between the earth's surface and a shell of field lines at $L=R_O/R_E$. The unit of energy in the figure is equivalent megatons of TNT explosive energy; 1 MT = 4.2×10^{22} erg = 4.2×10^{15} joule.

Usually β_p varies considerably along a field line, although in most observed cases of distributions stable over periods of days, the largest β_p is generally at the equator. The largest β_p can be used to estimate the saturation fluxes for any assumed pitch-angle distribution. A reasonable upper limit for β_p might be somewhat less than 1-perhaps of the order of 0.1. The limit on β_p is invoked in Section 7.3.2 to predict the maximum trapped fluxes that might occur following a high-altitude nuclear detonation.

If all the trapped particles are assumed to have the same energy, the maximum β_p can be computed for a pitch-angle distribution of the form (this is very nearly the distribution which would result from pitch-angle diffusion alone on moderate and high L-shells; see also Section 5.5.5 and the following)

$$j_o = \frac{2+n}{8\pi\mu_c^{n+1}} J_o(\mu_c^2 - \mu^2)^{n/2} \Big\} \; |\mu| \le \mu_c$$

$$= 0 \Big\} \; |\mu| > \mu_c \quad . \tag{5-56}$$

The omnidirectional flux in the equatorial plane is J_o. For all $n \ge 0$, the minimum β_p occurs at the equator. The maximum flux, in terms of the assumed pressure ratio, is

$$J_o = \frac{B_E^2 \beta_p}{8\pi L^6 p} / \left[1 - \mu_c^2 \; 8/(6+n)(4+n)\right] \tag{5-57a}$$

$$\approx 7.25 \times 10^{13} \frac{\beta_p}{p(\text{MeV/c})} \; \frac{(6+n)(4+n)}{L^6[(6+n)(4+n)-8] + 8L^3/\sqrt{4-3/L}} \tag{5-57b}$$

where the atmospheric cutoff has been substituted for μ_c.

5.4.2 Interchange Instability in the Outer Trapping Regions

A plasma may be expected to be confined by a magnetic field that provides a sufficiently great magnetic pressure on the exterior to counteract the particle pressure of the plasma that is seeking to escape. This is not always possible, though. The instability that results if two fluids (in the present case, a plasma and a magnetic field) can exchange positions with a consequent decrease in total

energy is known as the Rayleigh-Taylor instability (Reference 58). This instability is well known from early laboratory studies where it was called the fluting or interchange instability because a plasma boundary tends to break up into grooves or "flutes" as the plasma leaks out, carrying along the field lines (References 60, 61, and 62). Generally, whenever field lines at the plasma boundary are convex to the exterior, an instability results (Reference 63).

The criterion for stability at an interior point is rather complicated. Though the field lines may be convex in a direction toward which the particle density decreases, the plasma may be stable everywhere except on the extreme outer boundary. The plasma particle pressure in the exterior region may be greater than the interior pressure; the growth of instabilities thereby is restrained.

The total energy of all the particles on a field line is proportional to $\int H(M, J, \alpha, \beta)\, f(M, J, H)\, dMdJ$ where H is the Hamiltonian and M and J are the first two adiabatic invariants (References 64, 65, and 66). The Euler potentials, α and β (Section 3.4.1), are especially useful in treating hydromagnetic stability. The plasma is stable only if any exchange of two field lines and their associated trapped particles results in an increase in the total energy. With the assumptions that the adiabatic invariants M and J are preserved and that the Hamiltonian depends on only one spatial coordinate α, the necessary and sufficient criterion for stability (Reference 66) is

$$\int dM, dJ \left(\frac{\partial H}{\partial \alpha}\right)^2 \left(\frac{\partial f}{\partial H}\right)_{M, J} < 0 \quad . \tag{5-58}$$

The notation $(\partial / \partial H)_{MJ}$ refers to a partial derivative in which M and J are held fixed. Often the sufficiency criterion alone:

$$\left.\left(\frac{\partial f}{\partial H}\right)_{M, J} < 0 \quad \right\} \text{all } M, J \tag{5-59}$$

need be considered.

The stability criterion would be satisfied for almost any particle distribution if a minimum with respect to α and β existed in H. All the particles in such an energy well would have minimum energy and escape from the well would not be possible. In a dipole field, no energy wells occur, so examining the details of the distribution function is necessary to determine whether Equation 5-59 is satisfied.

The assumption that f depends only on one spatial coordinate is entirely justified for a geomagnetic field that has a high degree of

axial symmetry. The particle distribution function must be related, however, to the distribution in T, μ_o, L or T, B, L coordinates if meaningful comparisons are to be made with actually observed particle fluxes or intensities. Some of the details of the transformation are given because the intermediate results may be of general utility.

The distribution function f can be replaced by $N(M, J, \alpha)$, the number crossing the equator per unit magnetic flux, $d\alpha d\beta$. The total number of particles per energy interval and per μ_o interval in a magnetic flux tube of cross section $R_o dR_o d\phi$ is

$$N(T, \mu_o, R_o)\, R_o dR_o d\phi = J\, N(M, J, \alpha)\, d\alpha\, d\beta \quad . \tag{5-60}$$

The adiabatic invariants are related to energy and pitch angle through the Jacobian

$$J \equiv \frac{\partial(M, J)}{\partial(T, \mu_o)} = \left[\frac{\partial M}{\partial T}\frac{\partial J}{\partial \mu_o} - \frac{\partial M}{\partial \mu_o}\frac{\partial J}{\partial T}\right] \tag{5-61}$$

$$= \frac{\gamma p}{B_o} R_o \mu_o \mathcal{S}(\mu_o) \tag{5-62}$$

where $\mathcal{S}(\mu_o)$ is just vt_b/R_o, as defined in Equation 3-47. Now the coordinate β may be chosen equal to ϕ, the azimuthal angle or longitude. The corresponding α is $-M_E/R_o$ on the equator, where the magnetic flux element is

$$d\alpha\, d\beta = B_o R_o\, dR_o\, d\phi \quad . \tag{5-63a}$$

The relation between the previously defined two distribution functions is

$$N(T, \mu_o, R_o) = R_o \gamma p \mu_o \mathcal{S}(\mu_o)\, N(M, J, \alpha) \quad . \tag{5-63b}$$

The left-hand side of Equation 5-63b is related to the intensity (Equation 5-44). The relation between intensity and total number of trapped particles reduces to (References 68 and 69):

$$N(M, J, \alpha) = 2\pi m \frac{j_o(T, \mu_o)}{p^2} = \frac{N(M, J, R_o)}{B_o R_o} \tag{5-64a}$$

$$\sim \pi \frac{j_o(T, \mu_o)}{T} \quad \Big| \text{ low energies} \quad . \tag{5-64b}$$

The partial derivative with respect to H in the stability criterion can be replaced with a partial derivative with respect to R_o by the (not obvious) relation (Section 3.4.1; Reference 67):

$$\frac{\partial}{\partial R_o} = B R_o \frac{\partial}{\partial \alpha} = B R_o \frac{e}{c} \frac{\partial \beta}{\partial t} \left(\frac{\partial}{\partial H} \right)_{M,J} . \qquad (5\text{-}65)$$

However $R_o \partial\beta/\partial t$ is just the azimuthal drift velocity; therefore, $(e/c)\partial\beta/\partial t$ is always negative regardless of the sign of the electrical change. Finally, the interchange stability criterion (Equation 5-59) is

$$\left(\frac{\partial}{\partial L} \frac{j_o(T, \mu_o)}{p^2} \right)_{M,J} > 0 \quad \left\{ \text{all } M, J \right. . \qquad (5\text{-}66)$$

In the natural trapped radiation belts, most of the energy is retained by fast protons. If the protons by themselves are stable, the trapped electrons should not be able to overcome the inertia of the protons. It is probably safe to assert that the entire trapped particle belts are stable against interchange of field lines. The proton intensities are not well known for all values of M; however, all the available data indicate that the natural trapped radiation is stable as far out as $L \approx 5$ to 6 (References 67 through 71). That $N(M, J, \alpha)$ increases with radial distance may be taken as good evidence that particles are being added continually from outside (Reference 70). If particles were not continually added, the outer boundary would be subject to instabilities and the consequent loss of particles would lead to a reversal of the gradient (Equation 5-66).

The artificial electron belts resulting from the Starfish high-altitude nuclear explosion are another matter entirely. When a simplified model of the artificial electron distribution is constructed and $\partial(j_o/p^2)/\partial L$ is integrated over J, the necessary stability criterion (Equation 5-58) clearly is not satisfied (Reference 69). The results of such a computation are depicted in Figure 5-11. How a plasma behaves following the onset of instability is not very well understood. If indeed the electrons are subject to instability and the resulting hydromagnetic motion preserves M and J, then electrons might be expected to move outward with a softening of their energy spectrum. A softening of the energy spectrum of the Starfish trapped electrons may have been observed, though an interpretation on the basis of hydromagnetic instabilities is uncertain (Reference 69).

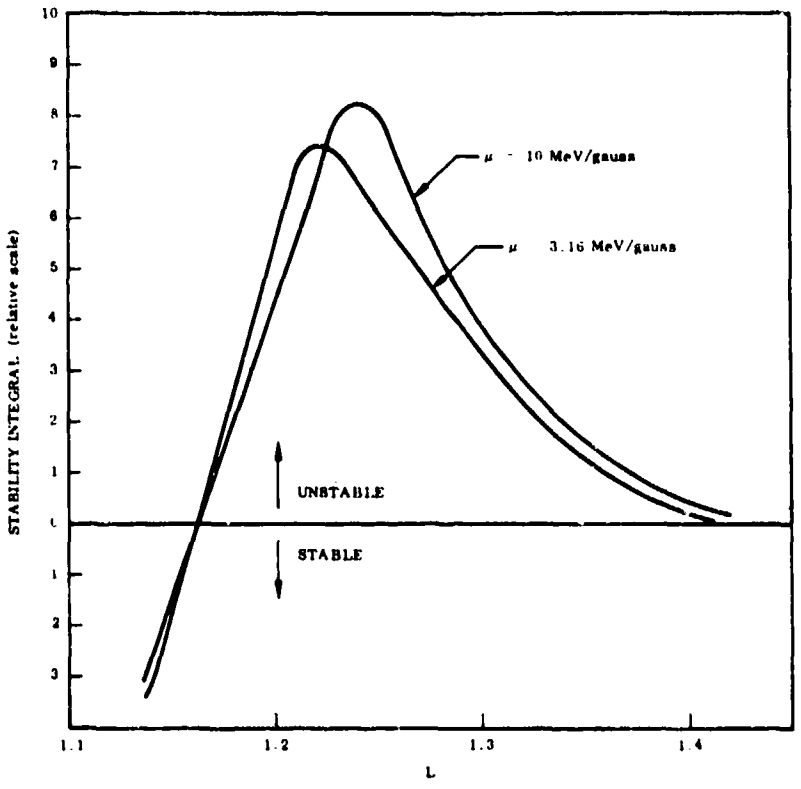

Figure 5-11. The stability function, $d(j_o/p^2)/dL$, integrated over J, the second adiabatic invariant, for the Starfish trapped electron belts (Reference 69).

The preceding discussion of hydromagnetic stability was incomplete because currents flowing in the ionosphere were ignored. In the trapped radiation belts, the field lines are effectively "frozen" into the material. If an entire field line is to exchange its position with another, the finite transverse conductivity in the ionosphere results in a relative motion of material and field lines at the lower ends of the lines. Equations 3-100 and 3-101 relate the velocity with which field lines are dragged through a plasma to the induced currents; thus:

$$\bar{J} = \bar{\bar{\sigma}} \cdot \bar{v} \times \bar{B} \qquad (5\text{-}67)$$

where $\bar{\bar{\sigma}}$ is the conductivity tensor. Substituting this in Equation 3-100, however, gives a force:

$$\bar{F} = (\bar{\bar{\sigma}} \cdot \bar{v} \times \bar{B}) \times \bar{B} \qquad (5\text{-}68)$$

contrary to the direction of motion. This force is thought to be adequate to restrain the field lines and prevent interchange.

The stability of the earth's radiation belts retaining the electric fields induced by plasma motion in the ionosphere has been analyzed (Reference 71). The energetic trapped protons can be stabilized by the ionospheric conductivity during the day, even if the simple stability criteria were violated. At night, when ionospheric electron densities are low, the ionosphere cannot be very effective in preventing instabilities.

4.3 Radial Motion of Trapped Particles as a Consequence of Nonadiabatic Behavior—Resonant Acceleration

The interchange instability leads to nonconservation of the third adiabatic invariant, Φ. If the instability occurs in a dipole field, trapped particles tend to move outwards, initially preserving the adiabatic invariants M and J. But, the stability criterion (Equation 5-67) now seems to be well satisfied in the trapped radiation belts. The interior (particle) pressure is counterbalanced by more than sufficient exterior (particle) pressure so that any mixing of particles on different L-shells might be expected to result in particles being transported inward by diffusion (References 68, 70, and 72 through 75). In fact, any process that involves nonconservation of Φ could result in inward (or outward) motion of trapped particles. Here then is a relatively uncomplicated mechanism for maintaining the radiation belts against atmospheric and other losses. Enough particles exist in the solar wind to supply all the trapped particles, provided they can get down to low enough altitudes.

Invariance of Φ requires that magnetic and electric fields do not change appreciably within the particles' drift periods (Section 3; References 64 and 65). If the fields fluctuate in a regular fashion, some particles possibly can be accelerated—somewhat as particles are accelerated in a cyclotron or betatron. Several instances have been noted in which a recurring geomagnetic fluctuation apparently resulted in acceleration of trapped electrons (References 69 and 76).

The requirements for an accelerating field seem to be met by a coherent worldwide magnetic variation with periods of about 1 hour, sometimes referred to as Dp2 or DP2 variations (References 77 and 78). Intense groups of nearly monoenergetic electrons in the lower

radiation belt were observed to be associated with several such fluctuations (Reference 76). The drift periods of these electrons were similar to the periods of the fluctuations, which exhibited several complete cycles.

Whenever the magnetic fluctuation fields are known, the electric fields in the ionosphere can be derived with the aid of known ionospheric conductivities. The majority of the electric field in the DP2 fluctuations appears to be a curl-free field ($\nabla \times \bar{E} = 0$)—derivable from a potential field (References 78 and 79). Conductivities along field lines are very large, which in turn leads to potential gradients that are nearly transverse to the field above the ionosphere. One component of the electric field will be in an azimuthal (ϕ) direction. This component is primarily responsible for particle acceleration (Reference 76). A particle with the proper drift period and phase is in resonance and experiences an accelerating force on each circuit of the earth. The situation is not exactly equivalent to the acceleration of charged particles in a cyclotron. Instead, a particle drifts inward and the resulting increase of kinetic energy is a consequence of conservation of M and J.

TRAJECTORIES OF PARTICLES CONSERVING ONLY THE FIRST AND SECOND ADIABATIC INVARIANTS. If the first and second adiabatic invariants are preserved, this simple relation (Reference 80):

$$\Phi = \pi\left(\frac{J^2}{Mm}\right)\left(\frac{\sin \alpha_o}{\mathcal{J}(\alpha_o)}\right)^2 \qquad (5\text{-}69)$$

results from Equations 3-46, 3-75, and 3-76. $\mathcal{J}(\alpha_o)$ is just that part of J that depends on the pitch angle. Equation 5-69 relates the equatorial pitch angle α_o to the flux invariant Φ. Equation 5-69 alternatively may be regarded as a relation between L and the pitch angle:

$$L = 2B_E R_E^2 \left(\frac{Mm}{J^2}\right)\left(\frac{\mathcal{J}(\alpha_o)}{\sin \alpha_o}\right)^2 . \qquad (5\text{-}70)$$

Once L and α_o are known, the mirror field B_m can be found immediately. Since M is assumed constant, the momentum squared must be proportional to B_m as a trapped particle moves across L-shells. Numerical relations between L, α_o, and B_m are given in Figures 3B-15 through 3B-19. Those figures are plotted for arbitrary values of the parameter $J^2/Mm = 2I^2 B_m$.

Of course, the distribution function $N(M, J, \alpha)$ is conserved for a group of particles that moves inward or outward together with changes in the geomagnetic field (this is because the flux $d\alpha d\beta$ is conserved). The intensity j_o therefore is seen from Equation 5-64 to be proportional to momentum squared.

When the equatorial pitch angle is large, the momentum squared is nearly inversely proportional to L^3 as a particle crosses L-shells. For mirror latitudes less than about 20 degrees, the momentum squared is nearly (within an error of less than 1 percent):

$$p^2 \cong \frac{2mB_E M}{L^3}\left[1 + \frac{3}{2\pi R_E}\sqrt{\frac{LJ^2}{B_E Mm}}\right]. \qquad (5\text{-}71)$$

Or, in terms of the initial mirror latitude λ_{m1},

$$p^2 \cong p_1^2\left(\frac{L_1}{L}\right)^3\left[1 + \frac{q}{2}\sin\lambda_{m1}\left(\sqrt{\frac{L}{L_1}} - 1\right)\right]. \qquad (5\text{-}72)$$

The subscripts 1 refer to the specified initial values.

At low energies, the square of momentum may be replaced by the kinetic energy. Equations 5-71 and 5-72 then give directly the energy gain or loss resulting from cross L-shell drift.

5.4.4 Stochastic Acceleration and L-Shell Diffusion

Most geomagnetic fluctuations are not obviously periodic (except for the daily variation). They are randomly distributed in time, with characteristic periods from fractions of a minute up to many hours. A schematic representation of the power spectrum of geomagnetic fluctuations observed on the earth's surface was presented in Figure 2-7.

That random, isolated magnetic disturbances can cause irreversible changes in the particle distribution is demonstrated readily for the type of disturbance known as a sudden commencement. During a sudden commencement, the geomagnetic field is rapidly compressed (Section 2.6.2), especially on the sunlit side of the earth. Particles continue to drift adiabatically in the distorted field, but now particles that were previously all on a single L-shell may be on quite different

invariant surfaces. The end result is that, if the compressed field is released sufficiently slowly, trapped particles will be spread over a finite range of L-shells (Reference 75). Repeated compressions and expansions of the geomagnetic field thereby can result in diffusion of particles.

Any magnetic field fluctuation with a characteristic period near the drift period can cause nonconservation of the third adiabatic invariant Φ, and acceleration of particles. The acceleration of a charged particle by random electromagnetic field fluctuations is called stochastic acceleration (References 73 and 81). Again (as in the treatment of particle collisions), a Fokker-Planck-type equation is useful in describing a process that is determined by the outcomes of many random events. The Fokker-Planck diffusion equation, for the number of particles trapped in a magnetic flux tube at R_o per unit area in the equatorial plane $N(M, J, R_o)$, is expected to be of the form:

$$\frac{\partial N(M, J, R_o)}{\partial t} = - \frac{\partial}{\partial R_o} \left[\langle \Delta R_o \rangle \, N(M, J, R_o) \right] + \frac{1}{2} \frac{\partial^2}{\partial R_o^2} \left[\langle (\Delta R_o)^2 \rangle \, N(M, J, R_o) \right] + \bar{Q} \qquad (5\text{-}73a)$$

$$= - \frac{\partial}{\partial R_o} \left[D_1 \, N(M, J, R_o) \right] + \frac{1}{2} \frac{\partial^2}{\partial R_o^2} \left[D_2 \, N(M, J, R_o) \right] + \bar{Q} \qquad (5\text{-}73b)$$

A source $\bar{Q}$ has been included here. A one-dimensional diffusion equation is valid if the diffusion proceeds with a time scale that is large compared to all other time parameters. If at any point on a field line they are transferred to another field line, the particles are rapidly "smeared" over a new invariant surface. Only on very high L-shells need the invariant surfaces be specified by more than one parameter. In the extreme outer radiation belts, a two-dimensional diffusion equation involving R_o or L and some other coordinate (such as pitch angle α_o or mirror point field B_m) would be necessary (References 28, 82, and 83).

A particular solution of Equation 5-73 is available for the case when the distribution function $N(M, J, \alpha, \beta)$ is constant everywhere. Liouville's theorem must apply to N. It is only necessary that particles should follow dynamical trajectories (Φ need not be conserved) in order that N remain unchanged after the exchange of particles between two invariant surfaces. The stability criterion (Equation 5-58)

guarantees that energy is not lost or gained. When the distribution function $B_o R_o N(M, J, \alpha)$ (Section 5.4.2) is inserted in the Fokker-Planck equation, the time rate of change must be zero. A solution (References 28, 82, 86, and 87) is:

$$D_1 = \frac{R_o^2}{2} \frac{\partial}{\partial R_o}\left(\frac{D_2}{R_o^2}\right) \quad . \tag{5-74}$$

The relation between the two Fokker-Planck coefficients should hold when sources and losses are included in the diffusion equation. Therefore, only one coefficient need be computed:

$$D = \frac{1}{2} D_2 \quad . \tag{5-75}$$

The simplified radial, or cross-L, diffusion equation may be rewritten:

$$\boxed{\frac{\partial N(M, J, R_o)}{\partial t} = -\frac{\partial}{\partial R_o}\left\{\frac{D}{R_o^2} \frac{\partial}{\partial R_o}\left[R_o^2 N(M, J, R_o)\right]\right\} + \bar{Q}} \tag{5-76}$$

The motion of a particle during a geomagnetic disturbance should be derivable directly from the equations of motion of an individual particle. The drift velocity is perpendicular to the field lines. The rate of change of R_o must be a single-valued function of the meridian plane component of the drift velocity V_D (References 81, 84, 88, 89, and 90):

$$\frac{dR_o}{dt} = V_{D[\text{meridian plane}]} \frac{\sqrt{1 + 3\sin^2\lambda}}{\cos^3\lambda} \tag{5-77}$$

where λ is the latitude of the particle at the instant an electric field is applied.

The diffusion coefficient D for a dipole field may be computed after breaking the disturbance field B into symmetric (S) and asymmetric (A) parts:

$$\begin{aligned}\tilde{B}_1 = {} & [-S(t)\cos\theta - A(t)\, r \sin 2\theta \cos\phi]\,\hat{r} \\ & + [S(t)\sin\theta - A(t)\, r \cos^2\theta \cos\phi]\hat{\theta} + [A(t)\, r \cos\theta \sin\phi]\hat{\phi}\end{aligned} \tag{5-78}$$

where $\hat{r}$, $\hat{\theta}$, and $\hat{\phi}$ are the unit vectors in an earth-centered spherical coordinate system and θ is the polar angle or colatitude. The spherical harmonic expansion of $\bar{B}_1$ has been terminated at the first-order terms. The induced electric field $\bar{E}_1$, associated with the magnetic disturbance, is (Equation 3-107)

$$\bar{E}_1 = \frac{1}{7} r^2 \frac{dA}{dt} \sin\theta \sin\phi \hat{r} - \frac{2}{7} r^2 \frac{dA}{dt} \cos\theta \sin\phi \hat{\theta}$$

$$r\left[\frac{1}{2}\frac{dS}{dt}\sin\theta - \frac{2}{21} r \frac{dA}{dt}(3 - 7\sin^2\theta)\cos\phi\right]\hat{\phi} \quad . \qquad (5\text{-}79)$$

The time average of the displacement is complicated; the computation has been performed with the result (Reference 89):

$$D_{[mag]}(L, \lambda_m) = 2\pi^2\left(\frac{5}{7}\right)^2 \Gamma(\lambda_m) \frac{R_E^2 L^{10}}{B_E^2}\left[\nu^2 P_A(\nu)\right]_{\nu=1/t_d} \qquad (5\text{-}80a)$$

$$= 16.55\, \Gamma(\lambda_m) R_E^2 L^{10}\left[\nu^2 P_A(\nu)\right]_{\nu=1/t_d} \quad . \qquad (5\text{-}80b)$$

The power spectrum is evaluated at the drift frequency. The function $\Gamma(\lambda_m)$ is presented in Figure 5-12. As might have been expected, $D_{[mag]}$ depends only on the asymmetric A part of the fluctuations. The magnetic fluctuations have been decomposed by Fourier analysis so that the power spectrum $P_A(\nu)$ is the Fourier transform of the average of $A(t)\,A(t + t')$:

$$P_A(\nu) = 4 \int_0^\infty dt' \overline{[A(t)\,A(t + t')]} \cos 2\pi\nu t' \quad . \qquad (5\text{-}81)$$

the flux of energy transported by magnetic fluctuations between the frequencies ν and $\nu + d\nu$ is proportional to $P_A(\nu)d\nu$.

A similar result follows for curl-free electric fields. When the disturbance field $\bar{E}_1$ is everywhere normal to the static magnetic field, the diffusion coefficient (References 82, 88, and 89) is

$$D_{[el]}(L, \lambda_m) = \frac{L^6}{8B_E^2} \sum_k \left[P_k(L, \nu)\right]_{\nu = 1/t_d} \quad . \qquad (5\text{-}82)$$

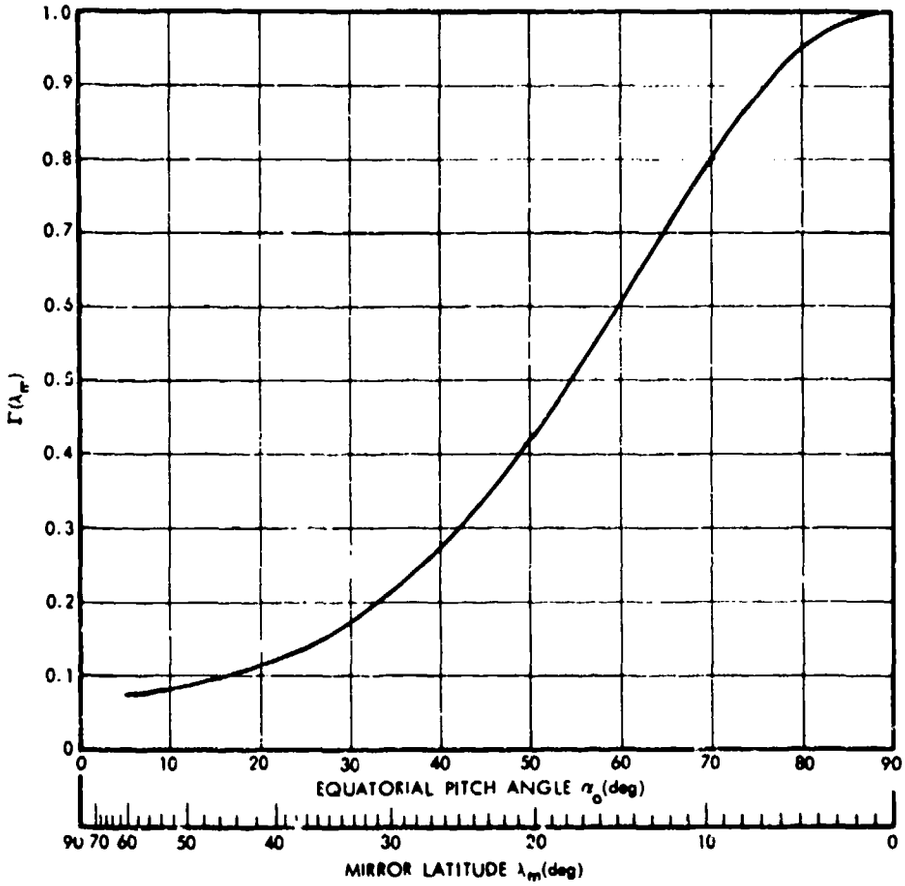

Figure 5-12. Latitude-dependent part of the radial diffusion coefficient (Reference 89).

The power spectrum, $P_k(L, \nu)$, here an explicit function of L, corresponds to the k'th component of the harmonic analysis of the electric field:

$$E_{\phi\,1}(L, \phi, t) = \sum_{k=0}^{\infty} E_{k\phi}(L, t) \cos\left(k\phi + \psi(L, t)\right) \qquad (5\text{-}83)$$

where ψ is merely a phase correction. The electric field diffusion coefficient $D_{[el]}$ depends on the mirror latitude only through the drift period t_d. The variation of drift period with mirror latitude is so slight (Equation 3-50) that $D_{[el]}$ is quite insensitive to mirror

latitude. Generally, the magnetic fluctuation diffusion coefficient $D_{[mag]}$ is much more sensitive to mirror latitude than is the electric field diffusion coefficient $D_{[el]}$. The magnetic diffusion coefficient falls so rapidly with increasing mirror latitude that magnetic acceleration effects are most important near the equatorial plane.

The magnetic fluctuation diffusion coefficient might be computed from a knowledge of magnetic disturbances observed on the earth's surface (Section 2.7). But the asymmetric part of the disturbance is proportional to radial distance, so ground-based magnetometers are sensitive primarily to S-variations. The relation between A and S is provided by the model chosen for the magnetic field. Some theoretical models have been constructed (References 89 and 91). Observational data collected with artificial satellites may be employed to further refine the models (Reference 92). Attempts have been made recently (References 93 and 94) to perform direct measurements of electric fields in the magnetosphere.

The spectral behavior of magnetic variations is not known with any more certainty than is the spatial dependence. The crude spectrum of Figure 2-17 is proportional, below about 1 hertz, approximately to the -2 power of frequency. A $P \propto \nu^{-2}$ frequency dependence is in agreement with most computations based on sudden commencements and other disturbances with a fast rise time succeeded by a slow recovery. For this special case, the diffusion coefficient is independent of drift period and is just proportional to L^{10}. Other assumed types of magnetic fluctuations yield quite different diffusion coefficients. Generally, for a power spectrum of the form:

$$P_A(\nu) \propto \nu^{-n} \tag{5-84a}$$

the diffusion coefficient (Reference 89) is

$$D_{[mag]} \propto L^{6+2n} M^{2-n} \propto L^{12-n} p^{4-2n} . \tag{5-84b}$$

EMPIRICAL COMPUTATIONS OF DIFFUSION COEFFICIENTS FROM OBSERVATIONAL DATA. The observation of an uncomplicated, unequivocal example of radial diffusion remains elusive. Because the motions of individual particles cannot be traced, observations of temporal changes in the trapped particle distribution must be relied on. But a radial motion of a group of particles is subject to being interpreted as a convective fluid motion of the entire group. On the other hand, a decay of the trapped particle flux at a single, isolated location perhaps could be explained by some other, yet undiscovered, loss process.

That the Liouville distribution function $N(M, J, \alpha)$ increases with L is suggestive of radial transport but is hardly conclusive evidence. The most compelling evidence for radial diffusion perhaps should be sought in the lower L-shells where the sources and losses are best understood. It has been noted that the artificial Starfish electron belts near L = 1.25 did not decay as rapidly as predicted from atmospheric losses alone. Computed and observed decay times are compared in Figure 5-13. Below $L \approx 1.2$, the observed decay time τ and the decay time predicted from atmospheric loss time τ_a differ enough that a cross L-diffusion coefficient can be computed. The atmospheric loss is well understood. The apparent discrepancy could only be explained by the addition of electrons diffusing from higher L-shells. The decay of the Starfish electrons can be represented by a simple empirical relation:

$$\frac{\partial N(M, J, R_o, t)}{\partial t} = - \frac{N(M, J, R_o, t)}{\tau} \tag{5-85a}$$

where τ is the time required for a decrease by a factor $1/e = 0.368$. The diffusion equation for this case can be solved analytically with the result (Reference 42):

$$D = \frac{\int_{R_{o1}}^{R_{o2}} \left[\frac{1}{\tau_a} - \frac{1}{\tau}\right] N(M, J, R_o, t)\, dR_o}{\left[\frac{1}{R_o^2} \frac{\partial}{\partial R_o}\left(R_o^2 N(M, J, R_o t)\right)\right]_{R_{o1}}^{R_{o2}}} \tag{5-85b}$$

where τ_a is the predicted atmospheric loss decay time. The momentum of particles is nearly proportional to B_o, so the relation between n and measured intensity j (Equations 5-64 and 5-72) is

$$N(M, J, R_o) \cong \frac{\pi R_o\, j_o(T, \mu_o)}{M\left[1 + \frac{3}{2\pi}\sqrt{R_o \frac{J^2}{Mm} \frac{B_E}{R_E^3}}\right]} . \tag{5-86}$$

Computations thus far have been practical only for particles with orbits restricted to the equatorial plane (where J = 0).

$$\langle \Delta\mu_o \rangle = -\frac{1}{2} C \frac{c^2}{v} \frac{m_e c^2}{T(T+2m_e c^2)} \frac{1}{\mu_o^3} \frac{(1-\mu_o^2)}{(1-\mu^2)} (\mu^2 - \mu_o^2 + \mu^2 \mu_c^2) \sum_k Z_k^2 \ln\Theta_{[min]k}^{-1} \tag{5-39}$$

$$\langle (\Delta\mu_o)^2 \rangle = C \frac{c^2}{v} \frac{m_e c^2}{T(T+2m_e c^2)} \frac{1}{\mu_o^2} \frac{(1-\mu_o^2)}{(1-\mu^2)} (\mu^2 - \mu^2 \mu_o^2) \sum_k n_k Z_k^2 \ln\Theta_{[min]k}^{-1} \tag{5-40a}$$

$$\equiv 2 \frac{c}{v} \frac{m_e c^2}{T(T+2m_e c^2)} D(\mu_o) \tag{5-40b}$$

$$\langle \delta T \Delta\mu_o \rangle = 0 \tag{5-41}$$

$$\langle (\Delta T)^2 \rangle \approx 0 \quad . \tag{5-42}$$

The number of orbital electrons in an atom of species k has been denoted by Z_k. Only the dynamical friction (Equation 5-38) is proportional to the total number of bound electrons – the other coefficients contain an extra Z factor. The minimum scattering angle in the center-of-mass frame is $\Theta_{[min]}$. The Fokker-Planck coefficients have been evaluated and can be found in References 10, 35, and 36.

The Fokker-Planck equation for the atmospheric loss of trapped electrons reduces to a diffusion-type equation for the distribution function at the equator $f_o(T, \mu_o)$ (in particles per unit energy, per steradian, per unit volume) (Reference 10):

$$\frac{\partial f_o(T,\mu_o)}{\partial t} = \frac{1}{2\pi v t_b} \frac{\partial}{\partial T} \left[f_o(T,\mu_o) v t_b \frac{\overline{dT}}{dt} \right] + \frac{1}{\mu_o t_b} \frac{\partial}{\partial \mu_o} \left[D(\mu_o) \mu_o t_b \frac{\partial f_o(T,\mu_o)}{\partial \mu_o} \right] \tag{5-43}$$

where t_b is the bounce period.

The energy loss part of Equation 5-43 could have been written in terms of the total number of particles in a magnetic flux tube per unit μ_o, per unit cross sectional area at the equator:

$$N_o(T, \mu_c) = 2\pi f_o(T, \mu_o) v \mu_o t_b \quad . \tag{5-44}$$

The pitch-angle deflection part of Equation 5-43 describes a diffusion process in pitch-angle space (for a further discussion of pitch-angle diffusion see Section 5.5.5).

The coefficients $\overline{dT/dt}$ and D are both extremely sensitive to μ_o near the atmospheric cutoff. It is primarily this fact that has prohibited analytic solution of Equation 5-43; the solution has been generally through numerical computations (References 10, 35, 36, 40, and 41). The results of a sample calculation, assuming injection strongly concentrated at one energy and pitch angle, are shown in Figure 5-5. In the figure, injection into the trapped-radiation belts was concentrated at an equatorial pitch angle α_o = arc cos μ_o = arc cos 0.25 and a kinetic energy of T = 1.5 MeV. The successive views represent "snapshots" at the times 90, 190, 365, and 900 days after the initial injection event. The flux intensity j($cm^{-2}sec^{-1}MeV^{-1}ster^{-1}$) is given as a function of μ and kinetic energy T. The effect of collisions is to broaden the distributions and degrade the energy. Eventually, of those injected at an intermediate pitch angle, the only trapped particles remaining have mirror points near the equatorial plane.

Below L ≈ 1.25, agreement of theory and observation leaves little doubt that, during periods of weak geomagnetic activity, electrons are lost primarily through atmospheric collisions. The electron fluxes resulting from the Starfish-high-altitude nuclear explosion decayed by as much as an order of magnitude within the first few days. During this time, several competing loss mechanisms may have been effective. After several weeks, the major irregularities in the pitch angle distributions disappeared and the decay leveled off to a nearly exponential behavior. By that time, the exponential decay rates were about the same everywhere on any L-shell. Observed and predicted decay rates are shown later in this section (Figure 5-13).

Above L ≈ 1.25, the decay after several weeks was exponential but the observed fluxes lay somewhat above the theoretical predictions. This seems to imply either an additional steady source of electrons or displacement of electrons toward lower L-shells (Reference 42). Diffusion of particles across L-shells seems to be the likeliest explanation. This topic is discussed in Section 5.4.

In the outer part of the trapped radiation belts, intensity variations occur over short time intervals that cannot be reconciled with slow diffusion and atmospheric loss. Lifetimes of some outer-belt particles may be as short as several days. Although the depletion of trapped-particle belts through atmospheric collisions is always effective, additional loss processes of comparable importance must be considered.

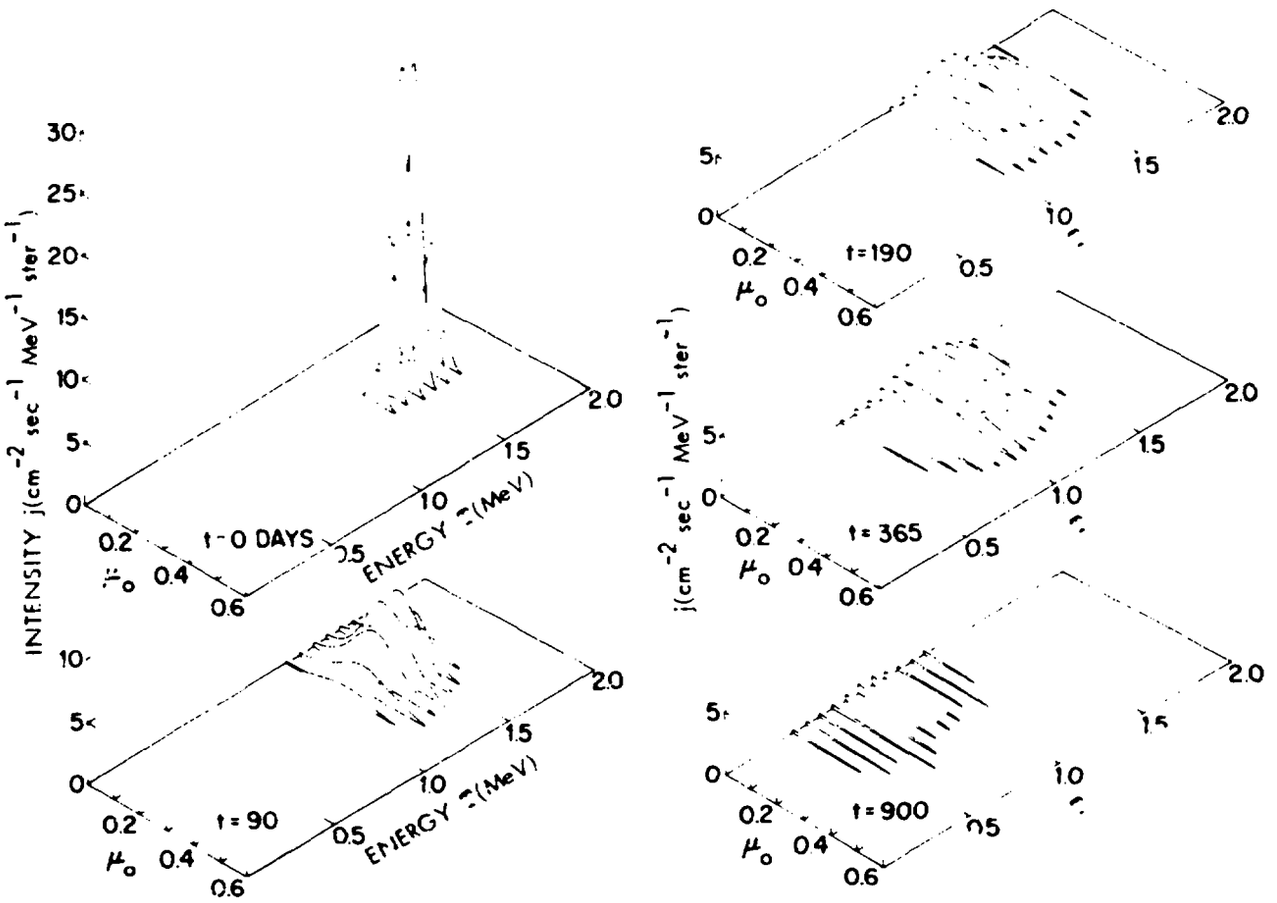

Figure 5-5. Diffusion of a group of electrons in energy, pitch angle space (Reference 40). Injection into the trapped radiation belts was concentrated at an equatorial pitch angle α_o = arc cos μ_o = arc cos 0.25 and a kinetic energy of T = 1.5 MeV. The successive views represent "snapshots" at the times 90, 190, 365, and 900 days after the initial injection event. The flux intensity j(cm^{-2} sec^{-1} MeV^{-1} ster^{-1}) is given as a function of μ and kinetic energy T.

5.3 INJECTION OF TRAPPED PARTICLES THROUGH NUCLEAR DECAYS

5.3.1 Injection of Trapped Particles

The source term, $q(T, \mu_o)$, in Equation 5-34 represents the instantaneous appearance of trapped particles with a given energy and pitch angle. Charged particles may be introduced in many ways--as products of fission fragment decays (the decay of fission fragments is discussed in Section 12), as products of neutron decays, as products of ionization, or as products of charge-transfer reactions (between atoms and ions). The decay of a neutron leaves behind a fast proton and a fast electron. This mechanism, which will be discussed in Section 5.3.2, therefore would appear a likely source of either kind of trapped particle.

The rate of injection $q(T, \mu, S, \psi)$ generally depends not only on energy, T, and pitch angle, μ, but also on location on the field line, S, and on azimuthal angle, ψ, referred to the field line. The rate of increase in $f(T, \mu, S)$ (averaged over ψ) due to injection in a segment δS of the field line is

$$\frac{df(T, \mu, S)}{dt} = \frac{\left[\int_o^{2\pi} q(T, \mu, S, \psi)\, d\psi\right] \delta S}{\pi \mu v t_b} \quad . \tag{5-45}$$

Note the factor μ in the denominator—isotropic injection does not result in isotropic trapping. With the aid of Liouville's equation (Equation 3-82) the rate of increase in $f_o(T, \mu_o)$ at the equator due to injection everywhere on the field line can be found. The result is

$$\frac{df(T, \mu_o)}{dt} = \frac{\oint \frac{dS}{\mu} \int_o^{2\pi} d\psi\, q(T, \mu, S, \psi)}{2\pi \oint \frac{dS}{\mu}} \quad . \tag{5-46}$$

The integration must follow a particle trajectory. If the injection rate is independent of ψ, the rate of increase is just $\overline{q(T, \mu_o)}$, as discussed in Section 5.2.4.

5.3.2 The Cosmic Ray Albedo Neutron Theory of Trapped Radiation Belt Formation

The albedo neutron theory of the trapped particle belts may be briefly outlined thus (References 11, 12, 43, and 44): Cosmic rays colliding with atmospheric nuclei produce neutrons; some of these neutrons, the albedo neutrons, leave the atmosphere, whereupon they decay leaving in their place charged particles that can be trapped. The expected numbers of trapped particles depend on the rates at

which neutrons leave at the top of the atmosphere. The outgoing neutron flux is very uncertain though it appears that a substantial portion of the high-energy trapped protons below $L \approx 1.5$ may be accounted for by decay of albedo neutrons (References 11 and 12).

Neutrons are produced by cosmic rays in (p,n) and similar reactions (References 45 and 46). The neutrons may decay in flight, with a half life of about 11 minutes or, more probably, may be lost in atmospheric collisions (Reference 47). Very few neutrons reach low enough altitudes that they can be easily detected. Direct observations of fast neutron fluxes is hindered by experimental difficulties so the neutron flux at high altitudes is poorly known. Most estimates of albedo neutron fluxes have been derived from the basic processes affecting neutrons rather than from extrapolations of observations (References 46 and 48 through 52). The number escaping, which is not a large fraction of the number produced, is therefore very uncertain.

High-energy neutrons, say at kinetic energies greater than 50 MeV, are deflected only slightly in the atmosphere. Therefore, the fast-neutron component of the albedo flux escapes nearly tangential to the horizon—being produced by cosmic rays with paths that do not intersect the earth's surface. The angular spread of the emergent beam of neutrons is determined primarily by the angular distribution of particles produced in cosmic ray "stars" (Reference 45). Fast secondary particles in turn may interact with other atomic nuclei; about three fourths of all neutron-generating interactions are due to secondary particles. Most of the albedo neutrons with kinetic energies greater than 1 GeV are in a beam less than 10 degrees wide. Only below 60 MeV is the width of the beam more than 60 degrees.

There is a latitude variation in the energies of cosmic rays which can penetrate the atmosphere; this is a consequence of the fact that cosmic rays cannot enter the forbidden regions discussed in Section 3.2.3. At latitudes beyond 60 to 70 degrees, solar cosmic rays can penetrate the atmosphere and contribute to the neutron albedo. The kinetic energies involved are moderate, 10 to 100 MeV, and the neutron production rates are expected to vary throughout the 11-year solar cycle. Neutrons are produced nearly isotropically in the center of mass reference frame. The angular distribution of albedo neutrons is therefore fairly broad (References 11 and 12).

Each neutron decay releases a proton with a kinetic energy nearly equal to that of the neutron. High-energy protons can be injected only when the projection of the initial velocity vector is tangent to the top of the atmosphere. The rate of injection can be approximated by:

$$\frac{df(\tau, \mu_o)}{dt} \cong \bar{q}(\tau) \frac{\oint \eta(\mu, S) \frac{dS}{u}}{\oint \frac{dS}{\mu}} \qquad (5\text{-}47)$$

where η is the fraction of the trajectory over which injection is possible and $\bar{q}'$ is an equivalent isotropic injection rate. Figure 5-6 shows how the pitch angle cone of halfwidth α_p at any point on a field line intersects the earth's atmosphere. Only within the shaded strip of the figure can neutrons be emitted (from the top of the atmosphere) that can decay at point P, thus releasing protons with the pitch angle α_p. Some pitch angle cones intersect the earth at all azimuthal angles; others do not intersect the earth anywhere (e.g. small pitch angles near the equator. It is evident that only a very small

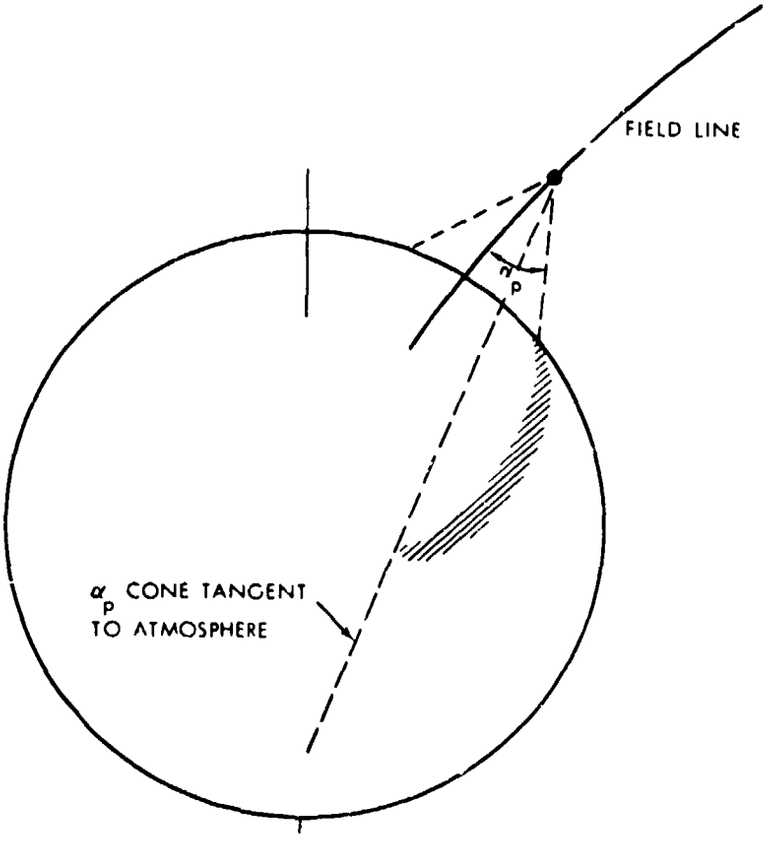

Figure 5-6. The intersection of a pitch angle cone with the earth's surface.

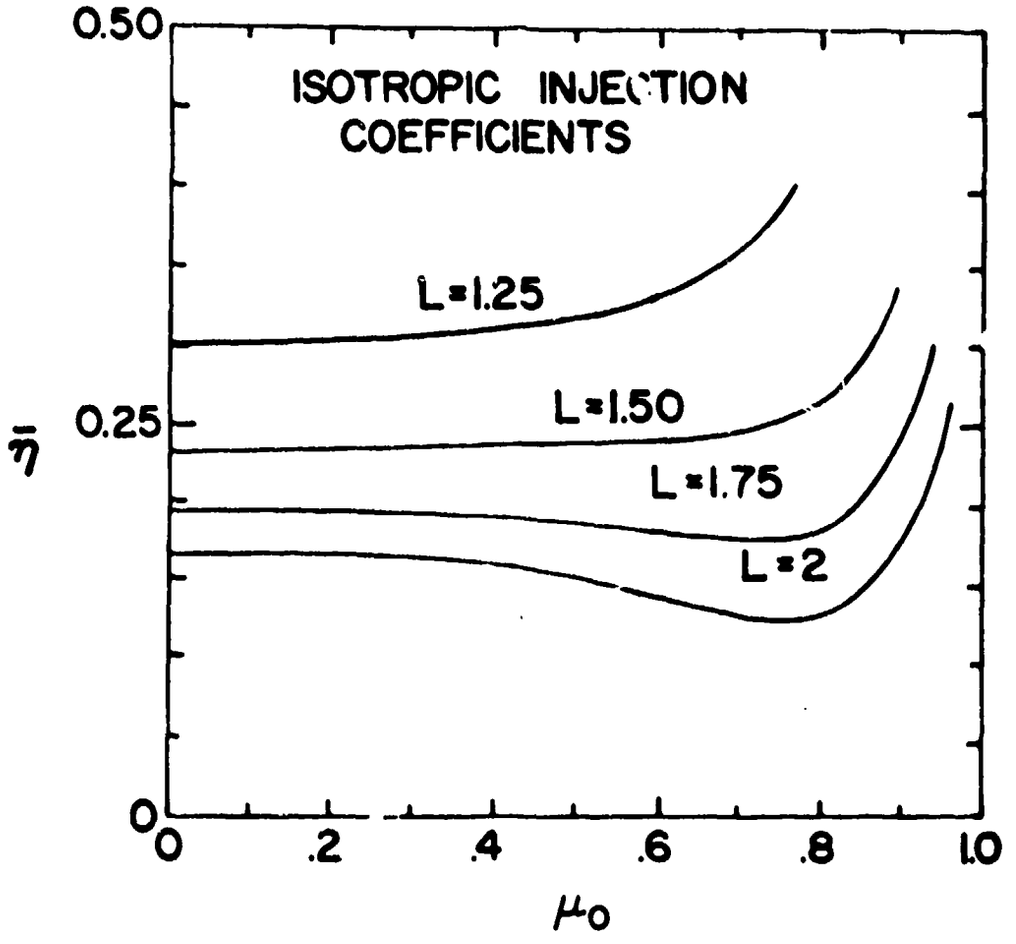

Figure 5-7. Equatorial pitch angle dependence of the average injection coefficient $\bar{\eta}$ for an isotropic neutron flux emerging from the atmosphere (References 11 and 12).

part of the pitch angle cone is within several degrees of being tangential to the atmosphere. Low-energy protons ($T \lesssim 50$ MeV) are injected nearly isotropically; η is then just the fraction of the pitch angle cone that intersects the earth. Some computed values of η are shown in Figures 5-7 and 5-8. In Figure 5-8, above $T \approx 50$ MeV, the effect of the finite width of the albedo neutron beam is included. The pitch angle dependence is nearly the same as in Figure 5-7.

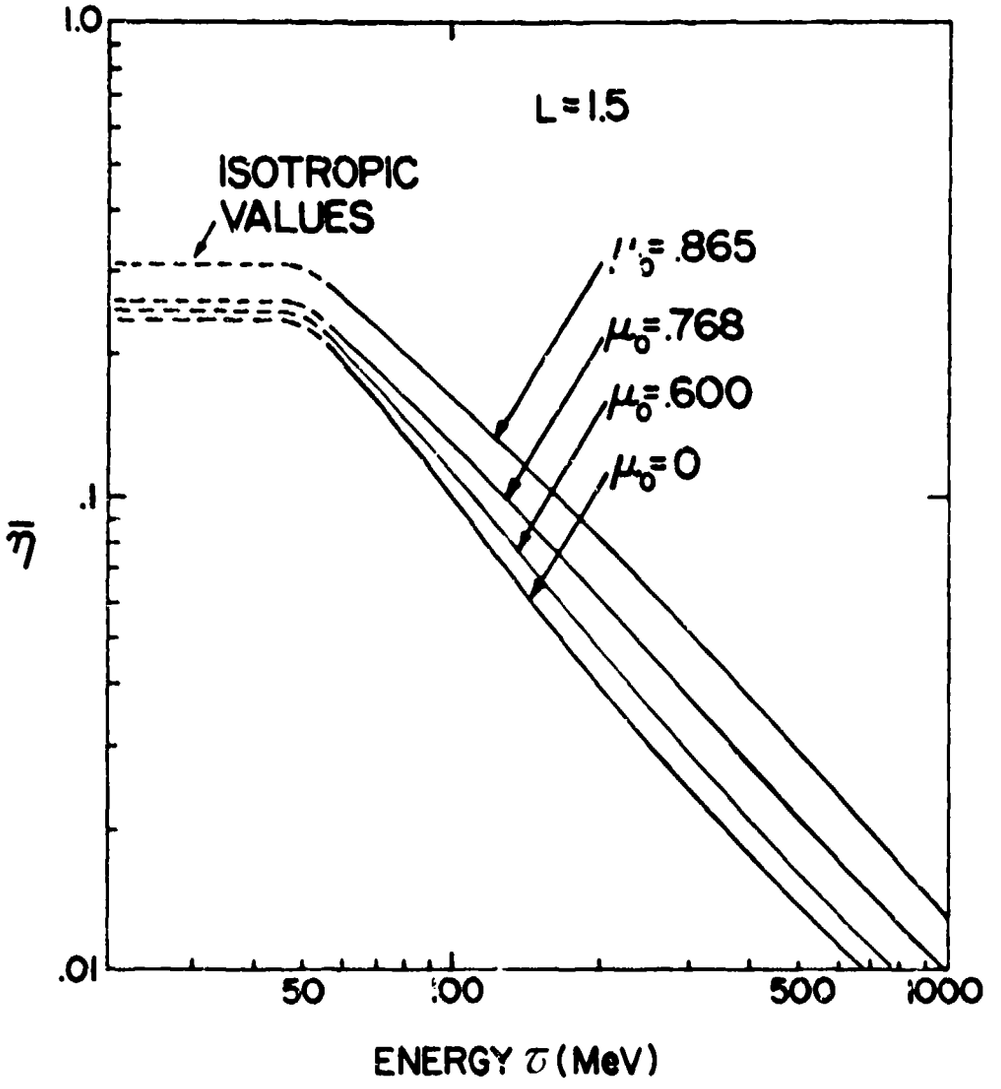

Figure 5-8. Energy dependence of average albedo neutron injection coefficient (References 11 and 12). Above $T \approx 50$ MeV, the effect of the finite width of the albedo neutron beam is included. The pitch angle dependence is nearly the same as in Figure 5-7.

The high-energy protons of the lower trapped radiation belt are fairly well accounted for by the albedo neutron-decay theory (Reference 12). The slope of the observed energy spectrum above 50 MeV is matched well by the predicted spectrum (Section 4.2). Some recent studies combining neutron decay and radial diffusion are discussed in Section 5.4.4. At lower kinetic energies, the numbers of trapped protons are much too great to be attributed solely to decay of fast neutrons. The low-energy albedo neutrons produced by solar cosmic rays might yield appreciable numbers of low-energy protons. However, these solar cosmic ray albedo neutrons cannot reach the equator at low altitudes; they cannot be responsible for an enhancement of trapping of protons with large pitch angles.

LOW ENERGY ALBEDO NEUTRONS. High-energy trapped protons can be attributed to decays of fast neutrons. The same source is relatively ineffective in producing trapped electrons; the low-energy trapped electron number density is nearly everywhere much larger than the trapped proton density. It has been suggested that the electrons could be injected by low-energy albedo neutrons (References 43 and 44). However, neutrons with kinetic energies below 1 MeV are deflected appreciably within the atmosphere. For that reason, considering a diffusion-type problem is necessary to obtain the albedo flux.

For any quantity that is transported through a material medium, in this case j (the number of neutrons per square centimeter per ster per second), a Boltzmann-type equation can be formulated. The Boltzmann equation (Equation 3-91) gives the rate of change of a number density in a volume element that follows the flow. The general transport equation for j in a plane-layered medium (References 53, 54, and 55) is

$$\zeta \frac{\partial j(T, \zeta, h)}{\partial h} + j(T, \zeta, h)\, n\sigma(T, \zeta) = q(T, \zeta, h) + \int_{T}^{\infty} dT' \int_{-1}^{1} d\zeta'\, j(T', \zeta', h)\, n\sigma(T', h)\, W(T', \zeta' \rightarrow T, \zeta) \tag{5-43}$$

where h is the depth measured perpendicular to the layers. The first term on the left denotes the rate of depletion (or augmentation) of a stream of particles moving at an angle arc cos ζ from the normal to the plane (note the similarity to Equation 3-34 when ζ is replaced by μ_0). The second term is the rate of loss by collisions, σ is the

total cross section, and n is the number density of scatterers. Particles are added to the stream by a source of strength q, or by scattering, with a fractional probability W, from all other energies, T', and angles, arc cosine ζ'. Slow neutrons scatter almost isotropically, in which case the scattering probability σW is equal to the product of a constant σ_s (which, of course, must be less than or equal to σ) and $W(T' \rightarrow T)$.

When Equation 5-48 is integrated over ζ, a simplified equation is obtained in terms of the omnidirectional neutron flux J and the flux across a constant-h surface F (Section 3.5.2; Reference 53):

$$4\pi \frac{\partial F(T)}{\partial h} + J(T)\, n\sigma = Q(T, h) + \int_T^\infty dT'\, J(T')\, n\sigma_s\, W(T' \rightarrow T) \qquad (5\text{-}49)$$

where Q now represents an average source strength:

$$Q(T, h) = \frac{1}{2} \int_{-1}^{1} d\zeta\, q(T, \zeta, h) \; . \qquad (5\text{-}50)$$

Equation 5-49 can be solved by standard numerical methods (References 48, 53, 54, 55, and 56).

Equation 5-49 has a form that resembles a conventional diffusion equation. In the lower atmosphere, where the mean path lengths are so short that j is nearly independent of ζ, the first term in Equation 5-49 may be replaced by

$$\frac{\partial}{\partial h}\left(D \frac{\partial J}{\partial h}\right) \; .$$

D is a diffusion coefficient (References 46, 51, 52, and 54). Unfortunately, the free paths of neutrons near the top of the atmosphere are large compared with other dimensional parameters. Consequently, the anisotropies are great enough that the diffusion equation solution does not give entirely reliable results for the flux at the top of the atmosphere.

An additional complication is that neutrons of energies much less than 1 eV cannot leave the earth's gravitational field. This has the effect of increasing the rate of neutron decays near the earth, though the albedo is diminished only slightly (Reference 46).

Various solutions to the neutron-transport problem have appeared. They are all normalized to measured fluxes of neutrons of cosmic rays observed at low altitudes. Figure 5-9 shows computed rates of neutron decays near the earth. These should be the same as the rates of electron injection (References 44, 45, and 46). The electrons released from slow neutron decays above the atmosphere are injected into the trapping regions nearly isotropically.

Albedo neutron decay is definitely inadequate as the sole source of trapped electrons (References 35, 43, and 44). Additionally, it is significant that the energy spectrum of trapped electrons is much different from that of the neutron decay component (Reference 57).

5.4 NONCONSERVATION OF THE THIRD ADIABATIC INVARIANT

15

5.4.1 Hydromagnetic Stability of Trapped Radiation

Simple two-particle interactions are inadequate to explain all the observations relevant to trapped particle sources and losses. The remainder of this chapter is concerned with the effects of plasma oscillations and collective behavior of large numbers of particles. A first consideration is whether the trapped radiation belts are always stable against gross instabilities, primarily involving violation of the third adiabatic invariant Φ.

The $\bar{J} \times \bar{B}$ term in the mechanical force equation (Equation 3-100) can be simplified readily with the aid of Maxwell's Equations (Equation 3-108). The result is

$$\bar{J} \times \bar{B} = -\nabla \frac{B^2}{8\pi} + \nabla \cdot \frac{\bar{B}\bar{B}}{4\pi} \qquad (5\text{-}51)$$

The expression on the right of Equation 5-51 may be identified with the divergence of the Maxwell stress tensor (Reference 58):

$$\bar{\bar{T}} = \frac{1}{4\pi} \begin{bmatrix} \frac{1}{2}B_x^2 + \frac{1}{2}B_y^2 + \frac{1}{2}B_z^2 & -B_xB_y & -B_xB_z \\ -B_yB_x & \frac{1}{2}B_x^2 - \frac{1}{2}B_y^2 + \frac{1}{2}B_z^2 & -B_yB_z \\ -B_zB_x & -B_zB_y & \frac{1}{2}B_x^2 + \frac{1}{2}B_y^2 - \frac{1}{2}B_z^2 \end{bmatrix} \qquad (5\text{-}52)$$

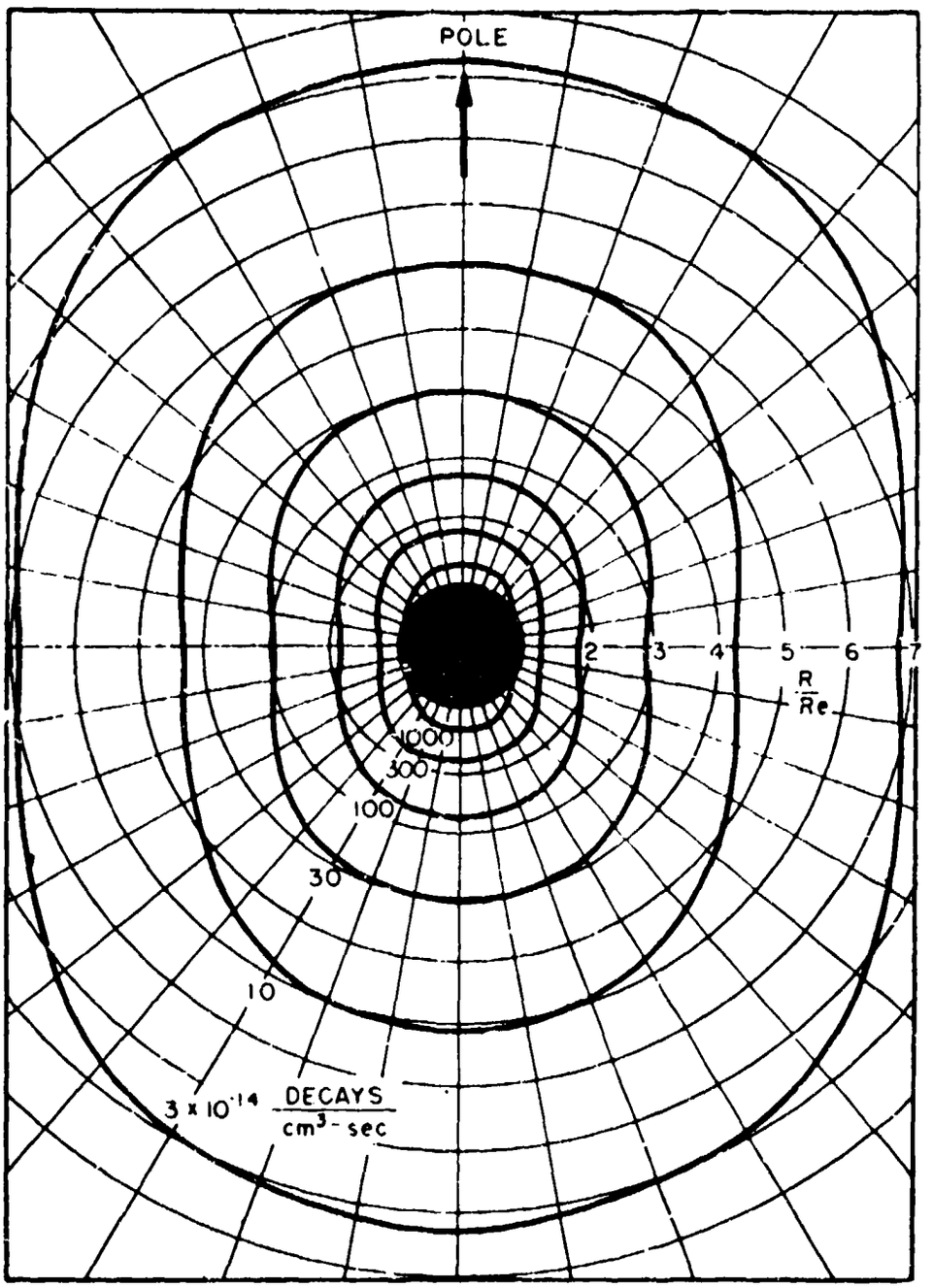

Figure 5-9. Neutron decay rate contours near the earth (Refcrence 46).

The mechanical force equation then can be written in the concise form:

$$\rho \frac{\partial \bar{v}}{\partial t} = - \nabla \cdot (\bar{\bar{T}} + \bar{\bar{P}}) \quad . \tag{5-53}$$

The magneto-mechanical stresses are equivalent to a pressure $B^2/8\pi$ transverse to the field lines and a tension $B^2/8\pi$ along the field lines (References 32, 58, and 59)

The ratio of the transverse particle pressure to the magnetic pressure is a useful criterion of the relative importance of particles versus field (Reference 60). If the ratio

$$\beta_p = \frac{\sum_{[\text{all particles}]} \gamma m v_\perp^2}{B^2/8\pi} \tag{5-54}$$

is much greater than unity, the medium behaves as a classical fluid and the magnetic field has little effect on the gross motion. Conversely, if β_p is extremely small, so little energy is contained in the particles that the effects of collective behavior are likely to be insignificant. When β_p is computed for observed naturally trapped particles, the result is generally much less than 1. If β_p (in any part of the radiation belts) should ever exceed about 0.1, the radiation belts would very likely exhibit all the types of plasma instabilities observed in mirror machines in the laboratory (References 60, 61, and 62).

The parameter β_p is nearly the ratio of particle kinetic energy to magnetic field energy. The magnetic field energy contained within a narrow range, δL, of L shells between the two conjugate intersections with the atmosphere is

$$\delta W = \frac{1}{2} R_E^3 B_E^2 \frac{\sqrt{L-1}}{L^{5/2}} \delta L \quad . \tag{5-55}$$

The total integrated magnetic energy between the earth's surface and a shell of field lines is shown in Figure 5-10. (The unit of energy in the figure is equivalent megatons of TNT explosive energy; 1 MT = 1.2×10^{22} erg.) The total kinetic energy of the particles trapped within an L shell is not expected to appreciably exceed the magnetic field energy.

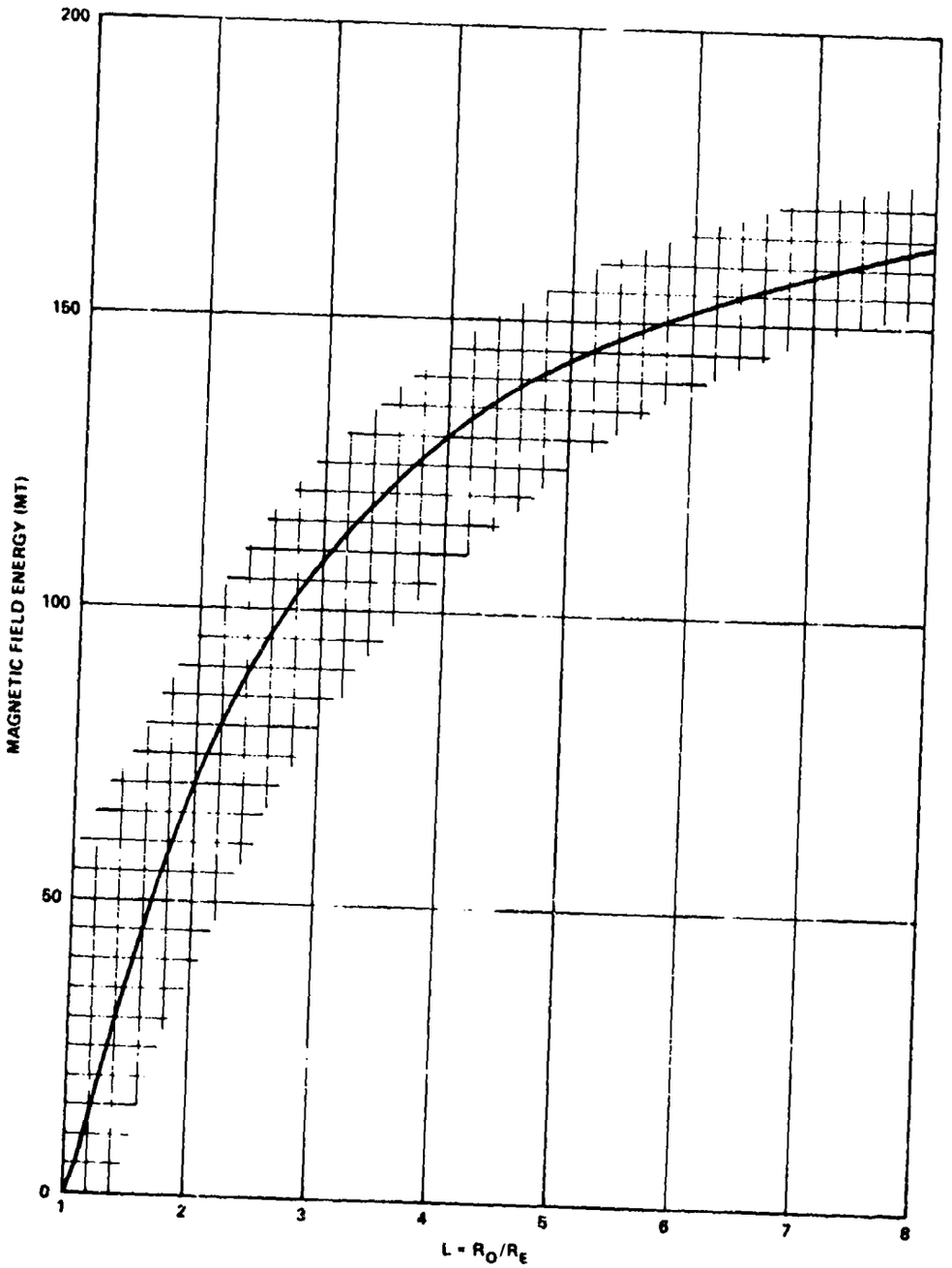

Figure 5-10. Total magnetic field energy in the volume contained between the earth's surface and a shell of field lines at $L=R_o/R_E$. The unit of energy in the figure is equivalent megatons of TNT explosive energy; 1 MT = 4.2×10^{22} erg = 4.2×10^{15} joule.

Usually β_p varies considerably along a field line, although in most observed cases of distributions stable over periods of days, the largest β_p is generally at the equator. The largest β_p can be used to estimate the saturation fluxes for any assumed pitch-angle distribution. A reasonable upper limit for β_p might be somewhat less than 1--perhaps of the order of 0.1. The limit on β_p is invoked in Section 7.3.2 to predict the maximum trapped fluxes that might occur following a high-altitude nuclear detonation.

If all the trapped particles are assumed to have the same energy, the maximum β_p can be computed for a pitch-angle distribution of the form (this is very nearly the distribution which would result from pitch-angle diffusion alone on moderate and high L-shells; see also Section 5.5.5 and the following)

$$j_o = \frac{2+n}{8\pi\mu_c^{n+1}} J_o(\mu_c^2 - \mu^2)^{n/2} \Big\} \; |\mu| \le \mu_c$$

$$= 0 \Big\} \; |\mu| > \mu_c \quad . \tag{5-56}$$

The omnidirectional flux in the equatorial plane is J_o. For all $n \ge 0$, the minimum β_p occurs at the equator. The maximum flux, in terms of the assumed pressure ratio, is

$$J_o = \frac{B_E^2 \beta_p}{8\pi L^6 p} / \left[1 - \mu_c^2 \; 8/(6+n)(4+n)\right] \tag{5-57a}$$

$$\approx 7.25 \times 10^{13} \frac{\beta_p}{p(\mathrm{MeV/c})} \; \frac{(6+n)(4+n)}{L^6[(6+n)(4+n)-8] + 8L^3/\sqrt{4-3/L}} \tag{5-57b}$$

where the atmospheric cutoff has been substituted for μ_c.

5.4.2 Interchange Instability in the Outer Trapping Regions

A plasma may be expected to be confined by a magnetic field that provides a sufficiently great magnetic pressure on the exterior to counteract the particle pressure of the plasma that is seeking to escape. This is not always possible, though. The instability that results if two fluids (in the present case, a plasma and a magnetic field) can exchange positions with a consequent decrease in total

energy is known as the Rayleigh-Taylor instability (Reference 58). This instability is well known from early laboratory studies where it was called the fluting or interchange instability because a plasma boundary tends to break up into grooves or "flutes" as the plasma leaks out, carrying along the field lines (References 60, 61, and 62). Generally, whenever field lines at the plasma boundary are convex to the exterior, an instability results (Reference 63).

The criterion for stability at an interior point is rather complicated. Though the field lines may be convex in a direction toward which the particle density decreases, the plasma may be stable everywhere except on the extreme outer boundary. The plasma particle pressure in the exterior region may be greater than the interior pressure; the growth of instabilities thereby is restrained.

The total energy of all the particles on a field line is proportional to $\int H(M, J, \alpha, \beta)\, f(M, J, H)\, dM dJ$ where H is the Hamiltonian and M and J are the first two adiabatic invariants (References 64, 65, and 66). The Euler potentials, α and β (Section 3.4.1), are especially useful in treating hydromagnetic stability. The plasma is stable only if any exchange of two field lines and their associated trapped particles results in an increase in the total energy. With the assumptions that the adiabatic invariants M and J are preserved and that the Hamiltonian depends on only one spatial coordinate α, the necessary and sufficient criterion for stability (Reference 66) is

$$\int dM, dJ \left(\frac{\partial H}{\partial \alpha}\right)^2 \left(\frac{\partial f}{\partial H}\right)_{M, J} < 0 \quad . \tag{5-58}$$

The notation $(\partial / \partial H)_{MJ}$ refers to a partial derivative in which M and J are held fixed. Often the sufficiency criterion alone:

$$\left.\left(\frac{\partial f}{\partial H}\right)_{M, J} < 0 \quad \right\} \text{all } M, J \tag{5-59}$$

need be considered.

The stability criterion would be satisfied for almost any particle distribution if a minimum with respect to α and β existed in H. All the particles in such an energy well would have minimum energy and escape from the well would not be possible. In a dipole field, no energy wells occur, so examining the details of the distribution function is necessary to determine whether Equation 5-59 is satisfied.

The assumption that f depends only on one spatial coordinate is entirely justified for a geomagnetic field that has a high degree of

axial symmetry. The particle distribution function must be related, however, to the distribution in T, μ_o, L or T, B, L coordinates if meaningful comparisons are to be made with actually observed particle fluxes or intensities. Some of the details of the transformation are given because the intermediate results may be of general utility.

The distribution function f can be replaced by $N(M, J, \alpha)$, the number crossing the equator per unit magnetic flux, $d\alpha d\beta$. The total number of particles per energy interval and per μ_o interval in a magnetic flux tube of cross section $R_o dR_o d\phi$ is

$$N(T, \mu_o, R_o)\, R_o dR_o d\phi = J\, N(M, J, \alpha)\, d\alpha\, d\beta \quad . \tag{5-60}$$

The adiabatic invariants are related to energy and pitch angle through the Jacobian

$$J = \frac{\partial(M, J)}{\partial(T, \mu_o)} = \left[\frac{\partial M}{\partial T}\,\frac{\partial J}{\partial \mu_o} - \frac{\partial M}{\partial \mu_o}\,\frac{\partial J}{\partial T}\right] \tag{5-61}$$

$$= \frac{\gamma p}{B_o}\, R_o \mu_o\, \delta(\mu_o) \tag{5-62}$$

where $\delta(\mu_o)$ is just vt_b/R_o, as defined in Equation 3-47. Now the coordinate β may be chosen equal to ϕ, the azimuthal angle or longitude. The corresponding α is $-M_E/R_o$ on the equator, where the magnetic flux element is

$$d\alpha\, d\beta = B_o R_o\, dR_o\, d\phi \quad . \tag{5-63a}$$

The relation between the previously defined two distribution functions is

$$N(T, \mu_o, R_o) = R_o \gamma p \mu_o\, \delta(\mu_o)\, N(M, J, \alpha) \quad . \tag{5-63b}$$

The left-hand side of Equation 5-63b is related to the intensity (Equation 5-44). The relation between intensity and total number of trapped particles reduces to (References 68 and 69):

$$N(M, J, \alpha) = 2\pi m\, \frac{j_o(T, \mu_o)}{p^2} = \frac{N(M, J, R_o)}{B_o R_o} \tag{5-64a}$$

$$\sim \pi\, \frac{j_o(T, \mu_o)}{T} \quad \text{low energies} \quad . \tag{5-64b}$$

The partial derivative with respect to H in the stability criterion can be replaced with a partial derivative with respect to R_o by the (not obvious) relation (Section 3.4.1; Reference 67):

$$\frac{\partial}{\partial R_o} = B R_o \frac{\partial}{\partial \alpha} = B R_o \frac{e}{c} \frac{\partial \beta}{\partial t} \left(\frac{\partial}{\partial H} \right)_{M,J} . \tag{5-65}$$

However $R_o \partial\beta/\partial t$ is just the azimuthal drift velocity; therefore, $(e/c)\partial\beta/\partial t$ is always negative regardless of the sign of the electrical change. Finally, the interchange stability criterion (Equation 5-59) is

$$\left(\frac{\partial}{\partial L} \frac{j_o(T, \mu_o)}{p^2} \right)_{M,J} > 0 \quad \left. \right\} \text{all } M, J \quad . \tag{5-66}$$

In the natural trapped radiation belts, most of the energy is retained by fast protons. If the protons by themselves are stable, the trapped electrons should not be able to overcome the inertia of the protons. It is probably safe to assert that the entire trapped particle belts are stable against interchange of field lines. The proton intensities are not well known for all values of M; however, all the available data indicate that the natural trapped radiation is stable as far out as $L \approx 5$ to 6 (References 67 through 71). That $N(M, J, \alpha)$ increases with radial distance may be taken as good evidence that particles are being added continually from outside (Reference 70). If particles were not continually added, the outer boundary would be subject to instabilities and the consequent loss of particles would lead to a reversal of the gradient (Equation 5-66).

The artificial electron belts resulting from the Starfish high-altitude nuclear explosion are another matter entirely. When a simplified model of the artificial electron distribution is constructed and $\partial(j_o/p^2)/\partial L$ is integrated over J, the necessary stability criterion (Equation 5-58) clearly is not satisfied (Reference 69). The results of such a computation are depicted in Figure 5-11. How a plasma behaves following the onset of instability is not very well understood. If indeed the electrons are subject to instability and the resulting hydromagnetic motion preserves M and J, then electrons might be expected to move outward with a softening of their energy spectrum. A softening of the energy spectrum of the Starfish trapped electrons may have been observed, though an interpretation on the basis of hydromagnetic instabilities is uncertain (Reference 69).

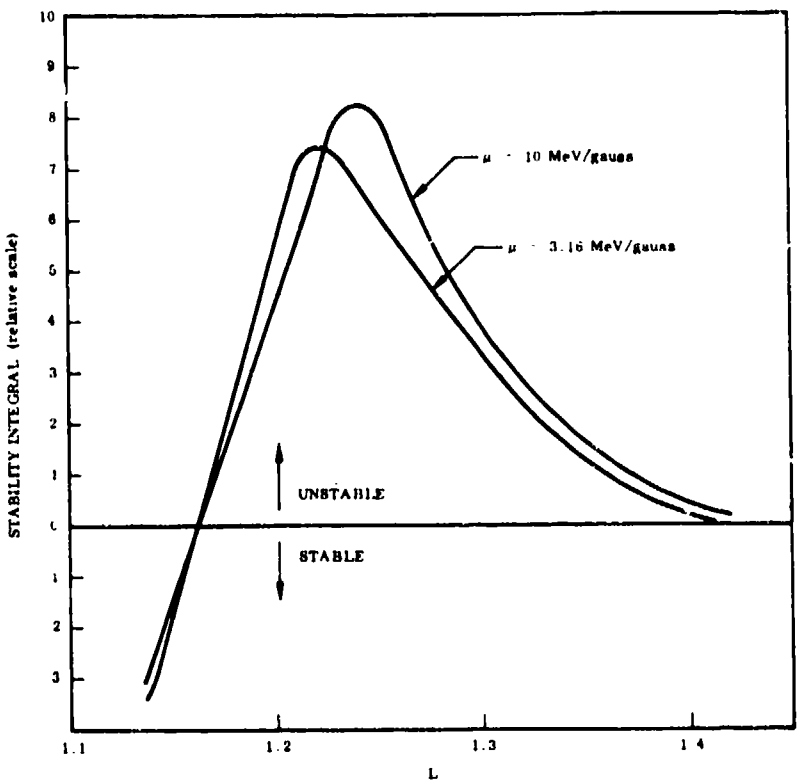

Figure 5-11. The stability function, $d(j_o/p^2)/dL$, integrated over J, the second adiabatic invariant, for the Starfish trapped electron belts (Reference 69).

The preceding discussion of hydromagnetic stability was incomplete because currents flowing in the ionosphere were ignored. In the trapped radiation belts, the field lines are effectively "frozen" into the material. If an entire field line is to exchange its position with another, the finite transverse conductivity in the ionosphere results in a relative motion of material and field lines at the lower ends of the lines. Equations 3-100 and 3-101 relate the velocity with which field lines are dragged through a plasma to the induced currents; thus:

$$\bar{J} = \overset{\bullet}{\sigma} \cdot \bar{v} \times \bar{B} \qquad (5\text{-}67)$$

where $\overset{\bullet}{\sigma}$ is the conductivity tensor. Substituting this in Equation 3-100, however, gives a force:

$$\bar{F} = (\bar{\bar{\sigma}} \cdot \bar{v} \times \bar{B}) \times \bar{B} \qquad (5\text{-}68)$$

contrary to the direction of motion. This force is thought to be adequate to restrain the field lines and prevent interchange.

The stability of the earth's radiation belts retaining the electric fields induced by plasma motion in the ionosphere has been analyzed (Reference 71). The energetic trapped protons can be stabilized by the ionospheric conductivity during the day, even if the simple stability criteria were violated. At night, when ionospheric electron densities are low, the ionosphere cannot be very effective in preventing instabilities.

5.4.3 Radial Motion of Trapped Particles as a Consequence of Nonadiabatic Behavior—Resonant Acceleration

The interchange instability leads to nonconservation of the third adiabatic invariant, Φ. If the instability occurs in a dipole field, trapped particles tend to move outwards, initially preserving the adiabatic invariants M and J. But, the stability criterion (Equation 5-67) now seems to be well satisfied in the trapped radiation belts. The interior (particle) pressure is counterbalanced by more than sufficient exterior (particle) pressure so that any mixing of particles on different L-shells might be expected to result in particles being transported inward by diffusion (References 68, 70, and 72 through 75). In fact, any process that involves nonconservation of Φ could result in inward (or outward) motion of trapped particles. Here then is a relatively uncomplicated mechanism for maintaining the radiation belts against atmospheric and other losses. Enough particles exist in the solar wind to supply all the trapped particles, provided they can get down to low enough altitudes.

Invariance of Φ requires that magnetic and electric fields do not change appreciably within the particles' drift periods (Section 3; References 64 and 65). If the fields fluctuate in a regular fashion, some particles possibly can be accelerated—somewhat as particles are accelerated in a cyclotron or betatron. Several instances have been noted in which a recurring geomagnetic fluctuation apparently resulted in acceleration of trapped electrons (References 69 and 76).

The requirements for an accelerating field seem to be met by a coherent worldwide magnetic variation with periods of about 1 hour, sometimes referred to as Dp2 or DP2 variations (References 77 and 78). Intense groups of nearly monoenergetic electrons in the lower

radiation belt were observed to be associated with several such fluctuations (Reference 76). The drift periods of these electrons were similar to the periods of the fluctuations, which exhibited several complete cycles.

Whenever the magnetic fluctuation fields are known, the electric fields in the ionosphere can be derived with the aid of known ionospheric conductivities. The majority of the electric field in the DP2 fluctuations appears to be a curl-free field ($\nabla \times \bar{E} = 0$)—derivable from a potential field (References 78 and 79). Conductivities along field lines are very large, which in turn leads to potential gradients that are nearly transverse to the field above the ionosphere. One component of the electric field will be in an azimuthal (ϕ) direction. This component is primarily responsible for particle acceleration (Reference 76). A particle with the proper drift period and phase is in resonance and experiences an accelerating force on each circuit of the earth. The situation is not exactly equivalent to the acceleration of charged particles in a cyclotron. Instead, a particle drifts inward and the resulting increase of kinetic energy is a consequence of conservation of M and J .

TRAJECTORIES OF PARTICLES CONSERVING ONLY THE FIRST AND SECOND ADIABATIC INVARIANTS. If the first and second adiabatic invariants are preserved, this simple relation (Reference 80):

$$\Phi = \pi\left(\frac{J^2}{Mm}\right)\left(\frac{\sin \alpha_o}{\mathcal{J}(\alpha_o)}\right)^2 \qquad (5\text{-}69)$$

results from Equations 3-46, 3-75, and 3-76. $\mathcal{J}(\alpha_o)$ is just that part of J that depends on the pitch angle. Equation 5-69 relates the equatorial pitch angle α_o to the flux invariant Φ. Equation 5-69 alternatively may be regarded as a relation between L and the pitch angle:

$$L = 2B_E R_E^2 \left(\frac{Mm}{J^2}\right)\left(\frac{\mathcal{J}(\alpha_o)}{\sin \alpha_o}\right)^2 \quad . \qquad (5\text{-}70)$$

Once L and α_o are known, the mirror field B_m can be found immediately. Since M is assumed constant, the momentum squared must be proportional to B_m as a trapped particle moves across L-shells. Numerical relations between L, α_o, and B_m are given in Figures 3B-15 through 3B-19. Those figures are plotted for arbitrary values of the parameter $J^2/Mm = 2I^2 B_m$.

Of course, the distribution function $N(M, J, \alpha)$ is conserved for a group of particles that moves inward or outward together with changes in the geomagnetic field (this is because the flux $d\alpha d\beta$ is conserved). The intensity j_o therefore is seen from Equation 5-64 to be proportional to momentum squared.

When the equatorial pitch angle is large, the momentum squared is nearly inversely proportional to L^3 as a particle crosses L-shells. For mirror latitudes less than about 20 degrees, the momentum squared is nearly (within an error of less than 1 percent):

$$p^2 \cong \frac{2mB_E M}{L^3}\left[1 + \frac{3}{2\pi R_E}\sqrt{\frac{LJ^2}{B_E Mm}}\right]. \qquad (5\text{-}71)$$

Or, in terms of the initial mirror latitude λ_{m1},

$$p^2 \cong p_1^2\left(\frac{L_1}{L}\right)^3\left[1 + \frac{q}{2}\sin\lambda_{m1}\left(\sqrt{\frac{L}{L_1}} - 1\right)\right]. \qquad (5\text{-}72)$$

The subscripts 1 refer to the specified initial values.

At low energies, the square of momentum may be replaced by the kinetic energy. Equations 5-71 and 5-72 then give directly the energy gain or loss resulting from cross L-shell drift.

5.4.4 Stochastic Acceleration and L-Shell Diffusion

Most geomagnetic fluctuations are not obviously periodic (except for the daily variation). They are randomly distributed in time, with characteristic periods from fractions of a minute up to many hours. A schematic representation of the power spectrum of geomagnetic fluctuations observed on the earth's surface was presented in Figure 2-7.

That random, isolated magnetic disturbances can cause irreversible changes in the particle distribution is demonstrated readily for the type of disturbance known as a sudden commencement. During a sudden commencement, the geomagnetic field is rapidly compressed (Section 2.6.2), especially on the sunlit side of the earth. Particles continue to drift adiabatically in the distorted field, but now those that were previously all on a single L-shell may be on quite diffe[illegible]

invariant surfaces. The end result is that, if the compressed field is released sufficiently slowly, trapped particles will be spread over a finite range of L-shells (Reference 75). Repeated compressions and expansions of the geomagnetic field thereby can result in diffusion of particles.

Any magnetic field fluctuation with a characteristic period near the drift period can cause nonconservation of the third adiabatic invariant Φ, and acceleration of particles. The acceleration of a charged particle by random electromagnetic field fluctuations is called stochastic acceleration (References 73 and 81). Again (as in the treatment of particle collisions), a Fokker-Planck-type equation is useful in describing a process that is determined by the outcomes of many random events. The Fokker-Planck diffusion equation, for the number of particles trapped in a magnetic flux tube at R_o per unit area in the equatorial plane $N(M, J, R_o)$, is expected to be of the form:

$$\frac{\partial N(M, J, R_o)}{\partial t} = -\frac{\partial}{\partial R_o}\left[\langle \Delta R_o \rangle \, N(M, J, R_o)\right] + \frac{1}{2}\frac{\partial^2}{\partial R_o^2}\left[\langle (\Delta R_o)^2 \rangle \, N(M, J, R_o)\right] + \bar{Q} \qquad (5\text{-}73a)$$

$$= -\frac{\partial}{\partial R_o}\left[D_1 \, N(M, J, R_o)\right] + \frac{1}{2}\frac{\partial^2}{\partial R_o^2}\left[D_2 \, N(M, J, R_o)\right] + \bar{Q} \qquad (5\text{-}73b)$$

A source $\bar{Q}$ has been included here. A one-dimensional diffusion equation is valid if the diffusion proceeds with a time scale that is large compared to all other time parameters. If at any point on a field line they are transferred to another field line, the particles are rapidly "smeared" over a new invariant surface. Only on very high L-shells need the invariant surfaces be specified by more than one parameter. In the extreme outer radiation belts, a two-dimensional diffusion equation involving R_o or L and some other coordinate (such as pitch angle α_o or mirror point field B_m) would be necessary (References 28, 82, and 83).

A particular solution of Equation 5-73 is available for the case when the distribution function $N(M, J, \alpha, \beta)$ is constant everywhere. Liouville's theorem must apply to N. It is only necessary that particles should follow dynamical trajectories (Φ need not be conserved) in order that N remain unchanged after the exchange of particles between two invariant surfaces. The stability criterion (Equation 5-58)

guarantees that energy is not lost or gained. When the distribution function $B_o R_o N(M, J, \alpha)$ (Section 5.4.2) is inserted in the Fokker-Planck equation, the time rate of change must be zero. A solution (References 28, 82, 86, and 87) is:

$$D_1 = \frac{R_o^2}{2} \frac{\partial}{\partial R_o}\left(\frac{D_2}{R_o^2}\right) . \tag{5-74}$$

The relation between the two Fokker-Planck coefficients should hold when sources and losses are included in the diffusion equation. Therefore, only one coefficient need be computed:

$$D = \frac{1}{2} D_2 . \tag{5-75}$$

The simplified radial, or cross-L, diffusion equation may be rewritten:

$$\boxed{\frac{\partial N(M, J, R_o)}{\partial t} = -\frac{\partial}{\partial R_o}\left\{\frac{D}{R_o^2} \frac{\partial}{\partial R_o}\left[R_o^2 N(M, J, R_o)\right]\right\} + \bar{Q}} \tag{5-76}$$

The motion of a particle during a geomagnetic disturbance should be derivable directly from the equations of motion of an individual particle. The drift velocity is perpendicular to the field lines. The rate of change of R_o must be a single-valued function of the meridian plane component of the drift velocity V_D (References 81, 84, 88, 89, and 90):

$$\frac{dR_o}{dt} = V_{D[\text{meridian plane}]} \frac{\sqrt{1 + 3\sin^2\lambda}}{\cos^3\lambda} \tag{5-77}$$

where λ is the latitude of the particle at the instant an electric field is applied.

The diffusion coefficient D for a dipole field may be computed after breaking the disturbance field B into symmetric (S) and asymmetric (A) parts:

$$\begin{aligned}\bar{B}_1 = {} & [-S(t)\cos\theta - A(t)\, r \sin 2\theta \cos\phi]\,\hat{r} \\ & + [S(t)\sin\theta - A(t)\, r \cos^2\theta \cos\phi]\hat{\theta} + [A(t)\, r \cos\theta \sin\phi]\hat{\phi}\end{aligned} \tag{5-78}$$

where $\hat{r}$, $\hat{\theta}$, and $\hat{\phi}$ are the unit vectors in an earth-centered spherical coordinate system and θ is the polar angle or colatitude. The spherical harmonic expansion of $\bar{B}_1$ has been terminated at the first-order terms. The induced electric field $\bar{E}_1$, associated with the magnetic disturbance, is (Equation 3-107)

$$\bar{E}_1 = \frac{1}{7} r^2 \frac{dA}{dt} \sin\theta \sin\phi \hat{r} - \frac{2}{7} r^2 \frac{dA}{dt} \cos\theta \sin\phi \hat{\theta}$$

$$+ r\left[\frac{1}{2} \frac{dS}{dt} \sin\theta - \frac{2}{21} r \frac{dA}{dt} (3 - 7 \sin^2\theta) \cos\phi\right] \hat{\phi} \quad . \qquad (5\text{-}79)$$

The time average of the displacement is complicated; the computation has been performed with the result (Reference 89):

$$D_{[mag]}(L, \lambda_m) = 2\pi^2 \left(\frac{5}{7}\right)^2 \Gamma(\lambda_m) \frac{R_E^2 L^{10}}{B_E^2} \left[\nu^2 P_A(\nu)\right]_{\nu = 1/t_d} \qquad (5\text{-}80a)$$

$$= 16.55\, \Gamma(\lambda_m) R_E^2 L^{10} \left[\nu^2 P_A(\nu)\right]_{\nu = 1/t_d} \qquad (5\text{-}80b)$$

The power spectrum is evaluated at the drift frequency. The function $\Gamma(\lambda_m)$ is presented in Figure 5-12. As might have been expected, $D_{[mag]}$ depends only on the asymmetric A part of the fluctuations. The magnetic fluctuations have been decomposed by Fourier analysis so that the power spectrum $P_A(\nu)$ is the Fourier transform of the average of $A(t)\, A(t + t')$:

$$P_A(\nu) = 4 \int_0^\infty dt' \left[\overline{A(t)\, A(t + t')}\right] \cos 2\pi\nu t' \quad . \qquad (5\text{-}81)$$

the flux of energy transported by magnetic fluctuations between the frequencies ν and $\nu + d\nu$ is proportional to $P_A(\nu)d\nu$.

A similar result follows for curl-free electric fields. When the disturbance field $\bar{E}_1$ is everywhere normal to the static magnetic field, the diffusion coefficient (References 82, 88, and 89) is

$$D_{[el]}(L, \lambda_m) = \frac{L^6}{8B_E^2} \sum_k \left[P_k(L, \nu)\right]_{\nu = 1/t_d} \quad . \qquad (5\text{-}82)$$

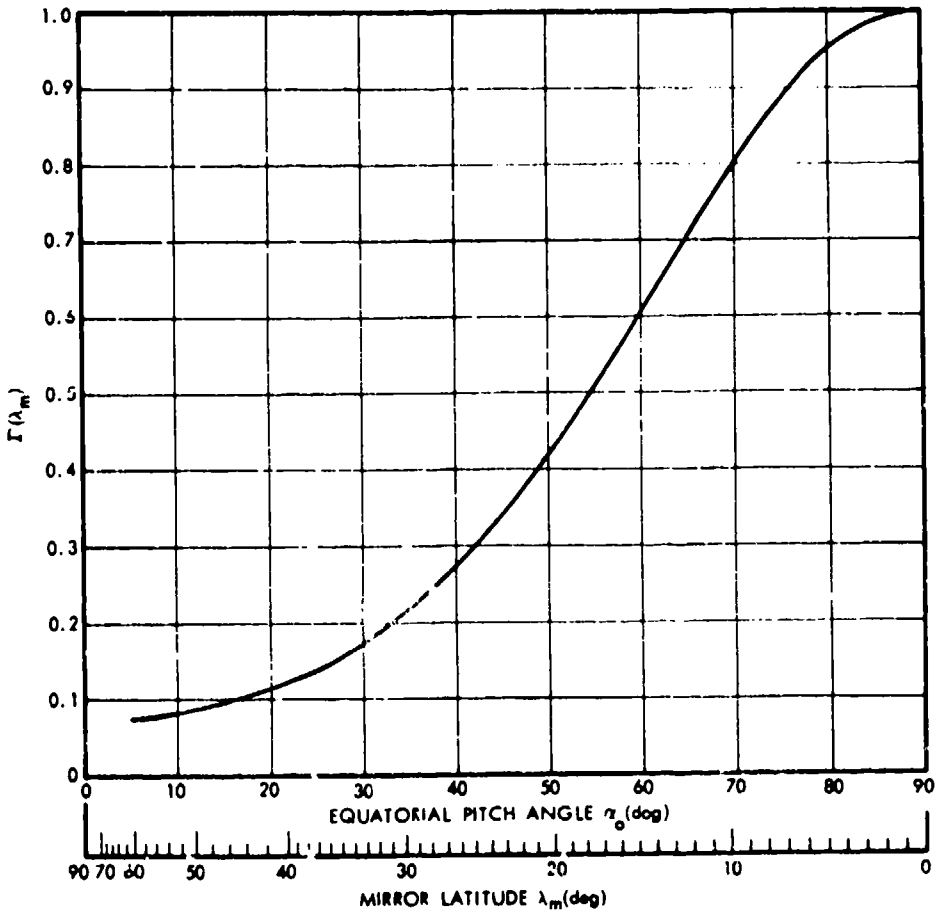

Figure 5-12. Latitude-dependent part of the radial diffusion coefficient (Reference 89).

The power spectrum, $P_k(L, \nu)$, here an explicit function of L, corresponds to the k'th component of the harmonic analysis of the electric field:

$$E_{\phi\,l}(L, \phi, t) = \sum_{k=0}^{\infty} E_{k\phi}(L, t) \cos\left(k\phi + \psi(L, t)\right) \qquad (5\text{-}83)$$

where ψ is merely a phase correction. The electric field diffusion coefficient $D_{[el]}$ depends on the mirror latitude only through the drift period t_d. The variation of drift period with mirror latitude is so slight (Equation 3-50) that $D_{[el]}$ is quite insensitive to mirror

latitude. Generally, the magnetic fluctuation diffusion coefficient $D_{[mag]}$ is much more sensitive to mirror latitude than is the electric field diffusion coefficient $D_{[el]}$. The magnetic diffusion coefficient falls so rapidly with increasing mirror latitude that magnetic acceleration effects are most important near the equatorial plane.

The magnetic fluctuation diffusion coefficient might be computed from a knowledge of magnetic disturbances observed on the earth's surface (Section 2.7). But the asymmetric part of the disturbance is proportional to radial distance, so ground-based magnetometers are sensitive primarily to S-variations. The relation between A and S is provided by the model chosen for the magnetic field. Some theoretical models have been constructed (References 89 and 91). Observational data collected with artificial satellites may be employed to further refine the models (Reference 92). Attempts have been made recently (References 93 and 94) to perform direct measurements of electric fields in the magnetosphere.

17

The spectral behavior of magnetic variations is not known with any more certainty than is the spatial dependence. The crude spectrum of Figure 2-17 is proportional, below about 1 hertz, approximately to the -2 power of frequency. A $P \propto \nu^{-2}$ frequency dependence is in agreement with most computations based on sudden commencements and other disturbances with a fast rise time succeeded by a slow recovery. For this special case, the diffusion coefficient is independent of drift period and is just proportional to L^{10}. Other assumed types of magnetic fluctuations yield quite different diffusion coefficients. Generally, for a power spectrum of the form:

$$P_A(\nu) \propto \nu^{-n} \tag{5-84a}$$

the diffusion coefficient (Reference 89) is

$$D_{[mag]} \propto L^{6+2n} M^{2-n} \propto L^{12-n} p^{4-2n} . \tag{5-84b}$$

EMPIRICAL COMPUTATIONS OF DIFFUSION COEFFICIENTS FROM OBSERVATIONAL DATA. The observation of an uncomplicated, unequivocal example of radial diffusion remains elusive. Because the motions of individual particles cannot be traced, observations of temporal changes in the trapped particle distribution must be relied on. But a radial motion of a group of particles is subject to being interpreted as a convective fluid motion of the entire group. On the other hand, a decay of the trapped particle flux at a single, isolated location perhaps could be explained by some other, yet undiscovered, loss process.

That the Liouville distribution function $N(M, J, \alpha)$ increases with L is suggestive of radial transport but is hardly conclusive evidence. The most compelling evidence for radial diffusion perhaps should be sought in the lower L-shells where the sources and losses are best understood. It has been noted that the artificial Starfish electron belts near $L = 1.25$ did not decay as rapidly as predicted from atmospheric losses alone. Computed and observed decay times are compared in Figure 5-13. Below $L \approx 1.2$, the observed decay time τ and the decay time predicted from atmospheric loss time τ_a differ enough that a cross L-diffusion coefficient can be computed. The atmospheric loss is well understood. The apparent discrepancy could only be explained by the addition of electrons diffusing from higher L-shells. The decay of the Starfish electrons can be represented by a simple empirical relation:

$$\frac{\partial N(M, J, R_o, t)}{\partial t} = - \frac{N(M, J, R_o, t)}{\tau} \tag{5-85a}$$

where τ is the time required for a decrease by a factor $1/e = 0.368$. The diffusion equation for this case can be solved analytically with the result (Reference 42):

$$D = \frac{\int_{R_{o1}}^{R_{o2}} \left[\frac{1}{\tau_a} - \frac{1}{\tau}\right] N(M, J, R_o, t)\, dR_o}{\left[\frac{1}{R_o^2} \frac{\partial}{\partial R_o}\left(R_o^2 N(M, J, R_o t)\right)\right]_{R_{o1}}^{R_{o2}}} \tag{5-85b}$$

where τ_a is the predicted atmospheric loss decay time. The momentum of particles is nearly proportional to B_o, so the relation between n and measured intensity j (Equations 5-64 and 5-72) is

$$N(M, J, R_o) \cong \frac{\pi R_o\, j_o(T, \mu_o)}{M\left[1 + \frac{3}{2\pi}\sqrt{R_o \frac{J^2}{Mm} \frac{B_E}{R_E^3}}\right]} . \tag{5-86}$$

Computations thus far have been practical only for particles with orbits restricted to the equatorial plane (where $J = 0$).

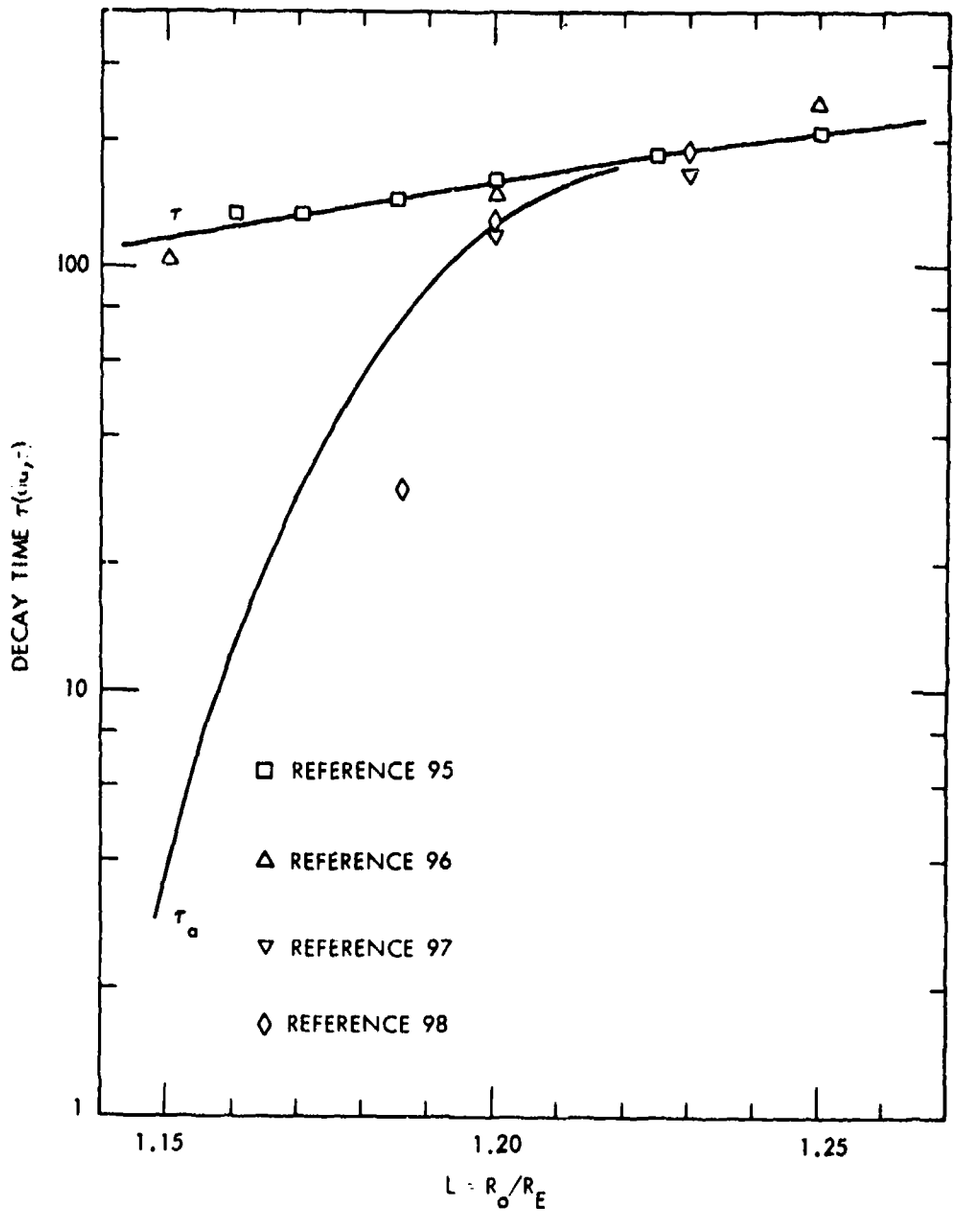

Figure 5-13. Decay time constants of the Starfish trapped electron belts (Reference 42). τ is the actual measured lifetime while τ_a is that computed for atmospheric losses alone.

Near the lower edge of the artificial radiation belts the intensity is approximately proportional to exp(138 x L). In this same region, τ_a drops very rapidly with decreasing altitude. τ and τ_a are compared in Figure 5-13. The computed diffusion coefficient (Figure 5-14) has a strong inverse dependence on L (Reference 42). This result is not easily reconciled with Equation 5-85. Perhaps a very large positive exponent in the magnetic fluctuation power spectrum is not necessary if the diffusion at low altitudes is principally due to curl-free electric fields, particularly the fields associated with recurring fluctuations (Section 5.4.3). Indeed, the particles noted in Section 5.4.3 that presumably had been accelerated by recurring field fluctuations were at $L \approx 1.15$ (Reference 76), below most of the trapped radiation regions. In the higher parts of the trapped electron belts, the decay time constants of Figure 5-15 have to be explained. The estimated intrinsic uncertainties, except where indicated in the figure, are generally of an order of magnitude comparable with the scatter of individual points. The data points attributed to Reference 98 are anomalously high because they include the effects of artificial electron belts. The higher characteristic energy of electrons released after a nuclear detonation results in lifetimes enhanced by a factor of 2 to 5. The higher set of data points attributed to Reference 104 represents only the electrons with more than 1-MeV kinetic energy. The solid curve at the left refers to computations of atmospheric losses (Reference 41). It should be evident from this figure that atmospheric decay cannot account for more than a small fraction of particle losses above $L \approx 1.5$. The trapped electrons resulting from the USSR high-altitude nuclear explosion of 1 November 1962 exhibited a radial spreading that can be explained by radial diffusion (References 106 and 107). When electrons restricted to the equatorial plane are considered, the resulting diffusion coefficient is represented by the single point at $L = 1.8$ in Figure 5-14. The L-dependence of the diffusion coefficients in the lower left of Figure 5-14 is so extreme that a nearly vertical line (with a negative slope) appears. Elsewhere, the diffusion coefficients agree with Equation 5-85. The individual points at $L = 1.7$, 2.1, and 2.2 were computed from observations on the decay of artificial electron belts (Section 6). The curve attributed to Reference 75 pertains to the diffusion of trapped protons.

An interesting case that seems to be attributable to radial diffusion was observed (References 108 and 109) in the outer radiation belts. There the electron distribution was greatly disturbed by a magnetic storm. After the storm, certain features of the radial distribution seemed to drift inward. Figure 5-16 illustrates how the perturbation in the

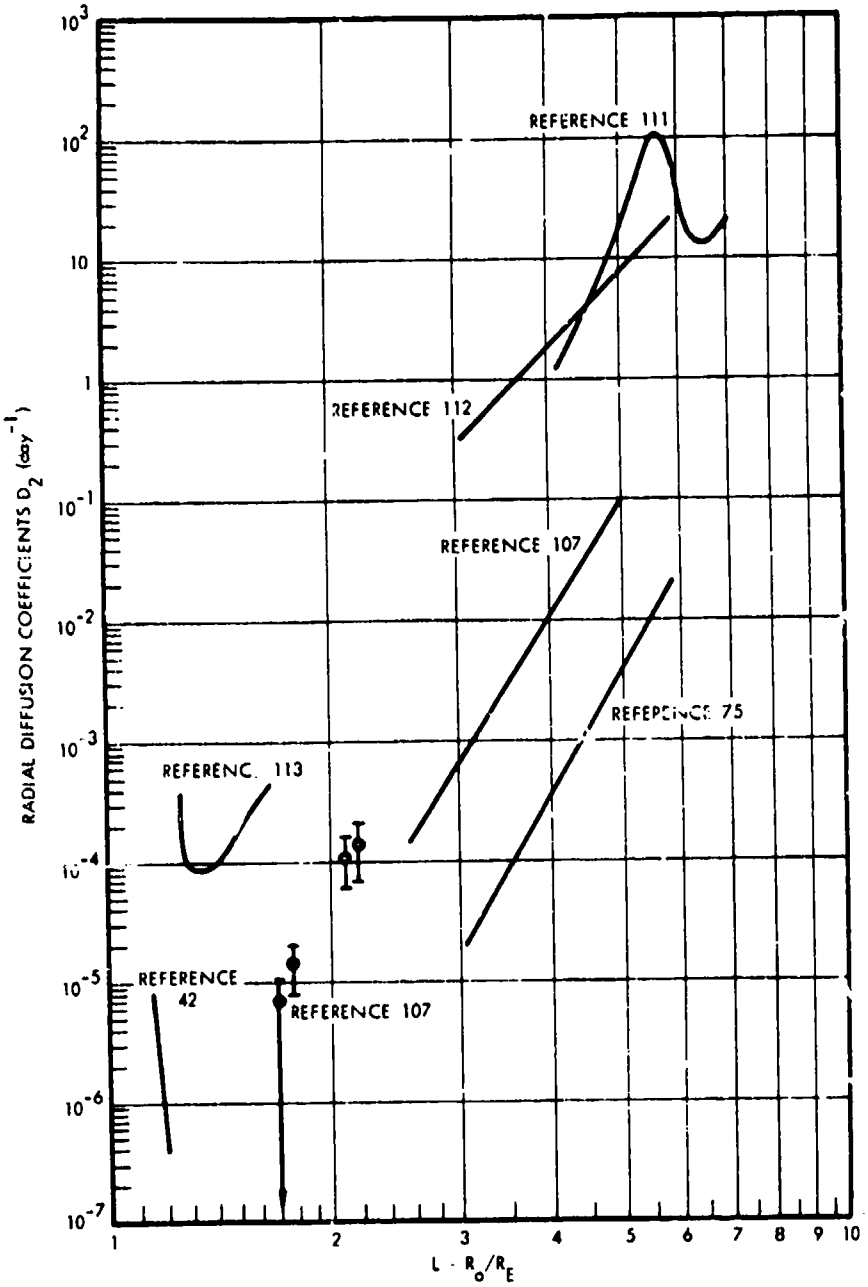

Figure 5-14. Radial diffusion coefficients for electrons with 90-degree equatorial pitch angles (Reference 110). The L-dependence of the diffusion coefficients in the lower left of Figure 5-14 is so extreme that a nearly vertical line (with a negative slope) appears. Elsewhere, the diffusion coefficients agree with Equation 5-85. The individual points at L = 1.7, 2.1, and 2.2 were computed from observations on the decay of artificial electron belts (Section 6). The curve attributed to Reference 75 pertains to the diffusion of trapped protons.

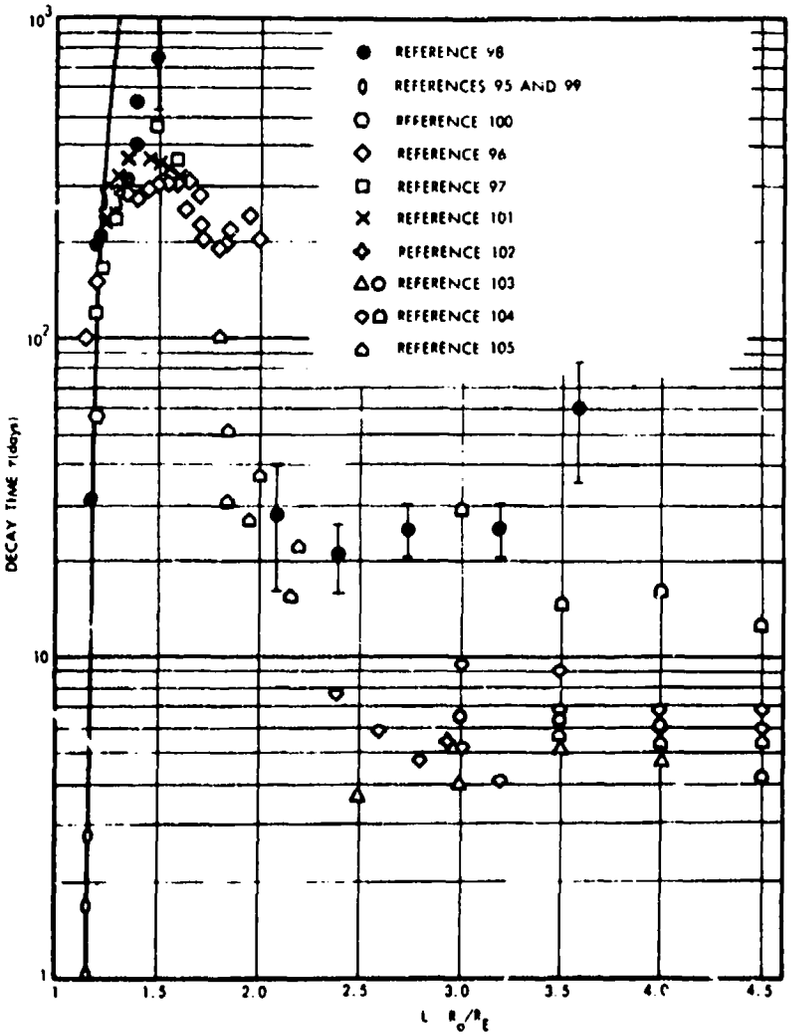

Figure 5-15. Decay time parameters for trapped electrons on intermediate L-shells. The estimated intrinsic uncertainties, except where indicated in the figure, are generally of an order of magnitude comparable with the scatter of individual points. The data points attributed to Reference 98 are anomalously high because they include the effects of artificial electron belts. The higher characteristic energy of electrons released after a nuclear detonation results in lifetimes enhanced by a factor of 2 to 5. The higher set of data points attributed to Reference 104 represents only the electrons with more than 1-MeV kinetic energy. The solid curve at the left refers to computations of atmospheric losses (Reference 41).

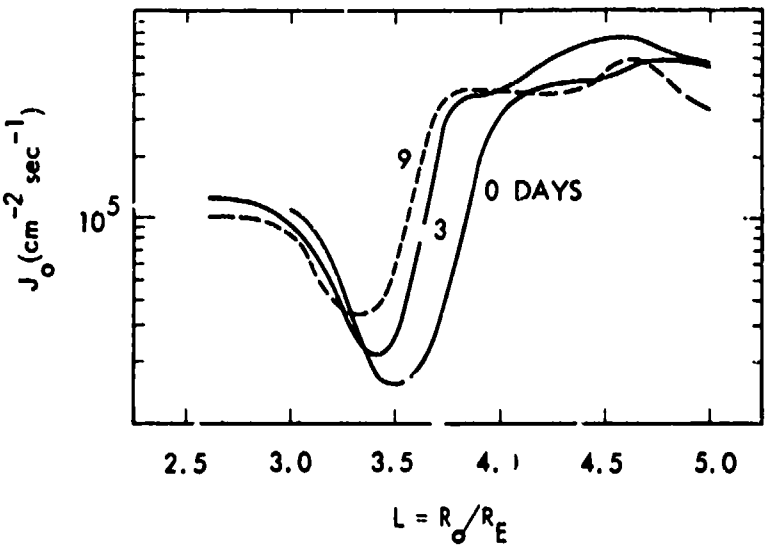

Figure 5-16. Inward motion of trapped electrons during a period of 9 days.

distribution moved inward while preserving its general shape. The omnidirectional fluxes on the equator of electrons with energies above 1.6 MeV are shown in Figure 5-16 (Reference 108). Though this is not obviously the result of pure radial diffusion, the inward motion can be described by a diffusion equation with the coefficients shown in Figure 5-14 (Reference 107).

The remainder of diffusion coefficient determinations have been primarily attempts to explain steady-state features of the trapped electron and proton belts (Reference 114). Most electron diffusion coefficients computed for the region between $L \approx 1.8$ and $L \approx 5$ exhibit the expected L^{10} form.

The low-energy trapped proton distributions seem to be consistent with the hypothesis that these protons originate in the outer magnetosphere and are transported by diffusion to lower L-shells (References 68, 75, and 115). Recent examination of the higher energy protons (Reference 116) indicates that radial diffusion plays an important part in determining the distribution of these particles below $L = 2$. When the albedo neutron source, atmospheric loss mechanisms, and radial diffusion are combined, the resulting distribution is consistent with the observed distribution of protons above

several MeV. Because of the scarcity of definitive measurements, the radial (L) dependence of proton diffusion coefficients is not yet certain to be at all near L^{10}.

5.5 NONCONSERVATION OF THE FIRST AND SECOND ADIABATIC INVARIANTS

5.5.1 Trapping Limits

That geomagnetic fluctuations and large-scale electric fields can alter the third adiabatic invariant has been demonstrated adequately. If Φ is not conserved in the trapped radiation belts, changes in the first and second adiabatic invariants might also be expected (References 28 and 89). The power density of geomagnetic fluctuations observed on the earth's surface falls rapidly with increasing frequency, but energy in moderately high-frequency oscillations near the gyrofrequency and bounce frequency is still sufficient to affect trapped particle motions. Properly, the Fokker-Planck diffusion equations for radial diffusion and pitch angle diffusion should include terms resulting from failure of all the adiabatic invariants (Reference 28).

One possible consequence of nonadiabatic behavior is that stable trapping of protons and heavy particles becomes less likely as the particles' kinetic energies increase. Section 3.2.3 noted that on any L-shell a maximum energy occurs above which trapped orbits are not possible. Actually, the maximum energies of protons observed in the trapped radiation belts seems to be somewhat lower than predicted by the simple theory (References 11 and 117). It has been suggested that this is because inhomogeneities in the magnetic field may be about the same size as the particles' gyro-radii. Therefore, M and perhaps J might not be strictly invariant (Reference 11). Analysis of naturally trapped proton data leads to an empirical formula for the maximum momentum of protons on any L-shell:

$$p(\mathrm{MeV/c}) \leq \frac{1800}{L^2} \quad . \tag{5-87}$$

This momentum limit is about 10 times lower than the limit derived from Störmer's theory for orbits in a strictly dipolar field (Equation 3-28). Protons with greater momenta presumably are not trapped with lifetimes comparable to their predicted lifetimes for energy loss in the atmosphere.

5.5.2 Nonconservation of the Second Adiabatic Invariant—Fermi Acceleration

If a trapped particle is to have its adiabatic invariants altered, the fluctuation fields must be aligned in such a fashion that particle acceleration can occur. Section 5.4.4 noted that only certain components of the fluctuation fields had any effect on the third adiabatic invariant, e.g., only the azimuthal component of a large-scale electric field can accelerate particles. Because the second invariant J depends on the longitudinal component of momentum, $\bar{p}_{\parallel}$, only the parallel part of the fluctuating electric field, $\bar{E}_{\parallel}$, should be expected to cause nonconservation of J.

A change in $\bar{p}_{\parallel}$ does not necessarily involve a change in J, however. For example: When a dipolar magnetic field is compressed, the field lines are shortened. Hence, the distance between mirror points, $|S_{m2} - S_{m1}|$, is decreased. But if the adiabatic invariant

$$J = \oint_{S_{m1}}^{S_{m2}} p_{\parallel} \, ds$$

is to be preserved, $p_{\parallel}$ must increase enough to offset the shortening of the trajectory. The resultant increase in the total momentum is a consequence of invariance of the magnetic moment invariant M. It has been called Fermi acceleration because a similar effect was invoked by Fermi in an attempt to explain cosmic ray acceleration (References 32 and 65). A simple explanation of Fermi acceleration may be constructed by referring to a charged particle spiralling about a field line as it enters a region where the field converges. In a static field, the particle is reflected with no change in its kinetic energy (Section 3.3.2). But, if the turning point is moving with a longitudinal velocity V_m toward the gyrating particle, a stationary observer would, after reflection, measure an increase by an amount of $2V_m$ in the particle's longitudinal velocity.

The energy gain (Fermi acceleration) in a single encounter with a moving magnetic mirror is (Reference 118)

$$\delta E = 2 p_{\parallel} \left\{ \frac{(1-v_{\parallel}^2/c^2)}{(1-v^2/c^2)} V_m + \left[\frac{(1-v_{\parallel}^2/c^2)}{(1-v^2/c^2)} (1 - 3v_{\parallel}^2/c^2) + 3 \frac{(1-v_{\parallel}^2/c^2)}{(1-v^2/c^2)} \frac{v_{\parallel}^2}{c^2} \right] V_m' v_{\parallel} \right\} \qquad (5\text{-}88a)$$

$$\cong 2 p_{\parallel} (V_m + V_m^2/v_{\parallel}) \ . \qquad (5\text{-}88b)$$

This formula is valid when the velocity of the moving mirror is considerably less than the speed of light. The mirror velocity is to be taken positive in head-on collisions and negative in collisions in which the mirror overtakes the particle.

The effects of hydromagnetic waves are equivalent to the accelerations incurred in many random encounters with moving magnetic mirrors. If some average frequency of encounters ν_m exists, the Fokker-Planck coefficients for the alteration of the parallel part of the momentum (Reference 119) are

$$\langle \Delta p_{\parallel} \rangle \approx \frac{2 \gamma^2 m^2 V_m^2}{p_{\parallel}} \nu_m \qquad (5\text{-}89)$$

$$\langle (\Delta p_{\parallel})^2 \rangle \approx 4 \gamma^2 m^2 V_m^2 \nu_m \ . \qquad (5\text{-}90)$$

If particle motions are influenced primarily by resonant encounters, then the frequency ν_m is equal to the bounce frequency or approximately $v_{\parallel}/S$, where S is the distance between mirror points. The Fokker-Planck coefficients thus are found to be related simply:

$$\langle \Delta p_{\parallel} \rangle = \frac{1}{2} \frac{d}{dp_{\parallel}} \langle (\Delta p_{\parallel})^2 \rangle \ . \qquad (5\text{-}91)$$

This equation has been derived elsewhere in other contexts and appears to be a general result for bounce resonant interactions between trapped particles and electromagnetic disturbances (References 105 and 120). The same relation could be obtained (as in Section 5.4.4) by presuming that the distribution function $f(p_{\parallel})$ = constant is highly stable against instabilities that derive their growth energy from the parallel momentum.

The order of magnitude of the diffusion coefficients can be estimated for general magnetic disturbances. The mirror velocity is nearly

$$V_m \cong 2\pi R_o \nu \frac{B_{||}}{B_o} \frac{\cos^3 \lambda_m (1 + 3 \sin^2 \lambda_m)}{9 \sin \lambda_m (1 + \frac{5}{3} \sin^2 \lambda_m)} \tag{5-92}$$

where $B_{||}$ is the parallel part of the disturbance amplitude and ν is the frequency. This formula is valid only when the mirror latitude λ_m is not too near zero. Since a continuous wave power spectrum must be presumed, particles out of resonance by an amount $\delta\nu$ clearly can interact only with a given train of waves for a time $\delta t \approx 1/2\delta\nu$. The change in the particles' momentum during the same time is

$$\delta p_{||} = 2\gamma m V_m \frac{\delta t}{t_b} \quad . \tag{5-93}$$

Averaged over time, this gives the Fokker-Planck coefficient

$$\left\langle (\Delta p_{||})^2 \right\rangle \approx \frac{16\pi^2}{9^2} \frac{R_E^2}{B_E^2} \frac{L^8 \cos^{16} \lambda_m}{\sin^2 \lambda_m} \frac{B_{||}^2}{2\delta\nu} \quad . \tag{5-94}$$

It can be shown (Reference 121) that, where δB is the average amplitude of waves in a narrow frequency band of width $\delta\nu$, the power spectral density is

$$P(\nu) \sim \frac{(\delta B)^2}{2\delta\nu} \quad . \tag{5-95}$$

The strength of geomagnetic fluctuations with periods of about 1 second can be estimated by presuming that disturbances originate on the exterior of the trapped radiation region (References 119 and 122 through 126). The trapped plasma behaves as an elastic medium; magnetic disturbances propagate inward by hydromagnetic waves. A hydromagnetic wave travels with the Alfvén velocity (References 59 and 63):

$$V_A = \frac{c}{\sqrt{1 + 4\pi\rho c^2/B^2}} \quad . \tag{5-96}$$

The Alfvén velocity increases with decreasing altitude until the density of the atmosphere ρ begins to increase faster than B. If hydromagnetic waves are not absorbed strongly, the amplitude of the waves above $r \approx 1.5\ R_E$ must increase with altitude. The amplitude of fluctuations on any L-shell above $L \approx 1.5$ is therefore likely to be greatest near the equator. The amplitude of hydromagnetic waves can be represented roughly as

$$B_{II} \sim B'_{II} \frac{L \cos^6 \lambda}{6} \tag{5-97}$$

where B'_{II} is the amplitude at $L = 6$ (Reference 119) (in $MeV^2/c^2/sec$). The corresponding Fokker-Planck diffusion coefficient is

$$\langle (\Delta p_{II})^2 \rangle \approx 34 \frac{[p(MeV/c)]^4}{\nu^2} \frac{L^6 \cos^{20} \lambda_m}{\sin^2 \lambda_m} P'_{II}(\nu)_{\nu = 1/t_b} \quad . \tag{5-98}$$

Using measured power spectra in the outer magnetosphere (Reference 127), an approximate lifetime of 1 MeV electron at $L \approx 6$ can be found with the aid of Equation 5-91:

$$\tau \approx \frac{p_{II}}{\langle \Delta p_{II} \rangle} \approx 2\ yr \quad . \tag{5-99}$$

Apparently, the Fermi acceleration bounce resonance process is significant only for particles mirroring very near the equatorial plane at times when the power density of magnetic fluctuations is far above the normal values. A similar result follows for other bounce-resonant interactions (Reference 120). That this is the most important mechanism for depletion of trapped particles in any region is therefore unlikely.

Some attempts have been made to include nonconservation of J in radial diffusion computations (Reference 28). The experimental evidence on radial diffusion has not yet, however, been adequate to test cases other than $J \approx 0$ ($\alpha_0 \approx 90$ degrees).

Whether longitudinal components of curl-free electric fields with periods near 1 second result in trapped particle losses is uncertain. Electric fields play such important roles in current auroral acceleration and precipitation theories that significant effects on trapped particle populations might be presumed. This is almost surely a valid conclusion in the outer parts of the magnetosphere (Section 5.6).

5.5.3 Nonconservation of the First Adiabatic Invariant—Wave Particle Interactions

The magnetic moment invariant M involves only the transverse part of the momentum. It does not follow, however, that changes in $\bar{p}_\perp$ and $\bar{p}_\parallel$ (and hence in M and J), are always independent. The effects of electromagnetic waves near the trapped particle's gyrofrequencies are somewhat more complicated than the effects of relatively slow magnetic fluctuations.

Electromagnetic waves of moderately high frequencies are propagated quite efficiently along magnetic field lines. While traveling from one "end" to the other along a field line, a wave has an opportunity to interact with many particles on the associated L-shell. Also, the wave might be reflected by the ionosphere and make several traversals of the field line before dying away. A wave propagating along a field line can be represented by the solutions to Maxwell's equations (in rectangular coordinates)(Reference 128):

$$\bar{E}_1 = \hat{x}\, E_\perp \cos\psi \pm \hat{y}\, E_\perp \sin\psi + \hat{z}\, E_\parallel \cos\psi \qquad (5\text{-}100a)$$

$$\bar{B}_1 = \mp\, \hat{x}\, B_\perp \sin\psi + \hat{y}\, B_\perp \cos\psi \qquad (5\text{-}100b)$$

$$\bar{J}_1 = \hat{x}\, J_\perp \sin\psi \mp \hat{y}\, J_\perp \cos\psi + \hat{z}\, J_\parallel \sin\psi \ . \qquad (5\text{-}100c)$$

The z-axis here is along the field line. The phase angle ψ is $\omega t - kz$ where k, the <u>wave number</u>, is equal to 2π divided by the wave length. Maxwell's equations (Equations 3-105 through 3-108) for the perturbed field of the wave reduce to:

$$B_\perp = \frac{kc}{\omega} E_\perp \qquad (5\text{-}101a)$$

$$J_\perp = \frac{1}{4\pi c} E_\perp \left(\omega - \frac{k^2 c^2}{\omega} \right) \qquad (5\text{-}101b)$$

$$J_\parallel = \frac{\omega}{4\pi c} E_\parallel \ . \qquad (5\text{-}101c)$$

(E and B are in conventional gaussian units, and J is in emu, see Appendix 3A). There is an arbitrariness in the sign of some components of the field vectors. Clearly, the <u>upper</u> signs pertain to a <u>right-handed</u> circularly polarized wave that rotates in the same sense as the gyrating electrons. The other signs yield a <u>left-handed</u>, circularly polarized wave. The relative phases of the rotating transverse wave

vectors are depicted in Figure 5-17. The wave vectors are depicted there as seen by a stationary observer looking in the negative z direction. The field components should be considered rotating clockwise (upper diagram) or counterclockwise (lower diagram) as viewed by a stationary observer looking in a direction contrary to the unperturbed magnetic field. The shaded area labelled f_1 represents the perturbation in the electron distribution function.

Longitudinal oscillations can be separated from transverse oscillations if propagation is strictly along the direction of the magnetic field. The mixture of transverse and longitudinal oscillations that would result from nonparallel propagation leads to elliptical polarization. Only purely circular polarization is considered here.

Gyrating particles interact with all components of an electromagnetic wave. If a wave consists entirely of longitudinal oscillations, the only force acting on a charged particle is along the direction of propagation. If it is moving along a field line with nearly the velocity of a longitudinal wave but slightly out of phase, the particle will be accelerated by the longitudinal electric field $\bar{E}_{1,\parallel}$. Given sufficient time, the gyrating particles adjust their speeds to the phase velocity of the wave so that they will eventually ride along in the "troughs" or "crests." The mechanism by which the transverse part of the velocity is altered in wave-particle interactions is considerably more complicated. When gyrating particles encounter circularly polarized waves, the $\bar{v} \times \bar{B}_1$ term in the equation of motion (Equation 3-3) has both longitudinal and transverse components.

An observer moving with a circularly polarized electromagnetic wave would sense no rotation of the field vectors. $\bar{E}_{1\perp}$ and $\bar{B}_{1\perp}$ would appear to maintain a fixed orientation with respect to the steady state field. But, to particles moving with longitudinal velocities different from the wave phase velocity, the wave rotates at a doppler-shifted frequency. Particles overtaking the wave experience a perturbed field that rotates in a direction contrary to the actual polarization. When the relative longitudinal velocity of wave and particle is just great enough that the particle senses a wave field rotating at its own gyro-frequency, the particle is in <u>resonance</u> with the wave. A particle that is just slightly out of resonance can be accelerated in a manner analogous to the acceleration by longitudinal oscillations. Only particles that are very near to resonance can be affected strongly

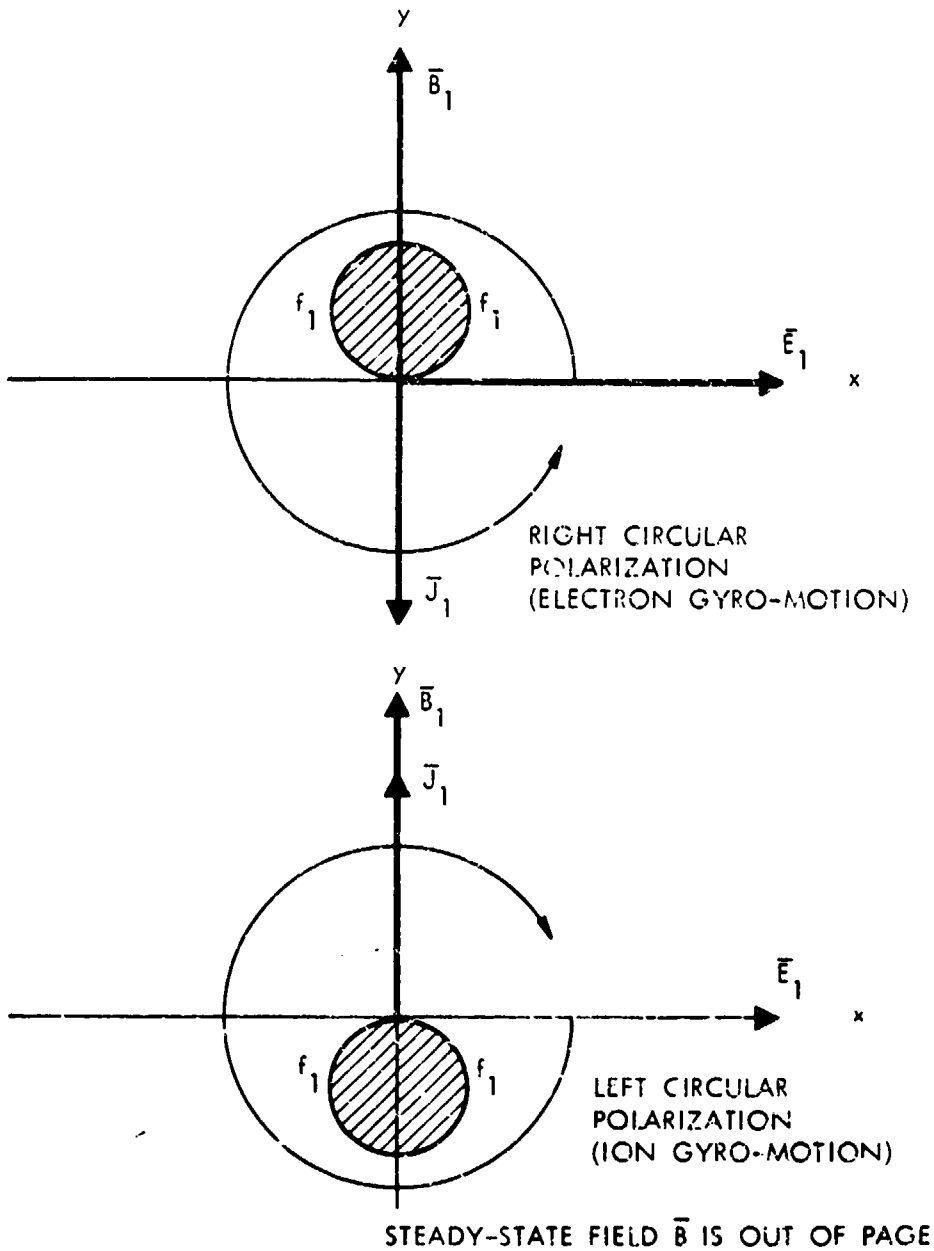

Figure 5-17. Relative phases of wave field vectors in a circularly polarized wave. The shaded area labeled f_1 represents the perturbation in the electron distribution function.

by wave particle interactions. Usually, positively and negatively charged particles may be in resonance with the same wave, although their longitudinal velocity components are entirely different. The longitudinal velocities of resonant particles are related to the wave phase velocities:

$$V_\omega = \frac{\omega}{k} \tag{5-102}$$

by the doppler frequency shift condition (Reference 129) for electrons:

$$v_{\parallel} = V_p \frac{\omega - \omega_e}{\omega} \tag{5-103a}$$

and for protons

$$v_{\parallel} = V_\omega \frac{\omega + \omega_i}{\omega} \quad . \tag{5-103b}$$

ω_e and ω_i are the gyro-frequencies, which include a factor of the inverse of the relativistic dilation factor γ. These two equations are valid for right-handed waves—rotating in the same sense as the electrons. They can be employed for waves of either polarity if ω is regarded as negative for left-handed waves.

From Equation 5-103, the rather odd result follows that a wave rotating in the same sense as the electrons but at a frequency below the electron gyro-frequency will be in resonance with electrons moving in a direction opposite to the wave. Protons in resonance with the same wave must be moving in the same direction as the wave but slightly faster.

In a coordinate frame moving together with a circularly polarized wave at the phase velocity V_ω, the E_1 force appears to be cancelled by the $\bar{v} \times \bar{B}_1/c$ force. The accelerating ($\bar{E}$) force on a resonant particle in this coordinate frame is zero, therefore its total energy remains constant (References 129 through 133). The momentum relative to the moving reference frame, which also must be conserved, is

$$p_W = \sqrt{p_\perp^2 + \gamma_W^2 (p_{\parallel} - m\gamma V_\omega)^2} \tag{5-104a}$$

$$\gamma_W = \frac{1}{\sqrt{1 - V_\omega^2/c^2}} \approx 1 \quad . \tag{5-104b}$$

Because some radiation belt particles have velocities near the speed of light, a fully relativistic formulation has been retained. When making the transition to a nonrelativistic formulation, both γ_W and the mass dilation factor γ must become nearly equal to 1. The phase velocity of most plasma waves is actually so small that γ_W seldom differs appreciably from 1.

According to Equation 5-104, an infinitesimal alteration of the transverse momentum $\delta p_\perp$ is related to an infinitesimal change in the longitudinal momentum $\delta p_\parallel$ or:

$$p_\perp \left[1 - \gamma_W^2 \left(p_\parallel - m\gamma V_\varphi \right) \frac{V_\varphi}{m\gamma c^2} \right] \delta p_\perp = - \gamma_W^2 \left(p_\parallel - m\gamma V_\varphi \right) \left(1 - \frac{p_\parallel V_\varphi}{m\gamma c^2} \right) \delta p_\parallel \quad . \tag{5-105}$$

In the nonrelativistic limit, this reduces to a much simpler formula (References 131, 134, and 135):

$$p_\perp \delta p_\perp \cong - \left(p_\parallel - m V_\varphi \right) \delta p_\parallel \quad . \tag{5-106}$$

Figures 5-18a and 5-18b illustrate the velocity-space diffusion trajectories of protons interacting with waves at the proper phase velocities. In constructing these relations between $v_\parallel$ and $v_\perp$ Equation 5-115 was utilized since it provides, in conjunction with Equations 5-103 and 5-105, a relation between phase velocity and frequency. At high velocities, these trajectories are very nearly circular; this means that the alteration of the particles' kinetic energies is slight. The corresponding velocity space trajectories would be indistinguishable from circles for most radiation belt electrons.

From the preceding equations, a simple relation follows for the change in the transverse part of the momentum relative to the change in the total momentum of electrons:

$$\frac{\delta p_\perp^2}{\delta p^2} \cong \frac{\omega_e}{\omega} \tag{5-107a}$$

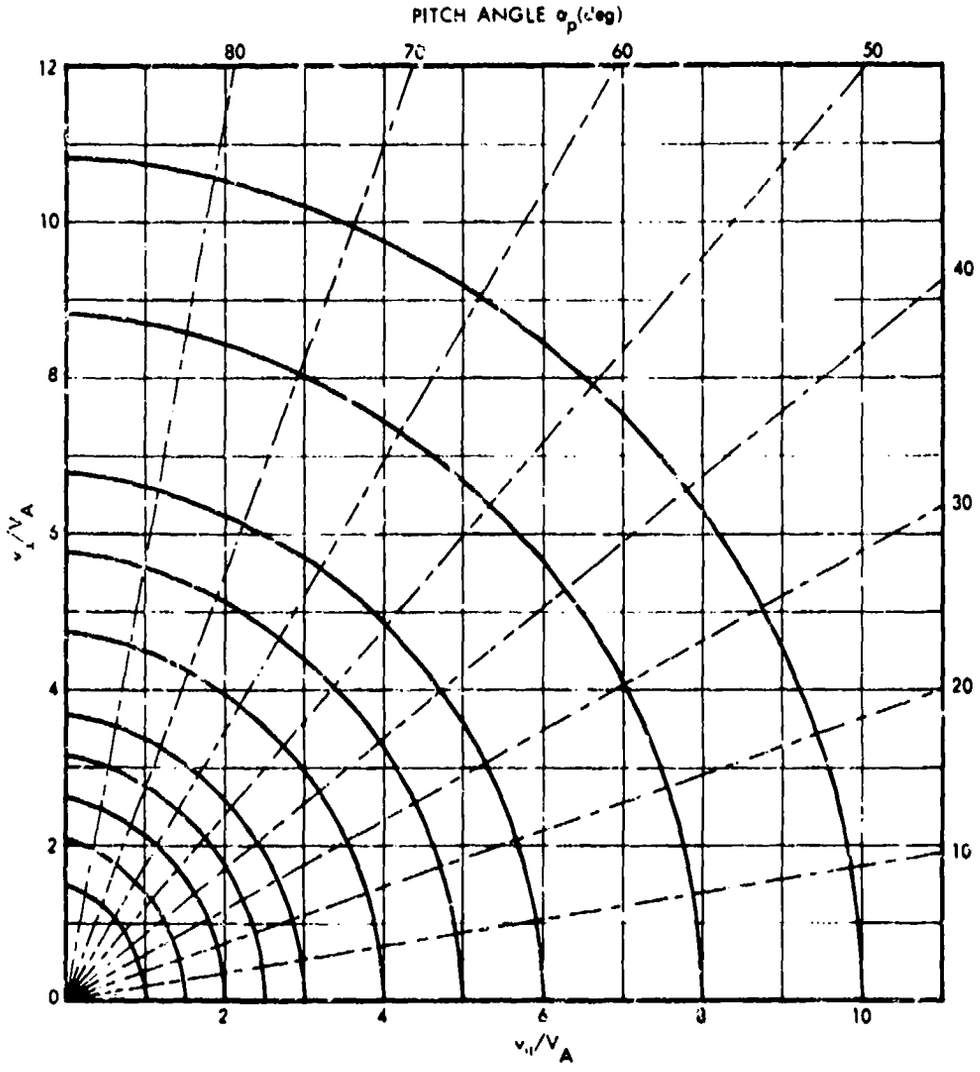

Figure 5-18a. Velocity space trajectories of a proton interacting with circularly polarized waves—velocity components are relative to the Alfvén velocity V_A.

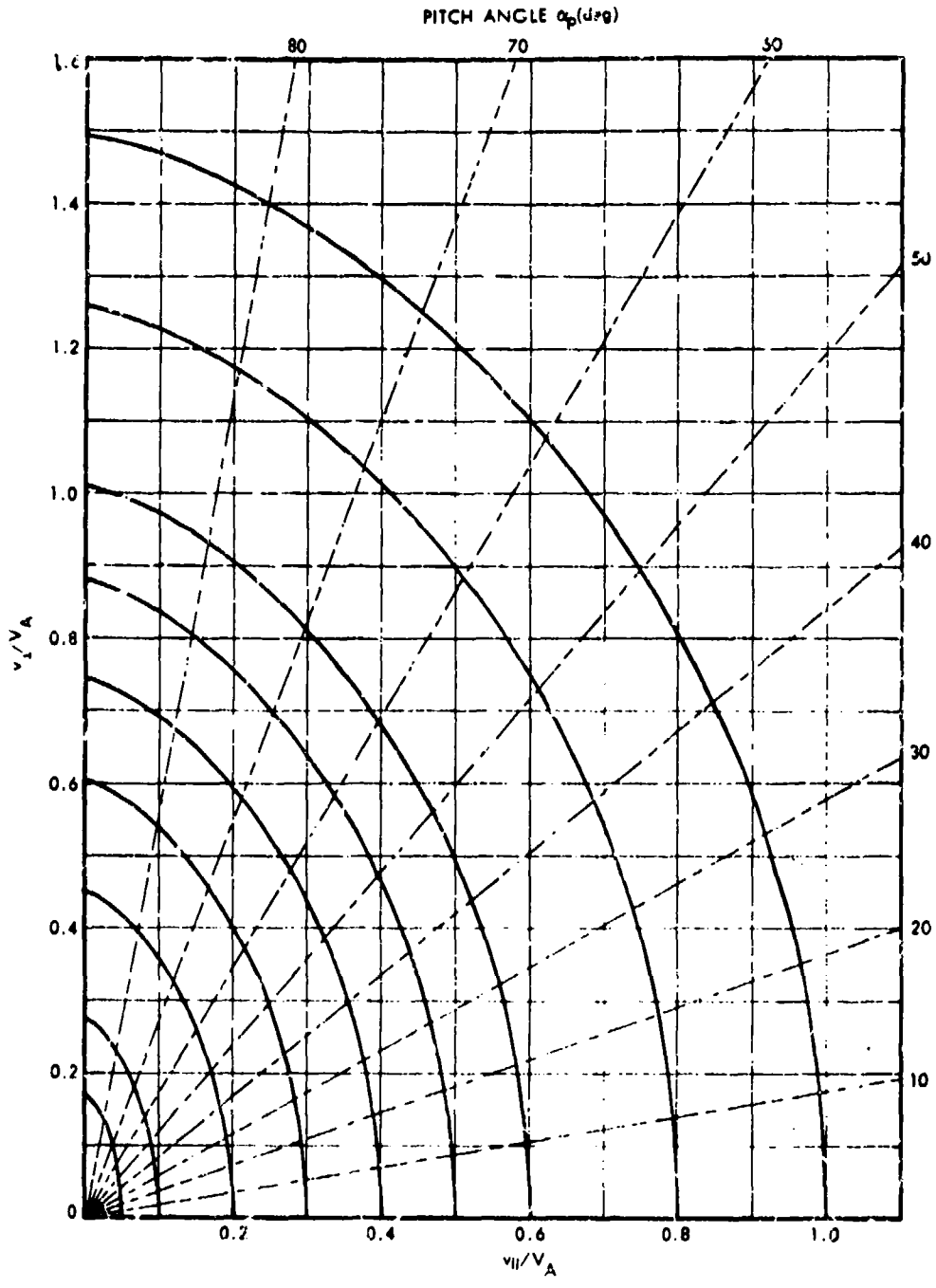

Figure 5-18b. Velocity space trajectories of a proton interacting with circularly polarized waves—velocity components are relative to the Alfvén velocity V_A.

or of protons or positive ions:

$$\frac{\delta p_-^2}{\delta p^2} \cong -\frac{\omega_i}{\omega} \qquad (5\text{-}107b)$$

Clearly, deflections of gyrating particles are much more important than changes in the total momentum whenever the frequency of the waves is much lower than the particles' gyro-frequencies. Also, oppositely charged particles are deflected in quite different directions by the same wave.

It should be especially emphasized that Equations 5-105 and 5-106 and the accompanying figures apply only to circularly polarized waves in a homogeneous plasma. There are many exceptions which allow a greater degree of acceleration than would seem to be permitted by the derived diffusion trajectories. A charged particle in a converging magnetic field experiences a turning force (Equation 3-42a) which may, under certain conditions, balance the accelerating force due to the wave (Reference 133). The particle then can be "held" in a localized region while being accelerated over many cycles of the wave. This mechanism has been suggested as a means for accelerating heavy ions at relatively low altitudes (Reference 136).

5.5.4 Propagation of Waves in a Plasma

In the preceding section it was pointed out that a charged particle in resonance with an electromagnetic wave exchanges energy with the wave. From a knowledge of the wave power spectrum one might derive diffusion coefficients that describe the changes in the particles' energy and pitch-angle distributions. However, the picture would not be complete because the resonant particles cause absorption or amplification of the waves. The effect of the particles on waves that propagate through the plasma is accounted for in the dispersion equation.

The equation-of-motion of particles interacting with a plasma wave is the Boltzmann equation (Equation 3-91). Let the distribution function be represented by a constant part f, plus a small part perturbed by the wave, f_1. When $f + f_1$, $\overline{E}_1$, and $\overline{B} + \overline{B}_1$ are substituted in the Boltzmann equation, the result, to first order in the perturbed quantities, is the Boltzmann-Vlasov equation (Reference 26):

$$\frac{\partial f_1}{\partial t} + \frac{1}{m\gamma}\overline{p} \cdot \nabla f_1 + \frac{\omega_c}{\gamma}(\overline{p} \times \hat{z}) \cdot \nabla_p f_1 + q\left[\overline{E}_1 + \frac{1}{m\gamma c}\overline{p} \times \overline{B}_1\right] \cdot \nabla_p f = 0 \qquad (5\text{-}108)$$

Collisions have been ignored here; they can do no more than absorb energy from all particles, more or less independent of their phase relationship with the waves. The wave field may be represented by the oscillatory parts of Equation 5-11, and f_1 may be represented by a function of the form $g \sin(\phi + \Psi)$.

The equations for longitudinal and transverse oscillations are separable for the special case of propagation along the direction of the external magnetic field. For a more thorough treatment of waves of various polarizations propagating at arbitrary angles to the magnetic field, see Reference 134, and particularly References 137 through 140. However, most of the interesting results follow from a simplified treatment, so the discussion here will be limited to parallel propagation.

Substitution of f_1 into the current equation

$$\bar{J}_1 = \frac{q}{c} \int\int\int d^3p \, \bar{v} f_1 \tag{5-109}$$

facilitates the elimination of g, E_1, and $E_\perp$. The result is the dispersion equation relating the frequency and wave number of curcularly polarized waves (References 133, 134, and 141):

$$\omega^2 - k^2 c^2 = - \sum_{\substack{\text{electrons} \\ \text{and ions}}} \omega^2_{p(e,i)} \int\int\int d^3p \, \frac{p_\perp}{2\gamma} \cdot \frac{i}{(\omega \mp \omega_c - k p_\parallel / m\gamma)} \left[\left(\omega - \frac{k p_\parallel}{m\gamma} \right) \frac{\partial f/n}{\partial p_\perp} + \frac{k p_\perp}{m\gamma} \frac{\partial f/n}{\partial p_\parallel} \right] \tag{5-110}$$

Note that the gyro-frequency still contains the factor $1/\gamma$. The upper signs pertain to right-handed (RH) waves, and the lower signs pertain to left-handed (LH) waves. The dispersion equation for longitudinally polarized waves is (after a partial integration with respect to $p_\parallel$):

$$\omega \sum_{\substack{\text{electrons} \\ \text{and ions}}} \omega^2_{p(e,i)} \int\int\int d^3p \, \frac{\omega}{\gamma^2} \frac{1}{(\omega - k p_\parallel / m\gamma)^2} \cdot \left(1 + \frac{p_\perp^2}{m^2 c^2} \right) \frac{f}{n} \cdot \tag{5-111}$$

The electron and ion plasma frequencies are (References 32, 58, and 128):

$$\omega_R = \sqrt{\frac{4\pi n e^2}{m}} \qquad (5\text{-}112a)$$

for electrons:

$$\omega_{pe}(\text{sec}^{-1}) = 5.641 \times 10^4 \sqrt{n_e(\text{cm}^{-3})} \qquad (5\text{-}112b)$$

and for protons:

$$\omega_{pi}(\text{sec}^{-1}) = 1.317 \times 10^3 \sqrt{n_i(\text{cm}^{-3})} \qquad (5\text{-}112c)$$

A useful parameter characterizing the ionization density of a magnetized plasma is the ratio of the squares of the electron plasma frequency and the electron gyro-frequency:

$$Q \equiv \frac{\omega_{pe}^2}{\Omega_e^2} = \frac{4\pi n_e m_e c^2}{B^2} \; . \qquad (5\text{-}113)$$

(There does not seem to be a well-established symbol for the quantity defined in Equation 5-113; the choice of Q is rather arbitrary.) Hereafter, to avoid confusion, the capital letter symbols Ω_c, Ω_e, Ω_i will be used to designate the part of the gyro-frequency that is independent of the particle momentum. The plasma density parameter, Q, is essentially the inverse of the magnetic energy per particle, a parameter that appears in much of the current literature (e.g., References 134 and 142 through 144). Figure 5-19 shows some typical values of Q throughout the magnetosphere. Generally, it is anticipated that the character of plasma waves changes dramatically as Q passes through the value of 1 (References 142 through 144). It might be further deduced that the interactions between waves and particles have different consequences inside and outside the plasmapause where Q may drop from a value greater than 1 to a value much less than 1. It likewise can be inferred that plasma oscillations are insignificant below the E layer of the ionosphere where Q falls rapidly toward zero.

Consider waves traveling in a plasma with an isotropic, low-temperature particle momentum distribution. Since electrical neutrality requires equality of the numbers of ions and electrons, the ion plasma frequency is negligible compared with the electron plasma-frequency. The dominant terms in the longitudinal-polarization dispersion equation, 5-111, are

$$\omega^2 = \omega_{pe}^2 + \omega_{pi}^2 = \Omega_p^2 \approx \omega_{pe}^2 \qquad (5\text{-}114)$$

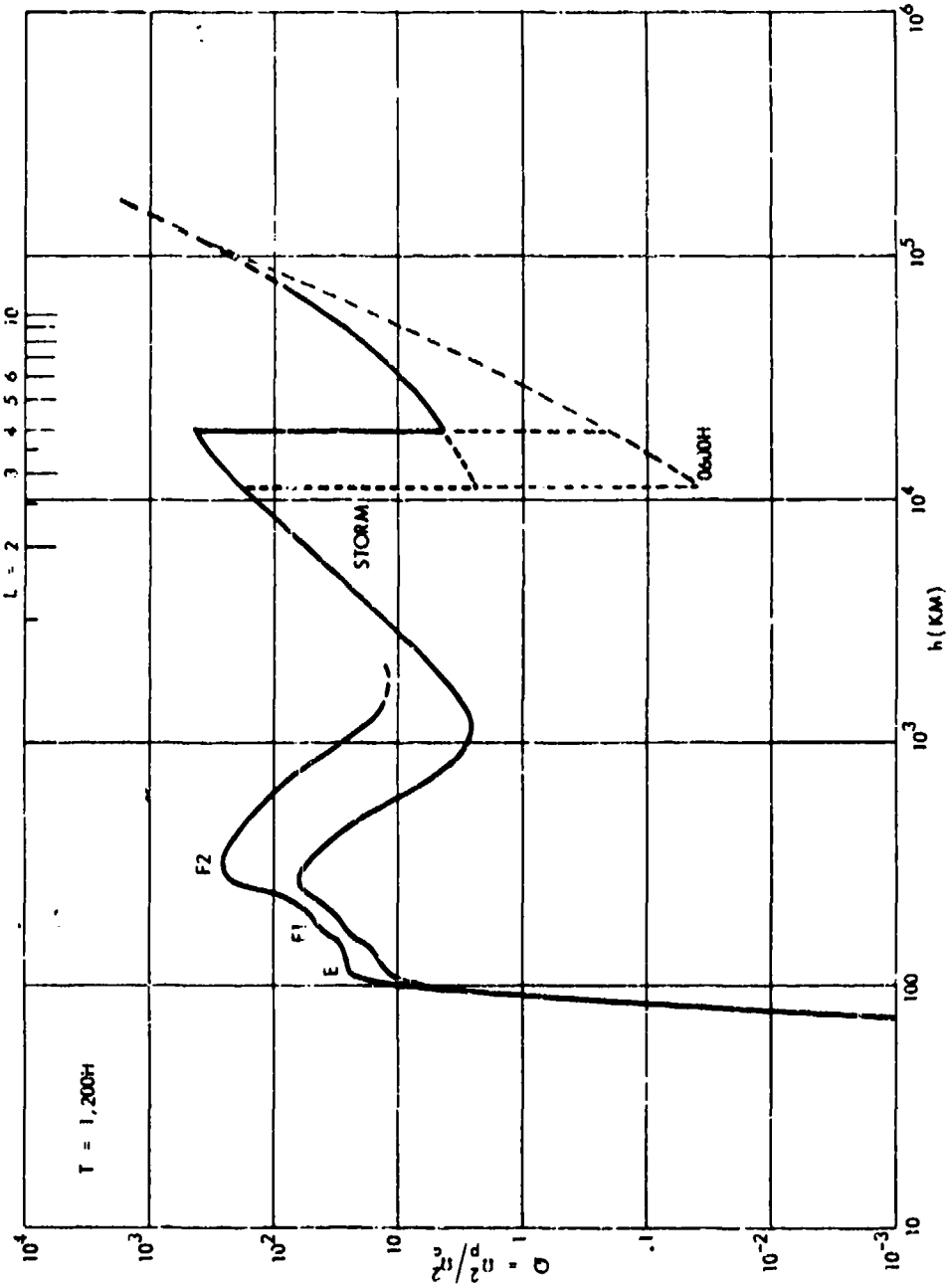

Figure 5-19a. The ratio of plasma frequency-squared to electron gyro-frequency-squared, on the morning and dayside of the magnetosphere. (In both parts of this figure, the values are representative of typical conditions in the equatorial regions. The data were adapted from Figure 5-2 and Reference 145.)

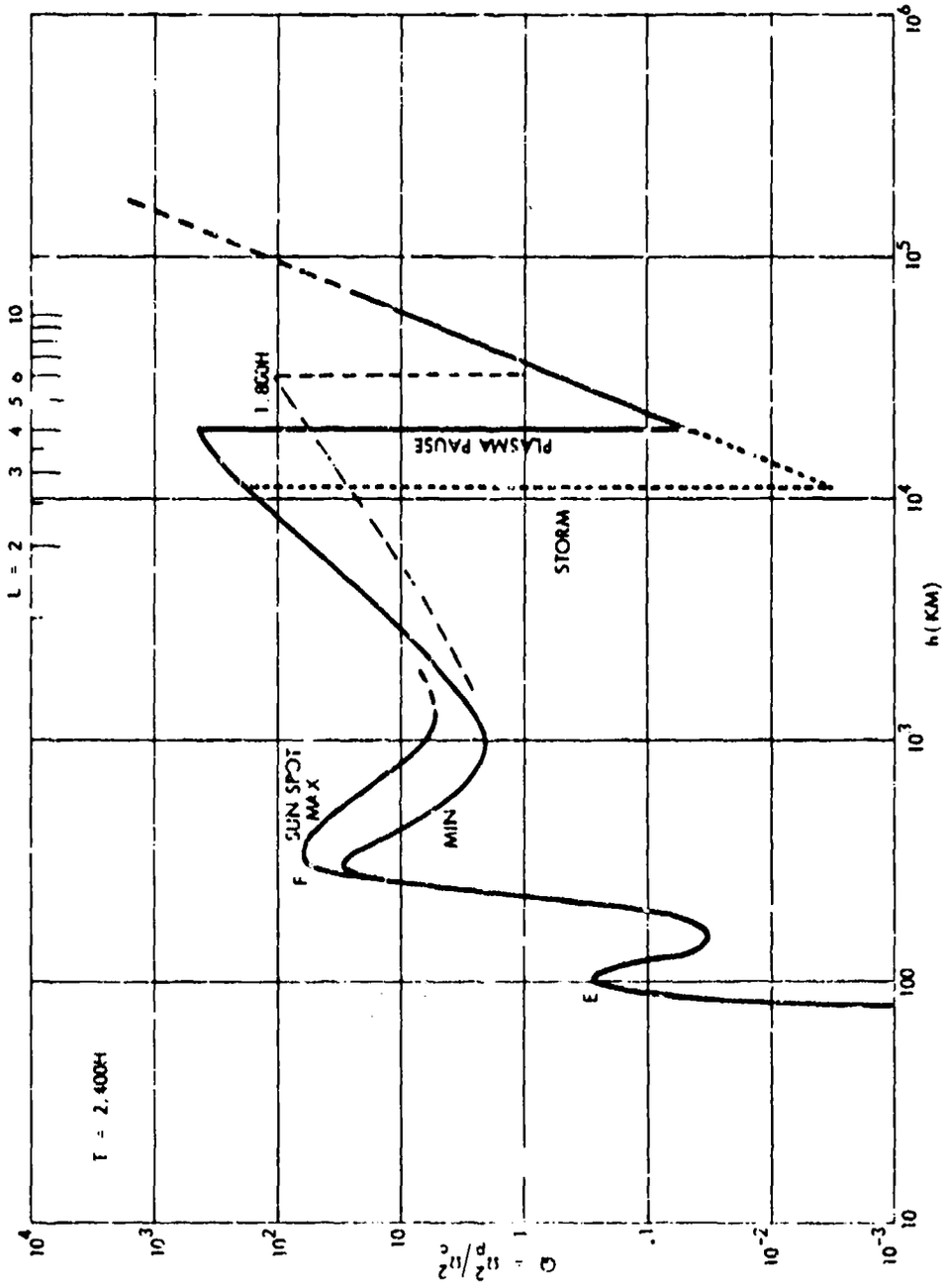

Figure 5-19b. The ratio of plasma frequency-squared to electron gyro-frequency-squared, on the evening and nightside of the magnetosphere.

That is, in a cold plasma, the only possible longitudinal waves are non-propagating electrostatic oscillations at the plasma frequency Ω_p (Reference 128).

Electrostatic-type waves propagating at large angles from the magnetic field have been observed (References 146 through 149), although their significance is not yet fully understood. Some electrostatic waves can exchange energy quite efficiently with trapped particles near the loss-cone of a typical trapped pitch-angle distribution (References 150 and 151). Electrostatic waves have been shown to be very effective in accelerating trapped particles (References 152 through 154) and might perhaps be shown to be responsible for many of the effects once attributed to circularly polarized electromagnetic waves. The treatment of electrostatic waves is slightly more complicated than the circularly polarized waves, and the interested reader is referred to the sources cited above and Reference 133. It is certainly agreed that most of the waves generated in the upper ionosphere are electrostatic in nature, although their effects on trapped particles are limited to the edge of the loss cone; for a particular example, see Reference 156.

The propagation of circularly polarized waves in a plasma consisting entirely of low-velocity particles is described by the cold-plasma dispersion equation (References 128 and 133)

$$\frac{V_\varphi}{c} \quad \frac{\omega}{kc} \sqrt{\frac{(\Omega_e - \omega)\ (\Omega_i + \omega)}{(\Omega_e - \omega)\ (\Omega_i + \omega) + \Omega_p^2}} \quad . \tag{5-115}$$

Again, a single equation, without the ± signs of Equation 5-110, suffices for both RH and LH polarization if ω is considered to be negative for LH waves and vice versa. The cold plasma dispersion equation is rather insensitive to small deviations from propagation strictly parallel to the external magnetic field (References 128 and 133)

Usually, in the magnetosphere, the wave frequency is low enough, and Q is sufficiently large that an adequate approximation to Equation 5-115 is

$$\frac{V_\varphi}{c} \sim \frac{\sqrt{\omega(\Omega_e - \omega)}}{\Omega_p} \Big\} \Omega_i < \omega << \Omega_e \tag{5-116}$$

The low-frequency right-handed waves to which Equation 5-116 applies are in the whistler mode; whistler-mode waves are one of the predominant types of magnetospheric VLF radio noise. At somewhat lower frequencies the RH waves are in the magnetosonic mode

$$\frac{V_\varphi}{c} \sim \frac{\sqrt{\Omega_e(\Omega_i + \omega)}}{\Omega_p} \Bigg\} \quad |\omega| < \Omega_i \quad . \tag{5-117}$$

The LH analog of the magnetosonic mode is the ion-cyclotron mode; ion-cyclotron waves also obey Equation 5-117 (with a negative frequency). The interaction of ions with ion-cyclotron waves is quite similar to the interaction of electrons with whistler waves.

Of considerable practical interest is the resonance condition relating the wave frequency to the velocity of a resonant particle. For an electron in resonance with a whistler mode wave, Equations 5-103a and 5-116 give

$$\frac{v_\parallel}{c} \approx \frac{1}{\Omega_p}\sqrt{\frac{(\Omega_e - \omega)^3}{\omega}} \quad . \tag{5-118}$$

The corresponding resonance condition for an ion in resonance with a wave in the ion-cyclotron mode is

$$\left|\frac{v_\parallel}{c}\right| \approx \frac{\sqrt{\Omega_e(\Omega_i + \omega)^3}}{\omega\,\Omega_p} \quad . \tag{5-119}$$

The resonance conditions for an electron-proton plasma are plotted in Figures 5-20 and 5-21, for electrons and ions, respectively. The plotted curves include the complete dispersion equation, 5-115, and the relativistic corrections. It is remarkable that the necessity for the relativistic corrections depends more upon the value of Q than upon the particles' speeds. For large values of Q (>> 1) the relativistic and non-relativistic resonance conditions are nearly identical. For very small values of Q the relativistic resonance condition in the vicinity of the gyro-frequency gives a resonant momentum about one-half that predicted by the simpler non-relativistic formula.

The resonant momenta very near the gyro-frequencies are actually slightly modified by the effects of finite plasma temperatures. A simple test of the necessity for finite-temperature corrections is to compare the kinetic energies of the important resonant particles with the mean thermal energies. Generally, the resonant velocities at low frequencies are far greater than the average thermal velocities. However, if a finite-temperature correction is needed, the form of the distribution function must be retained explicitly in Equations 5-110 and 5-111, rather than regarded as a Dirac delta-function around zero momentum. One case in which the finite-temperature corrections

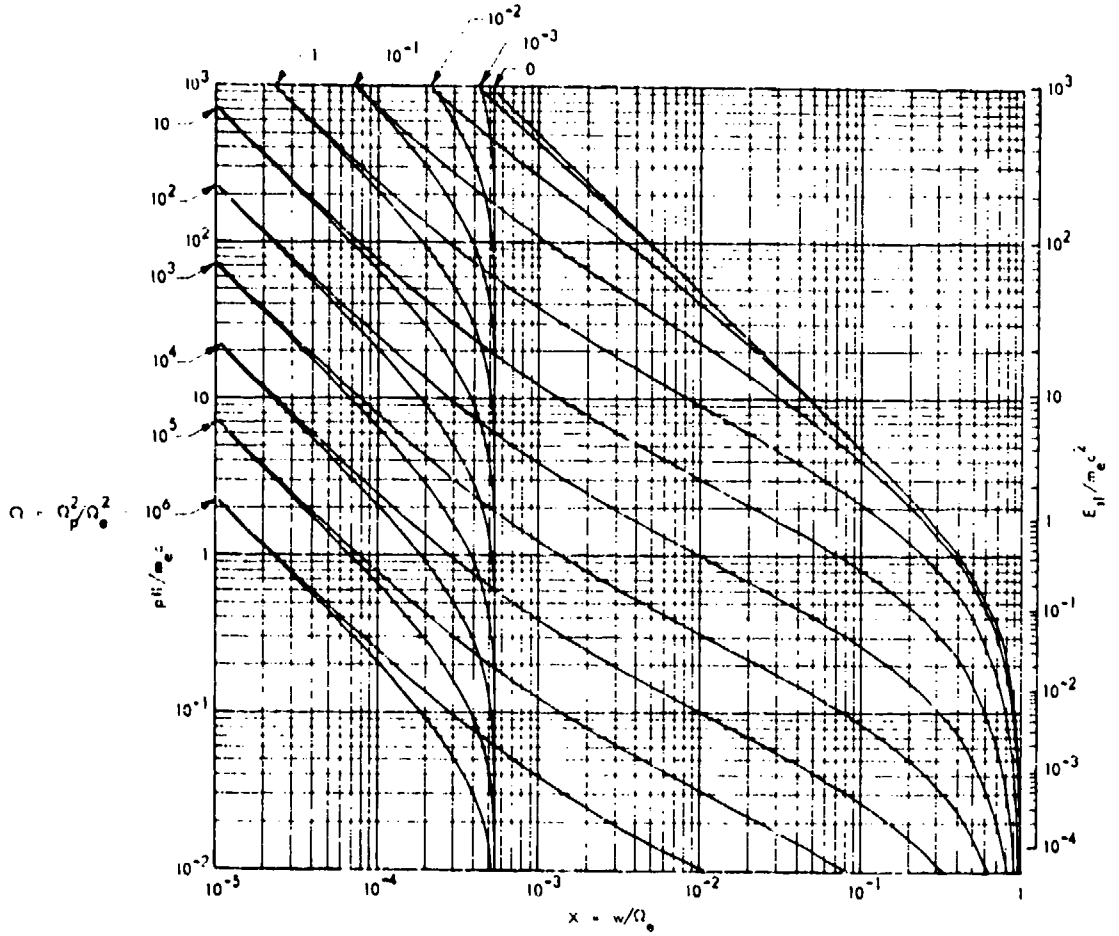

Figure 5-20. The relativistic resonance conditions for electrons interacting with circularly polarized waves in an electron-proton plasma. (On the right portion of the figure, for $\omega < \Omega_i$, the electrons can resonate only with right-handed, whistler mode waves. Below the ion gyro-frequency, resonance is possible with left-handed or right-handed waves; in the zero-frequency limit, those two resonances are identical.)

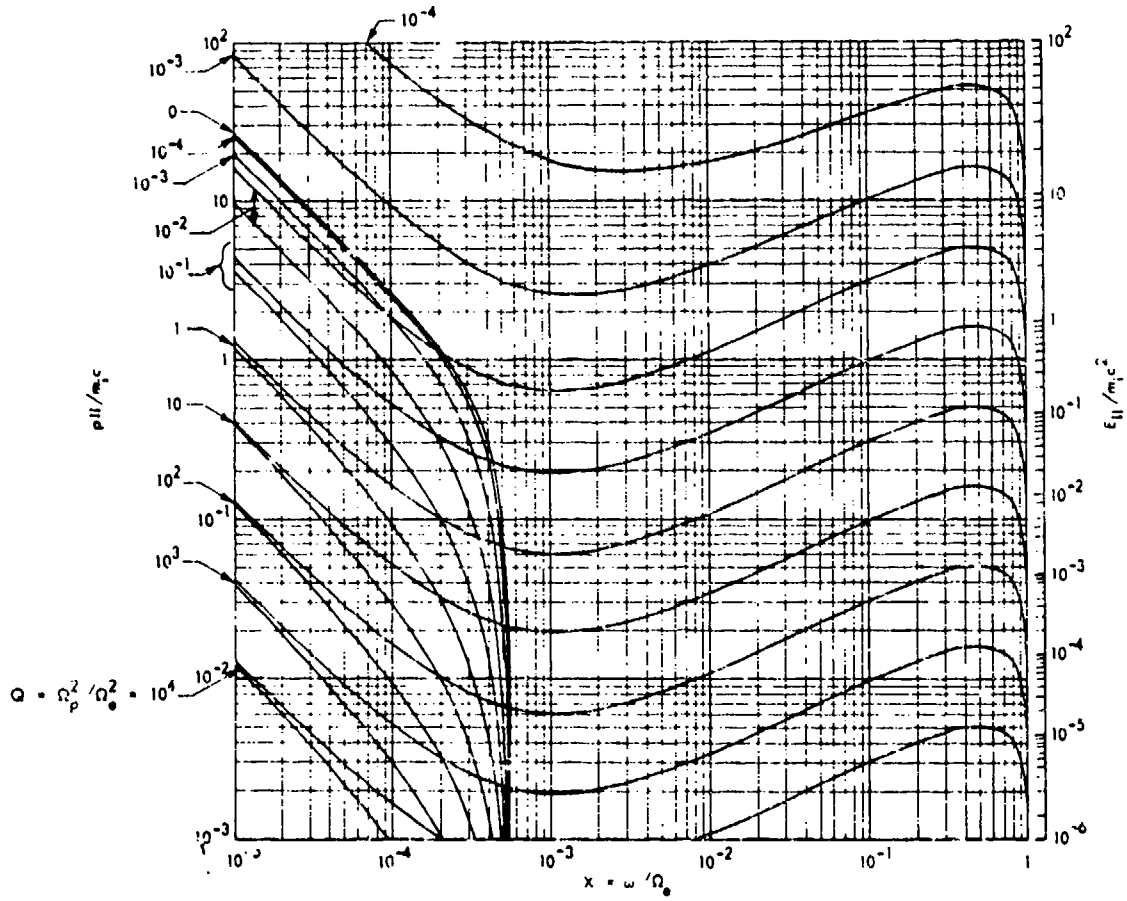

Figure 5-21. The relativistic resonance conditions for protons interacting with circularly polarized waves in an electron-proton plasma. (On the right-hand portion of the figure, the protons are in resonance only with right-handed waves. In practice only, the region around proton gyro-frequency is of interest; there is a minimum momentum below which resonance with right-handed waves is effectively prohibited.)

must be made is in the resonance of electrons with LH ion-cyclotron waves. That resonance is so near the ion gyro-frequency that the ions' temperature must be considered. The corrected ion-cyclotron wave phase velocity has a minimum near Ω_i, which, in turn, leads to a minimum resonant velocity (Reference 133). The computed minimum phase velocity and electron momentum are shown in Figure 5-22. The minimum energy of an electron resonating with ion-cyclotron waves inside the plasmasphere is of the order of several MeV.

AMPLIFICATION OF PLASMA WAVES-INSTABILITIES. The cold plasma dispersion equation (Equation 5-115) was derived subject to the assumption that the only contribution to the integral of Equation 5-110 was near $p=0$. Of course, most plasmas, and especially the magnetospheric plasma, include enough particles at finite momenta that the denominator of the integrand makes a large contribution at $p_{\parallel} = m\gamma(\omega+\omega_c)/k$. The denominator is singular at the resonant momentum, and only yields a finite result if a small imaginary part is added to the frequency or wave number (References 58, 133, and 134). This is equivalent to a multiplication of the amplitudes of the sinusoidal wave fields by an exponential growth or decay factor. Because the waves in the magnetospheric plasma pass through spatial inhomogeneities, it seems proper to consider the amplification rate δ, the imaginary part of the wave number. The growth rate, which is the imaginary part of the frequency, is ideally a characteristic parameter of an infinitely extensive homogeneous plasma. Either parameter can be derived from the basic dispersion equation; the amplification and growth rates are related through the group velocity V_g, or

$$\left|\frac{\mathrm{Im}(\omega)}{\mathrm{Im}(k)}\right| = \frac{\partial\omega}{\partial k} = V_g \quad . \tag{5-120}$$

For transverse circularly polarized waves, the group velocity is

$$V_g = c\,\frac{\sqrt{\left[(\Omega_i+\omega)(\Omega_e-\omega)+\Omega_p^2\right](\Omega_i+\omega)^3(\Omega_e-\omega)^3}}{(\Omega_i+\omega)^2(\Omega_e-\omega)^2+\Omega_p^2\left|\Omega_i\Omega_e+\omega(\Omega_e-\Omega_i)/2\right|} \tag{5-121}$$

A straightforward derivation of the amplification rate often yields a combination of two solutions -a growing wave solution, and a decaying wave solution. One of these solutions is not meaningful, and can be ruled out because it does not conserve energy. The convention followed here is that a positive amplification rate applies to growing waves in that case, the waves will grow until either a major part of the particles' kinetic energy is dissipated or the waves are restrained by an external agency. A negative amplification rate means that the particles absorb energy from the wave.

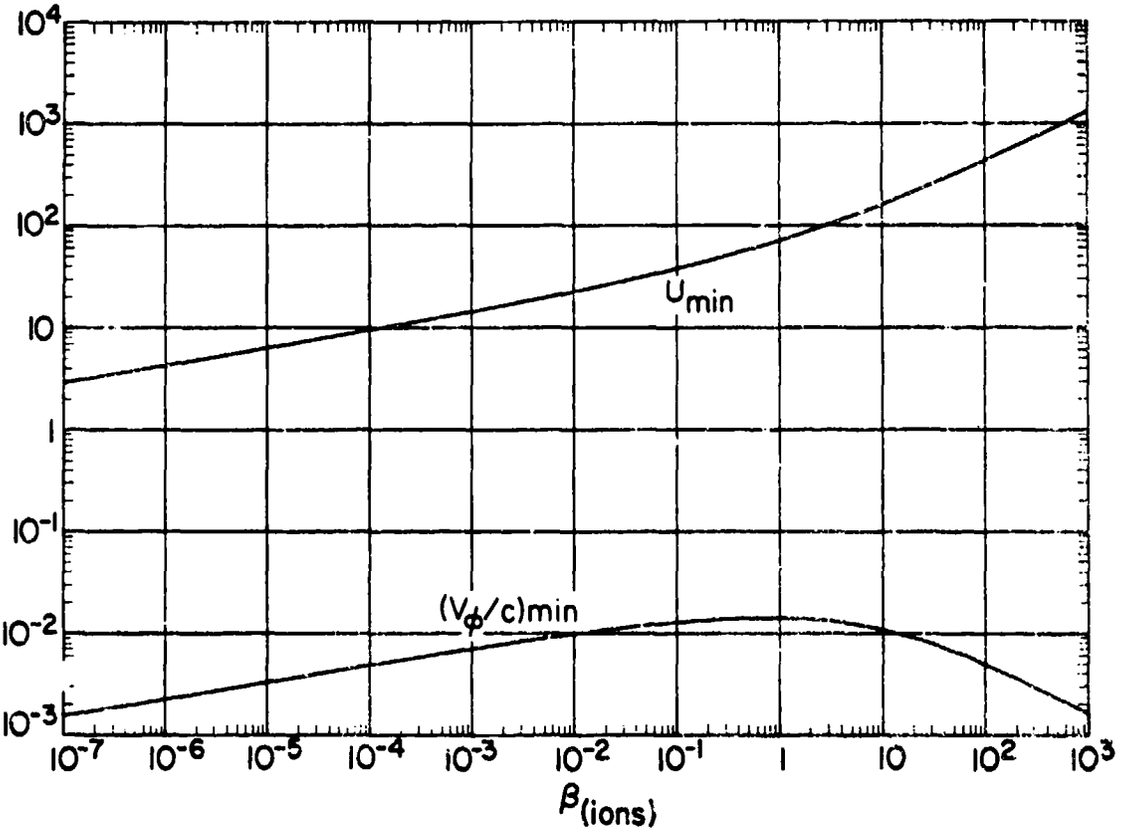

Figure 5-22. The minimum phase velocity and minimum resonant electron momentum for ion-cyclotron waves as a function of $\beta \frac{2Q\langle T\rangle_{avg}}{3m_e c^2}$ $\frac{2QT}{m_e c^2}$. (Note that this definition differs by a factor of 2/3 from the more conventional definition. The momentum is in dimensionless units, $U = p_{\|}\sqrt{Q}/m_e c^2$.)

The energy source needed to sustain wave growth is just the kinetic energy of the faster resonant particles. If it is assumed that the waves have not had sufficient time to exchange appreciable amounts of energy from the particles, the constant part of the distribution may be split into two parts: (1) an isotropic, low-temperature part, and (2) a non-thermal part that may comprise only a small fraction, η, of the total number of particles. The real part of the dispersion equation is merely the cold plasma equation, 5-115. The imaginary part, which gives δ, involves an integral over the non-thermal part of the distribution. If the non-thermal part of the distribution is represented by $f(\bar{p})$, now normalized so that

$$\int f(\bar{p}) d^3p = 1, \tag{5-122}$$

the imaginary part of the dispersion equation is

$$-2k\delta c^2 = \sum_{\text{ions + electrons}} \eta \omega_p^2 \{\text{sign}\} \cdot \int d_p^3 \frac{p_\perp}{2\gamma} (\omega + \omega_c) \frac{\delta/m\gamma}{(\omega + \omega_c - kp_\parallel/m\gamma)^2 + p_\parallel^2 \delta^2/m^2\gamma^2} \left[p_\parallel \frac{\partial f}{\partial p_\parallel} - \frac{\omega_c}{\omega + \omega_c} p_\parallel \frac{\partial f}{\partial p_\perp} \right]. \tag{5-123}$$

There is an ambiguity of sign in the above equation which will be resolved in the final result. The equation is of little interest itself except to demonstrate that the integrand is very sharply peaked at the resonant momentum. If δ is much less than the real part of the wave number k, the integration can be performed with the aid of the Dirac delta function

$$\text{delta}(x) = \frac{1}{\pi} \text{sign}(\epsilon) \lim_{\epsilon \to 0} \frac{\epsilon}{x^2 + \epsilon^2} . \tag{5-124}$$

The amplification rate is

$$\delta = \frac{\pi^2}{2} \frac{V_\varphi}{c^2} \sum_{\text{ions + electrons}} \text{sign}(\Omega_c) \eta \frac{\omega p^2}{\omega} \cdot \int_0^\infty p_\perp^2 dp_\perp \left[\frac{1}{1 - \frac{V_\varphi^2}{c^2} \frac{\omega + \omega_c}{\omega}} \right] \left\{ \frac{1}{\gamma} \left[p_\perp \frac{\partial f}{\partial p_\parallel} - p_\parallel \frac{\partial f}{\partial p_\perp} \right] + m V_\varphi \frac{\partial f}{\partial p_\perp} \right\}_{p_\parallel = p_R} . \tag{5-125}$$

The integrand must be evaluated at the resonant momentum p_R, a solution of the resonance relation

$$p_R^2\left(1 - \frac{V_\varphi^2}{c^2}\right) - \left|2p_R\, mV_\varphi \frac{\Omega_c}{\omega}\right| - m^2V_\varphi^2\left(1 - \frac{\Omega_c^2}{\omega^2}\right) = 0 \quad . \qquad (5\text{-}126)$$

The phase velocity is generally small compared with the speed of light, in which case the complicated denominator disappears and an integration by parts gives

$$\delta = \frac{\pi^2}{2}\frac{V_\varphi}{c^2} \sum_{\text{ions + electrons}} \text{sign}\,(\Omega_c)\,\eta\,\frac{\omega_p^2}{\omega}$$
$$\cdot \int_0^\infty p_\perp\, dp_\perp \frac{1}{\gamma}\left\{\left[p_\perp \frac{\partial f}{\partial p_\parallel} - p_\parallel \frac{\partial f}{\partial p_\perp}\right] - 2p_\parallel \frac{\omega}{\omega + \omega_c} f\right\}_{p_\parallel = p_R} . \qquad (5\text{-}127)$$

The last part of the integrand of the above equation is always negative and, by itself, would lead to wave absorption. The explanation for, and consequences of, the absorption are analogous to Landau damping in the simple theory of electrostatic waves (Reference 133). The damping effect arises because any distribution function begins at some point to fall off with increasing momentum; when that happens, there are more particles which tend to retard the wave than there are accelerating the wave. The actual Landau damping of transversely polarized waves is somewhat complicated by propagation at finite angles to the magnetic field, where the waves tend to behave as though they had also an appreciable electrostatic-mode component (References 157 and 158). All that is important here is that when the pitch-angle distribution is sufficiently anisotropic, the first part of the integral predominates and some waves can experience a growth in amplitude.

The non-relativistic approximation to the last equation is often presented in terms of the anisotropy (Reference 134):

$$A = \frac{\int_0^\infty p_\perp\, dp_\perp \frac{p_\perp}{p_\parallel}\left[p_\parallel \frac{\partial f}{\partial p_\perp} - p_\perp \frac{\partial f}{\partial p_\parallel}\right]_{p_\parallel = p_R}}{2\int_0^\infty p_\perp\, dp_\perp\, f_{p_\parallel = p_R}} . \qquad (5\text{-}128)$$

The necessary conditions for wave growth (in the presence of a single dominant resonant species) are simply

$$A > -\frac{\omega}{\Omega_c - \omega}\begin{cases}\text{electrons in RH waves}\\ \text{ions in LH waves}\end{cases} \qquad (5\text{-}129a)$$

$$A < -\frac{\omega}{\Omega_c + \omega} \left\{ \begin{array}{l} \text{electrons in LH waves} \\ \text{ions in RH waves} \end{array} \right.$$

The amplification rate by itself does not tell much about the behavior of plasma waves. The amplification rate is, merely, the linearized rate at which the amplitude of a perturbation begins to increase. A calculation which results in an amplification rate comparable with, or greater than, k is in obvious conflict with the condition for the validity of Equation 5-124. Such a result should be taken to mean only that the plasma is highly unstable to generation of waves. When the simple linearized theory leads to contradictions, or when the wave amplitudes have grown large, some form of nonlinear treatment must be employed. One successful analytic method for treating nonlinear growth is referred to as quasilinear theory. Quasilinear theory is a second order approximation in which the part of the distribution function that is constant in the linear theory is allowed to vary at a slow rate compared with the wave frequency. Quasilinear theory leads naturally to diffusion coefficients that describe the behavior of the plasma over extended time intervals. Some applications of quasilinear theory to magnetospheric waves are to be found in References 155 through 167.

A computational method that is beginning to prove its value in the solution of plasma problems is computer simulation. The most versatile plasma simulation programs are based on the simplest formulations of the equations-of-motion of a charged particle, or group of particles. The trajectories of many particles are numerically integrated over many steps; at each step all the field quantities are recomputed from the particle distribution and used to alter the particle trajectories in the next step of the integration. The method has many limitations, not the least of which is imposed by the storage capabilities and computation times of large digital computers. There are many awkward difficulties that still have to be overcome in the application to magnetospheric problems, particularly the large mass ratio of ions to electrons and the representation of the dipole field geometry. However, the successes of the method have been impressive; for notable examples, see References 166 through 170.

In spite of the limitations of the linearized theory, it may be advantageous to present some additional formulae to be used in estimating amplification rates. When the variables of integration are the cosine of the pitch angle, μ, and the total momentum, p, the amplification rate becomes

$$\delta = \frac{\pi^2}{2} \frac{V}{c} \frac{\varphi}{2} \sum_{\text{ions + electrons}} \text{sign}(\Omega_c)\ \eta \frac{\omega^2}{\omega} \frac{p}{}$$

$$\cdot \int_{p_R}^{\infty} dp \frac{1}{\gamma} \left\{ (p^2 - p_R) \left[1 - \frac{p_R^2}{p^2} \frac{\omega}{\omega + \omega_c} \right] \frac{\partial f}{\partial \mu} - 2pp_R \frac{\omega}{\omega + \omega_c} \right.$$

$$\left. \left[1 - \frac{v_\varphi^2}{c^2} \frac{\omega + \omega_c}{\omega} \omega_c \right] f \right\} \mu \, p_R/p \quad . \tag{5-130}$$

When the integration is restricted to a single plasma component, it may be helpful to change variables to the dimensionless set

$$X = \omega/\Omega_e \tag{5-131a}$$

$$U = V_\varphi/c \tag{5-131b}$$

$$W = p^2/m_e^2 c^2 \tag{5-131c}$$

$$Q = \Omega_p^2/\Omega_e^2 \tag{5-131d}$$

$$Q_H \quad Q_{HOT} = 4\pi n_{HOT} \, m_e c^2/B^2 \tag{5-131e}$$

$$Z \quad \delta c/\Omega_e \tag{5-131f}$$

where Q_H refers to the "hot" component. A large amplification rate occurs for Z near 1. The amplification rate for the electron component and the resonance condition are

$$Z = -\frac{\pi^2}{4} \frac{UQ_H}{X} \int_{W_R}^{\infty} dW \frac{1}{\gamma} \left\{ \sqrt{W} \left(1 - \frac{W_R}{W} \right) \left(1 + \frac{W_R}{W} \frac{X}{1/\gamma - X} \right) \frac{\partial f}{\partial \mu} \right.$$

$$\left. 2\sqrt{W_R} \frac{X}{1/\gamma - X} \left(1 + \frac{W_R}{\gamma} \frac{X}{1/\gamma - X} \right) f \right\}_{\mu \sqrt{W_R/W}} \tag{5-132}$$

$$W_R = \frac{(1-X)(R+X)}{Q^2 X^2} \left[\sqrt{(1-X)(R+X)+Q} - X \sqrt{\frac{1}{X^2} (1-X)(R+X)+Q} \right]^2$$

(5-133)

Equation 5-132 and all the following forms of the amplification rate can also be used for the ion component if the following set of variables is used:

$$R = m_e/m_i \tag{5-133a}$$

$$\hat{X} = -\omega/\Omega_i = -X/R \tag{5-133b}$$

$$\hat{W} = p^2/m_i^2c^2 \tag{5-133c}$$

$$\hat{Q} = \omega_{pi}^2/\Omega_i^2 = Q/R \tag{5-133d}$$

$$\hat{Q}_H = 4\pi n_{HOT} m_i c^2/B^2 \tag{5-133e}$$

$$\hat{Z} = \delta c/\Omega_i \quad . \tag{5-133f}$$

The resonance condition for the ions is

$$\hat{W}_R = \frac{(1-\hat{X})(1+R\hat{X})}{\hat{Q}^2\hat{X}^2}\left[\sqrt{(1-\hat{X})(1+R\hat{X})+\hat{Q}} - \hat{X}\sqrt{\frac{1}{\hat{X}^2}(1-\hat{X})(1+R\hat{X})+\hat{Q}}\right]^2 . \tag{5-134}$$

If the distribution function is separable, i.e.,

$$f(\mu, p) = g(\mu)\, h(p) \tag{5-135}$$

and, moreover, the pitch-angle distribution is of the trapped-type form

$$g(\mu) = \frac{1}{2\pi^{3/2}} \frac{\Gamma(\frac{n+3}{2})}{\Gamma(\frac{n+2}{2})} (1-\mu^2)^{n/2} \tag{5-136}$$

$$\propto (\sin\alpha_p)^n$$

then the amplification rate reduces to

$$\chi = -\frac{\sqrt{\pi}}{8}\frac{\Gamma(\frac{n+3}{2})}{\Gamma(\frac{n+2}{2})}\frac{U^2 Q_H}{X} \times \int_{W_R}^{\infty} dW \left\{ n\left(\frac{1/\gamma - X}{X} + \frac{W_R}{W}\right) - 2\left(1 + \frac{W_R}{\gamma}\frac{X}{1/\gamma - X}\right)\right\}\left(1 - \frac{W_R}{W}\right)^{n/2} h(W) \quad . \tag{5-137}$$

The anisotropy (Equation 5-128) for this case is just $A = n/2$. If the momentum distribution is Maxwellian-like, as defined by the formula

$$h(W) = \frac{W^{\nu/2}}{\Gamma(\frac{\nu+3}{2}) W_o^{(\nu+3)/2}} \exp(-W/W_o) \quad , \tag{5-138}$$

the amplification rate is

$$\chi = -\frac{\sqrt{\pi}}{8}\frac{\Gamma(\frac{n+3}{2})}{\Gamma(\frac{n+2}{2})\Gamma(\frac{\nu+3}{2})}\frac{U^2 Q_H}{X W_o^{3/2}} \int_{W_R}^{\infty} dW \left\{ n\left(\frac{1/\gamma - X}{X} + \frac{W_R}{W}\right) - 2\left(1 + \frac{W_R}{\gamma}\frac{X}{1/\gamma - X}\right)\right\}\left(1 - \frac{W_R}{W}\right)^{n/2} W^{\nu/2} \exp(-W/W_o) \tag{5-139}$$

The above equations are well-suited to numerical computations only in the non-relativistic limit when γ is near 1; then, Equation 5-139 reduces to

$$\gamma \propto \frac{\sqrt{\pi}}{8} \frac{\Gamma(\frac{n+3}{2})}{\Gamma(\frac{n+2}{2})\,\Gamma(\frac{\nu+3}{2})} \frac{U^2 Q_{II}}{X\sqrt{W_0}} \exp\left(-\frac{W_R}{W_0}\right)$$

$$\cdot \int_0^\infty dy \left\{ \left[n\frac{1-X}{X} - 2 \right] + n \frac{W_R/W_0}{y + W_R/W_0} \right\} y^{n/2} \left(y + W_R/W_0\right)^{\nu/2 - n/2} \exp(-y) \qquad (5\text{-}140a)$$

$$- UQ_{II} \left\{ G_1 \left[\frac{n}{X} - \frac{2}{1-X} \right] + G_2 \frac{n}{1-X} \right\} . \qquad (5\text{-}140b)$$

Some numerical values of the functions G_1 and G_2 are given in Figure 5-23 for selected values of the parameters n and ν. (In much of the current literature, e.g., Reference 134, the G_2 term is ignored; then the instability condition, Equation 5-129, follows immediately for A = n/2.)

However, another form of the amplification rate results if one of the variables of integration is the wave-frame momentum, p_W (Equation 5-104). If the remaining variable is x, the factor within the square brackets of Equation 5-110 is simply (Reference 171)

$$\left[p_\perp \frac{\partial f}{\partial p_{II}} - \frac{\omega_c}{\omega + \omega_c} p_{II} \frac{\partial f}{\partial p_\perp} \right]$$

$$= \left[p_\perp \frac{\partial x}{\partial p_{II}} - \frac{\omega_c}{\omega + \omega_c} p_{II} \frac{\partial x}{\partial p_\perp} \right] \frac{\partial f}{\partial x} . \qquad (5\text{-}141)$$

The amplification rates above have been applied mainly to trapped-type distributions. A trapped-type distribution is unstable to generation of waves whose polarization is in the same sense as the gyro-rotation of the particles, i.e., electrons excite whistler-mode waves, etc. Beams of particles localized around some pitch angle, usually in the loss cone, have been suggested as an agency for exciting plasma waves (References 172, 173, and 174). There is one interaction of this type which might be important to electron trapping and loss, i.e., the interaction between relativistic electrons and ion-cyclotron waves (References

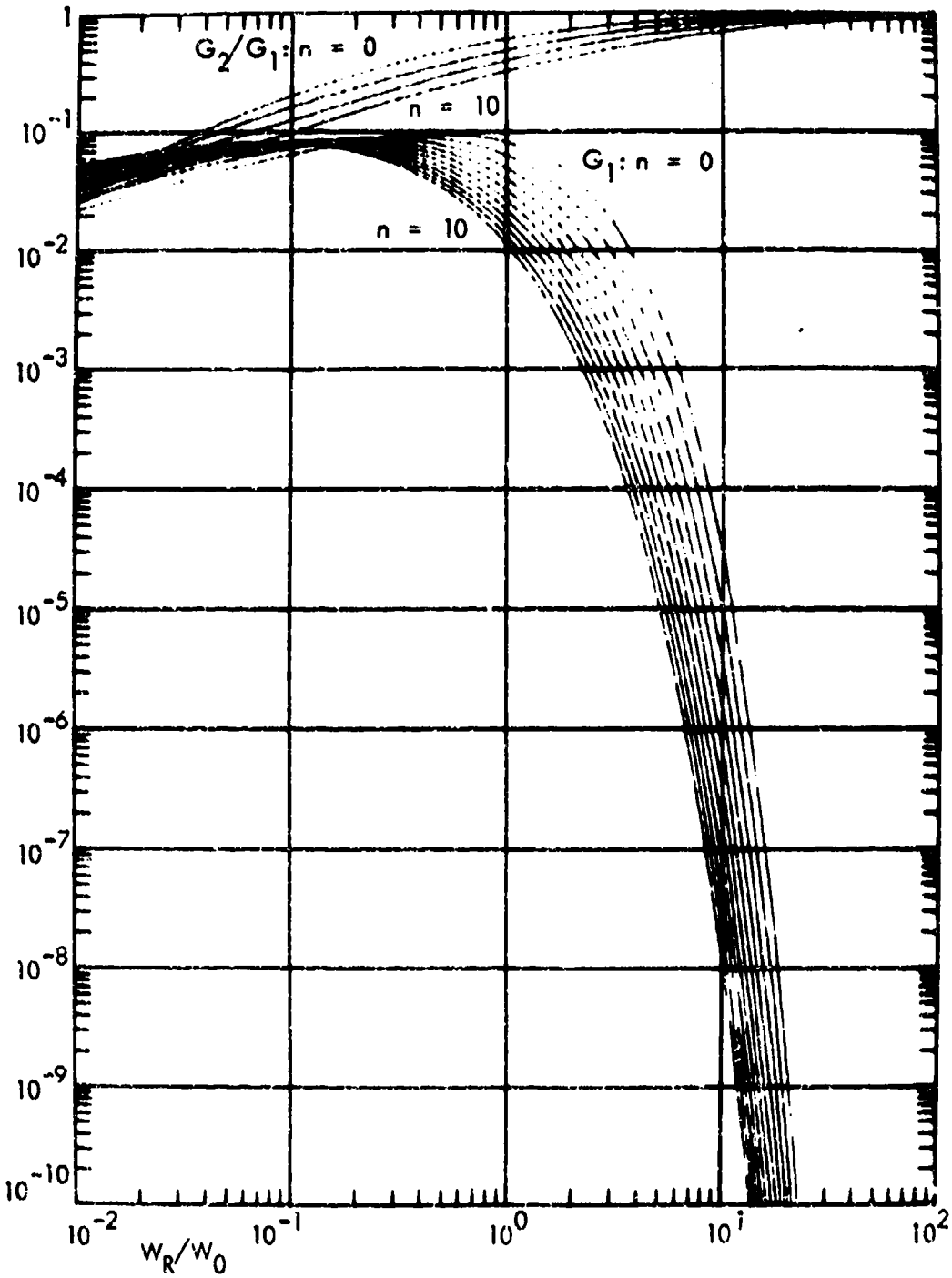

Figure 5-23a. The functions G_1 and G_2/G_1 used in evaluating the wave amplification rates of Equation 5-140b; $\upsilon = 0$. (The lower curves are G_1 for n from zero to 10 in increments of 1. The upper curves are G_2/G_1 for n = 0, 2, 5, and 10.)

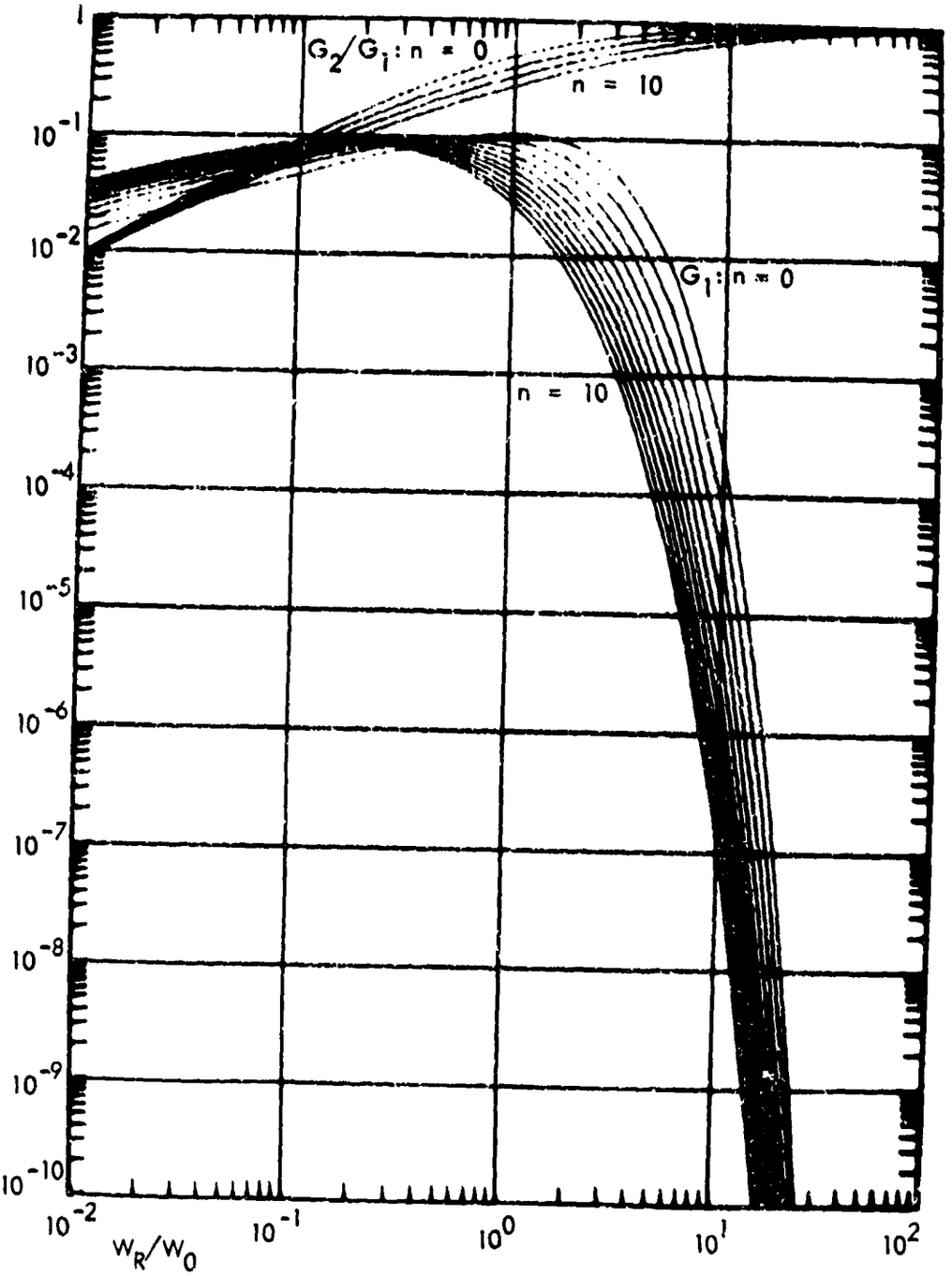

Figure 5-23b. The functions G_1 and G_2/G_1 used in evaluating the wave amplification rates of Equation 5-140b; υ ?.

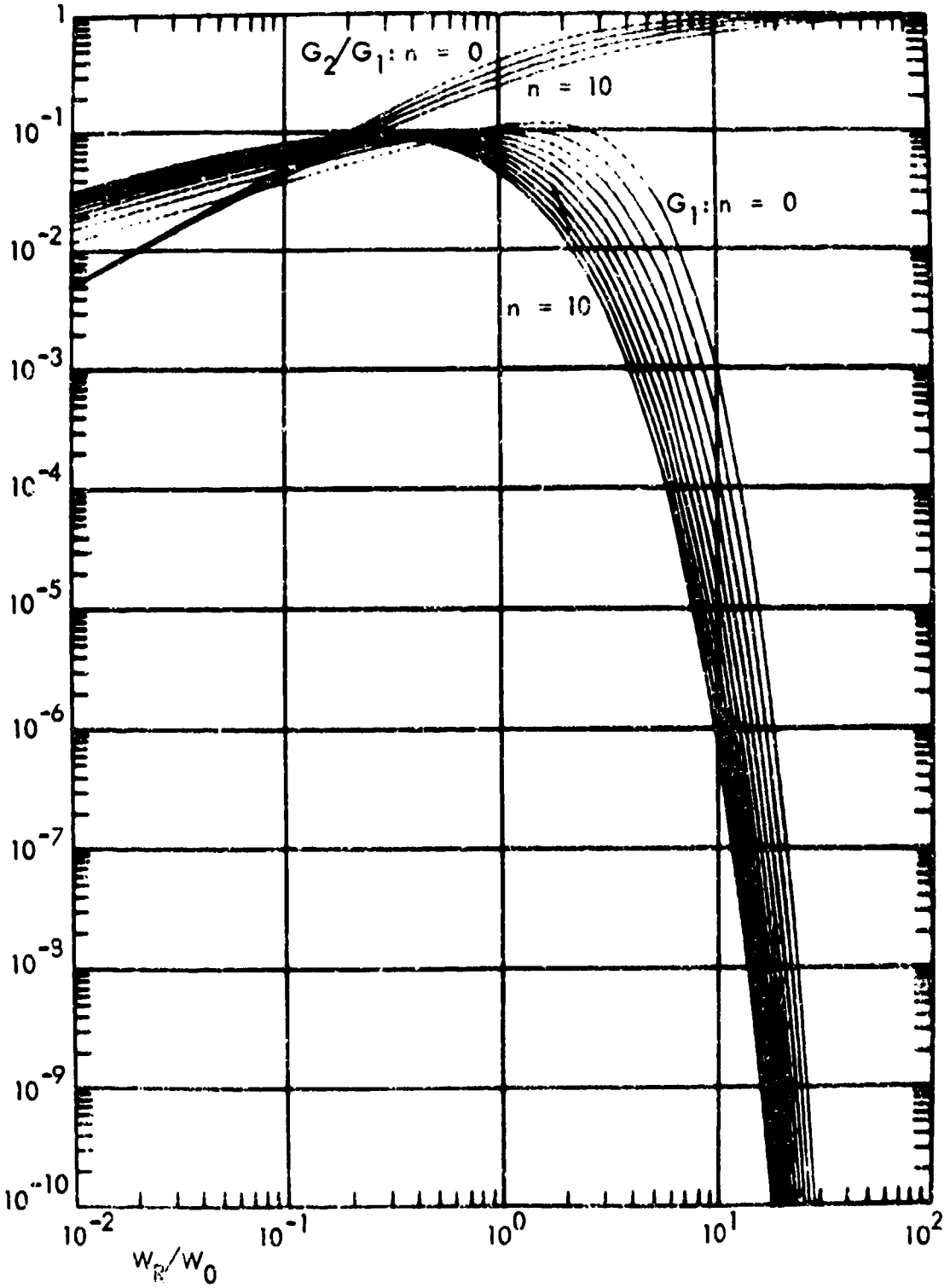

Figure 5-23c. The functions G_1 and G_2/G_1 used in evaluating the wave amplification rates of Equation 5-140b; $\upsilon = 4$.

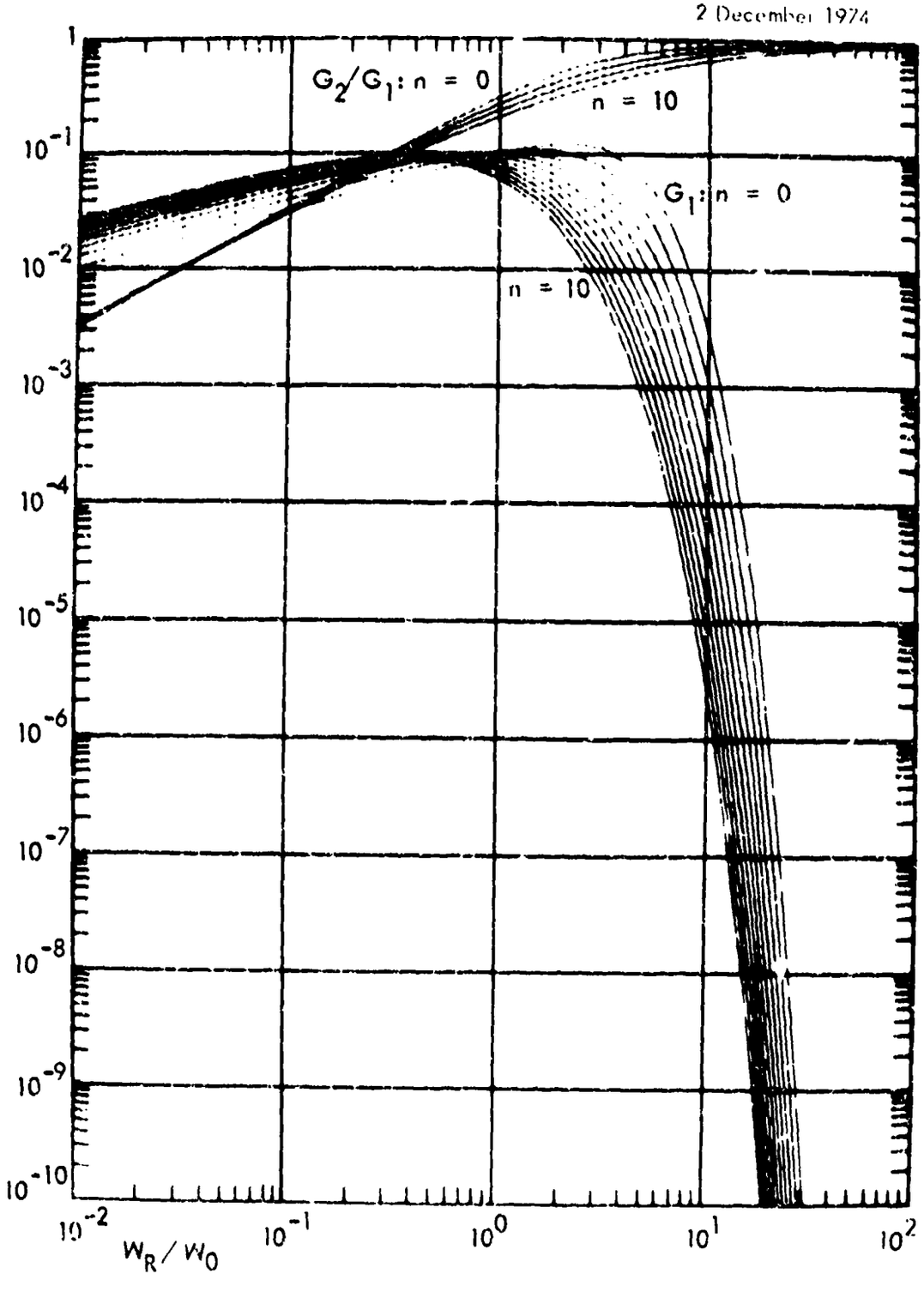

Figure 5-23d. The functions G_1 and G_2/G_1 used in evaluating the wave amplification rates of Equation 5-140b; $v = 6$.

175, 176, and 177). The resonance is near the ion gyro-frequency, or near X = -1 in Equation 5-133. A beam-like distribution to be substituted in Equation 5-132 is

$$f \approx 3 \frac{(\mu_c^4 - \mu^4 - 2\mu_c^2 + 2\mu^2}{(1 - \mu_c^2)^3} \frac{1}{W_0^{3/2}} \exp(-W/W_0) \quad . \qquad (5\text{-}142)$$

The amplification rate for this case is

$$Z \approx \sqrt{\pi}\ \Omega_H \sqrt{\frac{W_R}{1+W_R}} \left(\frac{W_R}{W_0}\right)^{3/2} \exp(-W_R/W_0) \quad . \qquad (5\text{-}143)$$

The maximum amplification rate for electrons confined to the loss cone with energies of several MeV is of the order of $Z \approx \Omega_H$. This instability could be responsible for turning some electrons injected by a high-altitude nuclear explosion into the trapped part of the distribution (References 176 and 177).

5.5.5 Pitch-Angle Diffusion and the Loss of Trapped Particles

PITCH ANGLE DIFFUSION. The scattering of trapped particles by electromagnetic waves very much resembles the scattering by bound and free electrons in the atmosphere. Fokker-Planck coefficients can be derived for the wave-particle interactions and included in the pitch angle diffusion Equation 5-21. The Fokker-Planck equation for wave-particle interactions, neglecting energy losses, has just two coefficients: $\langle \Delta\mu \rangle$ and $\langle (\Delta\mu)^2 \rangle$ (References 134 through 135). As in Section 5.4.4, a simple relation can be constructed between two Fokker-Planck coefficients if a particular solution of the diffusion equations is known. An isotropic pitch angle distribution [$f(T, \mu)$ independent of μ] is a steady state solution of the pitch angle diffusion equation. This is essentially because, near resonance, as many particles will be subject to acceleration as subject to deceleration (Section 5.5., Reference 26). The rate of change of the distribution function f is therefore zero, and the Fokker-Planck equation reduces to a simple differential equation relating two diffusion coefficients. After some simplification, the diffusion equation for the pitch angle distribution of trapped particles is

$$\frac{\partial f(\mu)}{\partial t} = \frac{\partial}{\partial \mu}\left[D \frac{\partial f(\mu)}{\partial \mu}\right] \tag{5-144a}$$

$$D \equiv \frac{1}{2}\left\langle (\Delta \mu)^2 \right\rangle \quad . \tag{5-144b}$$

The single diffusion coefficient D can be estimated if the variation in the pitch angle is known for a single interaction with a wave of known characteristics. The pitch angle alteration is found from the changes in the momentum components. From Equations 5-104 and 5-105, the relation between pitch angle and the longitudinal part of the momentum is

$$\delta \mu \approx \left(\frac{1}{p} - \frac{p_{\parallel} m \gamma V_{\varphi}}{p^3}\right) \delta p_{\parallel} \quad . \tag{5-145}$$

The change in $p_{\parallel}$ is just the acceleration $q\bar{v} \times \bar{B}_1/c$ multiplied by the time δt during which a particle is near resonance. A particle that is an amount δk away from exact resonance falls out of phase with the wave in a time roughly equal to $2/v_{\parallel}\delta k$. With this substitution for δt and neglecting terms of order V_{φ}/v, the diffusion coefficient becomes

$$D \approx \frac{m \omega_c^2 (1 - \mu^2)}{p \gamma \mu} \frac{B_{\perp}^2/\delta k}{B^2} \quad . \tag{5-146}$$

The factor $B_{\perp}^2/\delta k$ has the form of a power spectrum (amplitude squared per unit wave number, Section 5.5.2; Equation 5-95). It represents the magnetic fluctuation energy in a band of width:

$$\delta \omega \approx \frac{\omega}{k} \delta k = V_{\varphi} \delta k \quad . \tag{5-147}$$

As in the case of radial diffusion and bounce resonance diffusion, all that is needed to fully determine the effects of pitch angle scattering is a knowledge of the spectrum of waves. In practice, the major obstacle in this approach is the difficulty of measuring the amplitudes of waves that are not readily transmitted through the ionosphere and atmosphere. The spectrum of whistlers and very low frequency (VLF) noise observed on the ground is largely irrelevant because these waves already may have lost significant amounts of energy to the trapped particles (Reference 123).

When the energy exchanged between waves and particles is not negligible, the energy diffusion terms in the Fokker-Planck equation also must be taken into account. But because energy and pitch angle are interrelated, the Fokker-Planck equation should transform to an equation in one variable. The differential operators are generally of the form (Reference 119):

$$\frac{\delta}{\delta p} = p_W \left(\frac{\partial p_W}{\partial p_\perp} \frac{\partial}{\partial p_\parallel} - \frac{\partial p_W}{\partial p_\parallel} \frac{\partial}{\partial p_\perp} \right) \tag{5-148a}$$

$$\cong p_\perp \frac{\partial}{\partial p_\parallel} - \left(p_\parallel - m\gamma V_\varphi \right) \frac{\partial}{\partial p_\perp} \quad . \tag{5-148b}$$

When the distribution function is a function of p_W and some other variable, for example, x, the differential operator (Equation 5-148) is just

$$\frac{\delta}{\delta p} = p_W \left(\frac{\partial p_W}{\partial p_\perp} \frac{\partial x}{\partial p_\parallel} - \frac{\partial p_W}{\partial p_\parallel} \frac{\partial x}{\partial p_\perp} \right) \frac{\partial}{\partial x} \quad . \tag{5-149}$$

In terms of the pitch angle cosine μ:

$$\frac{\delta}{\delta p} = \frac{p_\perp}{p} \left[\frac{p_\perp^2}{p^2} + \gamma_W^2 \left(p_\parallel - m\gamma V_\varphi \right) \left(\frac{p_\parallel}{p^2} - \frac{V_\varphi}{m\gamma c^2} \right) \right] \frac{\partial}{\partial \mu} \tag{5-150a}$$

$$\cong \frac{p_\perp}{p} \left(1 - \frac{p_\parallel m\gamma V_\varphi}{p^2} \right) \frac{\partial}{\partial \mu} \quad . \tag{5-150b}$$

The diffusion equation properly should have the form

$$\frac{\partial f}{\partial t} \approx \frac{p_W^4}{p^4} \left(1 - \frac{m V_\varphi p \mu}{\partial p_W^2} \right) \frac{\partial}{\partial \mu} \left[D \left(1 - \frac{m V_\varphi p \mu}{\partial p_W^2} \right) \frac{\partial f}{\partial \mu} \right] \quad . \tag{5-151}$$

(p and γ are not constants, but functions of p_W and μ). The diffusion coefficient D is the same as was given in Equation 5-146 (Reference 135 contains another derivation of D). However, when the momentum-space diffusion trajectories differ appreciably from true circles, the V_φ terms are not negligible and Equation 5-151 has no longer the form of a simple diffusion equation, such as Equation 5-144.

In practice, the diffusion coefficients are computed with the aid of the quasilinear theory. The averages along the field lines are formed according to Equation 5-21f and the proper diffusion equation (assuming negligible energy loss) is Equation 5-21g. Most wave particle interactions take place near the equator (Reference 134); this does not mean that the averaged diffusion equation is equivalent to the simple diffusion Equation 5-21e.

THE SELF-CONSISTENT THEORY, LIMITS ON TRAPPING. If the radiation belts are regarded as a closed system, the trapped particles must reach some sort of equilibrium with the waves they generate. The greatest number of particles that can be trapped is just sufficient to maintain growing waves against absorption in the ionosphere or escape from the trapping region. Any excess in the number of trapped particles results in enhanced wave generation and pitch-angle diffusion. A group of waves travelling along a field line is amplified by an amount $\exp(\delta V_g t_W)$, where t_W is the time the wave spends in the region of interaction. In equilibrium this is just balanced by the wave losses due to imperfect reflection at the ionosphere; the amplitude at the ionosphere is diminished by 1 minus the reflection coefficient R_W. The equilibrium condition is (Reference 134)

$$\delta V_g t_W \approx \ell n R_W \quad . \tag{5-152}$$

The parameters R_W and t_W are both highly uncertain. An upper limit to t_W would be the wave travel time for a complete traverse of the field line. The varying conditions along the field line ensure that waves and particles fall out of resonance long before they have reached the limits of their travel.

When a bunch of trapped particles excites waves that can grow appreciably during a single bounce period, a large fraction of the particles may be lost immediately. This case is known as strong diffusion Above some limiting kinetic energy weak diffusion prevails, and most particles require many bounces to diffuse into the loss cone The time scale for weak diffusion, 1/D, is much longer than the bounce period Weak diffusion does seem to apply to trapped electrons with energies above 1.6 MeV (Reference 134). A computed trapping limiting for somewhat lower electron energies is shown in Figure 5-24. The largest fluxes do seem to approach the trapping limit on high L-shells.

Although attempts have been made to improve and verify the trapping limit theory, particularly in regard to the strong and weak diffusion limits (Reference 180), it still suffers from many uncertainties in the

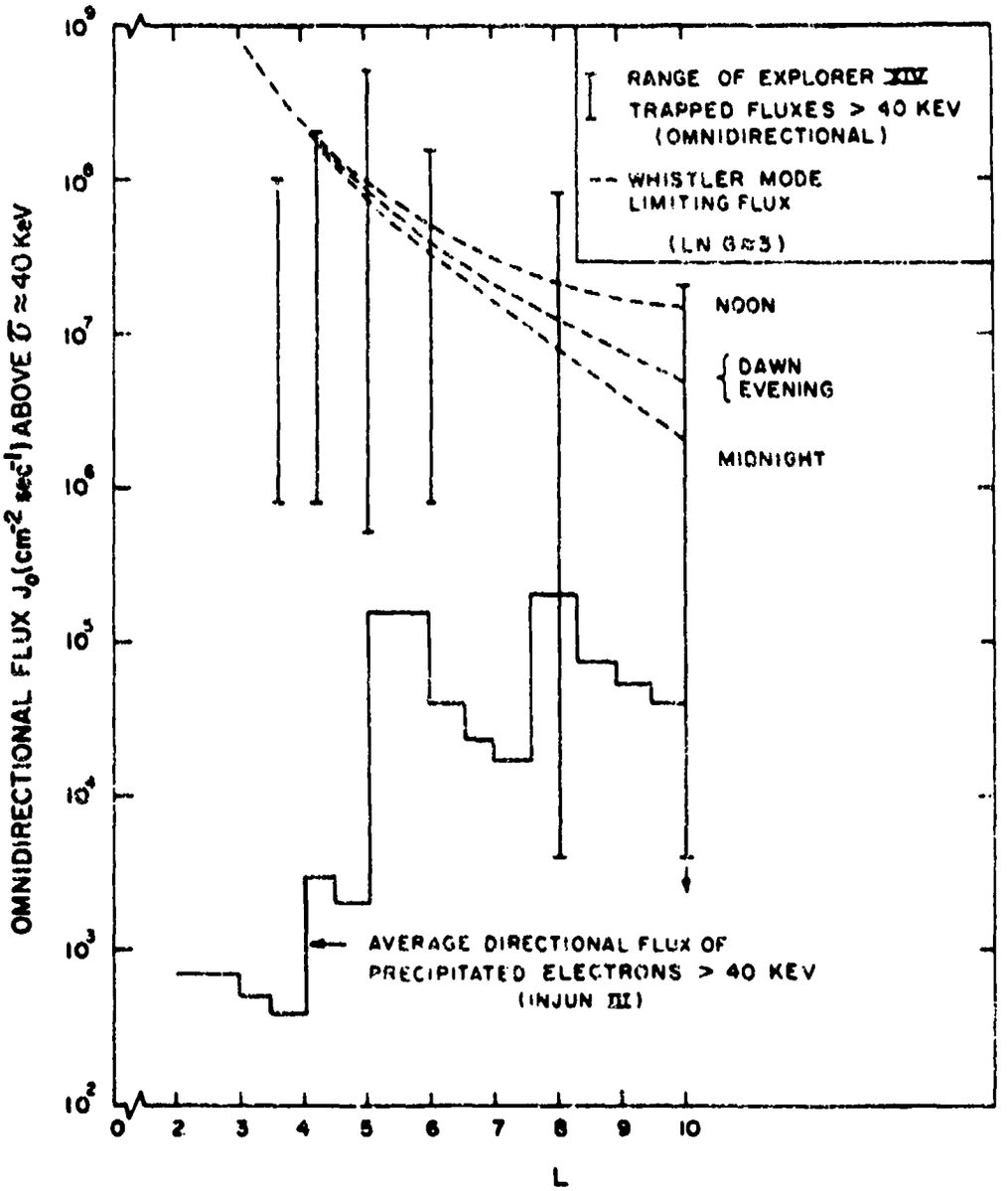

Figure 5-24. Limits on trapping of high-energy electrons (Reference 134). (An assumed wave reflection coefficient of 0.1 was used to derive the dashed curves. Observed fluxes were obtained from References 108, 178, and 179.)

evaluation of inter-related parameters. The theory might, however, be of considerable value in its application to transient events, such as the injection of an intense artificial radiation belt (Reference 181).

The "slot" in the trapped electron distribution is a particular feature of the radiation belts that might be due to wave-particle interactions. Trapped electrons seem to be distributed between two belts separated by a distinct gap between $L \approx 3$ and $L \approx 5$. In Figure 5-24, the observed fluxes below $L \approx 4$ are well below the fluxes predicted by the simple theory. The electron flux in the slot is apparently kept low by a combination of the effects of very efficient reflection and diffusion of wave energy toward lower L-shells (References 182 and 138). When a whistler-mode wave deviates from strictly parallel propagation and its frequency approaches the local lower hybrid resonant frequency,

$$\omega_{LH} = \sqrt{\frac{(\Omega_i^2 + \omega_{pi}^2)\,\Omega_i\Omega_e}{\Omega_i\,(\Omega_i+\Omega_e) + \omega_{pi}^2}} \quad , \tag{5-153}$$

it can experience nearly perfect reflection at the upper ionosphere (References 124, 133, and 182). The necessary conditions seem to be met in the region of the slot. The equilibrium condition (Equation 5-152) is satisfied in the slot region only if δ and the electron flux are very small.

Trapped electron and proton diffusion coefficients have been computed in a semi-self-consistent model in which the deviations from parallel wave propagation have been explicitly taken into account (References 137, 138, and 139). Some sample diffusion coefficients are shown in Figure 5-25. The peak in the diffusion coefficients near 90-degree pitch angles occurs because waves propagating at finite angles to the magnetic field appear to the resonant particles like a mixture of electrostatic and electromagnetic waves. The particles can resonate at all harmonics of the gyro-frequency. The resonance near 90-degree pitch angles is the zero-order, so-called Landau resonance (References 137 and 138).

THE RING CURRENT AND THE PLASMAPAUSE. During periods of geomagnetic disturbance, intense electrical currents are carried by trapped protons near the equator in the region from $L \approx 3$ to $L \approx 6$, or beyond (Reference 183). This ring current is related in a way that is not yet fully understood to the more stable trapped particle belts. The

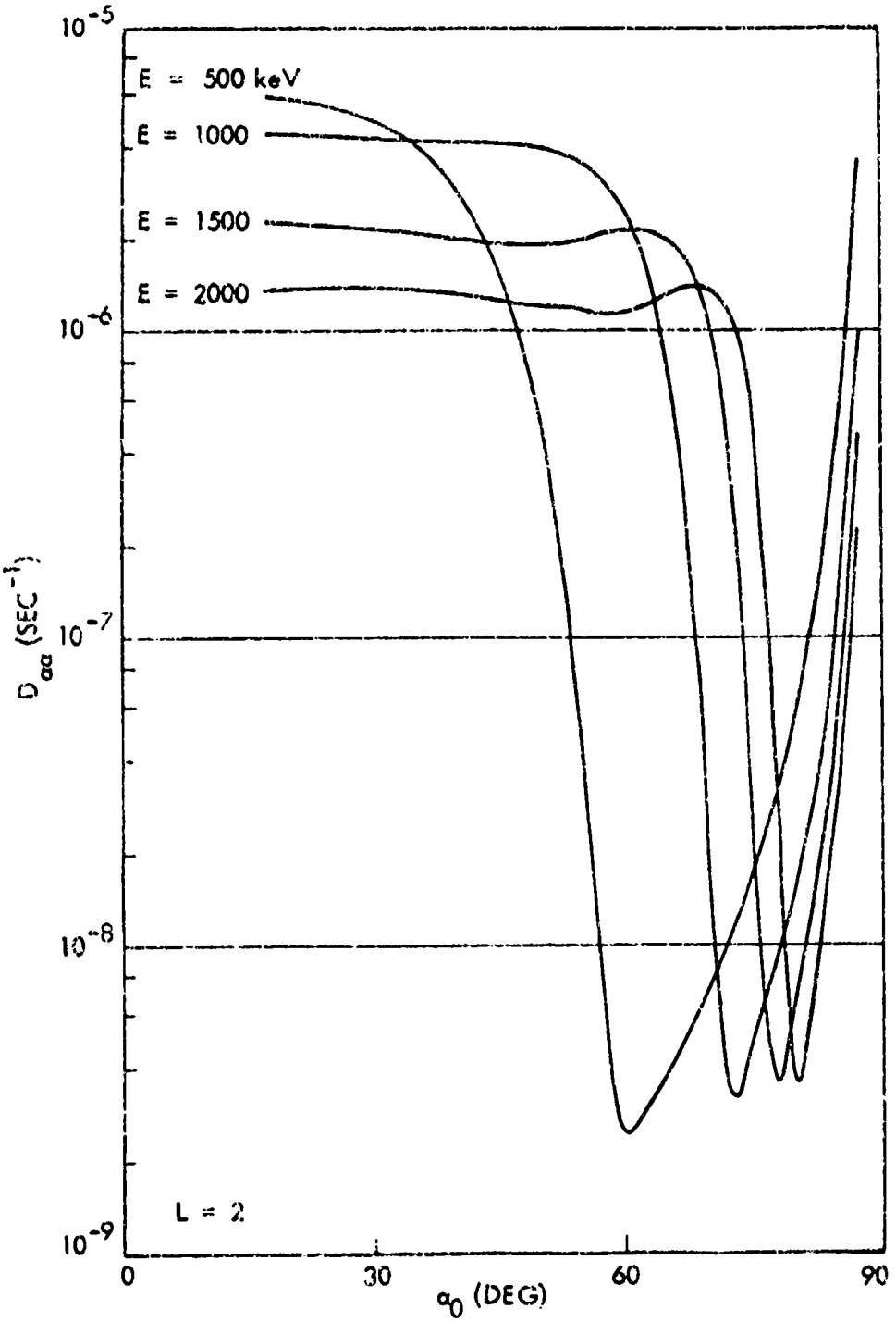

Figure 5-25a. Sample diffusion coefficients for electrons at L = 2. (Energies are listed with each curve in keV (References 137 and 138 and personal communication from L.R. Lyons).)

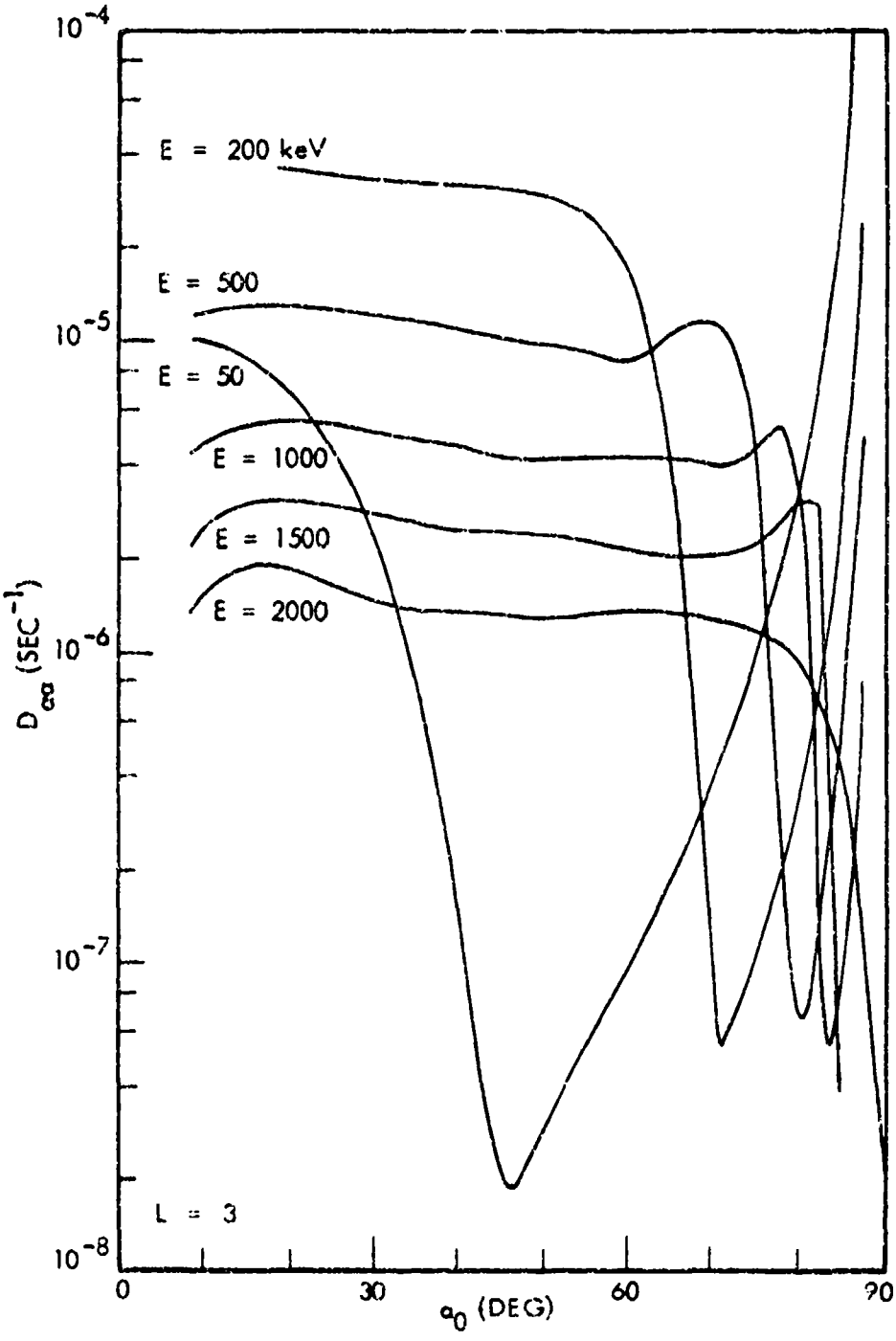

Figure 5-25b. Sample diffusion coefficients for electrons at L = 3. (Energies are listed with each curve in keV.)

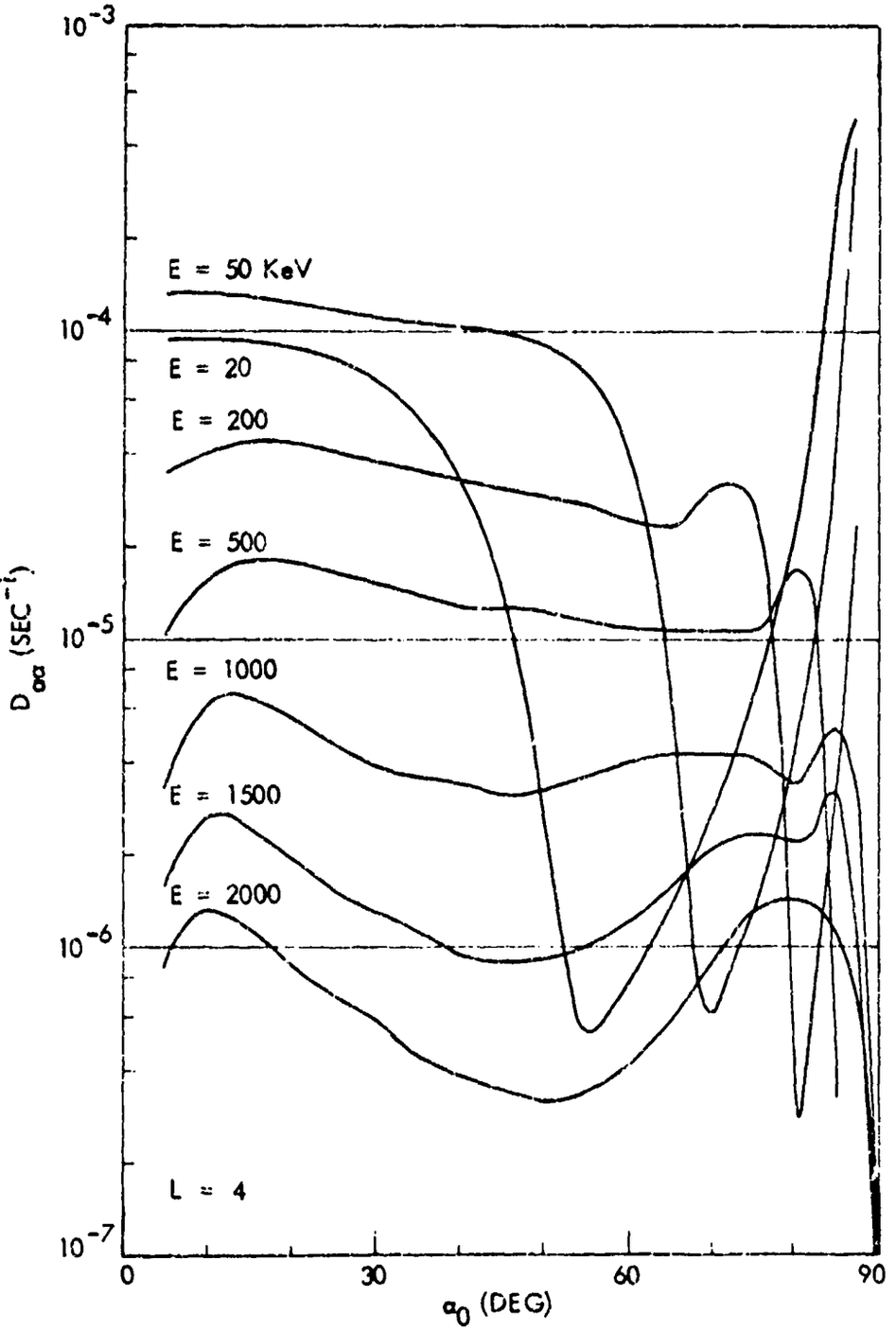

Figure 5-25c. Sample diffusion coefficients for electrons at L = 4. (Energies are listed with each curve in keV.)

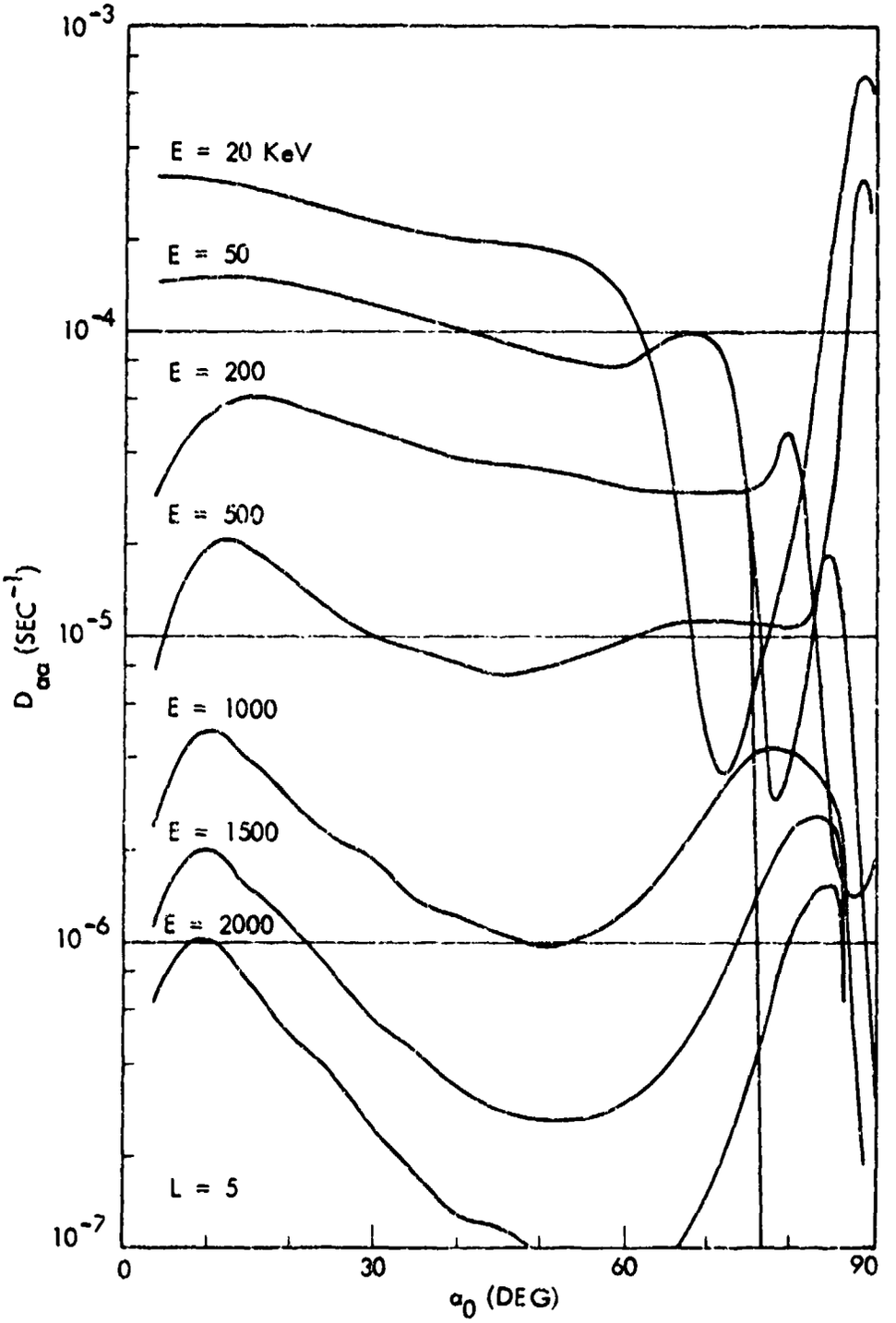

Figure 5-25d. Sample diffusion coefficients for electrons at L = 5. (Energies are listed with each curve in keV.)

ring current is established in a time that may be as short as 1 hour. During this time, protons of energies less than 100 keV must enter the magnetosphere and be transported as far inward as $L \approx 3$. One mechanism that will accomplish this is Bohm diffusion (Reference 185) which takes place at the maximum rate possible. Particles experiencing Bohm diffusion are displaced by one gyro-radius within as little as one gyro-period. Rapid alterations in the ring current may be accepted as evidence of intense wave turbulence during geomagnetic storms—intense enough that the slow radial diffusion discussed in Section 5.4.4 is no longer valid.

The rapid pitch-angle diffusion and loss of ring-current protons must be primarily due to wave-particle interactions in the vicinity of the plasmapause. One possible mechanism is the interaction of protons and ion-cyclotron waves. At the plasmapause, the ring current encounters a tremendous increase in the plasma ionization density (see Figure 5-19). The increase in the number of ions leads to a change in the anisotropy (Equation 5-128) which results in a large increase in the wave generation rate (References 186 and 187). There are, however, some major difficulties with this theory; the expected large rates of precipitation of protons into the atmosphere have not been observed where they were expected (Reference 188). Thus, it remains likely that other processes are involved, such as the interaction of protons with electrostatic-type waves.

ARTIFICIAL STIMULATION OF PLASMA WAVES-COLD PLASMA INJECTION. It has been suggested that the deposition of large amounts of cold ionized plasma in the trapped radiation belts might stimulate the generation of plasma waves (References 142 through 144). Presumably, this might be a mechanism for artificially altering the distribution of trapped particles. If it were feasible, it would require comparably small inputs of energy to achieve significant results.

To see how the injection of cold plasma would affect wave amplification, note that an amplification rate generally has a form like Equations 5-127 or 5-140: an integration over the momentum or energy spectrum multiplied by a factor that depends on the anisotropy of the "hot" part of the particle distribution. The energy dependence part, as in Figure 5-23, has a broad maximum where the resonant momentum is nearly equal to the average momentum. In terms of the dimensionless parameter

$$K = \frac{W_R}{W_O} = \frac{P_R^2}{P_O^2} \quad ; \qquad (5\text{-}154)$$

the maximum is near $K \approx 1$. For values of K greater than 1, the energy-dependent factor falls very sharply. The relation of K to wave frequency for whistler waves is approximately

$$K \sim \frac{(1-X)^3}{XQW_o} \quad . \tag{5-155}$$

However, the anisotropy part of the amplification rate has a cutoff frequency above which waves cannot grow; in the formulation of Equation 5-140, the cutoff frequency is

$$X = \frac{n}{n(1-G_2/G_1) + 2} \quad . \tag{5-156}$$

Comparison of the above equations reveals that for very small values of the plasma density parameter, Q, and small values of the anisotropy parameter, n, the cutoff frequency corresponds to a large value of K. Frequencies below the cutoff correspond to very small amplification rates. As Q is increased, the amplification rate near the cutoff frequency increases dramatically. Figure 5-26 shows how the amplification rate depends upon frequency. For any given value of Q (or of QW_o), there is a fastest growing mode whose frequency shifts toward lower values as Q is increased. For values of Q greater than about $1/W_o$, the maximum amplification rate is somewhat less than

$$Z \sim Q_H \sqrt{W_O} \quad . \tag{5-157}$$

As Q is decreased, the band of amplified waves becomes narrower and the maximum amplification rate drops more sharply than can be illustrated on the figure.

The simplified picture of stimulation of waves suffers some deficiencies. For large anisotropies ($n > 2$), the cutoff frequency is near 1 and K passes through the value 1 as the frequency is decreased. This means that for sufficiently large anisotropies, the maximum growth rate is near the limit of Equation 5-157. The main effect of increasing the plasma density in a highly anisotropic plasma is to increase the width of the band where waves will be generated, shifting the peak growth rate toward lower frequencies and lower phase velocities.

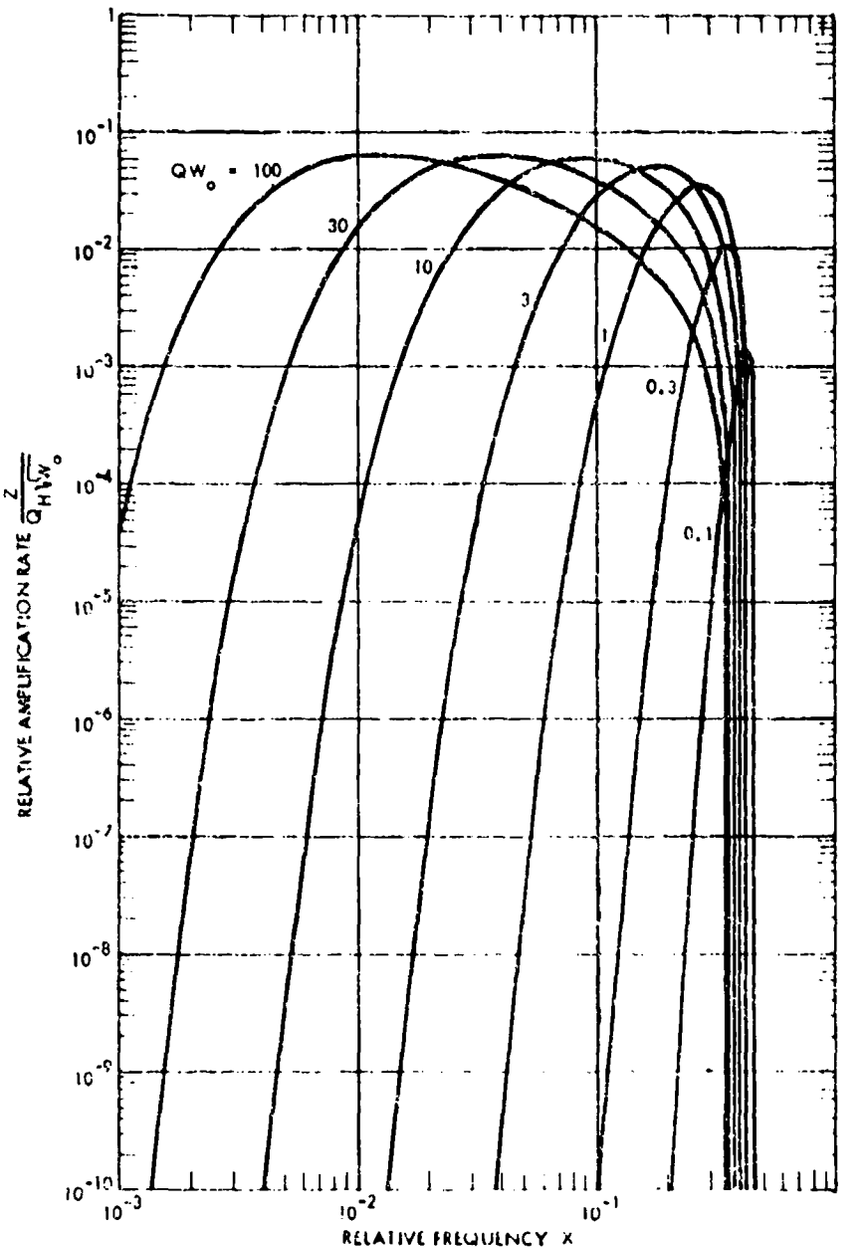

Figure 5-26a. The amplification rates of whistler-waves as a function of frequency for a (sin α_p) pitch-angle distribution. (The momentum distribution is Maxwellian (u = 0). The waves are labelled by their values of Q multiplied by the temperature W_o.)

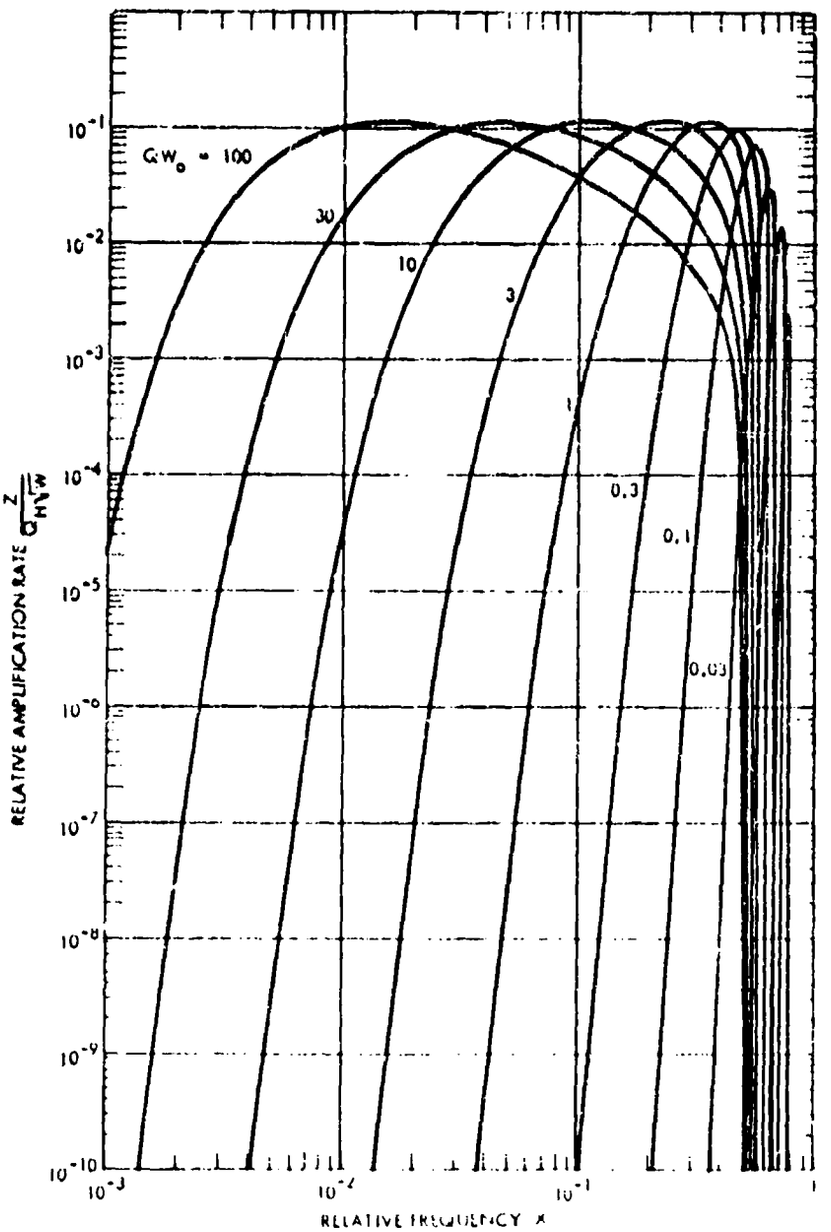

Figure 5-26b. The amplification rates of whistler-waves as a function of frequency for a $(\sin \alpha_p)^2$ pitch-angle distribution. (The momentum distribution is a Maxwellian ($v = 0$). The waves are labeled by their values of Q multiplied by the temperature W_o.)

Many detailed calculations of the effects of cold plasma injection have been performed (References 188 through 195). They are in agreement on the validity of the effect. However, the sensitivity to the trapped particle distribution is so great that a practical application in the trapped radiation belts would be conditional upon an ability to predict the particle distribution with far more accuracy and reliability than is now possible (Reference 195).

A special caution is perhaps necessary in applying some of the computed results here and elsewhere. The location of the cutoff frequency is very sensitive to the form of the pitch-angle distribution. Since the value of G_1 depends so strongly upon K, or on frequency, the largest growth rates at low-ionization densities may vary by many orders of magnitude for various particle distributions (Reference 195). Some calculations have been done with a bi-Maxwellian distribution with two separate temperatures, $T_\perp$ and $T_\parallel$; that type of distribution is probably a poor representation of the actual trapped particle distribution.

Again, a self-consistent model is necessary to predict the actual effects of cold plasma in the magnetosphere. From the discussion of the last sections, and particularly Equation 5-152, it is evident that the trapped particle distribution may adjust itself to compensate for changes in the wave spectrum. It appears that for this reason it would be very difficult to effect a discernible alteration in the trapped electron distribution with any conceivable amounts of cold plasma (Reference 180).

Another approach to artificial stimulation of waves in the magnetosphere is by electromagnetic waves transmitted from large antennae on the Earth's surface. For many years it has been known that powerful radio transmitters can trigger a peculiar type of very-low-frequency (VLF) emission from the magnetosphere. For a general discussion of the subject, see References 196 through 200. Again, the expectations of dramatic rearrangements of trapped particles are low. It is unlikely that enough wave energy could be "pumped" into the magnetosphere to affect a large proportion of the total number of particles. The likeliest applications of triggered VLF emissions are likely to be in communications and probing the physical state of the magnetosphere.

5.6 CONVECTION IN THE OUTER MAGNETOSPHERE AS A SOURCE OF TRAPPED PARTICLES

Much of the kinetic energy possessed by trapped particles now appears to have been acquired after their introduction into the magnetosphere. The solar wind is a likely source of charged particles, but solar wind particles have rather low energies, compared with the thousands or millions of electron volt energies of trapped particles. A number of investigators have attempted to explain injection at the outer part of the trapping region through a two-step process: Convection of low-energy plasma down to the trapping region followed by (or concurrent with) in situ acceleration of the charged particles (References 201 through 206).

Most convection theories embody the presumptions that, within the plasmasphere ($L \sim 3-4$), the plasma is constrained effectively to rotate with the earth and that the outer edge of the magnetosphere remains fixed with respect to the sun and solar wind. The basic convective mechanism has been described in Section 1. One model is sketched in Figure 5-27 (Reference 154). The upper sketch in the figure refers to the situation that would prevail if the plasmasphere were stationary. In the lower sketch, the plasmasphere is rotating with respect to the solar wind orientation and a shear exists throughout the outer magnetosphere. In the upper half of the figure is shown an equatorial plane cross section of the postulated circulation of plasma in the magnetosphere. The solar wind is assumed to drag the plasma back along the outer boundary, thus establishing two closed convection cells. If a shear motion due to the rotation of the inner plasmasphere is introduced, the convection cells are distorted as in the lower half of Figure 5-27. The convective motion brings charged particles down to the trapping region and also results in the establishment of complicated electric fields that can accelerate the particles. Details of this and other convective processes are to be found in the previously cited references.

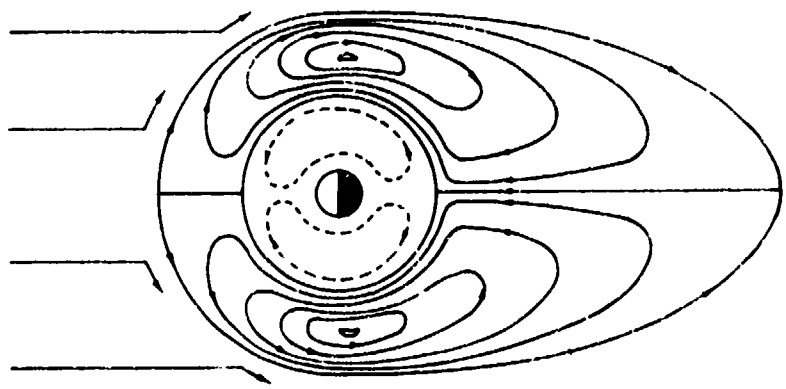

NO ROTATION OF PLASMASPHERE

SUN

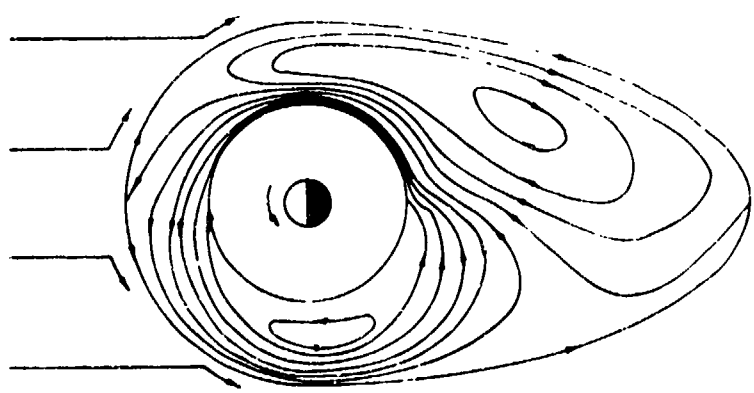

INCLUDING DRAG ON ROTATING PLASMASPHERE

Figure 5-27. Convection in the equatorial plane of the magnetosphere (Reference 154). The upper sketch in the figure refers to the situation that would prevail if the plasma sphere were stationary. In the lower sketch, the plasma sphere is rotating with respect to the solar wind orientation and a shear exists throughout the outer magnetosphere.

REFERENCES

1. W.N. Hess. The Radiation Belt and Magnetosphere, Blaisdell, Waltham, Mass., 1968, 541 pp.

2. H. Bethe. "Quantenmedranik der Ein-und Zwei-Electronenproblem," Hbd. Phys., 2nd ed., ed. by Smekal, Springer, Berlin, 273-560, esp. 515-524, 1933.

3. H. Bethe and J. Askin. "Passage of Radiation Through Matter," Experimental Nuclear Physics, 1, ed. by E. Segré, Wiley, New York, 166-357, 1953.

4. R.D. Evans. The Atomic Nucleus, McGraw-Hill, New York, 1955, 567-599.

5. H. Goldstein. Classical Mechanics, Addison Wesley, Cambridge, Mass., 1950, 383 pp, esp. 58-92.

6. C. Møller. Ann. d. Phys., 14, 531, 1932.

7. N.F. Mott and H.S.W. Massey. The Theory of Atomic Collisions, 3rd ed., Oxford, London, New York, 1965, 840 pp.

8. J.L. Delcroix. Introduction à la théorie des gaz ionisés, Dunod, Paris, 1959, trans. Introduction to the Theory of Ionized Gases, Interscience, New York, 1960, 146 pp.

9. B. Kwal. J. Phys. Rad., 12, 805, 1951.

10. W.M. MacDonald and M. Walt. "Distribution Function of Magnetically Confined Electrons in a Scattering Atmosphere," Ann. Phys., 15, 44-62, 1961.

11. A.M. Lenchek and S.F. Singer. "Geomagnetically Trapped Protons from Cosmic-Ray Albedo Neutrons," J. Geophys. Res., 67, 1263-1287, 1962.

12. A.M. Lenchek and S.F. Singer."The Albedo Neutron Theory of Geomagnetically Trapped Protons," Plan. Sp. Sci., 11, 1151-1208, 1963.

13. M.J. Berger and S.M. Seltzer. Tables of Energy Losses and Ranges of Electrons and Protons, NASA, SP-3012, 1964.

14. W.H. Barkas and M.J. Berger. Tables of Energy Losses and Ranges of Heavy Charged Particles, NASA, SP-3013, 1964.

15. W.N. Hess. "Summary of High Energy Nucleon-Nucleon Cross Section Data," Rev. Mod. Phys., 30, 368-401, 1958.

16. W.L. Fite, R.T. Brackman, and W.R. Snow. "Charge Exchange in Proton-Hydrogen Atom Collisions," Phys. Rev., 112, 1161-1169, 1958.

17. D.R. Bates and A. Dalgarno, "Electron Capture 3, Capture into Excited States in Encounters Between Hydrogen Atoms and Fast Protons," Proc. Phys. Soc. Lon., A66, 972, 1953.

18. R.F. Stebbings, W.L. Fite, and D.G. Hummer, "Charge Transfer Between Atomic Hydrogen and N^+ and O^+," J. Chem. Phys., 33, 1226- , 1960.

19. D. Rapp and I.B. Ortenburger. "Interchange of Charge Between Gaseous Molecules," J. Chem. Phys., 33, 1230- , 1960.

20. A.D. Anderson and W.E. Francis. "The Variation of the Neutral Atmospheric Properties With Local Time and Solar Activity from 100 to 10,000 km," J. Atm. Sci., 23, 110-124, 1966.

21. W.B. Hansen, "Structure of the Ionosphere," Satellite Environment Handbook, ed. by F.S. Johnson, Stanford Press, Stanford, Calif., 21-49, 1965.

22. H.C. Brinton, R.A. Pickett, and H.A. Taylor. "Thermal Ion Structure of the Plasmasphere," Plan Sp. Sci., 16, 899-909, 1968.

23. A. T. Nelms. Energy Loss and Range of Electrons and Protons, NBS, circular 577, 1956.

24. S. Chandrasekhar. "Stochastic Problems in Physics and Astronomy," Rev. Mod. Phys., 15, 1-89, 1943.

25. M. N. Rosenbluth, W. M. MacDonald, and D. L. Judd. "Fokker-Planck Equation for an Inverse-Square Force," Phys. Rev., 107, 1-6, 1957.

26. D. C. Montgomery and D. A. Tidman. Plasma Kinetic Theory, McGraw-Hill, New York, 1964, 286 pp.

27. E. N. Parker. Interplanetary Dynamical Processes, Interscience, New York, 1963.

28. G. Haerendel. "Diffusion Theory of Trapped Particles and the Observed Proton Distribution," Earth's Particles and Fields, ed. by B. M. McCormac, Reinhold, New York, 171-191, 1968.

29. H. B. Phillips. Vector Analysis, Wiley, New York, 1933, 231 pp.

30. S. Chandrasekhar. Principles of Stellar Dynamics, U. Chicago, Chicago, 1942; Dover, New York, 1960, 248 pp.

31. S. Chandrasekhar. "Dynamical Friction I General Considerations: The Coefficient of Dynamical Friction," Ap. J., 97, 255-262, 1943.

32. L. Spitzer. Physics of Fully Ionized Gases, Interscience, New York, 1956, 102 pp.

33. A. Omholt. "Studies on the Excitation of Aurora Borealis 1, The Hydrogen Lines," Geophys. Publ. Geophysica Norvegica, 20, 1, 1958.

34. G. T. Davidson. "Expected Spatial Distribution of Low-Energy Protons Precipitated in the Auroral Zones," J. Geophys. Res. 70, 1061-1068, 1965.

35. M. Walt and W. M. MacDonald. "The Influence of the Earth's Atmosphere on Geomagnetically Trapped Particles," Rev. Geophys., 2, 543-577, 1964.

36. W. M. MacDonald and M. Walt. "Diffusion of Electrons in the Van Allen Belt, 2 Particles with Mirroring Points at Low Altitude," J. Geophys. Res., 67, 1962, 5025-5033.

37. A.M. Lenchek and S. F. Singer. "Effects of the Finite Gyroradii on Geomagnetically Trapped Protons," J. Geophys. Res., 67, 4073-4075, 1963.

38. S. E. Vernov, E. V. Gorchakov, P. I. Shavrin, and K. N. Sharvina. "Radiation Belts in the Region of the South Atlantic Anomaly," Sp. Sci. Rev., 7, 490-533, 1967.

39. H.H. Heckman and G. H. Nakano. "East-West Asymmetry in the Flux of Mirroring Geomagnetically Trapped Protons," J. Geophys. Res., 68, 2117-2120, 1963.

40. M. Walt. "The Effects of Atmospheric Collision on Geomagnetically Trapped Electrons," J. Geophys. Res., 69, 3947-3958, 1964.

41. M. Walt. "Loss Rates of Trapped Electrons by Atmospheric Collisions," Radiation Trapped in the Earth's Magnetic Field, ed. by B. M. McCormac, Reidel, Dordrecht, Holland, 337-351, 1966.

42. L.L. Newkirk and M. Walt. "Radial Diffusion Coefficient for Electrons at Low L-Values," J. Geophys. Res., 73, 1013-1017, 1968.

43. W. N. Hess, J. Killeen, C. Y. Fan, P. Meyer, and J. A. Simpson. "The Observed Outer-Belt Electron Distribution and the Neutron Decay Hypothesis," J. Geophys. Res., 66, 2313-2314, 1961.

44. W. N. Hess and J. Killeen. "Spatial Distribution of Electrons from Neutron Decay in the Outer Radiation Belt," J. Geophys. Res., 66, 3671-3680, 1961.

45. B. Rossi. High Energy Particles, Prentice Hall, New York, 1952, 561 pp.

46. W. N. Hess, E. W. Canfield, and R. E. Lingenfelter. "Cosmic Ray Neutron Demography," J. Geophys. Res., 66, 665-677, 1961.

47. W. F. Libby. Radiocarbon Dating, U. Chicago, Chicago, 1952.

48. L. L. Newkirk. "Calculation of the Low-Energy Neutron Flux in the Atmosphere by the S_n Method," J. Geophys. Res., 68, 1825-1833, 1963.

49. R. E. Haymes. "Fast Neutron in the Earth's Atmosphere, 1. Variation With Depth," J. Geophys. Res., 69, 841-852, 1964.

50. R. E. Haymes. "Fast Neutrons in the Earth's Atmosphere, 2. Time Variation at High Altitudes," J. Geophys. Res., 69, 853-859, 1964.

51. R. E. Lingenfelter. "The Cosmic Ray Neutron Leakage Flux," J. Geophys. Res., 68, 5633-5640, 1963.

52. R. E. Lingenfelter and E. J. Flamm. "Neutron Leakage Flux from Interactions of Solar Protons in the Atmosphere," J. Geophys. Res., 69, 2199-2207, 1964.

53. S. Chandrasekhar. Radiative Transfer, Dover, New York, 1960, 385 pp, esp. 54-69.

54. E. H. Bareiss. "A Survey and Classification of Transport Theory Calculation Techniques," Second UN Int. Con. Peaceful Uses of At. Energy, 1958.

55. B. G. Carlson. "The Numerical Theory of Neutron Transport," Methods in Computational Physics, 1, ed. by B. Adler, S. Fernbach, and M. Rothenberg, Academic Press, New York, 1-42, 1963.

56. B. G. Carlson and G. I. Bell. "Solution of the Transport Method," Second UN Conf. on Peaceful Uses of At. Energy, 1958.

57. M. Walt and W. M. MacDonald. "Energy Spectrum of Electrons Trapped in the Geomagnetic Field," J. Geophys. Res., 66, 2047-2052, 1961.

58. S. Chandrasekhar. Plasma Physics, U. of Chicago, Chicago, 1960, 214 pp.

59. T. G. Cowling. Magnetohydrodynamics, Interscience, New York, 1957, 112 pp.

60. R. F. Post. "Some Observations on Plasma Instabilities in the Mirror Machine," Plasma Hydromagnetics, ed. by D. Bershader, Stanford U., Stanford, Calif., 1-39, 1962.

61. N. Rostoker. "Plasma Stability," Plasma Physics in Theory and Application, ed. by W. B. Kunkel, McGraw-Hill, New York, 120-146, 1966.

62. K. M. Watson. Stability of Trapped Electron Belts, Aerospace Corp., TR-1001, S2855-40-1; Air Force, BSD-TR-328, 1966, 28 pp.

63. J. G. Linhart. Plasma Physics, North Holland, Amsterdam, 1961, 214 pp.

64. T. G. Northrop and E. Teller. "Stability of the Adiabatic Motion of Charged Particles in the Earth's Field," Phys. Rev., 117, 215-225, 1960.

65. T. G. Northrop. The Adiabatic Motion of Charged Particles, Interscience, New York, 1963, 105 pp.

66. J. B. Taylor. "Equilibrium and Stability of Plasma in Arbitrary Mirror Fields," Phys. Fluids, 7, 767-773, 1964.

67. J. W. Dungey. "Effects of Electromagnetic Perturbations on Particles Trapped in the Radiation Belt," Sp. Sci. Rev., 4, 199-222, 1964.

68. J. W. Dungey, W. N. Hess, and M. P. Nakada. "Theoretical Studies of Protons in the Outer Radiation Belt," Sp. Res., 5, 399-403, 1965.

69. J. B. Cladis, G. T. Davidson, W. E. Francis, L. L. Newkirk, L. R. Tepley, M. Walt, and R. C. Wentworth. Search for Possible Loss Processes for Geomagnetically Trapped Particles, Lockheed M.S.C., M-57-65-1, DASA 1713, 1965, 128 pp.

70. M. P. Nakada, J. W. Dungey, and W. N. Hess. "On the Origin of Outer-Belt Protons 1," J. Geophys. Res., 70, 3529-3532, 1965.

71. D. B. Chang, L. D. Pearlstein, and M. N. Rosenbluth. "On the Interchange Stability of the Van Allen Belt," J. Geophys. Res., 70, 3085-3097, 1965.

72. E. N. Parker. "Geomagnetic Fluctuations and the Form of the Outer Zone of the Van Allen Radiation Belt," J. Geophys. Res., 65, 3117-3130, 1960.

73. L. Davis, Jr., and D. B. Chang. "On the Effect of Geomagnetic Fluctuations on Trapped Particles," J. Geophys. Res., 2169-2179, 1962.

74. B. A. Tverskoy. "Dynamics of the Radiation Belts of the Earth, 2.," Geomag. Aeron., 3, 351-366, 1964.

75. M. P. Nakada and G. D. Mead. "Diffusion of Protons in the Outer Radiation Belt," J. Geophys. Res., 70, 4777-4791, 1965.

76. W. L. Imhof, J. B. Cladis, and R. V. Smith. "Observation of an Energy-Selective Redistribution in the Inner Radiation Belt," Plan. Sp. Sci., 14, 569-577, 1966.

77. G. L. Pai and V. A. Sarabhai. "Periodic Fluctuations in the Geomagnetic Field During Magnetic Storms," Plan. Sp. Sci., 12, 855-865, 1964.

78. A. Nishida. "Geomagnetic DP2 Fluctuations and Associated Magnetospheric Phenomena," J. Geophys. Res., 73, 1795-1803, 1968.

79. T. Obayashi and A. Nishida. "Large-Scale Electric Field in the Magnetosphere," Sp. Sci. Rev., 8, 3-31, 1968.

80. R. L. Kauffmann. "Conservation of First and Second Adiabatic Invariants," J. Geophys. Res., 70, 2181-2186, 1965.

81. C.-G. Fälthammar. "Effects of Time Dependent Electric Fields on Geomagnetically Trapped Radiation," J. Geophys. Res., 70, 2503-2516, 1965.

82. J. G. Roederer. "Shell Splitting and Radial Diffusion of Geomagnetically Trapped Particles," Earth's Particles and Fields, ed. by B. M. McCormac, Reinhold, New York, 193-208, 1968.

83. G. Haerendel. "On the Violation of the Second and Third Adiabatic Invariants," J. Geophys. Res., 71, 1857-1868, 1966.

84. T.J. Birmingham, T.G. Northrop, and C.-G. Fälthammar. "Charged Particle Diffusion by Violation of the Third Adiabatic Invariant," Phys. Fluids, 10, 2389-2398, 1967.

85. A.T. Nelms. Energy Loss and Range of Electrons and Protons, NBS, circular 577, 1956.

86. J.W. Dungey. "Effects of Electromagnetic Perturbations on Particles Trapped in the Radiation Belts," Sp. Sci. Rev., 4, 199-222, 1965.

87. C.-G. Fälthammar. "On the Transport of Trapped Particles in the Outer Magnetosphere," J. Geophys. Res., 71, 1487-1491, 1966.

88. C.-G. Fälthammar. "Coefficients of Diffusion in the Outer Radiation Belt," Radiation Trapped in the Earth's Magnetic Field, ed. by B.M. McCormac, Reidel, Dordrecht, Holland, 398-402, 1966.

89. C.-G. Fälthammar. "Radial Diffusion by Violation of the Third Adiabatic Invariant," Earth's Particles and Fields, ed. by B.M. McCormac, Reinhold, New York, 157-169, 1968.

90. Al Ershkovich, G.A. Skuridin, L.S. Chesalin, and V.P. Shalimov. "Transport of Charged Particles in a Dipole Magnetic Field under the Influence of Electromagnetic Impulses," Kosm. Issled., 5, 792-795, 1967, trans: Cos. Res., 5, 673-675, 1967.

91. B.J. Conrath. "Radial Diffusion of Trapped Particles With Arbitrary Pitch Angle," J. Geophys. Res., 72, 6069-6076, 1968.

92. A. Nishida and L.J. Cahill, Jr. "Sudden Impulses in the Magnetosphere Observed by Explorer 12," J. Geophys. Res., 69, 2243-2255, 1964.

93. G. Haerendel and R. Lüst. "Electric Fields in the Upper Atmosphere," Earth's Particles and Fields, ed. by B.M. McCormac, Reinhold, New York, 271-285, 1968.

94. G. Haerendel, R. Lüst, and E. Reiger. "Motion of Artificial Ion Clouds in the Upper Atmosphere," Pl. Sp. Sci., 15, 1-18, 1967.

95. W. L. Imhof, J. B. Reagan, and R. V. Smith. "Long Term Study of Electrons Trapped on Low L-Shells," J. Geophys. Res., 72, 2371-2377, 1967.

96. C. E. McIlwain. "The Radiation Belts, Natural and Artificial," Science 142, 355- , 1963.

97. C. O. Bostrom and D. J. Williams. "Time Decay of the Artificial Radiation Belt," J. Geophys. Res., 70, 240-242, 1965.

98. J. A. Van Allen. "Lifetimes of Geomagnetically Trapped Electrons of Several MeV Energy," Nature 203, 1006- , 1964.

99. W. L. Imhof and R. V. Smith. "Longitudinal Variations of High Energy Electrons at Low Altitudes, J. Geophys. Res., 70, 569-577, 1965.

100. A. D. Bolyunova, O. L. Vaisberg, Yu. Galpernin, B. P. Polapov, V. V. Temny, and F. K. Shuyskaya. "Investigations of Corpuscles on the Electron-1 and Electron-2 Satellites," Space Research, North Holland, Amsterdam, 649-661, 1966.

101. D. S. Beall, C. O. Bostrom, and D. J. Williams. "Structure and Decay of the Starfish Radiation Belt, October 1963 to December 1965," J. Geophys. Res., 72, 3403-3427, 1967.

102. J. R. Burrows and I. B. McDiarmid. "A Study of Beta Decay Electrons Injected into the Geomagnetic Field in October 1962," Can. J. Phys., 42, 1529-1547, 1964.

103. D. J. Williams and A. M. Smith. "Daytime Trapped Electron Intensities at High Latitudes at 1100 Kilometers," J. Geophys. Res., 70, 541-556, 1965.

104. D. J. Williams, J. F. Arens, and L. J. Lanzerotti. "Observation of Trapped Electrons at Low and High Altitudes," J. Geophys. Res., 73, 5673-5696, 1968.

105. C. S. Roberts. "Cyclotron-Resonance and Bounce-Resonance Scattering of Electrons Trapped in the Earth's Magnetic Field," Earth's Particles and Fields, ed. by B. M. McCormac, Reinhold, New York, 317-336, 1968.

106. W. L. Brown. "Observations of the Transcient Behavior of Electrons in the Artificial Radiation Belts," Radiation Trapped in the Earth's Magnetic Field, ed. by B.M. McCormac, Reidel, Dordrecht, Holland, 610-633, 1966.

107. L. L. Newkirk and M. Walt. "Radial Diffusion Coefficient for Electrons at $1.76 < L < 5$," J. Geophys. Res., 73, 7231-7236,

108. L.A. Frank, J.A. Van Allen, and H.K. Hills. "A Study of Charged Particles in the Earth's Outer Radiation Zone with Explorer 14," J. Geophys. Res., 69, 2171-2191, 1964.

109. L.A. Frank. "Inward Radial Diffusion of Electrons Greater than 1.6 Million Electron Volts in the Outer Radiation Zone, J. Geophys. Res., 70, 3533-3540, 1965.

110. M. Walt. "Radial Diffusion of Trapped Particles," Particles and Fields in the Magnetosphere, ed. by B.M. McCormac, D. Reidel, Dordrecht, Holland, 410-415, 1970.

111. L.D. Kavanaugh, Jr. "An Empirical Evaluation of Radial Diffusion Coefficients for Electrons of 50-100 keV Form L = 4 to L = 7," J. Geophys. Res., 73, 2959-2965, 1968.

112. T.J. Birmingham. "Convection Electric Fields and the Diffusion of Trapped Magnetospheric Radiation," J. Geophys. Res., 74, 2169-2181, 1969.

113. T.A. Farley. "Radial Diffusion of Starfish Electrons," J. Geophys. Res., 74, 3591-3600, 1969.

114. J.G. Roederer. "Experimental Evidence on Radial Diffusion of Geomagnetically Trapped Particles," Earth's Particles and Fields, ed. by B.M. McCormac, Reinhold, New York, 143-155, 1968.

115. F. Söraas. Comparison of Post Storm Non-Adiabatic Recovery of Trapped Protons With Radial Diffusion, Goddard Space Flight Center, Z-612-69-241, 1969.

116. T.A. Farley, A.D. Tomassian, and M. Walt. "The Source of High Energy Protons in the Van Allen Radiation Belt," to be published (1970).

117. C.Y. Fan, P. Meyer, and J.A. Simpson. "Dynamics and Structure of the Outer Radiation Belt," J. Geophys. Res., 66, 2607-2640, 1961.

118. P. Morrison. "The Origin of Cosmic Rays," Hdb. d. Phys., 45/1, ed. by S. Flügge, Springer, Berlin, 1-87, esp. 24-30, 1961.

119. E.N. Parker. "Effect of Hydromagnetic Waves in a Dipole Field on the Longitudinal Invariant," J. Geophys. Res., 66, 693-708, 1961.

120. C.S. Roberts and M. Schulz. "Bounce Resonant Scattering of Particles Trapped in the Earth's Magnetic Field," J. Geophys. Res., 73, 7361-7376, 1968.

121. S.O. Rice. "Mathematical Analysis of Random Noise," Bell System Tech. J., 23, 24; Selected Papers on Noise and Stochastic Processes, ed. by N. Wax, Dover, New York, 130-294, 1954.

122. A.J. Dessler, W.E. Francis, and E.N. Parker. "Geomagnetic Storm Sudden-Commencement Rise Times," J. Geophys. Res., 65, 2715-2719, 1960.

123. W.E. Francis and R. Karplus. "Hydromagnetic Waves in the Ionosphere," J. Geophys. Res., 65, 3593-3600, 1960.

124. D.G. Wentzel. "Hydromagnetic Waves and the Trapped Radiation, 1. Breakdown of the Adiabatic Invariance," J. Geophys. Res., 66, 359-363, 1961.

125. D.G. Wentzel. "Hydromagnetic Waves and the Trapped Radiation, 2. Displacement of the Mirror Points," J. Geophys. Res., 66, 1641-1649, 1961.

126. A.J. Dragt. "Effect of Hydromagnetic Waves on the Lifetime of Van Allen Radiation Protons," J. Geophys. Res., 66, 1641-1649, 1961.

127. R.E. Holzer, M.G. McLeod, and E.J. Smith. "Preliminary Results from the OGO 1 Search Coil Magnetometer, Boundary Positions and Magnetic Power Spectra," J. Geophys. Res., 71, 1481-1486, 1966.

128. J. F. Denisse and J. L. Delcroix. Theorie des Ondes dans les Plasmas, Dunod, Paris, 1961, trans: Plasma Waves, Interscience, New York, 1963, 140 pp.

129. N.M. Brice. "Fundamentals of Very Low Frequency Emission Generation Mechanisms," J. Geophys. Res., 69, 1251-1258, 1964.

130. J.W. Dungey. "Loss of Van Allen Electrons Due to Whistlers," Plan. Sp. Sci., 11, 591-596, 1963.

131. J.W. Dungey. "Resonant Effect of Plasma Waves on Charged Particles in a Magnetic Field," J. Fluid Mech., 15, 74-82, 1963.

132. J.M. Cornwall. "Scattering of Energetic Trapped Electrons by Very-Low Frequency Waves," J. Geophys. Res., 69, 1251-1258, 1964.

133. T. H. Stix. The Theory of Plasma Waves, McGraw-Hill, New York, 1962, 268 pp.

134. C.F. Kennel and H.E. Petschek. "Limit on Stably Trapped Particle Fluxes," J. Geophys. Res., 71, 1-28, 1966.

135. R. Gendrin. "Pitch Angle Diffusion of Low Energy Protons Due to Gyroresonant Interaction With Hydromagnetic Waves," J. Atm. Terr. Phys., 30, 1313-1330, 1968.

136. J.B. Cladis. "Effect of Magnetic Field Gradient on Motion of Ions Resonating with Ion Cyclotron Waves," J. Geophys. Res., 78, 8129-8135, 1973.

137. L.R. Lyons, R.M. Thorne, C.F. Kennel, "Electron Pitch-Angle Diffusion Driven by Oblique Whistler-Mode Turbulence," J. Plasma Phys., 589, 1971.

138. L.R. Lyons, R.M. Thorne, "Pitch-Angle Diffusion of Radiation Belt Electrons within the Plasmasphere," J. Geophys. Res., 77, 3455-3474, 1972.

139. L.R. Lyons, R.M. Thorne. "Parasitic Pitch Angle Diffusion of Radiation Belt Particles by Ion Cyclotron Waves," J Geophys. Res., 77, 5608-5616, 1972.

140. A.L. Brinca. "On the Stability of Obliquely Propagating Whistlers," J.Geophys. Res., 77, 3495-3507, 1972

141. T.F. Bell and O. Buneman. "Plasma Instabi[illegible]in the Whistler Mode Caused by a Gyrating Electron Stream, [illegible]ys. Rev., A 133, 25-26, 1964.

142. N. Brice. "Artificial Enhancement of Energetic Particle Precipitation through Cold Plasma Injection: A Technique for Seeding Substorms," J. Geophys. Res., 75, 4890-4892, 1970.

143. N. Brice and C. Lucas. "Influence of Magnetospheric Convection and Polar Wind on Loss of Electrons from the Outer Belt," J. Geophys. Res., 76, 900-908, 1971.

144. N. Brice. "Harnessing the Energy in the Ra[illegible]ation Belts," J. Geophys. Res., 76, 4698-4701, 1971.

145. C.R. Chappell. "Recent Satellite Measurements of Morphology and Dynamics of the Plasmasphere," Rev. Geophys. Sp. Sci., 10, 951-979, 1972.

146. C.F. Kennel, R.W. Fredericks, and F.L. Scarf. "High Frequency Electrostatic Waves in the Magnetosphere," Particles and Fields in the Magnetosphere, B.M. McCormac, ed., Reidel, Dordrecht-Holland, 1970, pp. 257-265.

147. C.F. Kennel, F.L. Scarf, R.W. Fredericks, J.H. McGehee, and F.V. Coroniti. "VLF Electric Field Observations in the Magnetosphere," J. Geophys. Res., 75, 6136-6152, 1970.

148. F.V. Coroniti, R.W. Fredericks, and R. White. "Instability of Ring Current Protons Beyond the Plasmapause During Injection Events," J. Geophys. Res. 77, 6243-6248, 1972.

149. F.V. Coroniti, R.W. Fredericks, C.F. Kennel, and F.L. Scarf. "Fast Time Resolved Spectral Analysis of VLF Banded Emissions," J. Geophys. Res., 76, 2366-2381, 1973.

150. R.F. Post and M.N. Rosenbluth. "Electrostatic Instabilities in Finite Mirror Confined Plasmas," Phys. Fluids, 9, 730-749, 1966.

151. J.M. Cornwall and M. Schulz. "Electromagnetic Ion-Cyclotron Instabilities in a Multicomponent Plasma," J. Geophys. Res., 76, 7791-7796, 1971.

152. D.W. Swift. "A New Interpretation for VLF Chorus," J. Geophys. Res., 73, 7447-7456, 1968.

153. D.W. Swift. "Particle Acceleration by Electrostatic Waves," J. Geophys. Res., 75, 6324-6328, 1970.

154. G. Laval and R. Pellat. "Particle Acceleration by Electrostatic Waves Propagating in an Inhomogeneous Plasma," J. Geophys. Res., 75, 3255-3256, 1970.

155. L.R. Lyons. "Electron Diffusion Driven by Magnetospheric Electrostatic Waves," J. Geophys. Res., 79, 575-580, 1974.

156. J.M. Kindel and C.F. Kennel. "Topside Current Instabilities," J. Geophys. Res., 76, 3055-3078, 1971.

157. D. A. Tidman and R.K. Jaggi. "Landau Damping of Transverse Waves in the Exosphere by Fast Particle Fluxes," J. Geophys. Res., 67, 2215-2221, 1962.

158. F.E. Scarf. "Landau Damping and the Attenuation of Whistlers," Phys. Fluids, 5, 6-13, 1962.

159. R.D. Engel. "Nonlinear Stability of the Extraordinary Wave in a Plasma," Phys. Fluids, 8, 939-950, 1965.

160. J. Rowlands, V.D. Shapiro, and V.I. Shevchenko. "Quasi-linear Theory of Plasma Cyclotron Instability," Sov. Phys. JETP, 23, 651-660, 1966.

161. C.F. Kennel and R. Englemann. "Velocity Space Diffusion from Weak Plasma Turbulence in a Magnetic Field." Phys. Fluids, 9, 2377-2388, 1966.

162. W.J. Cocke and J.M. Cornwall. "Theoretical Simulation of Micropulsations," J. Geophys. Res., 2843-2856, 1967.

163. A.A. Galeev and R.Z. Sagdeev. Nonlinear Plasma Theory, Benjamin, New York, 1969.

164. P.J. Palmadesso and G. Schmidt. "Collisionless Damping of a Large Amplitude Whistler Wave," Phys. Fluids, 14, 1411-1418, 1971.

165. P.J. Palmadesso and G. Schmidt. "Stability of a Large Amplitude Whistler Wave," Phys. Fluids, 15, 485-492, 1972.

166. S.L. Ossakow, E. Ott, and I. Haber. "Nonlinear Evolution of Whistler Instabilities," Phys. Fluids, 15, 2314-2326, 1972.

167. S. L. Ossakow, E. Ott, and I. Haber. "Theory and Computer Simulation of Whistler Turbulence and Velocity Space Diffusion in the Magnetospheric Plasma," J. Geophys. Res., 78, 2945-2958, 1973.

163. S. L. Ossakow, E. Ott, and I. Haber. "Simulation of Gyroresonant Electron-Whistler Interaction in the Outer Radiation Belts," J. Geophys. Res., 78, 3970-3975, 1973.

169. S. Cuperman, Y. Salu, W. Bernstein, and D. J. Williams. "A Computer Simulation of Cold Plasma Effects on the Whistler Instability for Geostationary Orbit Plasma Parameters," J. Geophys. Res., 78, 7372-7387, 1973

170. R. A. Helliwell and T. L. Crystal. "A Feedback Model of Cyclotron Interaction between Whistler-Mode Waves and Energetic Electrons in the Magnetosphere," J. Geophys. Res., 78, 7357-7371, 1973.

171. G. Haerendel. "On the Balance Between Radial and Pitch Angle Diffusion," Particles and Fields in the Magnetosphere, ed. by B.M. McCormac, D. Reidel, Dordrecht, Holland, 416-428, 1970.

172. R. L. Dowden. "Doppler Shifted Cyclotron Generation of Exospheric Very-Low-Frequency Noise ('Hiss')," Plan. Sp. Sci., 11, 361-369, 1963.

173. J. A. Jacobs and T. Watanabe. "Amplification of Hydromagnetic Waves in the Magnetosphere by a Cyclotron Instability Process With Applications to the Theory of Hydromagnetic Whistlers," J. Atm. Terr. Phys., 28, 235-253, 1966.

174. R. L. Dowden. "Use of Electron and Proton Beams for Production of Very Low Frequency and Hydromagnetic Emissions," J. Geophys. Res., 78, 684-696, 1973.

175. R. M. Thorne and C. F. Kennel. "Relativistic Electron Precipitation During Magnetic Storm Main Phase," J. Geophys Res., 76, 4446-4453, 1971.

176. G. T. Davidson. "Enhancement of Artificial Electron Belts through Interactions of Electrons with Ion Cyclotron Waves," J. Geophys. Res., 78, 7569-7571, 1973.

177. G. T. Davidson. "Finite Temperature Effects on the Diffusion of Charged Particles in the Magnetosphere," J. Geophys. Res., (submitted 1974).

178. L.A. Frank. "A Survey of Electrons E>40 KeV Beyond 5 Earth Radii with Explorer 14," J. Geophys. Res., 70, 1593-1626, 1965.

179. B.J. O'Brien. "High Latitude Geophysical Studies with Satellite Injun 3. 3. Precipitation of Electrons into the Atmosphere," J. Geophys. Res., 69, 13-14, 1964.

180. J. Etcheto, R. Gendrin, J. Solomon, and A. Roux. "A Self-Consistent Theory of Magnetospheric ELF Hiss," J. Geophys. Res., 78, 8150-8166, 1973.

181. M. Schulz. "Wave-Particle Interaction in the Magnetospheric Plasma," Aerospace Corp. rept. ATR-74(7420)-1, 1974.

182. C.T. Russell and R.M. Thorne. "On the Structure of the Inner Magnetosphere," Cosm. Electrodyn., 1, 67-89, 1970.

183. S.I. Akasofu and C.I. Meng. "A Study in Polar Magnetic Storms," J. Geophys. Res., 74, 293-313, 1969.

184. J.M. Cornwall. "Diffusion Processes Influenced by Conjugate Point Wave Phenomena," Radio Sci., 3, 740-744, 1968.

185. J.M. Cornwall, F.V. Coroniti, and R.M. Thorne. "Turbulent Loss of Ring Current Protons," J. Geophys. Res., 75, 4699-4709, 1970.

186. J.M. Cornwall, F.V. Coroniti, and R.M. Thorne. "Unified Theory of SAR Arc Formation at the Plasmapause," J. Geophys. Res., 76, 4428-4445, 1971.

187. P.F. Mizera. "Observations of Precipitating Protons with Ring Current Energies," J. Geophys. Res., 79, 581-588, 1974.

188. H.B. Liemohn. "Cyclotron-Resonance Amplification of VLF and ULF Whistlers," J. Geophys. Res., 72, 39-55, 1967.

189. J.C. Lee and F.W. Crawford. "Stability Analysis of Whistler Amplification," J. Geophys. Res., 75, 85-96, 1970.

190. S. Cuperman and R.W. Landau. "On the Enhancement of the Whistler Mode Instability in the Magnetosphere by Cold Plasma Injection," J. Geophys. Res., 79, 128-134, 1974.

191. S. Cuperman and Y. Salu. "Optimum Cold Plasma Density for Maximum Whistler Instability: Numerical Versus Analytical," J. Geophys. Res., 79, 135-137, 1974.

192. C.S. Lin. "Further Discussion of the Cyclotron Instability," J. Geophys. Res., 79, 2894-2897, 1974.

193. E. Mark. "Growth Rates of the Ion Cyclotron Instability in the Magnetosphere," J. Geophys. Res., 79, 3218-3220, 1974.

194. H.B. Liemohn. "Stimulated Amplification of VLF and ULF Waves in the Magnetosphere by Localized Injections of Plasma Clouds and Particle Beams," University of Washington and Battelle Memorial Institute rept., 1972.

195. B.M. McCormac, J.E. Evans, S.B. Mende, G.T. Davidson, and C.R. Chappell. "Magnetospheric Chemical Release Study," Lockheed Palo Alto Res. Lab. rept. LMSC D354601, Palo Alto, Cal, 1973.

196. R.A. Helliwell. "Low-Frequency Waves in the Magnetosphere," Rev. Geophys., 7, 281-303, 1969.

197. R.A. Helliwell. "Intensity of Discrete VLF Emissions," Particles And Fields in the Magnetosphere, ed. by B.M. McCormac, Reidel, Dordrecht, Holland, 292-301, 1970.

198. R.L. Dowden. "Electron Energy Spectrum and Structure Deduced from Analysis of VLF Discrete Emissions by Using the Helliwell Criterion," J. Geophys. Res., 76, 3034-3045, 1971.

199. R.L. Dowden. "VLF Discrete Emissions Deduced from Helliwell's Theory," J. Geophys. Res., 76, 3046-3054, 1971.

200. R.N. Sudan and E. Ott. "Theory of Triggered VLF Emissions," J. Geophys. Res., 76, 4463-4476, 1971.

201. W.I. Axford and C.O. Hines. "A Unifying Theory of High-Latitude Geophysical Phenomena and Geomagnetic Storms," Can. J. Phys., 39, 1433-1464, 1961.

202. W.I. Axford, H.E. Petschek, and G.L. Siscoe. "Tail of the Magnetosphere," J. Geophys. Res., 70, 1231-1236, 1965.

203. W.I. Axford. "Some Aspects of the Structure and Dynamics of the Terrestrial Magnetosphere," Natural and Electromagnetic Phenomena Below 30 kc/s., ed. by D.F. Bleil, Plenum Press, New York, 5-32, 1964.

204. J.W. Dungey. "The Reconnection Model of the Magnetosphere," Earth's Particles and Fields, ed. by B.M. McCormac, Reinhold, New York, 385-392, 1968.

205. H.E. Taylor and E.W. Hones. "Adiabatic Motion of Auroral Particles in a Model of the Electric and Magnetic Fields Surrounding the Earth," J. Geophys. Res., 70, 3605-3628, 1965.

206. J.H. Piddington. "The Magnetospheric Radiation Belt and Tail Plasma Sheet," Pl. Sp. Sci., 16, 703-716, 1968.

207. R.D. Richtmyer. "Difference Methods for Initial Value Problems," Interscience, New York, 1957.

208. B. Carnahan, H.A. Luther, and J.O. Wilkes. "Applied Numerical Methods," Wiley, New York, 1969.

209. G.E. Forsythe and W.R. Wason. "Finite Difference Methods for Partial Differential Equations," Wiley, New York, 1960.

210. M. Schulz and L.J. Lanzerotti. "Particle Diffusion in the Radiation Belts," Springer, New York, 1974.

$$\eta_d(E) = \frac{1.95 \times 10^4}{E} \left(\frac{Z}{A}\right)^2 \frac{\rho}{E_d} \left(15.2 - \ell n \left[\frac{(A+1)^2}{A}\right] - \ell n\, E_d + \ell n\, E\right) \quad (8\text{-}6)$$

where Z is atomic number, ρ the density in grams per cubic centimeter, E_d is in eV, and E is in MeV. This relationship is valid for a range of proton energies for which the coulomb interaction is dominant for primary displacements and for which elastic scattering is dominant for secondary displacements. In addition, the energy must be low enough so that the contribution of proton nuclear elastic scattering and inelastic reactions to the displacement cross section is small compared to the coulomb contribution. For electrons, the evaluations are more complex but have been performed and illustrate the rapid rise above threshold to a slowly increasing function of energy above 0.5 MeV (Reference 12).

These evaluations are crude and correspond only to initial displacements rather than actual defects, but they are of qualitative and intuitive importance in comparing displacement production by particles of differing type and energy. For example, Table 8-1 gives values of η_d and ν for 1-MeV electrons, 10-MeV protons, and 100-MeV protons incident on Si. The measured carrier removal rate per unit particle fluence, $-dn/d\Phi$, also is given for comparative purposes (Reference 9).

Table 8-1. Comparison of theoretical displacement parameters with measured carrier removal in silicon.

Particle	η_d (cm^{-1})	ν	n-Si $-dn/d\Phi$ (carriers/cm)	p-Si $-dn/d\Phi$ (carriers/cm)
1-MeV Electrons	4.6	1.3	0.2	0.005
10-MeV Protons	1100.0	6.0	100.0	100.0
100-MeV Protons	130.0	7.0	—	—

RADIATION DEFECT FORMATION PROCESSES. After the primary displacement or ionization processes, several intermediate entities often occur before the final radiation defect sites are established. These will be discussed for displacement processes in the bulk material and ionization near the surface.

For displacement due to electrons irradiating the bulk crystal, secondary displacements are few so that the distribution of defects is approximated closely, at the first stage, by isolated, closely spaced interstitial vacancy (I-V) pairs (Reference 7). Often the vacancy is mobile and migrates to defect or impurity atom sites [oxygen (O) or phosphrous (P)] or, conv rsely, the impurities may migrate to form stable sites. Another possibility is that the vacancy may recombine. As a consequence of these possibilities, the defect sites will depend on type (n or p) of Si and on impurities. They are more easily annealable than are heavy particle sites.

Much information has been accumulated on the physical structure of these sites (Reference 12). The relative number of such sites is a strong function of temperature. Protons have more secondaries per primary displacement and increased primary displacements per centimeter than do electrons. This suggests that the primary stage consists of closely spaced, small defect clusters. The increased cluster size for protons compared to electrons means that annealing will be less probable but migration of vacancies (or interstitials) should not be impeded. This indicates a strong dependence of the resulting stable defect sites on the type silicon, impurity atoms, resistivity, and residual impurities (O, P).

In terms of ionization-induced defect sites in surface layers [e.g., silicon dioxide (SiO_2) passivation layers], the final defect site may be (1) the initial ionized atom, (2) the result of the migration of the site, or (3) the result of impurity migration to the site. Very little is understood about the details of these processes, but the observed effects have been found to be dependent on the magnitude and distribution of the surface charge (Reference 10).

SEMICONDUCTOR TRANSPORT PROPERTIES DEPENDENCE ON RADIATION-INDUCED DEFECTS. The effects on both the bulk and surface semiconductor transport properties of radiation-induced defect sites are best understood in terms of the concept of a recombination center (Reference 8). Any defect site, whether natural or radiation-induced, may introduce defect energy levels into the forbidden energy band gap of a semiconductor. These levels may be described in terms of their cross section for capture or emission of free electrons and holes. In particular, those states may exist called recombination centers, which, after capturing a conduction electron (hole), will have a large capture cross section for a free hole (electron)leading, in effect, to a net loss of an electron-hole

SECTION 15

INDEX

-A-

-B-

-C-

-D-

-E-

-J-

-L-

-N-

-V-

-W-

-X-

-Y-

-Z-

DISTRIBUTION LIST

DEPARTMENT OF DEFENSE

Assistant to the Secretary of Defense
Atomic Energy
ATTN: Honorable Donald R. Cotter

Director
Defense Communications Agency
ATTN: Clyde W. Herr

Defense Communication Engineer Center
2 cy ATTN: Code R1035S, John W. Worthington

Defense Documentation Center
12 cy ATTN: TC

Director
Defense Intelligence Agency
ATTN: DT-1C, Jack Vorona
ATTN: DT-1, Mr. Knoll

Director
Defense Nuclear Agency
ATTN: RAAE, Captain Bauer
ATTN: STVL, E. Lavier
ATTN: STSI, Archives
ATTN: RAAE, Captain Motal
ATTN: DDST, Warren W. Berning
ATTN: RAAE, Major Clark
ATTN: RAAE, H. C. Fitz
3 cy ATTN: RAEV, Major Adams
2 cy ATTN: STTL, Technical Library
3 cy ATTN: RAAE, Charles A. Blank
ATTN: SPAS, James Moulton

Director of Defense Research & Engineering
ATTN: Honorable Thomas C. Reed
ATTN: ADI&C
ATTN: DD/S&SS, John B. Walsh
ATTN: DDS&SS, Richard S. Ruffine
ATTN: DDR&AT/EPS
ATTN: NTA, James P. Wade
ATTN: DDS&SS, Daniel J. Brockway
ATTN: Captain K. W. Ruggles

Commander
Field Command
Defense Nuclear Agency
ATTN: FCT, William S. Isengard
ATTN: FCPR

Director
Joint Strategic Target Planning Staff, JCS
ATTN: Document Control
ATTN: JPST, Major J. S. Green

Chief
Livermore Division Field Command, DNA
Lawrence Livermore Laboratory
ATTN: FCPRL

Director
National Security Agency
ATTN: Technical Library

DEPARTMENT OF DEFENSE (Continued)

Interservice Nuclear Weapons School
ATTN: Document Control

OJCS/J-2
The Pentagon
ATTN: J-2, Intelligence

OJCS/J-3
The Pentagon
ATTN: J-3, Environmental Services Division
ATTN: J-3, Operations Analyses Branch
ATTN: J-3, Operations

OJCS/J-5
The Pentagon
ATTN: J-5, Plans & Policy, R&D Division

OJCS/J-6
The Pentagon
ATTN: J-6

Weapons Systems Evaluation Group
ATTN: Document Control

DEPARTMENT OF THE ARMY

Commander
U.S. Army SATCOM Agency
ATTN: Technical Library

Assistant Chief of Staff for Force Development
Department of the Army
ATTN: Director of Chemical & Nuclear Operations

Director
Ballistic Missile Defense Advanced Tech Center
Huntsville Office
ATTN: CRDABH-O, W. Davies
ATTN: Melvin T. Capps

Chief of Research, Development & Acquisition
Department of the Army
ATTN: CRD-NCB
ATTN: NCB Division
ATTN: ABMDA-OO

Department of the Army
Office of the Chief of Engineers
ATTN: Fernand DePercin

Commander
Harry Diamond Laboratories
2 cy ATTN: AMXDO-NP

Commander
U.S. Army Electronics Command
ATTN: AMSEL-RD-P, Hans Bomke
ATTN: AMSEL-XL-D, Stanley Kronenberg
ATTN: AMSEL-RD-P, Park Richmond
ATTN: AMXSEL-TL-IR, E. J. Hunter

DEPARTMENT OF THE ARMY (Continued)

Commanding Officer
U.S. Army Electronics Command
Atmospheric Sciences Laboratory
ATTN: H. Ballard
ATTN: Robert Rubio
ATTN: Robert Olsen

Commander
U.S. Army Material Command
ATTN: Robert Jones

Commander
U.S. Army Materiel Command
ATTN: AMCRD-WN-RE, John F. Corrigan

Director
U.S. Army Ballistic Research Laboratories
ATTN: J. Mester
ATTN: Franklin E. Niles
ATTN: J. Heimerl
ATTN: DRL, Don Snider
ATTN: M. Kregl
ATTN: Technical Library

Commander
U.S. Army Missile Command
ATTN: AMSMI-XS, Chief Scientist
ATTN: AMSMI-ABL

Commander
U.S. Army Nuclear Agency
ATTN: CDINS-E

Chief
U.S. Army Research Office (Durham)
ATTN: CRDARD-DCS, Hermann R. Robl
ATTN: CRDARD-P, Robert Mace

Commander
Whippany Field Office (BDMSC-WS-W)
Bell Telephone Laboratories
ATTN: John Turner

Commander
White Sands Missile Range
ATTN: Willis W. Webb, AMSEL-NL-SD
ATTN: Marvin P. Squires, STEWS-TE-NT

DEPARTMENT OF THE NAVY

Chief of Naval Operations
Navy Department
ATTN: Code 604C3, Robert Piacesi
ATTN: OP 985

Chief of Naval Research
Navy Department
ATTN: Code 461, Jacob L. Warner
ATTN: Code 427, CDR Ronald J. Oberle
ATTN: Code JTC, John G. Dardis
ATTN: Code 461, Thomas P. Quinn
ATTN: Code 464, Grayson Joiner

Commander
Naval Electronic Systems Command
Naval Electronic Systems Command Headquarters
ATTN: PME 117-T
ATTN: ELEX03

DEPARTMENT OF THE NAVY (Continued)

Commander
Naval Electronics Laboratory Center
ATTN: Technical Library for T. J. Keary
ATTN: William F. Moler
ATTN: Code 2200, Verne E. Hildebrand
ATTN: Jurgen Richter
ATTN: Ilan Rothmuller
ATTN: William Pappert

Director
Naval Research Laboratory
ATTN: Donald J. Horam
ATTN: Code 7750, Timothy P. Coffey
ATTN: Wahab Ali
ATTN: James D. Kurfess
ATTN: W. Neil Johnson
ATTN: Gerald H. Share
ATTN: Robert L. Kinzer
ATTN: Code 7127, Charles Y. Johnson
ATTN: Jack Brown
ATTN: Code 2027, Technical Library
ATTN: Klaus Hain
ATTN: Frederick W. Raymond
ATTN: E. L. Brancato
ATTN: Jack Davis
ATTN: Richard L. Statler
ATTN: S. L. Ossakow
ATTN: Francis J. Campbell

Commander
Naval Surface Weapons Center
ATTN: Code 1224, Navy Nuclear Programs Office
ATTN: Code 730, Technical Library

Commander
Naval Weather Service Command
Naval Weather Service Headquarters
ATTN: Robert H. Martin

Commanding Officer
Navy Astronautics Group
6 cy ATTN: W. J. Gleason

Superintendent
Naval Postgraduate School
ATTN: E. A. Milne
ATTN: Technical Library
ATTN: J. N. Dyer

Commanding Officer
Nuclear Weapons Training Group, Pacific
ATTN: Nuclear Warfare Department

Commander
Nuclear Weapons Training Group, Atlantic
ATTN: Nuclear Warfare Department

DEPARTMENT OF THE AIR FORCE

ADC/DO
ATTN: DOF

ADC/XP
ATTN: XPQDQ
ATTN: XPQD, Maj G. Kuch
ATTN: Hqs. 14th Aerospace Force
ATTN: Paul Major

DEPARTMENT OF THE AIR FORCE (Continued)

AF Cambridge Research Laboratories, AFSC
ATTN: LI, Phillip Newman
ATTN: C. Stergis
ATTN: L. Katz
ATTN: LKB, Kenneth S. W. Champion
ATTN: LI, Wolfgang Pfister
ATTN: LKD, Rocco S. Narcisi
ATTN: OP, John S. Garing
ATTN: OPR, E. Lee
ATTN: OPR, F. Delgreco
ATTN: OPR, Harold Gardner
ATTN: SUOL, AFCRL Research Library
ATTN: OPR, R. O'Neill
ATTN: OPR, T. Connolly
ATTN: E. Murad
ATTN: W. Pittenger
ATTN: A. Faire
ATTN: John McClay
ATTN: Jack Kenneally
ATTN: R. Huffman
ATTN: W. Swider
ATTN: L. Weeks
ATTN: J. Rodgers
ATTN: A. T. Stair
ATTN: T. J. Keneshea
ATTN: F. R. Innes
ATTN: Joseph Kelly
ATTN: D. Columb
6 cy ATTN: OPR, James C. Ulwick

Aerospace Research Laboratories, AFSC
ATTN: T. O. Terman
ATTN: Technical Library

AF Weapons Laboratory, AFSC
ATTN: DYT, Capt Dennis Hollars
ATTN: CA, Arthur H. Guenther
ATTN: SUL
ATTN: DYT, Capt David Goetz
ATTN: DYT, Joseph Janni
ATTN: DYT, Gary D. Cable
ATTN: DYT, Capt Richard Harris
ATTN: DYT, Major Gregory Canavan
ATTN: DYT, Major Daniel Matuska

AFTAC
ATTN: TN
ATTN: Maj R. Wiley
ATTN: TNE, Lt Col E. C. Thomas
ATTN: Technical Library

Headquarters
Air Force Systems Command
ATTN: DLXP, Capt Robel
ATTN: SCTSW, Weapons & Weapon... ...ts Div.
ATTN: SDSS/DLSE
ATTN: Lt Col B. C. Healy
ATTN: Lt Col H. Simmons
ATTN: Lt Col W. Beam

Commander
Foreign Technology Division, AFSC
ATTN: TD-BTA, Library
ATTN: TDPSS, Kenneth N. Williams

HQ USAF/IN
ATTN: IN

DEPARTMENT OF THE AIR FORCE (Continued)

HQ USAF/RD
ATTN: RDSA
ATTN: RDQPN
ATTN: RDPS
ATTN: RD
ATTN: RDPM

Commander
Rome Air Development Center, AFSC
ATTN: J. J. Simons
ATTN: EMTLD, Document Library
ATTN: Col R. Paltauf
ATTN: V. Coyne

SAMSO/DY
ATTN: DYE, Lt Col W. F. Herdrich

Commander in Chief
Strategic Air Command
ATTN: XPFS, Maj Brian G. Stephan

4th Weather Wing, MAC
2 cy ATTN: AESB

USAF&TAC/CB
ATTN: CRT, Mr. Creasi

ENERGY RESEARCH & DEVELOPMENT ADMINISTRATION

FERMI National Laboratory
ATTN: Document Control for A. C. Wahl
ATTN: Document Control for Leo Leibowitz
ATTN: Document Control for S. Gabelnick
ATTN: Document Control for W. A. Chupka
ATTN: Document Control for David W. Green
ATTN: Document Control for Gerald Reedy

Division of Military Application
U.S. Energy Research & Development Administration
ATTN: Document Control for Rudolf J. Engelmann
ATTN: Document Control for Colonel T. Cross
ATTN: Document Control for Frank A. Ross
ATTN: Document Control for Donald I. Gale
ATTN: Document Control for David H. Slade

University of California
Lawrence Livermore Laboratory
ATTN: L-517, J. F. Tinney
ATTN: Dept. L-3, Tech. Info. Department
ATTN: F. Charles Gilbert
ATTN: R. Yoder
ATTN: J. Watson

Los Alamos Scientific Laboratory
ATTN: Document Control for Herman Hoerlin
ATTN: Document Control for John S. Malik
ATTN: Document Control for J. Judd
ATTN: Document Control for E. W. Hones, Jr.
ATTN: Document Control for Martin Tierney, J-10
ATTN: Document Control for William Maier
ATTN: Document Control for H. M. Peek
ATTN: Document Control for S. Rockwood
ATTN: Document Control for Donald Kerr

ENERGY RESEARCH & DEVELOPMENT ADMINISTRATION (Continued)

Sandia Laboratories
Livermore Laboratory
ATTN: Doc. Con. for Thomas B. Cook, Org. 8000

Sandia Laboratories
ATTN: Doc. Con. for 3141, Sandia Rpt. Coll
ATTN: Doc. Con. for Craig Hudson, Org. 1751
ATTN: Doc. Con. for Org. 9220
ATTN: Doc. Con. for J. C. Eckhardt, Org. 1250
ATTN: Doc. Con. for Morgan L. Kramm, Org. 5720
ATTN: Doc. Con. for Frank P. Hudson, Org. 1722
ATTN: Doc. Con. for Clarence R. Mehl, Org. 5230

U.S. Energy Research & Development Administration
Division of Headquarters Services
ATTN: Doc. Con. for D. Kohlstad
ATTN: Doc. Con. for Joseph D. Lafleur
ATTN: Doc. Con. for Richard J. Kandel
ATTN: Doc. Con. for H. H. Kurzweg
ATTN: Doc. Con. for George L. Rogosa

U.S. Energy Research & Development Administration
Brookhaven Area Office
ATTN: A. W. Castleman, Jr.
ATTN: J. Chernik

OTHER GOVERNMENT AGENCIES

Central Intelligence Agency
ATTN: RD/SI for NED/OSI - 2G48, Hqs.

Department of Commerce
National Bureau of Standards
ATTN: D. Garvin
ATTN: D. R. Lide
ATTN: B. Stiener
ATTN: K. Kessler
ATTN: Stanley Abramowitz
ATTN: M. Scheer
ATTN: Office of Director
ATTN: Charles W. Beckett
ATTN: J. Cooper
ATTN: M. Krauss
ATTN: G. A. Simmatt
ATTN: L. G. Evantman

Department of Commerce
National Oceanic & Atmospheric Administration
Environmental Research Laboratories
ATTN: R43, Donald J. Williams
ATTN: Robert B. Doeker
ATTN: RX1, Robert W. Knecht
ATTN: George C. Reid, Aeronomy Lab.
ATTN: E. E. Ferguson
ATTN: Donald J. Williams
ATTN: R43, Herbert B. Sauer

Director, Air Resources Laboratories
National Oceanic & Atmospheric Administration
ATTN: J. K. Angell
ATTN: L. Machta

OTHER GOVERNMENT AGENCIES (Continued)

Department of Commerce
Office of Telecommunications
Institute for Telecom Science
ATTN: William F. Utlaut
ATTN: Glenn Falcon
ATTN: Lester Berry

Department of Transportation
Transportation Research System Center
ATTN: F. Marmo

Department of Transportation
Office of the Secretary
ATTN: Allen J. Grobecker
ATTN: R. Underwood
ATTN: Samuel C. Coroniti
10 cy ATTN: Richard L. Strombotne, TST-8

NASA
Scientific & Technical Information Facility
ATTN: ACQ Branch
ATTN: SAR/DLA-385

National Aeronautics & Space Administration
George C. Marshall Space Flight Center
ATTN: W. A. Oran
ATTN: C. R. Baugher
ATTN: N. H. Stone
ATTN: W. T. Roberts
ATTN: R. D. Hudson
ATTN: R. Chappell

National Aeronautics & Space Administration
Goddard Space Flight Center
ATTN: Gilbert D. Mead, Code 641
ATTN: J. Siry
ATTN: James I. Vette
ATTN: S. J. Bauer
ATTN: Technical Library
ATTN: A. Tempkin
ATTN: G. Levin
ATTN: J. P. Heppner
ATTN: R. F. Benson
ATTN: E. J. Meyer
ATTN: M. Sugiura
ATTN: H. A. Taylor
ATTN: A. C. Aiken

National Aeronautics & Space Administration
Johnson Space Center
ATTN: Classified Library, Code BM6
ATTN: Owen Garriot

National Aeronautics & Space Administration
Ames Research Center
ATTN: C. P. Sonett
ATTN: N-245-4, Ilia G. Poppoff
ATTN: N-245-3, Palmer Dyal
3 cy ATTN: M-254-4, R. Whitten

OTHER GOVERNMENT AGENCIES (Continued)

National Aeronautics & Space Administration
ATTN: E. R. Schmerling
ATTN: L. D. Kavanagh, Jr.
ATTN: A. Schardt
ATTN: J. Naugle
ATTN: G. K. Oertel
ATTN: H. H. Kurzweg
ATTN: Lieutenant Colonel J. F. Lehans
ATTN: R. Fellows
ATTN: M. Dubin
ATTN: R. T. Schiffer
ATTN: P. Eaton
ATTN: N. Roman
ATTN: O. Cauffman
ATTN: L. Fong
ATTN: M. Tepper
ATTN: J. Findlay
ATTN: G. Sharp

National Science Foundation
ATTN: E. P. Todd
ATTN: M. K. Wilson
ATTN: L. R. Megill
ATTN: W. H. Cramer
ATTN: F. Gilman Blake
ATTN: Fred D. White
ATTN: Robert Manka
ATTN: R. S. Zapolsky
ATTN: Rolf Stuclair
ATTN: W. O. Adams

U.S. Arms Control & Disarmament Agency
ATTN: Office of Director
ATTN: Reference Info. Center
ATTN: Pierce S. Corden

U.S. Geological Survey
ATTN: Robert D. Regan

Department of Commerce
National Oceanic & Atmospheric Administration
ATTN: Gerald A. Peterson
ATTN: Ronald L. Lavoie
ATTN: Wayne McGovern
ATTN: Edward S. Epstein
ATTN: John W. Townsend, Jr.

DEPARTMENT OF DEFENSE CONTRACTORS

Aerodyne Research, Inc.
ATTN: M. Camac

American Science & Engineering Corporation
ATTN: Document Control

Analytical Systems Engineering Corporation
ATTN: J. A. Caruso

Battelle Memorial Institute
ATTN: Radiation Effects Information Center
ATTN: Donald J. Hamman

Bell Telephone Laboratories, Inc.
ATTN: Lyman J. Fretwell
ATTN: Arnold S. Boxer
ATTN: L. H. Sessler, Jr.
ATTN: W. Brown

DEPARTMENT OF DEFENSE CONTRACTORS (Continued)

Aeronomy Corporation
ATTN: S. A. Bowhill

Aerospace Corporation
ATTN: F. Keller
ATTN: D. Cohn
ATTN: J. B. Blake
ATTN: J. Sorrels
ATTN: L. W. Aukerman
ATTN: Julian Reinheimer
ATTN: J. Stevens
ATTN: J. Woodford
ATTN: R. Mortensen
ATTN: V. Wall
ATTN: T. Friedman
ATTN: V. Josephson
ATTN: Harris Mayer
ATTN: George Paulikas
ATTN: G. Millburn
ATTN: S. P. Bower
ATTN: T. Taylor
ATTN: N. Cohen
ATTN: R. D. Rawcliffe

Albright College
ATTN: Moo Ung Kim

The Boeing Company
ATTN: Glen Keister

The Trustees of Boston College
ATTN: Library
ATTN: Chairman, Department of Chemistry
ATTN: R. L. Carlvilland
ATTN: R. Eather
ATTN: R. Helblom

Brown Engineering Company, Inc.
ATTN: J. E. Cato
ATTN: C. E. Wayne
ATTN: R. Walters
ATTN: J. Dabkins

University of California at Los Angeles
Office of Extramural Support
ATTN: T. A. Farley, Space Science Laboratory

University of California at Riverside
ATTN: Alan C. Lloyd
ATTN: James N. Pitts, Jr.
ATTN: Leo Zaponte

University of California at San Diego
ATTN: Peter M. Banks
ATTN: C. E. McIlwain, Physics Dept.

University of California, Berkeley Campus
ATTN: Kinsie A. Anderson

Calspan Corporation
ATTN: W. Wurster
ATTN: C. E. Treanor
ATTN: Robert A. Fluegge
ATTN: M. G. Dunn
ATTN: Technical Library

DEPARTMENT OF DEFENSE CONTRACTORS (Continued)

University of Colorado
Office of Research Services
ATTN: Charles A. Barth, LASP
ATTN: Jeffrey A. Pearce
ATTN: A. Phelps
ATTN: C. Lineberger
ATTN: E. C. Beaty

The Trustees of Columbia University
ATTN: Richard N. Zare
ATTN: Security Officer, H. M. Foller

Comsat Laboratories
ATTN: Document Control

University of Denver
Colorado Seminary
ATTN: Juan G. Roederer
ATTN: D. Murcray
ATTN: B. Van Zyl

Epsilon Laboratories, Inc.
ATTN: Henry Miranda
ATTN: C. Accardo

ESL, Inc.
ATTN: James Marshall

Extranuclear Laboratories, Inc.
ATTN: Wade Fite

General Dynamics Corporation
Convair Division
ATTN: Library 2-98-00, D. H. McCoy

General Electric Company
Space Division
ATTN: Technical Information Center
ATTN: M. H. Bortner, Space Science Laboratory
ATTN: Joseph C. Peden, CCF 8301
ATTN: T. Baurer
ATTN: P. Zavistanos
ATTN: F. Alyea
ATTN: A. Simisgalli

General Electric Company
TEMPO-Center for Advanced Studies
ATTN: Tim Stephens
ATTN: Don Chandler
ATTN: W. S. Knapp
ATTN: B. Gambill
51 cy ATTN: DASIAC, M. Dudash

General Research Corporation
ATTN: John Ise, Jr.

General Research Corporation
ATTN: J. Zokrskowski

Grumann Aerospace Corporation
ATTN: Michael D. Agostino

DEPARTMENT OF DEFENSE CONTRACTORS (Continued)

Geophysical Institute
University of Alaska
ATTN: S. I. Akasofu
ATTN: A. Belon
ATTN: Neil Brown
ATTN: T. N. Davis
ATTN: Technical Library
ATTN: R. Parthasoratny
ATTN: H. Cole
ATTN: D. J. Henderson
ATTN: J. S. Wagner

Harvard College Observatory
ATTN: J. Patrick Henry

HRB-Singer, Inc
ATTN: Tech. Information Center, E. J. McBride

HSS, Inc.
ATTN: M. Schuler
ATTN: D. Hansen
ATTN: H. Stewart

IBM Corporation
ATTN: Daniel C. Sullivan

IIT Research Institute
ATTN: Technical Library
ATTN: R. B. Cohen

University of Illinois
ATTN: J. Schroeder

University of Illinois
ATTN: Chalmers Sechrist

University of Illinois
Physics Department
ATTN: William J. Otting

Institute for Defense Analyses
ATTN: IDA, Librarian, Ruth S. Smith
ATTN: Joel Bengston
ATTN: Hans Wolfhard
ATTN: Ernest Bauer

Intelcom Rad Tech
ATTN: R. H. Neynaber

Jaycor, Inc.
ATTN: James Young

Johns Hopkins University
Applied Physics Laboratory
ATTN: Document Control

Kaman Sciences Corporation
ATTN: Frank H. Shelton
ATTN: Library

DEPARTMENT OF DEFENSE CONTRACTORS (Continued)

Lockheed Missiles & Space Company, Inc.
ATTN: J. H. Hockenberry, D/60-01
ATTN: J. T. Hart, Jr., D/61-03
ATTN: W. P. Minmaugh, D/69-50
ATTN: R. D. Moffat, D/81-01
ATTN: S. I. Weiss, D/68-01
ATTN: E. E. Crowther, D/60-01
ATTN: D. L. Crowther, D/62-25
ATTN: Q. A. Riepe, D/60-80
ATTN: Dewey Churchill
ATTN: J. Cretcher
ATTN: D. F. McClinton
ATTN: R. H. Olds

Lockheed Missiles & Space Company
ATTN: W. L. Imhof, D/52-12
ATTN: G. H. Nakano, D/52-12, B/205
ATTN: R. P. Caren, D/62-20
ATTN: R. K. Landshoff
ATTN: James W. Schallov
ATTN: E. A. Smith
ATTN: T. D. Passell
ATTN: R. D. Meyerott
ATTN: G. T. Davidson, D/52-12
ATTN: John E. Evans, D/52-14
ATTN: R. D. Sharp, D/52-12
ATTN: W. D. Frye, D/52-21
ATTN: Technical Information Center, D/Coll.
ATTN: Richard G. Johnson, D/52-12
ATTN: Billy M. McCormac, D/52-14
ATTN: W. E. Francis, D/52-12
ATTN: D. C. Fisher, D/52-14
ATTN: A. D. Anderson, D/52-12
ATTN: J. B. Reagan, D/52-12
ATTN: R. A. Breuch, D/52-21
ATTN: L. L. Newkirk, D/52-21
ATTN: John B. Cladis, D/52-12
ATTN: Martin Walt, D/52-10

M. I. T. Lincoln Laboratory
ATTN: James H. Pannell, L-246
ATTN: W. E. Morrow

Maxwell Laboratories, Inc.
ATTN: Victor Fargo

McDonnell Douglas Corporation
ATTN: A. D. Goedeke
ATTN: O. K. Moe
ATTN: W. Olsen

University of Minnesota
ATTN: J. R. Winkler

Mission Research Corporation
ATTN: Dave Sowle
ATTN: Conrad L. Longmire
ATTN: D. Sappenfield
ATTN: D. Archer
ATTN: D. Holland
ATTN: M. Scheibe
ATTN: R. Bogusch
ATTN: P. Fischer
ATTN: R. Hendrick

DEPARTMENT OF DEFENSE CONTRACTORS (Continued)

The Mitre Corporation
ATTN: B. Troutman
ATTN: R. Greeley
ATTN: P. Grant
ATTN: Library

Mount Auburn Research Associates
ATTN: Sheldon Kabales

National Academy of Sciences
ATTN: Edward P. Dyer
ATTN: William C. Bartley
ATTN: John R. Sievers

Pennsylvania State University
Industrial Security Office
ATTN: J. S. Nesbet
ATTN: R. Simoniatis
ATTN: L. Hale

Photometrics, Inc.
ATTN: Irving L. Kofsky

Physical Dynamics, Inc.
ATTN: K. Watson
ATTN: Joseph Workman
ATTN: A. Thompson

Physical Sciences, Inc.
ATTN: R. L. Taylor
ATTN: K. Wray

University of Pittsburgh of the
Commonwealth Systems of Higher Education
ATTN: Frederick Kaufman
ATTN: M. Biondi

R & D Associates
ATTN: William J. Karzas
ATTN: Robert E. Lelevier
ATTN: William R. Graham, Jr.
ATTN: Forest Gilmore
ATTN: R. P. Turco
ATTN: H. A. Ory
ATTN: R. G. Lindgren
ATTN: A. Latters

R & D Associates
ATTN: J. Rosengren
ATTN: R. Latter
ATTN: H. Mitchell

The Rand Corporation
ATTN: Cullen Crain
ATTN: Technical Library
ATTN: Paul Tamarkin

Rice University
Department of Space Science
ATTN: Ronald F. Stebbings
ATTN Joseph Chamberlain

DEPARTMENT OF DEFENSE CONTRACTORS (Continued)

Rockwell International Corporation
Space Division
ATTN: William Atwell

Sanders Associates, Inc.
ATTN: Jack Schwartz
ATTN: Edward A. Colson

Science Applications, Inc.
ATTN: Robert W. Lowen
ATTN: Daniel A. Hamlin
ATTN: David Sachs

San Diego State University Foundation
ATTN: F. A. Wolf

Smithsonian Astrophysical Observatory
ATTN: A. Dalgarno

Space Data Corporation
ATTN: Edward F. Allen

Stanford Research Institute
ATTN: Ray L. Leadabrand
ATTN: M. Baron
ATTN: Allen M. Peterson
ATTN: James P. Peterson
ATTN: E. Kindermann
ATTN: Felix T. Smith
ATTN: Walter G. Chesnut
ATTN: John Lomax

Stanford University
ATTN: D. L. Carpenter
ATTN: R. A. Helliwell

DEPARTMENT OF DEFENSE CONTRACTORS (Continued)

Technology International Corporation
ATTN: W. P. Boquist

TRW Systems Group
ATTN: J. M. Sellen, Jr.
ATTN: Benjamin Sussholtz
ATTN: J. R. McDougall
ATTN: Technical Information Center, S-1930
ATTN: R. Watson
ATTN: F. Scarf
ATTN: J. F. Frichtenicht

United Aircraft Corporation
Research Laboratories
ATTN: H. Michels
ATTN: Robert Bullis

Utah State University
ATTN: D. Burt
ATTN: Kay Baker
ATTN: D. Baker
ATTN: C. Wyatt

Visidyne, Inc.
ATTN: Oscar Manley
ATTN: J. W. Carpenter

Wayne State University
ATTN: R. Kummler
ATTN: P. K. Rol
ATTN: W. E. Kauppila

Yale University
ATTN: G. J. Schultz